

# Dissertation

submitted to the  
Combined Faculties for the Natural Sciences and for Mathematics  
of the Ruperto-Carola University of Heidelberg, Germany  
for the degree of  
Doctor of Natural Sciences

Put forward by

**Dipl. Phys. Helene Margarethe Hoffmann**

born in Homburg (Saar), Deutschland

Oral examination: 11.5.16



**Micro radiocarbon dating of the  
particulate organic carbon fraction  
in Alpine glacier ice:  
method refinement, critical evaluation  
and dating applications**

This work is dedicated to Dietmar Wagenbach,  
who was the main advisor of this project  
and sadly did not live to see this work finished.

**Referees:**

Prof. Dr. Ingeborg Levin  
Prof. Dr. Werner Aeschbach



## Abstract:

This work focuses on radiocarbon dating of the Particulate Organic Carbon fraction (POC) of Alpine glacier ice. This organic carbon fraction was chosen, because the initially preferred Dissolved Organic Carbon fraction (DOC) was found to be biased by incorporation of in situ produced  $^{14}\text{C}$  at high Alpine sites. Concentrations of POC in high Alpine ice are generally very low, ranging on average between 10 and 50  $\mu\text{gC}$  per kg ice. Thus, POC  $^{14}\text{C}$  dating of Alpine ice cores, where available masses for dating are not exceeding a few hundred grams of ice, becomes a large challenge. Within this work, a unique sample preparation system (REFILOX), with a process blank reproducibly at a total carbon mass of  $(1.5 \pm 1.0) \mu\text{gC}$  or even below detection limit for combustion at 340 °C, has been deployed. This system was complemented by the setup of a gas ion source for direct  $\text{CO}_2$  AMS (Accelerator Mass Spectrometry)  $^{14}\text{C}$  measurements. Together, these novel sample preparation systems allow reliable dating of samples down to 2  $\mu\text{gC}$  with a relative error not exceeding 10% for ages up to 15 000 years BP. For comprehensive age interpretation, POC age biasing effects such as input of old Saharan dust or sediment material have been investigated. The Saharan dust consistently featured an age range of 2200-2800 years BP and the sediment samples showed ages up to more than 20 000 years BP. POC combustion temperature investigations revealed that such biases by incorporated aged material can be avoided best by combustion at a temperature not higher than 340 °C. A first application of the method to ice block samples from Titlis glacier (Swiss Alps, 3020 m a.s.l.) yielded a consistent basal ice age of almost 5000 years BP. Additionally, 16 samples from an ice core drilled at the high Alpine glacier saddle Colle Gnifetti (Swiss Alps, 4500 m a.s.l.) have been POC micro-radiocarbon dated and revealed a so far not fully explained systematic age offset to younger ages than proposed by the annual layer counting based working chronology.

## Zusammenfassung:

Der Schwerpunkt dieser Arbeit liegt auf der Datierung der partikulären organischen Kohlenstofffraktion (POC) aus alpinem Gletschereis. Diese Fraktion wurde gewählt, da die ursprünglich bevorzugte gelöste organische Kohlenstofffraktion (DOC) durch in situ Produktion von  $^{14}\text{C}$  verfälscht ist. Die Konzentration von POC in hochalpinem Eis ist insgesamt sehr niedrig, typischerweise in einem Bereich von 10-50  $\mu\text{gC}$  pro kg Eis. Aus diesem Grund stellt die POC  $^{14}\text{C}$ -Datierung alpiner Eisbohrkerne, bei denen oft nur wenige hundert Gramm Eis zur Verfügung stehen, eine große Herausforderung dar. In dieser Arbeit wurde ein neuartiges System zur Probenaufbereitung (REFILOX) entwickelt, dessen Prozessblank stabil bei einer Kohlenstoffmasse von  $(1,5 \pm 1,0) \mu\text{gC}$  liegt. Für die Verbrennung bei 340 °C sogar darunter. Zusätzlich zu diesem System wurde eine sogenannte Gasionenquelle für direkte AMS (Beschleunigermassenspektrometrie)  $^{14}\text{C}$  Messungen an  $\text{CO}_2$  in Betrieb genommen. Durch Kombination dieser beiden Systeme sind nun verlässliche Datierung von Proben bis hin zu 2  $\mu\text{gC}$  mit einem relativen Fehler unter 10% für den Altersbereich bis zu 15 000 Jahren vor heute möglich. Für eine verlässliche Altersinterpretation wurden zudem mögliche Effekte untersucht, die das POC Alter verfälschen können, wie zum Beispiel der Eintrag von Saharastaub oder Sediment. Das Alter des Saharastaubs liegt sehr konstant in einem Altersbereich von 2200-2800 Jahren vor heute, die Sedimentproben wurden zum Teil sogar auf mehr als 20 000 Jahre datiert. Untersuchungen zur Verbrennungstemperatur zeigten, dass die beste Abtrennung von solchem bereits gealtertem Material bei einer Temperatur nicht höher als 340 °C erfolgt. Eine erste Anwendung der Methode zur Datierung basaler Eisblöcke vom Titlisgletscher (Schweizer Alpen, 3020 m a.s.l.) ergab ein belastbares basales Alter von annähernd 5000 Jahren vor heute. In einer weiteren Anwendung wurden 16 Proben eines Eiskerns vom hochalpinen Gletschersattel Colle Gnifetti (Schweizer Alpen, 4500 m a.s.l.) mit der Mikro- $^{14}\text{C}$ -Methode datiert. Die Ergebnisse zeigten eine systematische Abweichung zu jüngeren Altern als die der durch Zählung von Jahresschichten bisher bestimmten Alter der Arbeitschronologie. Der Grund für diese Abweichung ist noch nicht abschließend geklärt.



# Contents

<b>1. Introduction</b>	<b>1</b>
<b>2. Theoretical background - Dating methods for Alpine glacier ice samples</b>	<b>5</b>
2.1. Dating of Alpine ice cores . . . . .	5
2.2. Radiocarbon dating . . . . .	8
2.3. <sup>14</sup> C measurement by Accelerator Mass Spectrometry (AMS) . . . . .	14
<b>3. Theoretical background - Particulate organic material in Alpine ice</b>	<b>19</b>
3.1. General sources of organic material in Alpine ice samples . . . . .	19
3.2. Possible sources of <sup>14</sup> C age biased organic material . . . . .	26
<b>4. State of the art and new insights into micro-radiocarbon dating of high Alpine ice samples</b>	<b>29</b>
4.1. The problem of in situ produced radiocarbon in the Dissolved Organic Carbon (DOC) . . . . .	29
4.2. Principle of the method and state of the art of POC dating . . . . .	37
<b>5. Methods - Implementation of the gas ion source at the MICADAS-AMS Mannheim</b>	<b>41</b>
5.1. Setup of the Gas Inlet System (GIS) . . . . .	41
5.2. Characterisation of the system performance . . . . .	42
<b>6. Methods - Optimisation of the POC extraction system</b>	<b>49</b>
6.1. General remarks on filtration media for POC separation . . . . .	49
6.2. Pre-existing offline filtration system at the IUP Heidelberg . . . . .	50
6.3. Process blank reduction . . . . .	51
6.4. Development and setup of the online cleaning - filtration - combustion unit REFILOX	54
6.5. Sample handling in the REFILOX system . . . . .	57
6.6. Characterisation of the two POC extraction systems (offline and REFILOX) . . . .	60
6.7. Calibration of REFILOX combustion temperatures . . . . .	71
<b>7. Results - Systematical investigation of <sup>14</sup>C age biasing effects in glacier ice</b>	<b>79</b>
7.1. Introductory remarks . . . . .	79
7.2. Site descriptions and presentation of radiocarbon results . . . . .	80
7.3. Discussion of radiocarbon results . . . . .	86
7.4. General implications for interpretation of POC derived radiocarbon ice ages . . . .	92
<b>8. Results - POC based <sup>14</sup>C dating of selected small Alpine glacier caps</b>	<b>95</b>
8.1. Cold Alpine ice patches . . . . .	95
8.2. Site descriptions . . . . .	95
8.3. Presentation of radiocarbon results . . . . .	97

<b>9. Results - POC based <sup>14</sup>C dating of a new ice core from the high Alpine firn saddle Colle Gnifetti (Swiss Alps)</b>	<b>101</b>
9.1. Glaciological site description, available ice cores and dating challenges . . . . .	101
9.2. Sample selection, presentation of radiocarbon results and blank correction . . . . .	105
9.3. Discussion of POC <sup>14</sup> C results . . . . .	109
9.4. Discussion of potential reasons for the age difference between POC <sup>14</sup> C dating and annual layer counting . . . . .	112
9.5. Comparison with previous Colle Gnifetti ice core dating studies . . . . .	119
 <b>10. Outlook</b>	 <b>125</b>
 <b>A. Appendix</b>	 <b>157</b>
A.1. Appendix to Chapter 4 . . . . .	157
A.2. Appendix to Chapter 6 . . . . .	159
A.3. Appendix to Chapter 7 . . . . .	166
A.4. Appendix to Chapter 8 . . . . .	168
A.5. Appendix to Chapter 9 . . . . .	168

# 1. Introduction

*This is radio carbon - measure and cry  
(freely adapted from Fury in The Slaughterhouse)*

Between September 2014 and October 2015, the air temperature over large parts of the Arctic exceeded the long-term average value to more than 3 °C and surface melting occurred on more than 50% of the Greenland ice sheet. This is the highest positive temperature deviation since the year 1900 (NOAA, 2015). Simultaneously, the new report AR5 of the Intergovernmental Panel on Climate Change (IPCC) states the human influence on climate as "clear" (IPCC, 2014). For the investigation of climate change in the past and the developments of future perspectives, analyses of proxy data retrieved from climate archives are indispensable (Masson-Delmotte et al., 2013). Within the large range of climate archives, tree rings, stalagmites, sea sediments and ice cores are the most prominent. For ice bodies, apart from the stratified archiving of past climate conditions, the basal age itself contains important climate information about the time of glacier formation onset.

Ice cores from polar regions allow reconstructions of climate parameters like for example dust concentrations and temperature (Johnsen et al., 2001) for up to 800 000 years back in time (see e.g. Lambert et al. (2008); Jouzel et al. (2007)). A new Antarctic drilling project aiming for the recovery of 1.5 million year old ice (Fischer et al., 2013) is aiming to extend these records even further. Mid-latitude glaciers in general (see e.g. Thompson et al. (2000); Fujita et al. (2004)), and Alpine glaciers especially, are not able to cover such large ranges and are restricted to centennial up to millennial time scales (Jenk et al., 2009; May, 2009; Wagenbach et al., 2012; Bohleber et al., 2013). Because of their close vicinity to human settlements, they are more important sources of information about the anthropogenic influences (e.g. short lived aerosol emissions) on climate change than the polar ice cores. The interpretation of any climate archive and the establishment of a reliable chronology is a crucial step. For glaciers also the constraint of a maximum age yields important information about the time of formation onset. Polar ice cores are mainly dated by the technique of annual layer counting based on the seasonal variations of different parameters (e.g.  $\delta^{18}\text{O}$ , major ions, see e.g. Svensson et al. (2008)) the identification of absolute time markers like volcanic eruptions (Zielinski et al., 1994; Narcisi et al., 2005; Sigl et al., 2015) and matching with other climate records. However, the dating of ice cores from Alpine glaciers is very challenging. Because of their typically small scale extensions, complex bedrock geometry and highly variable accumulation regimes, which lead to a very non-linear depth relationship, annual layer counting is restricted to the last few hundred years (Wagenbach and Geis, 1989; Bohleber, 2008; Wagenbach et al., 2012). The signal of volcanic eruptions is often masked by frequent inputs of sulphate-rich Saharan dust (Preunkert and Legrand, 2001). Additionally, the application of flow modelling (see e.g. Lüthi and Funk (2000)) is complicated by the complex and often unknown bedrock topography.

## 1. Introduction

---

For the older and deeper parts of such ice cores, or for ice bodies where no stratigraphic dating is possible at all, alternative dating methods must be applied, for the retrieval of an absolute age. This can be achieved by analyses of different radionuclide species contained in the ice matrix. These species are  $^{210}\text{Pb}$ , originating from soil and rocks, which can be used for datings up to 100 years before present (see e.g. Gägger et al. (1983)), and  $^{39}\text{Ar}$  from the atmosphere, which allows dating for the last 1000 years. For  $^{39}\text{Ar}$  however, the application is currently still very limited due to small concentrations resulting in high required ice masses of ca. 4 kg. It is thus unrealistic for an ice core application at present, nevertheless with a future perspective of required masses below 1 kg ice (Ritterbusch et al., 2014). Thus, for ice samples older than 1000 years, radiocarbon dating of organic material incorporated in the ice matrix is the only option for the determination of ages up to 20 000 years BP. The main challenge of this method lies in the generally very low organic carbon concentration in Alpine ice samples in the microgram range. Organic carbon in ice samples for  $^{14}\text{C}$  dating can be separated in Dissolved Organic Carbon (DOC) and Particulate Organic Carbon (POC). The DOC fraction is present in concentrations of ca. 50-100  $\frac{\mu\text{gC}}{\text{kg}}$  (May, 2009; Preunkert et al., 2011), which is a factor of two to ten more than the concentration of POC, which lies on average in the range of 10-50  $\frac{\mu\text{gC}}{\text{kg}}$  (Steier et al., 2006; Jenk et al., 2009). It was therefore initially attempted to use the DOC fraction for  $^{14}\text{C}$  dating, especially for ice core samples from the high Alpine firn saddle of Colle Gnifetti (Swiss Alps, 4500 m a.s.l.). The DOC at such an high altitude, low accumulation glacier was however found to be significantly biased by the incorporation of in situ produced  $^{14}\text{C}$  (see May (2009) and this work) and is therefore not usable for dating. The main focus of this work lies thus on  $^{14}\text{C}$  dating of the POC fraction, which has already been applied for a high Alpine ice core by Jenk et al. (2009).

The aim of this work is therefore to improve and apply the existing method of POC based micro radiocarbon dating of Alpine ice samples. Additionally to the aim of further minimisation of the required sample mass, for the first time special effort was put into analyses of the key question whether the incorporated organic matter does really represent the age of the surrounding ice. Especially for the POC fraction, this assumption is not a priori true, because it can be influenced by already aged organic material (e.g. from soils and glacial sediment). At the beginning of this work, the already existing system at the IUP Heidelberg had a very high and variable process blank of  $\approx 6 \mu\text{gC}$ , and was therefore not usable for the required POC concentrations. A main focus must be thus on the reduction of the contamination during sample preparation (process blank), ideally below an absolute mass of 1  $\mu\text{gC}$ , to make the method applicable for ice core studies with sample sizes below 1 kg for the average POC concentrations stated above. Also the  $^{14}\text{C}$  dating of samples in the microgram range is a large challenge. Conventional Accelerator Mass Spectrometry (AMS) commonly used for  $^{14}\text{C}$  dating requires carbon masses of 1 mg as graphite, which is a hundred times more than the typical POC sample sizes recovered from ice. Graphitisation of very small samples is possible (Liebl et al., 2010), but cumbersome, time consuming and susceptible to isotope fractionation and contamination. Therefore, within this work a so-called gas ion source at the MICADAS-AMS of the Klaus-Tschira-Laboratory in Mannheim was established, which enables  $^{14}\text{C}$  dating of  $\text{CO}_2$  samples down to 3  $\mu\text{gC}$ . Along with these technical method improvements, a systematic investigation of potentially age biasing effects in the POC fraction is carried out, by analyses of samples with either known age or material composition. This will support a more reliable interpretation of POC  $^{14}\text{C}$  ages in terms of ice ages. In a last step, the improved POC  $^{14}\text{C}$  dating method is applied to date ice samples from selected small Alpine glacier caps and a new ice core from the high Alpine firn saddle Colle Gnifetti (Switzerland).

---

The main steps to achieve the aims stated above can be summarised to:

1. The implementation and characterisation of a gas ion source for the MICADAS AMS system at the Klaus-Tschira-Lab in Mannheim to enable reliable radiocarbon measurements of sample sizes down to 3  $\mu\text{g}$  carbon as  $\text{CO}_2$ .
2. The development of a new sample preparation system to extract POC from ice samples with a minimal process blank ( $\approx 1 \mu\text{gC}$ ) and a high reliability.
3. Investigation of potentially age biasing effects by analysis of selected samples of known age and structure (ice and other material) and application of the method as a dating tool to high Alpine ice samples including a new ice core from Colle Gnifetti.



## 2. Theoretical background - Dating methods for Alpine glacier ice samples

### 2.1. Dating of Alpine ice cores

*The dating of ice cores from compared to polar ice sheets small scale summit ranges of Alpine glaciers is a big challenge and can only be successful by combination of a whole set of different methods, which will be presented shortly in the following.*

#### 2.1.1. Stratigraphic methods

##### Annual layer counting

Similar to dendrochronological methods, under certain premises it is possible to establish an ice core chronology by counting annual layers of snow accumulation over the entire core length. The main prerequisite is here, that the glacier body is cold, which means there is no substantial melting of ice throughout the year. The most common parameter to count such layers is the temperature driven variation in water isotope ratios  $\delta^{18}\text{O}$  and  $\delta\text{D}$  (Dansgaard, 1964). This method has been very successfully applied to ice cores from polar ice sheets (Johnsen et al., 2001; Rasmussen et al., 2013). In combination with other stratigraphical methods, for polar ice sheets chronologies for up to 800 000 yBP could be established (Petit et al., 1999; Parrenin et al., 2007). For high Alpine ice cores (above ca. 3000-4000 m a.s.l.) the water isotope method is complemented by other tracers that show seasonal signals. These seasonal trends are due to a shift of the planetary boundary layer with large mixing rates and material transport to high altitudes in summer, whereas in winter the summit regions above at least 4000 m a.s.l. are already in the free troposphere and shielded from the near ground mixing (Preunkert and Legrand, 2001). Compared to other ions, ammonium ( $\text{NH}_4$ ) shows an extraordinarily high summer to winter amplitude in concentration and is therefore the most commonly used tracer for annual layer counting. Emitted mainly from animal waste, biomass decomposition and, in modern times, fertilizers and ammonia production power plants (Buijsman et al., 1987), the emission peaks are in phase with the convection intensity. For example, in recent times summer to winter concentration ratios of a factor of 14 have been observed at the high Alpine glacier site of Col du Dome, 4250 m a.s.l. (Preunkert et al., 2000). Nevertheless, for ice cores from high Alpine sites with low net accumulation like Colle Gnifetti, which will be mainly discussed in this work, the application of these annual layer counting methods is very limited. A low net accumulation rate is however crucial for the conservation of long time scales. The most prominent problems for dating by annual layer counting of Colle Gnifetti are:

1. **Complex accumulation regime:** The net accumulation at Colle Gnifetti is mainly controlled by strong wind erosion, which leads to a systematical bias to the conservation of wet summer snow and even the possibility of losing the snow deposition of a complete year. Together with the small geometry, a resulting high spatial variation of accumulation and a complex glacier flow, this leads to a rapid layer thinning and a very non-linear age depth-

## 2. Theoretical background - Dating methods for Alpine glacier ice samples

---

relationship. Missing layers and the bias to summer snow conservation thus make the layer counting and interpretation of signals extremely difficult (Bohleber et al., 2013).

- 2. Technical limits of depth resolution:** The main technical limit to annual layer counting is the depth resolution of the retrieved impurity signal. For the routinely applied method of continuous flow analysis limited to a maximum depth resolution of ca. 0.5-1 cm (Kaufmann et al., 2008; Bigler et al., 2011). Because of the rapid layer thinning with depth at Colle Gnifetti this resolution limit is only applicable for the last 200-400 yBP (see e.g. Döscher et al. (1996); Bohleber et al. (2013)). Recently, the technique of laser ablation ICP-MS allowed a significant improvement in resolution up to several hundred micrometers (Sneed et al., 2015), but is so far restricted to layer counting in the calcium and sodium signal, where the seasonal amplitude of the signal is about 4-5 times lower than for the  $\text{NH}_4$  (Preunkert et al., 2000). Calcium and sodium also have the potential of additional noise in the seasonal signal caused by frequent Saharan dust inputs (Tomadin et al., 1996) which can be an additional source of counting uncertainty.

### Absolute time markers

A very important tool for dating of ice cores is the identification of absolute time markers within the ice. Such absolute markers are used to back up and constrain the relative dating methods of annual layer counting and age depth models. The most common markers are the traces of volcanic eruptions, which mainly show up as strong increases in the conductivity, acidity and sulfate signals (Legrand and Mayewski, 1997). In the more recent past some major eruptions have been historically documented (e.g. Tambora 1815 or Krakatau 1883 A. D.) and thus can be linked to ice core records. However, volcanic reconstructions from polar ice core records reach further back in time, up to 9000 yBP (Zielinski et al., 1994; Sigl et al., 2015), where historical records are sparse or non-existent. Still it is a challenge to link different records on base of such eruptions, because a clear identification and assignment to a certain eruption can be difficult. The most powerful tool to identify a single eruption is the evidence of volcanic ash (tephra), which carries a characteristic structure and chemical composition for each eruption (Narcisi et al., 2005; Dunbar and Kurbatov, 2011). Nevertheless, for high Alpine ice cores, the identification of certain volcanic eruptions is not evident. This is due to the regular occurrence of desert dust inputs by long range transport from low latitude arid regions, mainly the Sahara (Wagenbach and Geis, 1989; Maupetit and Delmas, 1994; Thevenon et al., 2012), which also contain high amounts of sulphate, masking or imitating volcanic signals (see e.g. Schwikowski et al. (1999)).

Big saharan dust events themselves can function as a valuable absolute time marker. Some of them can even be identified by eye by their characteristic yellow / red colour. Important events are for example recorded for the years 1977 and 1901 A.D. (Haeberli et al., 1983). In very recent times (the past 50 years) an important absolute time marker is the so called "bomb peak" in 1963, an enrichment of nuclear reaction products in the atmosphere caused by extensive above-ground tests of nuclear weapons. This very distinct peak is usually identified by enhanced tritium contents (Schotterer et al., 1998). However, at Colle Gnifetti absolute time markers based on the assignment of volcanic eruptions and Saharan dust horizons to documented events in the past is only possible for the last 200-400 years, which equals about half of the glacier thickness. For older events, an unambiguous assignment is extremely difficult, if not even impossible, because of the fast increasing dating uncertainty due to rapid layer thinning and non-linearity of the time scale.

### 2.1.2. Modelling of ice dynamics

Mathematical flow models offer an additional possibility to determine an age depth relationship. The simplest 2D-flow model for a glacier was developed by Nye (see e.g. Cuffey and Paterson (2010)). It assumes an infinite horizontal ice extension and constant thickness, which is reasonable only near ice divides of the large ice sheets. A 2D-model for mountain glaciers, recently applied at the Institute for Environmental Physics Heidelberg, is the ice slap model developed by Bohleber (2008), which is a progression of the Nye model to a tilted plane. In recent times, 3D-modelling of cold mountain glaciers becomes more important (Lüthi, 2000; Gagliardini et al., 2013; Gilbert et al., 2014) and is currently also being applied to the high Alpine firn saddle of Colle Gnifetti (pers. comm. Carlo Licciulli). All these models have an increasing uncertainty with depth, which is mainly due to insufficiently known or represented boundary conditions at bedrock. It is therefore crucial to supply models with absolute dates in larger depths.

### 2.1.3. Radiometric methods

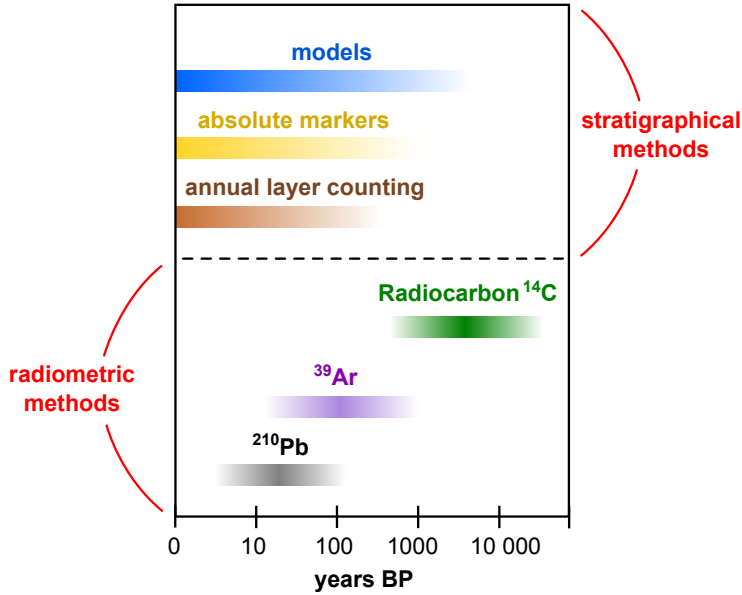
Apart from the absolute time markers discussed above, it is possible to measure the activity of several radionuclides contained in the ice matrix and to calculate the time of incorporation into the ice. The most important radionuclides for this dating method are:

- **$^{210}\text{Pb}$ :** The isotope  $^{210}\text{Pb}$  has a half life of  $T_{1/2}=22.3$  a and is part of the  $^{238}\text{U}$  decay chain. It is terrigenously formed by decay of  $^{222}\text{Rn}$ , which degasses rather constantly from soil and rocks. By adsorption to aerosol, the  $^{210}\text{Pb}$  is deposited onto the glacier.  $^{210}\text{Pb}$ -dating has been applied to Alpine glaciers in the past (Gäggeler et al., 1983; Picciotto et al., 1967) but has the disadvantages of large required ice volumes because of very low concentrations and a limited applicability to the last ca. 200 years because of the short half life.
- **$^{39}\text{Ar}$ :** Cosmogenic  $^{39}\text{Ar}$  has a half life of  $T_{1/2}=269$  a and is present in the atmosphere and thus also in air bubbles of glacier ice in very constant concentrations. The principle of dating by use of  $^{39}\text{Ar}$  has been known for a long time (Loosli, 1983), but because of the very low concentrations, only the development of Atom Trap Trace Analysis (ATTA) (Chen et al., 1999; Welte et al., 2010) made the method lately applicable for groundwater (Ritterbusch et al., 2014) and larger ice samples in the order of ca. 4 kg. By half life, this method is limited to ca. 1000 years before present.
- **$^{14}\text{C}$ :** Cosmogenic  $^{14}\text{C}$  has a half life of  $T_{1/2}=5700$  a and is therefore the best option for dating of the basal parts of Alpine ice cores with expected ages up to 10 000 yBP (Jenk et al., 2009). By incorporation into  $\text{CO}_2$   $^{14}\text{C}$  takes part in the global carbon cycle and is deposited onto the glacier as part of the organic aerosol. This dating technique was up to now also complicated by rather large required ice masses of ca. 1 kg.

## 2. Theoretical background - Dating methods for Alpine glacier ice samples

### 2.1.4. Summary of the dating methods

The various dating methods available for Alpine ice cores and their applicable time scales are schematically summarised in Fig. 2.1.



Most of the described methods are limited to an age range of up to 1000 years before present. By combination of several methods, this time range is relatively reliable. Up to now, for the deeper parts of Alpine ice cores, only modelled chronologies have been available, where accuracy is largely decreasing with depth. For the basal parts of ice cores,  $^{14}\text{C}$  offers in principle the unique possibility to get an absolute date, which on one hand could give a direct age estimation of the ice and could also help the models to constrain the not well determined ice flow parameters.

**Fig. 2.1.:** Overview of different dating techniques for Alpine ice cores and their applicable time ranges

## 2.2. Radiocarbon dating

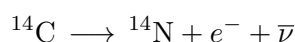
### 2.2.1. Environmental $^{14}\text{C}$ as a dating tool

Radiocarbon is naturally present in two stable isotopes:  $^{12}\text{C}$  with an abundance of 98.9% and  $^{13}\text{C}$  with an abundance of 1.1% (Mook, 2000). The third, radioactive isotope is  $^{14}\text{C}$ , which is the base for the equally named dating method. In equilibrium, when  $^{14}\text{C}$  production, biosphere uptake and decay are balanced, the ratio between  $^{14}\text{C}$  and  $^{12}\text{C}$  is nowadays approximately  $< 10^{-12}$  (Mook, 2000).

$^{14}\text{C}$  is constantly produced in the upper atmosphere, predominantly in the lower stratosphere, by reactions of nitrogen with thermal neutrons, which themselves are products from reactions of high energetic cosmic irradiation (described first by Libby (1946)):



The so created radiocarbon is oxidised almost immediately to CO and  $\text{CO}_2$  and mixed homogeneously within the troposphere (Nydal, 1968). Finally, the  $^{14}\text{CO}_2$  is fixed within the living biosphere by photosynthesis and thus takes part in the global carbon cycle (schematically shown in Fig. 2.2).  $^{14}\text{C}$  has a half life of  $(5700 \pm 30)$  years (Roberts and Southon, 2007) and decays via  $\beta^-$  decay back to  $^{14}\text{N}$



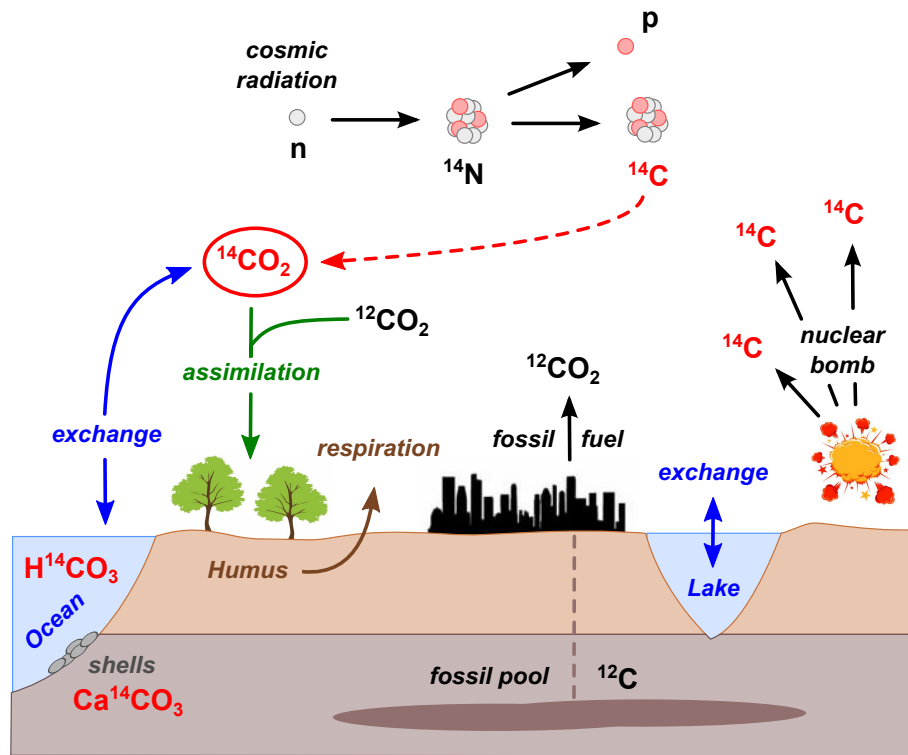


**Fig. 2.2.:** Schematic view of the pathways for  $^{14}\text{C}$  in the carbon cycle. Adapted from (Mook, 2000)

with a maximum electron energy of 156 keV. While the residence time of  $^{14}\text{C}$  within the atmosphere (in the order below ten years) is very low compared to its half life (Craig, 1957), the residence time in other reservoirs of the cycle like the ocean or groundwater can be substantial and is not directly comparable to the atmospheric values. This needs to be regarded at  $^{14}\text{C}$  age interpretation.

### 2.2.2. Isotope fractionation and normalisation

Isotope fractionation means the partial separation of different isotopes during phase changes (like evaporation and condensation) or chemical reactions, which results in an enrichment of one isotope relative to another. During sample preparation in the lab, this can happen for example in incomplete combustion processes or incomplete cryogenic transfer of a  $\text{CO}_2$  sample. For the radiocarbon dating method, the most important fractionation process happens during fixation of  $^{14}\text{CO}_2$  via photosynthesis. Plants in general prefer the uptake of  $^{12}\text{C}$  over  $^{13}\text{C}$  over  $^{14}\text{C}$  (Baertschi, 1953). Thus, the plant material is depleted in the rare carbon isotopes compared to the surrounding atmosphere. The isotopic signature of a sample is usually expressed as the  $^{13}\text{C}/^{12}\text{C}$  ratio of the sample compared to the  $^{13}\text{C}/^{12}\text{C}$  ratio of a standard material, the Vienna Pee Dee Belemnite (VPDB), a fossil carbonate sample, and noted as:

$$\delta^{13}\text{C} = \left( \frac{\left( \frac{^{13}\text{C}}{^{12}\text{C}} \right)_{\text{sample}} - \left( \frac{^{13}\text{C}}{^{12}\text{C}} \right)_{\text{VPDB}}}{\left( \frac{^{13}\text{C}}{^{12}\text{C}} \right)_{\text{VPDB}}} \right) \cdot 1000 \text{‰} \quad (2.1)$$

## 2. Theoretical background - Dating methods for Alpine glacier ice samples

---

Table 2.1 gives an overview of typical  $^{13}\text{C}$  contents of different materials (adapted from Stuiver and Polach (1977)) Since  $^{14}\text{C}$  is also effected by fractionation, samples of different material must be normalised to a common standard material, which then makes the radiocarbon ages comparable. This standard value is the postulated mean of wood and set to  $\delta^{13}\text{C} = -25 \text{‰}$ . In other words, the  $^{14}\text{C}$  activity of the sample is translated to the activity it would have, if it were made of wood.

**Tab. 2.1.:** Typical  $\delta^{13}\text{C}$  values of some natural materials

Material	$\delta^{13}\text{C}$ [‰]
C4-plants (maize, millet)	-13 to -7
C3-plants (wheat, oats, rice)	-27 to -19
Tree leaves, straw	-32 to -22
Bone collagen, cellulose	-24 to -18

The normalisation factor  $\text{norm}_{13/12}$  can then be expressed by the  $^{13}\text{C}/^{12}\text{C}$  ratios (Stenström et al., 2011):

$$\text{norm}_{13/12} = \frac{\left(\frac{^{13}\text{C}}{^{12}\text{C}}\right)_{\text{wood}}}{\left(\frac{^{13}\text{C}}{^{12}\text{C}}\right)_{\text{sample}}} \quad (2.2)$$

From there, the  $^{14}\text{C}$ -normalisation  $\alpha_{14/12}$  can be calculated, because it is approximately given by the square of the  $^{13}\text{C}$ -normalisation factor (Stuiver and Robinson, 1974):

$$\text{norm}_{14/12} = \text{norm}_{13/12} \cdot \text{norm}_{14/13} \approx (\text{norm}_{13/12})^2 \quad (2.3)$$

Insertion of Eq. 2.2 and Eq. 2.1 into Eq. 2.3 then yields:

$$\text{norm}_{14/12} = \left(\frac{1 - \frac{25}{1000}}{1 + \frac{\delta^{13}\text{C}}{1000}}\right)^2 = \left(\frac{0.975}{1 + \frac{\delta^{13}\text{C}}{1000}}\right)^2 \quad (2.4)$$

Which can be Taylor approximated to:

$$\text{norm}_{14/12} \approx \left(1 - \frac{2(25 + \delta^{13}\text{C})}{1000}\right) \quad (2.5)$$

The relation 2.5 is then used to normalise all measured  $^{14}\text{C}$  activities of samples.

### 2.2.3. Reporting of $^{14}\text{C}$ -results

#### Basic principle of radiocarbon dating

Because of the compared to half life very fast transfer of  $^{14}\text{C}$  into the biosphere, the  $\frac{^{14}\text{C}}{^{12}\text{C}}$  of the living biomass should always be in equilibrium with the atmospheric  $\frac{^{14}\text{C}}{^{12}\text{C}}$  ratio. When the living organism dies, it is disconnected from the source and the radiometric clock is set.

If at a later point in time the activity of the sample  $A_S$  is measured and the starting activity  $A_0$  is known, the time  $t$  since the death of the organism can be calculated:

$$A_S = A_0 \cdot e^{-\lambda t} \quad \Leftrightarrow \quad t = -\frac{1}{\lambda} \cdot \ln \left( \frac{A_S}{A_0} \right) \quad (2.6)$$

with  $\lambda = \frac{\ln 2}{T_{1/2}}$  as the decay constant of  $^{14}\text{C}$ . The determination of a radiocarbon age  $t$  of a sample thus involves two steps:

1. Measurement of the present activity  $A_S$  of the sample
2. Knowledge of the starting activity  $A_0$  at time of death

The first point comprises the technical measurement, which will be discussed in section 2.3, the second includes the age calibration and be addressed in section 2.2.4.

### Formal notation

In the past, several ways to report radiocarbon values have been established and documented well (Stuiver and Polach, 1977) (Donahue et al., 1990), so here only a short overview of the most common notations will be given. First, all measured sample activities have to be normalised, to account for the fractionation according to equation 2.5, which gives the *normalised standard activity*  $A_{SN}$  of a sample:

$$A_{SN} = A_S \cdot \text{norm}_{14/12} = \left( \frac{0.975}{1 + \frac{\delta^{13}\text{C}}{1000}} \right)^2 \approx A_S \cdot \left( 1 - \frac{2(25 + \delta^{13}\text{C})}{1000} \right) \quad (2.7)$$

To make  $^{14}\text{C}$  values comparable, all results are reported relative to the  $^{14}\text{C}$  activity  $A_{OxI}$  of a universal standard material, which is oxalic acid (NIST: SRM 4990 B (OxI)) from a crop of 1955 sugar beet. This oxalic acid has a  $\delta^{13}\text{C}$  value of close to -19 ‰ and is normalised to that value. Since the OxI standard material is already influenced by anthropogenic effects, bomb test  $^{14}\text{C}$  and fossil fuel combustion, the activity of the OxI standard is defined relative to a pre-industrial *absolute radiocarbon standard*, which is wood grown in the year 1890 (decay corrected to the year 1950) and has 95% of the oxalic acid activity. Therefore, the *normalised standard activity* of that standard material is:

$$A_{ON}(\text{OxI}) = 0.95 A_{OxI} \cdot \left( 1 - \frac{2(19 + \delta^{13}\text{C})}{1000} \right)$$

The OxI standard is no longer available, nowadays the new oxalic acid standard OxII (SRM 4990 C) is used (Stuiver, 1983), which has a  $^{13}\text{C}$  ratio of -17.8 ‰, is also referred to the 1890 wood as:

$$A_{ON}(\text{OxII}) = 0.7459 A_{OxII} \cdot \left( 1 - \frac{2(25 + \delta^{13}\text{C})}{1000} \right) \quad (2.8)$$

Apart from these normalisations, it was agreed to reference all radiocarbon measurements to the year 1950,  $A_{abs}$  then gives the *absolute international standard activity*, which can be expressed by  $A_{ON}$  in the year of measurement  $y$ :

$$A_{abs} = A_{ON} \cdot e^{\lambda(y-1950)} \quad (2.9)$$

## 2. Theoretical background - Dating methods for Alpine glacier ice samples

---

All normalised  $^{14}\text{C}$  measurements should be reported relative to this standard value. To directly report relative deviations of measured activities from this standard, the most commonly used notation is the  $\Delta$ -notation:

$$\Delta^{14}\text{C} = \left( \frac{A_{\text{SN}}}{A_{\text{abs}}} - 1 \right) \cdot 1000 \text{‰} \quad (2.10)$$

This notation includes no decay correction of the sample and is therefore not constant over time. Also, the sample activity can directly be referred to the reference year 1950 (modern) and is then reported as *percent modern carbon pmC*:

$$\text{pmC} = \frac{A_{\text{SN}}}{A_{\text{abs}}} \cdot 100 \text{‰} = \frac{A_{\text{SN}}}{A_{\text{ON}}} \cdot e^{-\lambda(y-1950)} \cdot 100 \text{‰} \quad (2.11)$$

Again this notation includes no decay correction of the sample and changes over time. For example, the result will be different if the sample is measured today and ten years from now, because the relation does not take into account the decay of the sample in the meantime. In this work,  $^{14}\text{C}$ -ratios will therefore be dimensionless reported as *Fraction modern carbon*  $F^{14}\text{C}$ , which includes decay corrections for both, sample and standard:

$$F^{14}\text{C} = \frac{A_{\text{SN}} \cdot e^{\lambda(y-1950)}}{A_{\text{abs}}} = \frac{A_{\text{SN}}}{A_{\text{ON}}(\text{OxII})} \quad (2.12)$$

This connected to the  $\Delta^{14}\text{C}$  notation via:

$$F^{14}\text{C} = \left( \frac{\Delta^{14}\text{C}}{1000} \right) \cdot e^{-\lambda(y-1950)}$$

### 2.2.4. Calibration of radiocarbon ages

#### Conventional $^{14}\text{C}$ -ages and the calibration curve

The primary result of any radiocarbon measurement is the so-called *conventional radiocarbon age*  $t$  calculated from Eq. 2.6 using the normalised sample and standard activities according to:

$$t = -\frac{1}{\lambda_L} \ln \left( \frac{A_{\text{SN}}}{A_{\text{ON}}} \right) = -8003 \ln \left( \frac{A_{\text{SN}}}{A_{\text{ON}}} \right) = -8003 \ln \left( \frac{A_{\text{SN}} \cdot e^{\lambda(y-1950)}}{A_{\text{abs}}} \right) \quad (2.13)$$

with  $\lambda_L$  as the decay constant based on the Libby half life of  $^{14}\text{C}$ , 5568 years (Stuiver, 1983). This calculation assumes, that the atmospheric content of  $^{14}\text{C}$  was constant over time. This assumption is however insufficient. The production rate of  $^{14}\text{C}$  is dependent on the strength of cosmic radiation, which itself among other things is modulated by the changing activity of the sun and the earth magnetic field (Hughen et al., 2004). Because of these atmospheric  $^{14}\text{C}$  variations, the conventional age of a sample will not represent the real age of the sample. To determine this real or calibrated age of the sample, the atmospheric  $^{14}\text{C}$  content of the past must be known as precisely as possible, which led to the assembly of an independent calibration curve, which compares the measured  $^{14}\text{C}$ -content of a sample (the conventional age) with the  $^{14}\text{C}$  content of an independently dated sample.

The independently dated samples that make up the calibration curve are mostly tree rings, dated by dendrochronology, for the last ca. 20 000 years BP (see e.g. Becker (1993)) and corals,

speleothems and varved sediments for the time range up to 50 000 years BP (see e.g. Hughen et al. (2006)).

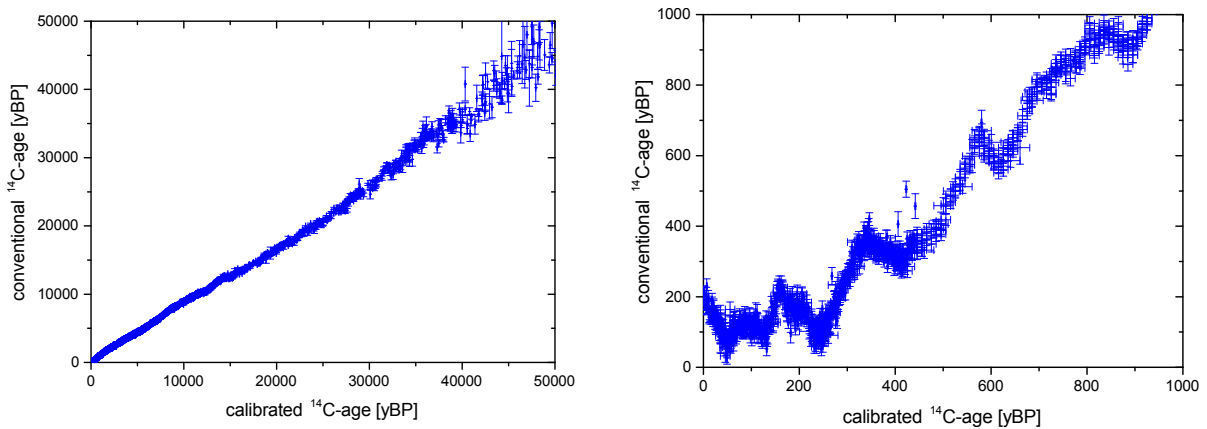


**Fig. 2.3.:** The radiocarbon calibration curve IntCal13 (Reimer et al., 2013). The left panel shows the complete record up to 50 000 yBP with increasing uncertainties to the very old ages, on the right is a zoom to the last 1000 yBP.

All these separately dated records together make up the calibration curve, which is constantly updated and in some parts still under discussion (Muscheler et al., 2008). The latest version for atmospheric  $^{14}\text{C}$ -contents is the IntCal13 curve, published by Reimer et al. (2013).

### Age calibration and difficulties

For practical applications of this calibration procedure, several computing programs are available, of which the most prominent is probably OxCal (Bronk Ramsey, 1995).

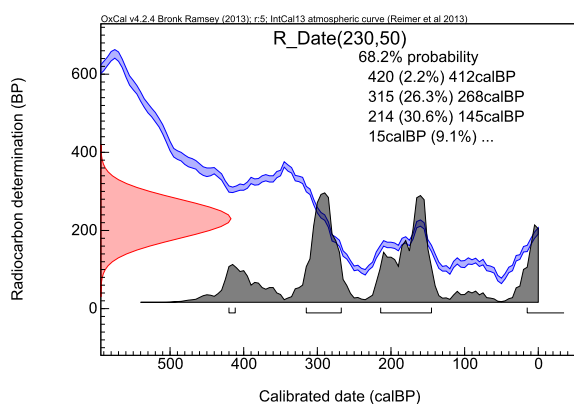


**Fig. 2.4.:** Large variations in the calibration curve makes  $^{14}\text{C}$  dating of samples younger than 400 years extremely difficult.

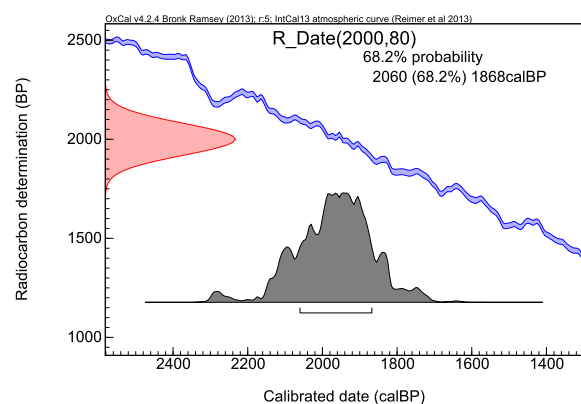


**Fig. 2.5.:** Example of an uncritical age calibration. No multiple age assignments are possible. The  $1\sigma$  probability of the calibrated age is given.

## 2. Theoretical background - Dating methods for Alpine glacier ice samples

Simplified, the program searches the calibration curve via Monte Carlo simulations for intersections with the measured age and gives a probability for every matching section (see Fig. 2.5). The red age span on the y-axis is the measured  $^{14}\text{C}$  age as input for the program. The grey age spans on the x-axis mark the most probable calibrated  $^{14}\text{C}$  ages derived from agreements of the measured age with the calibration curve (blue). The precision of the calibrated age is therefore not only dependent on the measurement error but also on the course of the calibration curve.

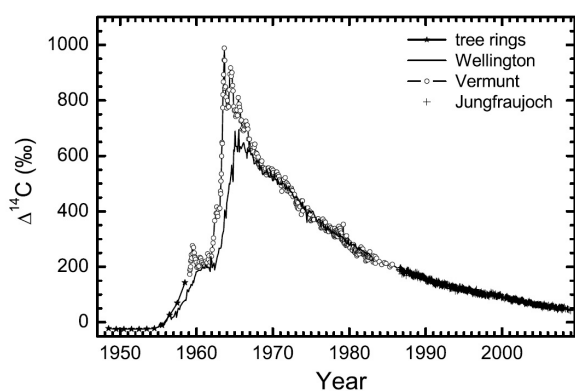


**Fig. 2.6.:** Atmospheric enrichment of  $\Delta^{14}\text{C}$  during the bomb peak period. Figure taken from Levin et al. (2010).

Large plateaus lead to large possible age ranges, whereas steep parts allow a more precise age determination. If the variation become too large (see Fig. 2.4), a distinct age assignment can become impossible because of different age options for one measured  $^{14}\text{C}$ -content. This is especially the case in the 20th century during the period of the so-called bomb peak. Between 1950 and 1963 excessive aboveground nuclear bomb tests have been carried out, which led to a strong atmospheric  $^{14}\text{C}$  enrichment (see Fig. 2.6). The strong decline after the test ban in 1963 is due to  $\text{CO}_2$  uptake of the ocean and biosphere as well as ongoing Suess effect, which means atmospheric  $^{14}\text{C}$  depletion due to enhanced fossil fuel combustion.

The overall precision of the radiocarbon dating method is thus depending on three factors:

1. Statistical measurement error combined with uncertainties introduced within sample preparation
2. Error (width) of the calibration curve
3. Shape and course of the calibration curve

### 2.3. $^{14}\text{C}$ measurement by Accelerator Mass Spectrometry (AMS)

In the early years of radiocarbon analyses, the  $^{14}\text{C}$  ratio of a sample was determined by counting the decay of  $^{14}\text{C}$ . Because the  $\frac{^{14}\text{C}}{^{12}\text{C}}$  ratio even in modern samples is as low as  $10^{-12}$ , this type of measurement needs comparably large amounts of sample material in the range of grams (Arnold and Libby, 1949) and the measurement takes a long time to provide a good counting statistics. The development of Accelerator Mass Spectrometry (AMS) brought massive improvements by measuring the  $\frac{^{14}\text{C}}{^{12}\text{C}}$  directly instead of the decay rate. For conventional AMS  $^{14}\text{C}$  analyses therefore only ca. 0.5-1 mg of carbon in form of graphite is needed.

#### 2.3.1. The MICADAS $^{14}\text{C}$ -AMS system

The basic steps of mass selecting processes in every AMS facility are (detailed explanation below):

1. Selective ionisation of distinct species by negative ionisation in a sputter ion source (suppression of nitrogen for  $^{14}\text{C}$  analyses)

## 2.3 $^{14}\text{C}$ measurement by Accelerator Mass Spectrometry (AMS)

2. Pulsed injection (fast beam switching) of ions into the accelerator using an electric field in the low energy (LE) magnet
3. Acceleration of ions in a tandem accelerator to energies between several hundred kilovolts up to ca. 10 megavolts
4. Switch to positive ion charge by stripping of electrons and destruction of molecules
5. Energy filtering and second mass selection in a magnetic sector field (high energy (HE) side)
6. Detection of selected ions as currents in Faraday cups or detectors for counting of single ions

Many AMS systems have been developed throughout the years for many different applications. During this work, only a very special and recently developed system for  $^{14}\text{C}$  measurements was used and will be briefly described here.

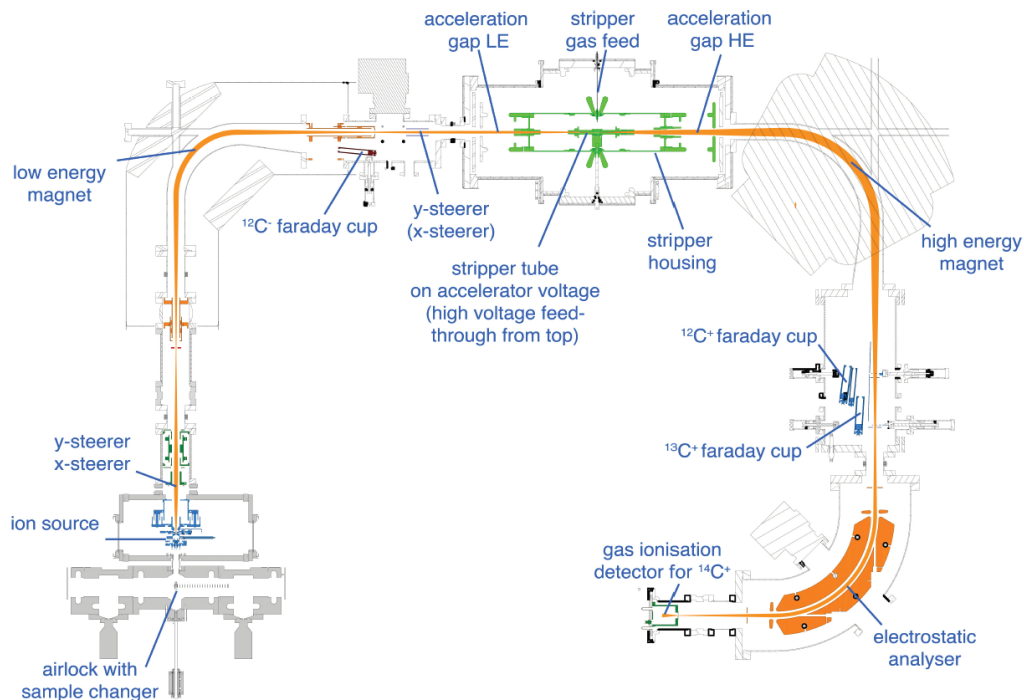


**Fig. 2.7.:** Schematic view of the MICADAS main components and the proposed ion pathway (red) (picture by Ionplus AG).

The so-called MICADAS (Mini CARbon DAting System) has been developed and set up by the ETH Zürich (Synal et al., 2004, 2007). The MICADAS system used for all  $^{14}\text{C}$  analyses in this work is hosted at the Klaus-Tschira-Center for Archaeometry in Mannheim (Kromer et al., 2013). A schematic view of the AMS system and its main components is shown in Fig. 2.7.

## 2. Theoretical background - Dating methods for Alpine glacier ice samples

---

### Ion source

The MICADAS hybrid ion source uses Cs<sup>+</sup> ions for sputtering of graphite targets. These ions are produced by evaporation of caesium from a reservoir and ionisation at a spherical ioniser. They are accelerated onto the graphite target with energies between 5 and 12 keV. The so created negative sample ions are extracted from the source with energies of up to 40 keV. For graphite samples, in normal measurement mode ion currents of 30-50 μA are reached at the low energy side, but largely dependent on Cs flow. The ion source is also capable of sputtering CO<sub>2</sub> samples directly, this will be discussed in section 2.3.2.

### Low energy mass separation

After extraction from the ion source, the LE mass separation is done by a dipole magnet, in whose focal plane a Faraday cup is mounted to monitor the ion currents extracted from the source. This allows a calculation of transmission through the accelerator unit. The low energy spectrometer is equipped with a fast beam pulsing system, that allows injections of beams into the accelerator in very short pulses (Suter et al., 1984). It is operated with injection times and sequences of <sup>12</sup>C (50 μs), <sup>14</sup>C (40 ms), <sup>13</sup>C (500 μs), <sup>14</sup>C (40 ms). This beam pulsation enables effectively simultaneous measurements of adjacent masses on the high energy side. In the focal plain of the HE magnet, a Faraday cup for <sup>13</sup>C is located close to the beamline of <sup>14</sup>C. Thus, if <sup>14</sup>C is injected to the accelerator, the <sup>13</sup>C beam is directed to the cup, and for the injection of <sup>13</sup>C, <sup>12</sup>C can be measured simultaneously. A third cup located between the <sup>13</sup>C and <sup>12</sup>C measures the <sup>13</sup>C breakup fragments of <sup>13</sup>CH<sup>-</sup> molecules destroyed in the stripper, which is a good parameter for background correction.

### Acceleration unit

The accelerator is a compact high voltage platform set to a terminal voltage of 200 kV inside a vacuum chamber. The stripper gas for ion charge switching and molecule destruction (N<sub>2</sub>) is inserted into the acceleration unit via a capillary and pumped continuously.

### High energy mass separation

At the high energy side of the accelerator, another magnet for impulse selection is located, in whose focal plane all HE faraday cups are located. Subsequently, the ion beam passes a spherical electrostatic analyser for energy selection. With this setup, under normal conditions a beam transmission through the accelerator of ca. 40% is achieved.

### <sup>14</sup>C detection

A gas ionisation chamber is used to detect the incoming <sup>14</sup>C ions. The detector window is made of a Si<sub>3</sub>N<sub>3</sub> foil (50 nm) and the detection gas is isobutane at a pressure of 20hPa (Synal et al., 2007). Data analysis, blank and standard corrections are done by a programme directly designed for the MICADAS system at ETH Zürich (Wacker et al., 2010). The machine background is in the order of  $\frac{^{14}\text{C}}{^{12}\text{C}}=10^{-15}$  and therefore dating of samples up to 50 000 years BP should be possible. The MICADAS system in Mannheim is able to measure modern graphite samples with a precision of ca. 2 ‰ and a high stability over time (Kromer et al., 2013).

2.3.2.  $^{14}\text{C}$  measurements via a Gas Ion Source

For conventional AMS  $^{14}\text{C}$  measurements, a mass of usually ca. 1 mg carbon is required as graphite. This is still too much for the application in  $^{14}\text{C}$  ice core dating, because typical sample sizes are in the order of micrograms of carbon and 1mg carbon would require about 20-40 kg ice for high Alpine POC concentration, which is not a realistic and manageable sample size. To deal with this issue, a micro-graphitisation system has been developed at the Vienna Environmental Research Accelerator (VERA), which allows sample preparation down to 5  $\mu\text{gC}$  (Liebl et al., 2010). Still, this system includes the process of graphitisation, which means the reduction of  $\text{CO}_2$ , which is produced by combustion of organic material during sample preparation, to graphite. This process is cumbersome, includes many steps and holds the risks of sample loss, isotope fractionation and possible contamination.

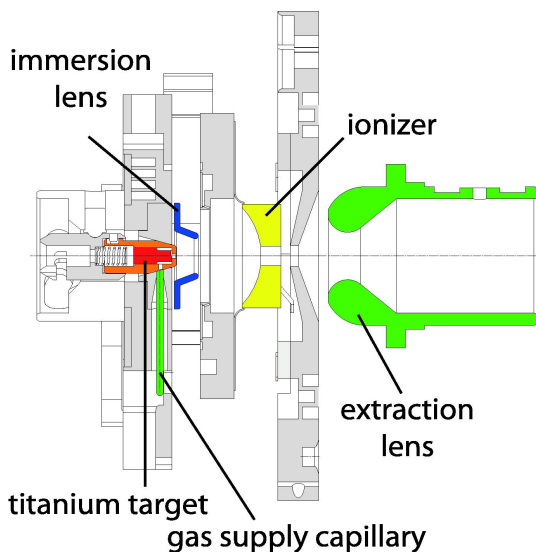


**Fig. 2.8.:** Schematic view of the MICADAS ion source with a gas target inserted. The  $\text{CO}_2$  is supplied by a capillary (60  $\mu\text{m}$  diameter), which feeds the target through a hole in the holder (Fahrni et al., 2013).

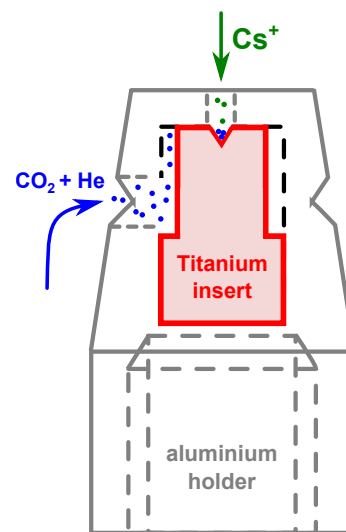


**Fig. 2.9.:** Cross section of a target for gas measurements. The  $\text{CO}_2$ -He-mixture is directed via a small slit to the front of the titan insert, where it is sputtered (modified from Ruff et al. (2007)).

To avoid this step, so called gas ion sources have been developed. This means, a  $\text{CO}_2$  sample does not have to be graphitised, but the  $\text{CO}_2$  gas can directly be inserted into the ion source. This has the advantage, that even very small samples down to a few  $\mu\text{gC}$  can be measured for  $^{14}\text{C}$ . The large disadvantage is, however, a much smaller dating precision of only a few percent relative error. Gas ion sources have for example been established at the AMS facilities in Oxford (Bronk Ramsey et al., 2004) and Erlangen (Uhl et al., 2007), but this work will focus on the setup designed at the ETH Zürich for the MICADAS AMS system, which was used during this work (Ruff et al., 2007), (Fahrni et al., 2013). The MICADAS has a built-in hybrid ion source, which can handle graphite and gas samples only by use of a different target type and no structural changes. At the position

## 2. Theoretical background - Dating methods for Alpine glacier ice samples

---

where otherwise the graphite is located, a titanium insert is placed inside the aluminium holder. This insert has a small slit (0.3 mm) on top. The CO<sub>2</sub> is transported to the target via a capillary (60 μm diameter) on a stream of helium as a carrier gas (see Fig. 2.8). It enters the target via a small hole in the aluminium holder and is guided via the slit to the front of the target (see fig. 2.9), where the sputtering process takes place. The CO<sub>2</sub> molecules are not directly sputtered by the caesium, but are bound at first to the surface of the Ti-insert, probably by forming titanium carbide (Fahrni et al., 2013). The sputter efficiency is much smaller than for graphite and ranges between 6 and 10 %, but still, LE ion currents of up to 20 μA can be achieved, which is almost half of the currents achieved with graphite samples. The characteristics of the particular gas ion source at the MICADAS in Mannheim, which was taken into operation within this work, will be discussed in chapter 5.

## 3. Theoretical background - Particulate organic material in Alpine ice

*Radiocarbon analyses of ice samples require the availability of a certain amount of organic material within the ice matrix. The possible sources and deposition processes for this organic matter will be discussed in the following chapter.*

### 3.1. General sources of organic material in Alpine ice samples

#### 3.1.1. Airborne material - aerosol

For high Alpine glaciers, the most prominent source of organic carbon is the deposition of carbonaceous aerosol. Aerosol is defined as a stable suspension of solid and liquid particles in a gas (e.g. Junge (1963)) and usually distinguished by size into different particle fractions (Colbeck and Lazaridis, 2014):

- **Ultrafine particles (< 100 nm)**  
Nucleation mode: Particles with diameter < 0.1  $\mu\text{m}$ , which are formed by nucleation processes  
Aitken mode: Particles with diameter 0.01  $\mu\text{m}$  - 0.1  $\mu\text{m}$  from vapour nucleation or particle growth by condensation
- **Fine particles: (< 2  $\mu\text{m}$ )**  
Accumulation mode: Particles with diameter 0.1  $\mu\text{m}$  - 3  $\mu\text{m}$ , formed by coagulation of smaller particles or by condensation. Removal of this size fraction from the atmosphere by wet and dry deposition is very slow
- **Coarse fraction > 2 $\mu\text{m}$**

Another classification criteria is the formation process of the aerosol particles, which divides them into (Poeschl, 2005):

- **Primary Aerosol:** Directly emitted in the condensed phase (solid or liquid) or as semi volatile vapours, which are condensable under atmospheric conditions. Typical sources are for example biomass burning, incomplete combustion of fossil fuels, volcanic eruptions, wind-driven suspension of soil and mineral dust, sea salt and biological materials (plant fragments, micro organisms etc.). These particles mainly make up the coarse fraction
- **Secondary aerosol:** Formed by chemical reactions, coagulation of gaseous precursors and condensation of volatile compounds. They involve a large variety of chemical species and are part of the fine and ultrafine particle fraction.

An overview of the different particle size classifications and formation processes is given in Fig. 3.1

### 3. Theoretical background - Particulate organic material in Alpine ice

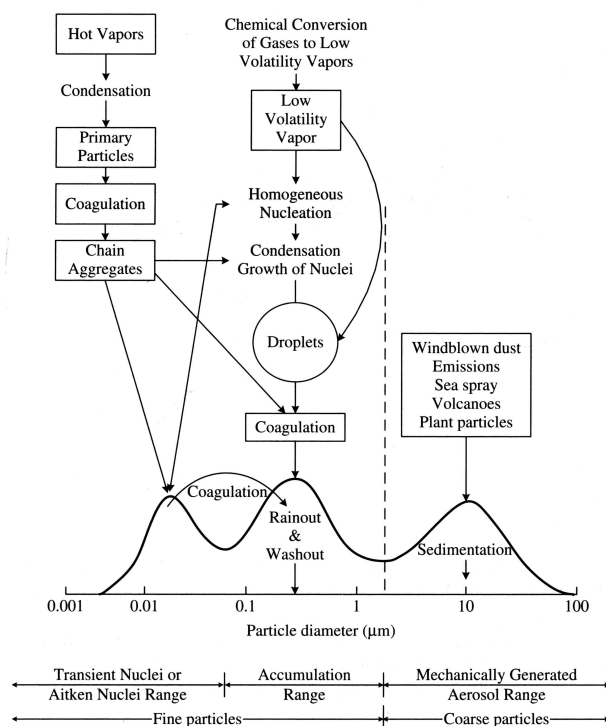


**Fig. 3.1.:** Schematic overview of the different aerosol particle sizes and formation pathways. Figure taken from Colbeck and Lazaridis (2014).

Atmospheric lifetimes of aerosol particles strongly depend on particle sizes. Very small particles coagulate very fast to larger particles and thus are removed from the system. The largest particles are removed by sedimentation (dry deposition) due to their high mass. These particle fractions therefore appear mostly in the vicinity of the source. The particle fraction with the longest atmospheric lifetime is the fine particle fraction with sizes up to a few micrometers. For those, wet deposition by rain and washout is the dominant deposition factor (Colbeck and Lazaridis, 2014). Because of their long lifetime in the range of up to several days, this particle fraction is the most important for long range transport.

For high Alpine glaciers, according to Wagenbach and Geis (1989) and Tomadin et al. (1996), the main source regions and composition of the deposited aerosol can by mineralogic composition and particle size investigations be narrowed down to:

- **Episodic long-range** dust transport, especially from the Saharan desert.  
(Fine particle fraction  $< 4 \mu\text{m}$ , mainly clay minerals)
- **Medium range** transport of regional soil dust during the summer by deep convective tropospheric mixing  
(highly variable grain sizes (1-100  $\mu\text{m}$ ), natural and anthropogenic origin)
- **Short range** transport of local periglacial debris onto the glacier surface by strong winds  
(Coarse particle fraction  $> 60 \mu\text{m}$ )

These transport schemes are schematically shown in Fig. 3.2. For the 20th century, the amount and composition of aerosol load deposited at high Alpine glacier sites has been widely investigated.

### 3.1 General sources of organic material in Alpine ice samples

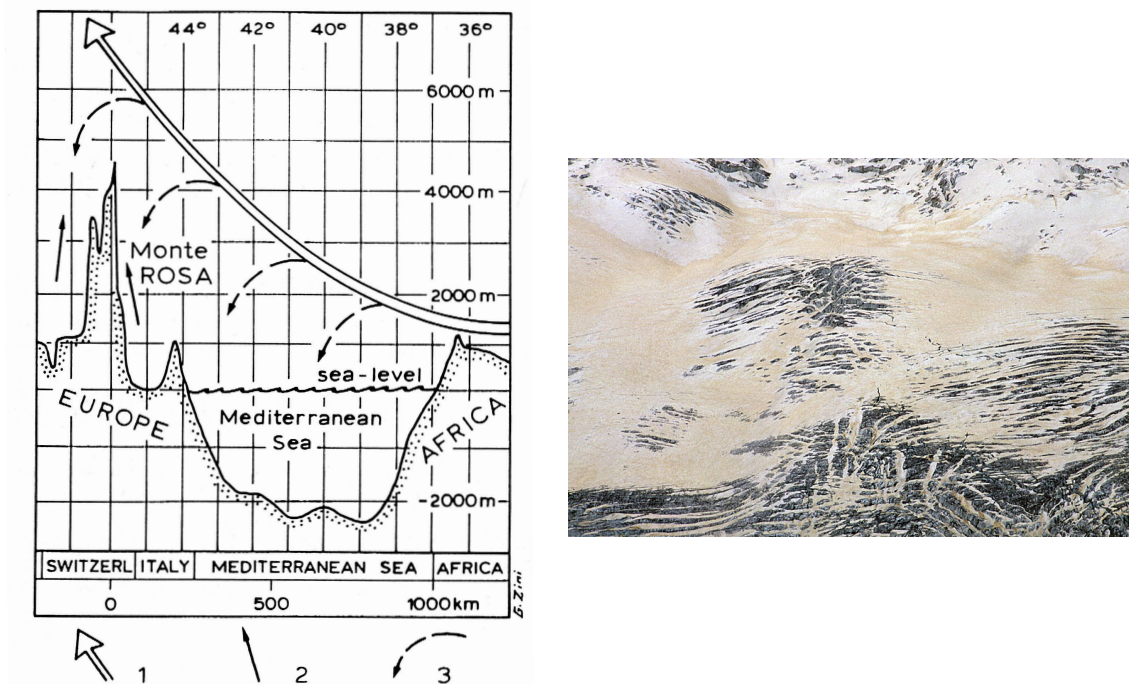


**Fig. 3.2.:** Left: Dust transport to high Alpine glaciers. 1: long range - Saharan dust, 2: mid and short range - local sources, 3: Eolian dust input to the Mediterranean basin. Taken from Tomadin et al. (1996). Right: A large deposit of Saharan dust on the north flank of Breithorn in the year 2004 (Monte Rosa Massif, Switzerland); picture taken from Swissheduc (2004).

It was found, that  $\text{NH}_4$  and  $\text{SO}_4$  nowadays make up the largest aerosol fraction, at least in summer, and are mainly deposited by mid-range transport from sources in middle Europe.

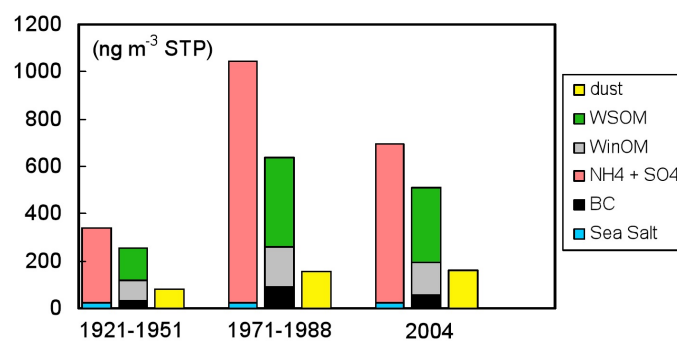


**Fig. 3.3.:** Temporal changes over the 20 th century of summer mass concentration of different aerosols derived from an ice core drilled at the Col du Dome site (Mont Blanc, France) WSOM: water soluble organic matter, WinOM: Water insoluble organic matter, BC: black carbon. Figure taken from Preunkert and Legrand (2013).

### 3. Theoretical background - Particulate organic material in Alpine ice

This is due to anthropogenic emissions (Preunkert and Legrand, 2001), which make up 50%-75% of the total amount of ammonium and sulphate (Fagerli et al., 2007). For pre-industrial times, the major source of sulphate is long range transport of Saharan dust (Wagenbach et al., 1996). An overview of the apportionment of the different aerosol fractions in industrial times is given in Fig. 3.3, taken from Preunkert and Legrand (2013). Apart from that inorganic aerosol, the organic aerosol fraction is the second largest and the target for the  $^{14}\text{C}$  dating method. Therefore, the composition and sources of this fraction will be discussed in detail in the following section.

#### 3.1.2. Organic aerosol in high Alpine glacier ice - origin and composition

Carbonaceous aerosol, which is the relevant fraction for radiocarbon analyses of ice, is primarily divided into the inorganic carbon fraction (IC) and the total organic carbon fraction (TOC). The IC mainly consists of carbonate particles originating from the mineral dust fraction. Counted as part of the TOC fraction is the elemental carbon (EC), which consists mainly of soot particles and other residues of burning and charring processes. This fraction can also be called black carbon (BC). The organic carbon fraction is subdivided into at least three parts (Legrand et al., 2013b): Volatile organic carbon (VOC), which is mainly defined as gaseous organic substances with low boiling points. The other two subdivisions are dissolved organic carbon (DOC) also called water soluble organic carbon (WSOC) and particulate organic carbon (POC), also called water insoluble organic carbon (WinOC). They are usually differentiated by size. All filterable components are counted for the POC fraction, the non-filterable components are called dissolved organic carbon (Gómez-Gutiérrez et al., 2007). The definition of filterability is not very sharp, usually substances that do not pass a filter with  $0.45\ \mu\text{m}$  pore size (see e.g. Zsolnay (2003)) are considered to be POC. The particulate organic aerosol can contribute up to 25% to the total aerosol budget. Fig. 3.4 gives an overview of all carbonaceous compounds.

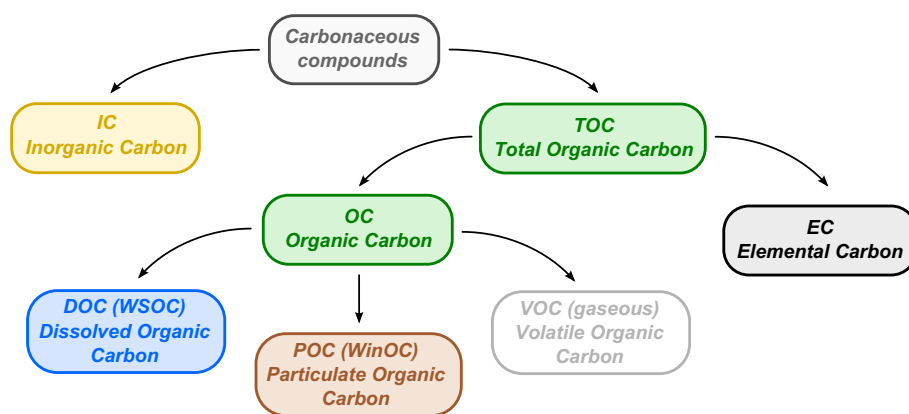


**Fig. 3.4.:** The fractions of carbonaceous compounds in glacier ice samples.

Organic aerosols are part of the primary (Jaenicke and Matthias, 1988) and secondary fraction (Gelencsér et al., 2007). DOC (WSOC) is mainly made up by secondary aerosol, formed by (photochemical) reactions of volatile organic compounds of natural and anthropogenic origin (Gelencsér et al., 2007). Because of the larger mean size of particles, POC is predominantly consistent of primary aerosol. Nevertheless, Jaenicke (1987) states that approximately 80-90% of the particulate organic aerosol in particle numbers is smaller than  $1\ \mu\text{m}$  and thus the small particle fraction also has a large contribution, at least in number.

The main focus of this work lies on analyses of the POC fraction of organic aerosol.

#### POC concentrations in Alpine ice samples

The reported concentrations of POC in high Alpine ice samples vary over a rather wide range, which is due to the different extraction methods and variations in in e.g. filter pore sizes. Steier et al. (2006) measured 25-300  $\frac{\mu\text{gC}}{\text{kg}}$  ice for samples from the high Alpine Grenzgletscher (manometrically quantified from  $\text{CO}_2$ ), Jenk et al. (2009) found POC contents of ca. 15-60  $\frac{\mu\text{gC}}{\text{kg}}$  for the high Alpine firn saddle of Colle Gnifetti and May (2009) extracted for the same site POC concentrations of ca. 5-50  $\frac{\mu\text{gC}}{\text{kg}}$  ice, also manometrically quantified. Legrand et al. (2007) retrieved 20-50  $\frac{\mu\text{gC}}{\text{kg}}$  for the POC (WinOC) fraction by a thermo-optical method (Pio et al., 1994) in pre-industrial snow samples from the Mont Blanc region. Despite of these variations, the overall average concentration of POC in high Alpine ice samples can be assumed to range between 10 and 60  $\frac{\mu\text{gC}}{\text{kg}}$ . The composition of POC can also be strongly dependent on the location and altitude of the sampling site, but the major components can be identified and quantified as follows:

#### Pollen

With average diameters of 10-100  $\mu\text{m}$  (Després et al., 2012), pollen are part of the largest aerosol fraction in size. Because of that, their occurrence in glacier ice and snow decreases strongly with altitude and distance from the source. Haeberli et al. (1983) found numbers of ca. 200-400 pollen per litre on average in high Alpine snow from Colle Gnifetti, which equals ca. 2-4  $\frac{\mu\text{gC}}{\text{kg}}$ . Depending on the season, this can increase by a factor of up to ten in spring and summer dust events. Referred to the mean POC contents stated above, this would result in ca. 3-40% of mass of the total POC.

#### Cellulose and plant debris

Also part of the largest aerosol fraction in size, but covering a large range of ca. 0.1 - 25  $\mu\text{m}$  (Sánchez-Ochoa et al., 2007) are plant fragments and cellulose, the latter being a major component of plant tissue and pollen. These components are also one of the largest mass fractions of primary organic aerosol (Després et al., 2012). Sánchez-Ochoa et al. (2007) give ca. 4-8% for the relative amount of cellulose within organic carbon measured on aerosol filters from the high Alpine observatory Sonnblick, and ca. 6-10 % for the relative contribution of plant debris to the organic matter in aerosol. Legrand et al. (2007) states ca. 20% for the relative mass contribution of cellulose to the water insoluble aerosol carbon fraction in industrial times measured in a Col du Dome ice core and  $8 \pm 5 \frac{\mu\text{gC}}{\text{kg}}$  for a sample from the early 20th century.

#### Fungal spores

One of the most common classes of aerosol POC are fungal spores and spore fragments directly originating from the living biosphere. They are also part of the large aerosol fraction showing typical sizes of  $> 2 \mu\text{m}$  - 10  $\mu\text{m}$  (Bauer et al., 2002), with a mean of about 3-5  $\mu\text{m}$  (Després et al., 2012). Heald and Spracklen (2009) modelled a global contribution of ca. 23% of fungal spores to the primary organic aerosol, whereas Bauer et al. (2002) found only ca. 2% for the relative amount of fungal spores in total carbon in Alpine snow samples, which is a more representative value for the POC analyses of this work.

### 3. Theoretical background - Particulate organic material in Alpine ice

---

#### Bacteria and microbes

Part of the smallest insoluble organic carbon aerosol fraction, around 1  $\mu\text{m}$  of diameter (Després et al., 2012) are bacteria and microbes. They have been observed in size ranges below 0.5  $\mu\text{m}$  and numbers in the range of  $10^4$  cells per ml in high Alpine Snow at Sonnblick observatory (Sattler et al., 2001). For snow samples from Mont Blanc containing Saharan dust range of  $10^2 - 10^3$  have been found (Chuvochina et al., 2011). With masses ranging from 5-90 fg/cell (Whitman et al., 1998), this gives total contributions to the organic carbon in glacier ice and snow of maximal ca.  $0.9 \frac{\mu\text{gC}}{\text{kg}}$  in ice, calculated with the highest cell masses and numbers. Bauer et al. (2002) states 0.02% for the relative amount of bacteria of total carbon in snow from Sonnblick observatory. Overall, it is possible to find rather large numbers of bacteria and microbes in Alpine glacier ice, but their mass contribution to the total POC is compared to other components negligible.

#### Elemental carbon

Elemental carbon particles (soot), are residues of incomplete combustion of biomass and fossil fuel. They are part of the fine aerosol fraction, with particle sizes ranging from 0.03-0.5  $\mu\text{m}$  for so called tar balls (Pósfai et al., 2004) up to about 2  $\mu\text{m}$  on average in snow samples (Schwarz et al., 2013). These particles have very high carbon contents of up to 90%, but contribute only small total carbon amounts to the POC fraction. For example ca.  $1.6 \frac{\mu\text{gC}}{\text{kg}}$  in pre-industrial ice core samples from Mt. Blanc (Legrand et al., 2007). Bauer et al. (2002) give 10-25 % for the amount of Elemental carbon in the modern organic aerosol fraction.

#### Soil dust

As discussed in Section 3.1.1, soil dust inputs onto high Alpine glaciers can have local sources as well as sources that require a long range transport of material. Therefore, they cover a wide range of particle sizes from ca. 0.5  $\mu\text{m}$  up to 20  $\mu\text{m}$ , with a mean of about 2.5-4.5  $\mu\text{m}$  (Wagenbach and Geis, 1989). For the high Alpine glacier Colle Gnifetti, it was observed that two thirds of the main mineral dust was of Saharan origin (Tomadin et al., 1996). This mineral dust is not itself organic, but can serve as a transport medium for organic species and bacteria (Griffin, 2007; Chuvochina et al., 2011) that adsorb onto the surfaces of clay and other mineral dust particles. The organic part of the soil dust thus carries all stages of biomass decomposition products, like dicarboxylic acids (Kawamura et al., 1996), leaf waxes or humic substances. The humic like substances (HULIS) were found to make up ca. 15% of the organic carbon in high Alpine aerosol samples collected at Sonnblick observatory (Feczko et al., 2007). For ice core samples from the high Alpine site Col du Dome (Mont Blanc), summer concentrations of 10-50  $\frac{\mu\text{gC}}{\text{kg}}$  have been measured (Guilhermet et al., 2013) for the industrial period. However, the fraction of HULIS present as POC is not clear and hard to estimate. Overall, the composition of soil derived organic dust is highly inhomogeneous, but can make up a significant amount of POC in Alpine ice samples.

#### Summary of the POC components

An overview of the main components of the particulate organic carbon fraction in Alpine ice and snow samples and their key parameters is given in Table 3.1. All numbers have been scaled to the typical total POC contents of high Alpine ice samples stated above ( $10-60 \frac{\mu\text{gC}}{\text{kg}}$ ). For the fungal spores, it was assumed that ca. one third of the total OC measured in ice samples is POC and the fungal spores only contribute to that POC fraction. The soil dust contribution could not be quantified reasonably. Overall, the stated contributions of the single components to the

### 3.1 General sources of organic material in Alpine ice samples

total POC fraction are highly dependent on source region, season, sampling method and local meteorological features. The values given in Table 3.1 should therefore be regarded as a rough estimation. In Fig. 3.5, The averaged fractions of the different POC components are shown in comparison to the average chemical composition of DOC, retrieved from an ice core from Col du Dome for the first half of the 20th century (Legrand et al., 2013b). It is striking, that for both organic carbon fractions more than one third of the composition remains so far unknown. For the POC, on which lies the main focus of this work, probably a large contribution to that unknown fraction must be attributed to soil dust. Age biasing effects potentially caused by this soil dust and unknown POC fraction will be addressed in the following section.

**Tab. 3.1.:** Major components, sizes and sub-fractions of the POC aerosol fraction in Alpine ice and snow samples. Fractions are calculated on the base of average total POC contents for high Alpine glacier ice ( $10\text{-}60 \frac{\mu\text{gC}}{\text{kg}}$ )

Component	Particle size range [ $\mu\text{m}$ ]	C-mass fraction of total POC
Pollen	10-100, mean: 20-40	3-40 % of POC in Colle Gnifetti snow (Haeberli et al., 1983)
Cellulose and plant debris	0.1-25	ca. 16-50 % of WinOC (POC) in Mt. Blanc ice (Legrand et al., 2007)
Fungal spores	> 2 - 10	ca. 2-6 % of POC in Alpine snow (Bauer et al., 2002)
Bacteria and microbes	smaller 0.5 - larger 1	0.02 -0.1 % in Alpine snow (Chuvochina et al., 2011)
Elemental carbon and soot	smaller 0.5 - larger 2	3-20 % of POC in Mt. Blanc ice (Legrand et al., 2007)
Soil dust	0.5 - 20 mean: 4-5	widely unknown, highly variable

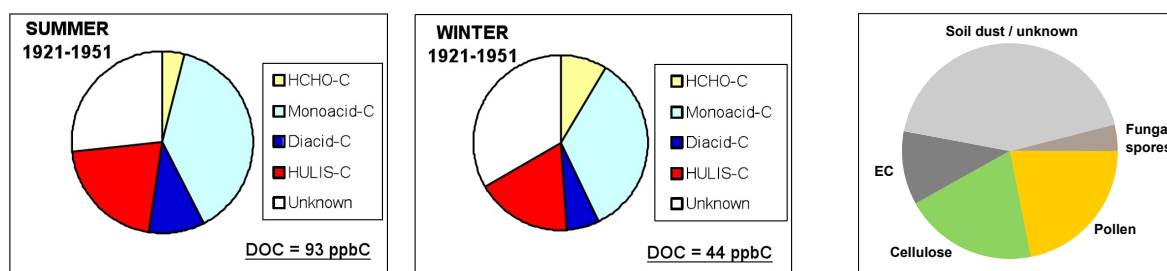


**Fig. 3.5.:** **Left panels:** Chemical winter and summer composition of DOC retrieved from a Col du Dome ice core (Mont Blanc) for the first half of the 20th century (adapted from Legrand et al. (2013b)). **Right panel:** Averaged POC composition of high Alpine glacier ice based on the summarised values in Table 3.1. Note the large unknown fraction.

## 3.2. Possible sources of $^{14}\text{C}$ age biased organic material

For the dating of Alpine ice samples via radiocarbon analyses of the incorporated organic matter, the main prerequisite is the assumption that the age of the organic material represents the age of the surrounding ice body. For the DOC fraction this assumption is likely true. DOC mainly consists of secondary aerosol, formed by coagulation of gaseous precursors directly emitted from the living biosphere (e.g. Pautler et al. (2012)). For the POC fraction however, this assumption is not a priori true. Some of the POC components discussed in Section 3.1.2 can undergo substantial ageing processes before they are deposited onto the glacier and will in this case no longer represent the age of the surrounding ice. This was already observed by Jenk et al. (2006) for Saharan dust influenced ice samples. In the following, these critical POC components and their possible so-called reservoir ages are discussed theoretically.

### 3.2.1. Soil dust from aged sources

The most important source for the deposition of already aged organic material on the glacier surface is soil dust. For high Alpine sites, a large fraction of this material originates from Saharan dust storms (Wagenbach and Geis, 1989; Wagenbach et al., 1996), but also local sources have to be considered. These local soils can inherit very high ages of the incorporated organic matter. This is especially the case in the surroundings of retreating glaciers, where ancient soils resurface again. Trumbore (2000) reports for the  $^{14}\text{C}$  ages of humic substances in boreal and temperate forest soils values up to 1500 years BP. Carcaillet (2001) retrieved  $^{14}\text{C}$  ages of up to 4000 y BP from charcoal particles collected in the top layer of soils in the French Alps. And Egli et al. (2001) found for  $^{14}\text{C}$  ages of soil organic matter in the proglacial area of Swiss glaciers even 150 - 10 000 years BP. They discovered rather high fractions of organic carbon up to almost 40% within the fine soil material fraction (< 2 mm particle size). Soil organic matter from local sources could therefore bias the  $^{14}\text{C}$ -derived ice ages significantly, if transported onto the glacier.



**Fig. 3.6.:** A Saharan dust storm over Italy in 2003 (MODIS, 2003).

Saharan dust (see e.g. large over storm in Fig. 3.6) has been studied intensely with respect to mineral composition, particle size distribution and origin (e.g. (Tomadin et al., 1996; Sode-mann et al., 2006; Thevenon et al., 2012)). Information the  $^{14}\text{C}$  ages of the organic particles transported to the European Alps along with the dust storms is however sparse. Saharan dust is a major contributor of carbonates (IC) to the total carbon fraction of glacier ice (Wagenbach et al., 1996). Carbonates are usually originating from the weathering of old ( $^{14}\text{C}$  free) carbonate rocks and thus carry a large age bias compared to the surrounding material.

The only direct  $^{14}\text{C}$  dating of a Saharan dust sample so far, collected on a buoy in the north east Atlantic has been performed by Eglinton et al. (2002). It yielded ages of ca. 1000 yBP for the total organic carbon fraction and ca. 2000 yBP for the black carbon (mainly microscopical charcoal). Additionally, Jenk et al. (2006) found  $^{14}\text{C}$  contents in the black carbon fraction (defined by combustion temperature) of pre-industrial ice core samples from Fiescherhorn glacier

(Switzerland) of ca.  $0.5 F^{14}\text{C}$ . This equals ca. 5000 years of  $^{14}\text{C}$  age for samples that visibly have been influenced by Saharan dust. Considering the termination of the African Humid Period ca. 5500 yBP (deMenocal et al., 2000), which could be regarded as the last major production period for organic material in that region, organic particles mobilised by desert dust storm could be able to reach ages up to more than 5000 yBP. Therefore, Saharan dust may have a major influence on the POC  $^{14}\text{C}$  ages of Alpine glacier ice samples, but the available data is so far incomplete. A more systematic investigation of Saharan dust  $^{14}\text{C}$  ages has been performed within this work and is discussed in section 7.3.1.

### 3.2.2. Cryoconite and fossil basal sediment

Similar to the eolian input of old soil organic material to the glacier surface, especially for basal glacier ice the incorporation of bedrock sediment into the ice matrix becomes important. This mostly happens in the ablation zone of glaciers, where the availability of liquid water allows sliding of the ice body over soft sediment beds (see Fig. 3.7 for an example from Svalbard). But also in cold high Alpine glaciers, which are frozen to bedrock, sediment particles have been observed in the basal sections of ice cores (Benn and Evans, 2010). These bedrock sediments can reach very high ages of up to 10 000 years BP or more for Alpine glaciers. This can nowadays be documented by dating of sediments released from retreating glacier fronts (see e.g. Joerin et al. (2006), Bardgett et al. (2007)). If organic material contained in these bedrock sediments, where even under cold and dark conditions microbial life is possible (Benn and Evans, 2010), is folded into the ice, the age of that material will not represent the surrounding ice age at all. Again, directly measured  $^{14}\text{C}$  ages of organics from subglacial sediments are not very numerous, most studies refer to dating of proglacial sediments.



**Fig. 3.7.:** Bedrock sediment folded into the basal ice of Tunabreen glacier, Svalbard (2013), Doug Benn for scale. Picture by Helene Hoffmann.



**Fig. 3.8.:** Water-filled cryoconite holes in the ablation zone of Grenzgletscher, Switzerland (2014), Pole for scale. Picture by Johanna Kerch.

Another source for age biased organic material in glacier ice can be so-called cryoconite. The accumulation of fine-grained debris on a glacier surface in the ablation zone can lead to the for-

### 3. Theoretical background - Particulate organic material in Alpine ice

---

mation of small meltwater filled holes (see Fig. 3.8), due to reduced albedo of the dark dust particles (Wharton et al., 1985). In such holes, more dust will accumulate, which leads to growth of the hole and onset of microbial activity. These microbes can reach high productivity rates (Takeuchi et al., 2001; Anesio et al., 2009). The material within these cryoconite holes therefore consists of a very broad mixture of eolian dust and wind blown sediment particles. Both materials can have very high intrinsic  $^{14}\text{C}$  ages, as stated above, but also a large amount of microbial activity with a modern  $^{14}\text{C}$  signature is present. Nowadays, these cryoconite holes inherit also a fraction of anthropogenic fossil fuel burning products (soot), which can shift the apparent  $^{14}\text{C}$  age of the organic material to very high values (Stubbins et al., 2012). For cold high Alpine glaciers this mixture of organic material does not play a major role, because temperatures are too low to allow formation of cryoconite holes. Nevertheless, at lower altitude glaciers, cryoconite can become a significant source of englacial organic material, when the holes are covered again with snow and slowly transported into the glacier by flow. Again, the  $^{14}\text{C}$  age of this material will not be representative for the surrounding glacier ice.

All these possible contributions of age biased organic material to the microscopic POC fraction of Alpine glacier ice must be considered carefully, when interpreting  $^{14}\text{C}$  contents of POC in terms of ice ages. They have been investigated systematically within this work (see section 7.3).

#### 3.2.3. Anthropogenic influences

Together with the naturally aged material, in recent times since the onset of the industrial revolution, also anthropogenic emissions are able to alter  $^{14}\text{C}$  ages of glacier ice POC. The burning of fossil fuel contributes directly to the POC fraction, mainly by soot particles deposited with the snow. They are highly depleted in  $^{14}\text{C}$  and can shift the ages of the dated organic material significantly to higher values (see e.g. Jenk et al. (2006)). This effect makes POC dating of ice samples, which are younger than the onset of industrialisation (i.e. younger than 100 years) very difficult, because always an estimation of the anthropogenic carbon contribution is needed. Another anthropogenic age biasing effect is the incorporation of organic material from the bomb peak period. Usually, bomb peak biased ice samples can be identified by enhanced tritium values. However, if by some mechanisms material from that time period is transported to the glacier interior (e.g. by crevasses), deep, old glacier parts can be dated too young in  $^{14}\text{C}$  analyses. Therefore, this possibility should also be considered with the interpretation of radiocarbon ages of glacier ice.

## 4. State of the art and new insights into micro-radiocarbon dating of high Alpine ice samples

### 4.1. The problem of in situ produced radiocarbon in the Dissolved Organic Carbon (DOC)

#### 4.1.1. Very high $^{14}\text{C}$ contents in DOC of high Alpine ice samples

At the start of micro-radiocarbon dating of Alpine ice samples at the IUP Heidelberg, it was initially envisaged to use the dissolved organic carbon fraction (DOC) for dating, because:

1. The total concentrations of DOC in ice are about a factor 5-10 higher than the particulate organic carbon (POC) concentrations (Stricker, 2008; May, 2009), which makes reliable measurements easier
2. DOC mainly consists of components directly emitted by the living biosphere (Singer et al., 2012; Pautler et al., 2012) and should not be influenced strongly by reservoir effects.

The development and application of a DOC extraction system for radiocarbon dating of ice samples at the Institute for Environmental Physics in Heidelberg is described in detail in May (2009).

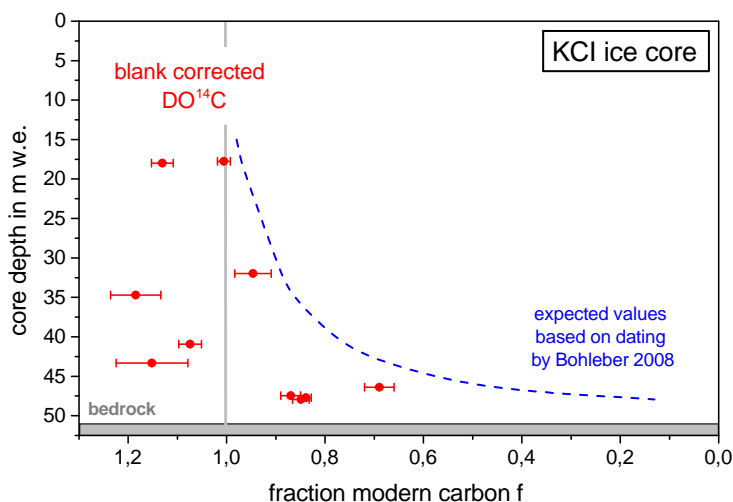


**Fig. 4.1.:** DOC  $^{14}\text{C}$  results of samples from an ice core from the high Alpine firn saddle Colle Gnifetti. Note the  $^{14}\text{C}$  values higher than modern even in large core depths and the large discrepancy to the age expectation based on a 2D-flow model (Bohleber, 2008). Figure modified from May (2009)

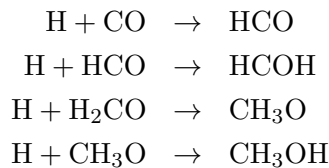
## 4. State of the art and new insights into micro-radiocarbon dating of high Alpine ice samples

---

However, the  $^{14}\text{C}$  results of these DOC analyses for ice cores drilled at the high Alpine firn saddle Colle Gnifetti (4500 m a.s.l., Swiss Alps) showed very high  $^{14}\text{C}$  values, partially even higher than the modern atmospheric content. This was found even in large core depths, which is not reasonable from a glaciological point of view (see Fig. 4.1). The large offset from the expected curve could not be explained by any artificial contamination during the sample preparation process or the incorporation of  $^{14}\text{C}$ -enhanced organic matter e.g. from the bomb peak period. As a consequence, another  $^{14}\text{C}$  source was needed to explain these enhanced values.

### 4.1.2. Hypothesis: in situ production of $^{14}\text{C}$ (May, 2009)

It has been known for many years, that  $^{14}\text{C}$  atoms can be produced within the ice matrix by spallation of oxygen within the water molecule, induced by cosmic radiation (Lal et al., 1987; van de Wal et al., 1994; Mazarik and Reedy, 1995). The main natural reaction paths for this in situ production are  $^{16}\text{O}(\text{n},\text{n}2\text{p})^{14}\text{C}$  and  $^{16}\text{O}(\mu,2\text{p})^{14}\text{C}$ , whereas the relative contribution of the muon reaction can be neglected at high altitudes (Mazarik and Reedy, 1995). Because of the high recoil energy of this neutron reaction, the water molecule bonds can be disrupted and the  $^{14}\text{C}$  is present within the ice matrix as a hot atom, which is quickly oxidised to different chemical species. Most commonly, these species are CO and  $\text{CO}_2$ , but also more complex volatile molecules like  $\text{CH}_4$  have been reported lately (Petrenko et al., 2009, 2013). It is also possible to hydrogenate the CO molecule to higher organic species via (Woon, 2002):



This is achieved by reaction of the CO with free H atoms produced during the disruption of the water molecule and with the ice surface acting as a catalyst. Also Yankwich et al. (1946) found in situ produced  $^{14}\text{C}$  in methanol and formic acid in the presence of water after the irradiation of nitrogenous solutions. It could therefore be possible, that short chained organic molecules formed during the process of in situ production of  $^{14}\text{C}$  could contribute to the DOC, the amount however remains unknown so far.

The natural neutron flux is strongly dependent on altitude and latitude, but the energy distribution of the incoming neutrons is overall very uniform. Gordon et al. (2004) found for mid-latitude neutron fluxes variances up to a factor of 15 from sea level to 3450 m a.s.l., but the shape of the energy distribution shown in Fig. 4.2 is very similar for all sites. It has three distinct peaks, one for the thermal neutrons in the low energy section and two for the fast and relativistic neutrons. Only the high energy fraction is able to take part in the  $^{14}\text{C}$  in situ production (Park et al., 2005). The production of in situ  $^{14}\text{C}$  in glacier ice is strongly dependent on the depth and snow accumulation rate. The absolute number of produced atoms per gram ice can according to Lal et al. (1987) be expressed as:

$$c_{\text{insitu}}(z) [\text{C}/\text{gram}] = \frac{P_0}{\frac{\rho A}{\Lambda} - \lambda} \cdot \left( e^{-\frac{\lambda z}{A}} - e^{-\frac{\rho z}{\Lambda}} \right) \quad (4.1)$$

## 4.1 The problem of in situ produced radiocarbon in the Dissolved Organic Carbon (DOC)

With  $\lambda = \frac{\ln 2}{T_{1/2}}$  as the decay constant of  $^{14}\text{C}$  and  $A = \frac{dz}{dt}$  as the accumulation rate.  $P_0$  denotes the production rate, which depends on altitude, latitude and ice density  $\rho$ ; and  $\Lambda$  is the adsorption mean free path length in  $\text{g}/\text{cm}^2$ .

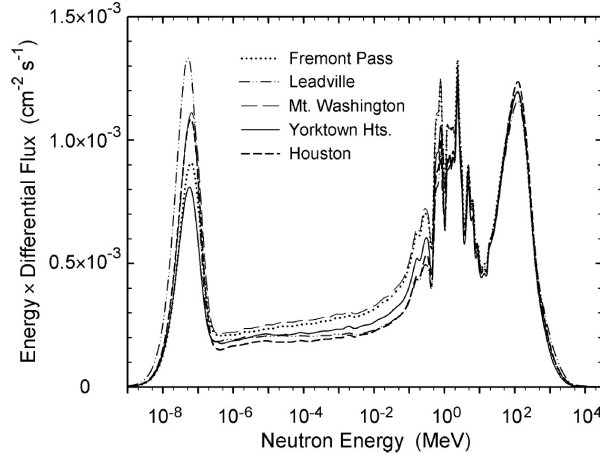


**Fig. 4.2.:** Neutron fluxes and energy spectra for several North American measurement sites scaled to sea level. Note the very similar shape of the energy distributions. Figure taken from Gordon et al. (2004)

For the mean free path length, Lal and Jull (1990) give a value of ca.  $\Lambda = 150 \text{ g} \cdot \text{cm}^{-2}$  for the top 10 m and a production rate of  $P_0 \approx 396 \text{ }^{14}\text{Cg}^{-1}\text{a}^{-1}$  for an altitude of 4500 m a.s.l.

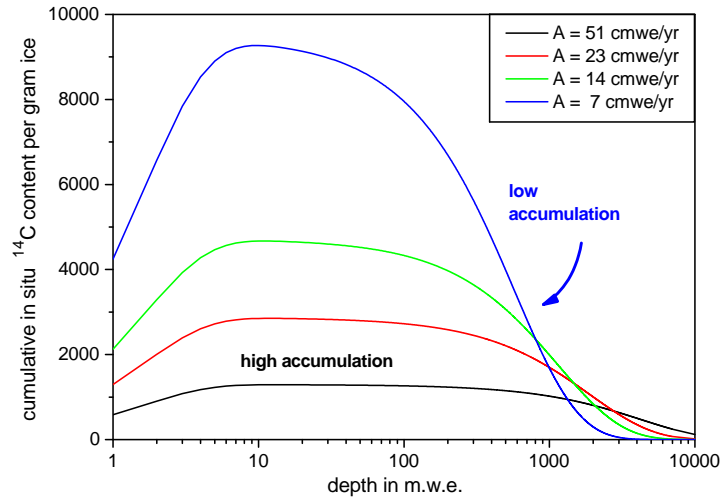


**Fig. 4.3.:** Theoretically produced number of  $^{14}\text{C}$  atoms per gram ice based on Eq. 4.1 depending on ice depth  $z$ , for different accumulation rates  $A$ . With  $P_0 \approx 396 \text{ }^{14}\text{Cg}^{-1}\text{a}^{-1}$ ,  $\Lambda = 150 \text{ g} \cdot \text{cm}^{-2}$  and  $\rho = 0.9\text{g}/\text{cm}^3$

Assuming that only 20% of this in situ produced  $^{14}\text{C}$  enters into the DOC fraction (e.g. as formic acid) and correcting the  $^{14}\text{C}$  results in Fig. 4.1 accordingly, the  $^{14}\text{C}$  contents already shift to

## 4. State of the art and new insights into micro-radiocarbon dating of high Alpine ice samples

overall more reasonable values (see Fig. 4.4).

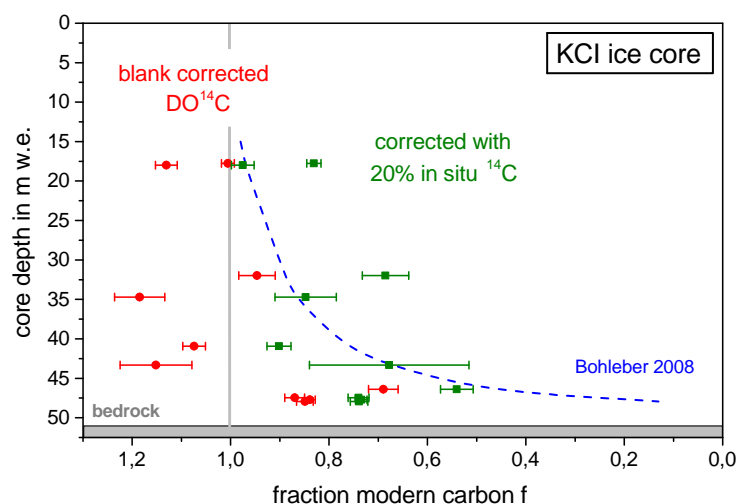


**Fig. 4.4.:** DOC- $^{14}C$  results of ice samples from an ice core from the high Alpine firn saddle Colle Gnifetti (red) together with a hypothetical correction (green) under assumption of a 20% in situ produced  $^{14}C$ -contribution to the DOC fraction (modified from May (2009))

If it could be proved that this in situ production indeed causes the enhanced DOC  $^{14}C$ -results, radiocarbon dating of ice cores via this organic carbon fraction is not possible in locations, which have a large in situ production (high latitudes, high altitudes and low accumulation). This is mainly due to:

- The strong dependence of in situ production on accumulation rate (see Fig. 4.3). The assumption of a constant accumulation rate over time is unrealistic and the real variation of this rate is not known.
- The exact fraction of in situ  $^{14}C$  incorporated in the DOC is not known.
- The production rate is modulated by solar activity and variable over time (Usoskin, 2008).

Therefore, the hypothetical correction of in situ production, which was performed here, must remain insufficient and the measured radiocarbon ages do not represent the real ice ages.

### 4.1.3. Proof of in situ production of $^{14}C$ -enriched DOC - irradiation experiments

To prove or rule out the hypothesis of in situ produced radiocarbon being incorporated in measurable amounts into the DOC fraction of glacier ice, neutron irradiation pilot experiments have been performed under the lead of B. May at the IUP Heidelberg. This was done in close cooperation with the University of Vienna (Institute of Isotope Research and Nuclear Physics) and the Helmholtz Centre Dresden Rossendorf. The main goals of these irradiation experiments were:

1. To prove the possibility to create  $^{14}C$ -enriched DOC from the irradiation of ice samples with fast neutrons.

## 4.1 The problem of in situ produced radiocarbon in the Dissolved Organic Carbon (DOC)

2. To quantify the fraction of produced  $^{14}\text{C}$  that enters the DOC fraction.
3. To investigate the production and DOC incorporation for different sample materials (liquid water, snow, natural and artificial ice).

### Setup of the neutron irradiation experiments

The available neutron source at the Helmholtz Centre Dresden Rossendorf is a Deuterium-Tritium-source (DT), which mainly produces fast neutrons at 14.5 MeV from the reaction



Therefore, the neutron energy is not high enough for the natural  ${}^{16}\text{O}(\text{n},3\alpha){}^{14}\text{C}$  reaction, which has an energy threshold at 15.53 MeV (Park et al., 2005), and only reactions of  ${}^{17}\text{O}(\text{n},\alpha){}^{14}\text{C}$  and  ${}^{18}\text{O}(\text{n},\text{n}'\alpha){}^{14}\text{C}$  could be studied with this setup. The key parameters for the investigated reactions are summarised in Table 4.1.

**Tab. 4.1.:** Overview of the key parameters for neutron reactions with different oxygen isotopes creating  $^{14}\text{C}$ . The cross sections are given for neutron energies of 14.5 MeV. Note the large variation of measured cross section for the  ${}^{17}\text{O}$  reaction.

O-Isotope	Abundance [%]	Neutron reaction	E-threshold [MeV]	Cross section [barn]
${}^{16}\text{O}$	99.757	${}^{16}\text{O}(\text{n},3\text{He}){}^{14}\text{C}$	15.53	$0,052 \pm 0.016$ (Park et al., 2005)
${}^{17}\text{O}$	0.038	${}^{17}\text{O}(\text{n},\alpha){}^{14}\text{C}$	none	$0.035 \pm 0.007$ (Verzilov et al., 1998) 0.087-0.25 (EXFOR, 2016)
${}^{18}\text{O}$	0.205	${}^{18}\text{O}(\text{n},\text{n}'\alpha){}^{14}\text{C}$	6.58	$0.027 \pm 0.005$ (Verzilov et al., 1998) 0.02-0.06 (EXFOR, 2016)

The reaction cross sections for the available neutron energy of 14.5 MeV are not very well determined, especially for the  ${}^{17}\text{O}$ -reaction. This results in a large scope of the number of theoretically created  $^{14}\text{C}$  atoms. According to Verzilov et al. (1998) and the EXFOR database (EXFOR, 2016), the ranges for the reaction cross sections were assumed to be 0.03-0.2 barn for the  ${}^{17}\text{O}$  and 0.03 barn for the  ${}^{18}\text{O}$  reaction.

For the experiment, the ice samples were contained in plastic jars and additionally sealed in PE-foil to avoid any contact with the surrounding lab air. Most of the samples have been equipped with neutron flux monitors (Nb for the high energetic and Au for the low energetic neutrons) at front and back, to survey the actual neutron flux at the position of the sample. The ice samples have been placed inside a polystyrene container, which was cooled by an atmosphere of liquid nitrogen for the whole process of irradiation, to prevent the samples from melting.

#### 4. State of the art and new insights into micro-radiocarbon dating of high Alpine ice samples

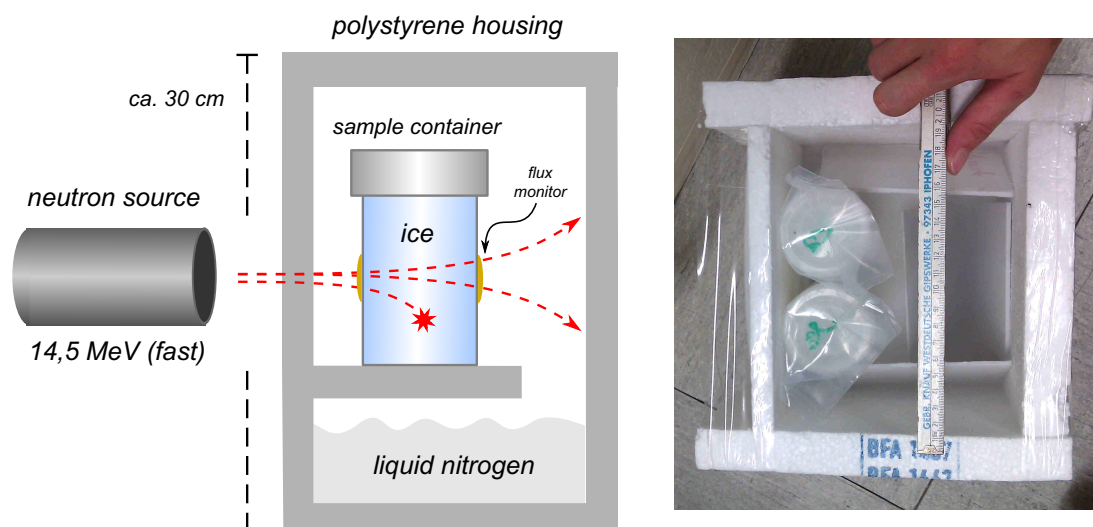


**Fig. 4.5.:** **Left:** Schematic view of the ice sample irradiation experiment. Samples have been kept in plastic containers sealed in PE-foil and have been equipped with flux monitors to observe the actual neutron flux. The ice samples were placed inside a polystyrene container and cooled by an atmosphere of liquid nitrogen to prevent them from melting during the irradiation. **Right:** Picture of the polystyrene container from top. The sample containers can be seen to the left. Picture by Helene Hoffmann

Four different material types have been irradiated and DOC was extracted afterwards: Liquid ultra pure water (ELGA-Labwater, 18 M $\Omega$ , 1-2 ppb TOC (ELGA, 2016), called MQ-water), degassed artificial blank ice (DOC-free) produced from ultra pure water, natural pre-industrial glacier ice (Grenzgletscher) and modern high Alpine snow (Colle Gnifetti). For every irradiated sample, a reference sample of the same type was kept in the same type of jar at the IUP. An overview of all sample parameters and neutron flux calculations needed for computing of  $^{14}\text{C}$  production is given in Appendix A.1.1. All irradiated samples stayed in the neutron source for 35-60 min and were exposed to neutron fluxes of ca.  $10^7$ - $10^8$  n/cm $^2$ /s. The theoretically produced number of  $^{14}\text{C}$ -atoms within the samples was calculated according to:

$$^{14}\text{C}_{\text{produced}} = \Phi_n \cdot t \cdot N_A \cdot \frac{m_s}{M_{\text{H}_2\text{O}}} \cdot (\sigma_{^{17}\text{O}} \cdot 3.8 \cdot 10^{-4}) \cdot (\sigma_{^{18}\text{O}} \cdot 2 \cdot 10^{-3}) \quad (4.3)$$

With  $\Phi_n$  as the neutron flux measured by the flux monitors,  $t$  as the irradiation time,  $N_A$  the Avogadro constant,  $m_s$  the sample mass in grams,  $M_{\text{H}_2\text{O}}$  the molar mass of water,  $\sigma_{^{17}\text{O}}$  and  $\sigma_{^{18}\text{O}}$  the cross sections of  $^{17}\text{O}$  and  $^{18}\text{O}$  weighted here with their relative natural abundances. The resulting numbers of theoretically produced in situ  $^{14}\text{C}$  atoms can be found in Table 4.2.

#### Main results and interpretation of the DOC - $^{14}\text{C}$ values of the irradiated samples

After neutron irradiation, all samples along with the not irradiated reference samples have been processed for DOC extraction according to the procedure described in May (2009). The resulting  $\text{CO}_2$  has been graphitised and measured for radiocarbon content at the Vienna Environmental Research Accelerator (VERA). Results of the DOC extraction (given as carbon concentration) and  $^{14}\text{C}$ -measurement are summarised in Table 4.2. The  $^{14}\text{C}$  results for the reference samples are

## 4.1 The problem of in situ produced radiocarbon in the Dissolved Organic Carbon (DOC)

all in the expected range. Water and blank ice approximately like the process blank, the Alpine snow modern, as it should be, and the glacier ice in the same range as it has been measured before (May, 2009). The rather high DOC mass for the blank water sample is probably due to the storage in a Polypropylene-jar and thus contamination of the liquid from diffusion of organic compounds from the jar wall. That would also explain the rather low  $^{14}\text{C}$  value of the reference sample. All other DOC masses are in characteristic ranges.

**Tab. 4.2.:** Extracted DOC concentrations, theoretically produced numbers of in situ  $^{14}\text{C}$  atoms and  $^{14}\text{C}$  contents for all irradiated and reference ice samples. Note the very enriched contents of the irradiated samples.

Sample type	DOC [ $\frac{\mu\text{gC}}{\text{kg}}$ ]	$^{14}\text{C}$ atoms produced	$^{14}\text{C}$ content [ $\text{F}^{14}\text{C}$ ]
MQ-water reference	605		$0.33 \pm 0.01$
MQ-water (60 min. irradiated)	353	$2.34\text{E}+08 - 5.22\text{E}+08$	$48.56 \pm 0.45$
Blank ice reference	58		$0.54 \pm 0.01$
Blank ice (36 min. irradiated)	71	$4.87\text{E}+08 - 1.09\text{E}+09$	$210.93 \pm 2.84$
Alpine snow reference	1907		$1.10 \pm 0.01$
Alpine snow (60 min. irradiated)	1943	$2.65\text{E}+08 - 5.90\text{E}+08$	$25.35 \pm 0.13$
Glacier ice reference	332		$0.642 \pm 0.01$
Glacier ice (60 min. irradiated)	271	$3.52\text{E}+08 - 7.85\text{E}+08$	$76.52 \pm 2.37$

The ranges given in the produced  $^{14}\text{C}$  numbers in Table 4.2 are due to the large uncertainty of the  $^{17}\text{O}$  cross section. Therefore the lower limit was calculated with  $\sigma_{17\text{O}}=0.02$  and the upper limit by use of  $\sigma_{18\text{O}}=0.3$ . The irradiated samples show very enhanced  $^{14}\text{C}$  contents, ranging from an approximately hundred times increase for the glacier ice to a more than 400 times larger content in the blank ice sample (see Fig. 4.6). These findings impressively show that incorporation of artificially produced in situ radiocarbon into the DOC fraction in ice is possible. It is able to alter the  $^{14}\text{C}$  age of an ice sample significantly. Apart from the striking high absolute  $^{14}\text{C}$  values, which are due to the high neutron fluxes and long irradiation times, the major question is how much of the produced  $^{14}\text{C}$  entered the DOC fraction. This was calculated from the ratio of the extracted number of  $^{14}\text{C}$  of the irradiated sample  $n_{14\text{C}}(\textit{irradiated})$  (where the number of  $^{14}\text{C}$  atoms found in the reference  $n_{14\text{C}}(\textit{reference})$  was subtracted) and the theoretically produced number of  $^{14}\text{C}$  atoms  $n_{14\text{C}}(\textit{produced})$ :

$$\frac{^{14}\text{C}_{\text{DOC}}}{^{14}\text{C}_{\text{produced}}} [\%] = \frac{n_{14\text{C}}(\textit{irradiated}) - n_{14\text{C}}(\textit{reference})}{n_{14\text{C}}(\textit{produced})} \cdot 100 \quad (4.4)$$

The results (Table 4.3) show that on average ca. 10 - 30% of the produced  $^{14}\text{C}$  atoms could be extracted in the DOC fraction. Only for the Alpine snow sample the fraction is significantly higher. This is probably due to the very different texture of this sample compared to the others. It had a very low density of  $0.36 \text{ g/cm}^3$ , large, open pores and thus a very large internal surface. That could lead to additional containment of  $^{14}\text{C}$  produced from nitrogen in the air space. This process is however based on the present data highly speculative and needs further investigations.

#### 4. State of the art and new insights into micro-radiocarbon dating of high Alpine ice samples

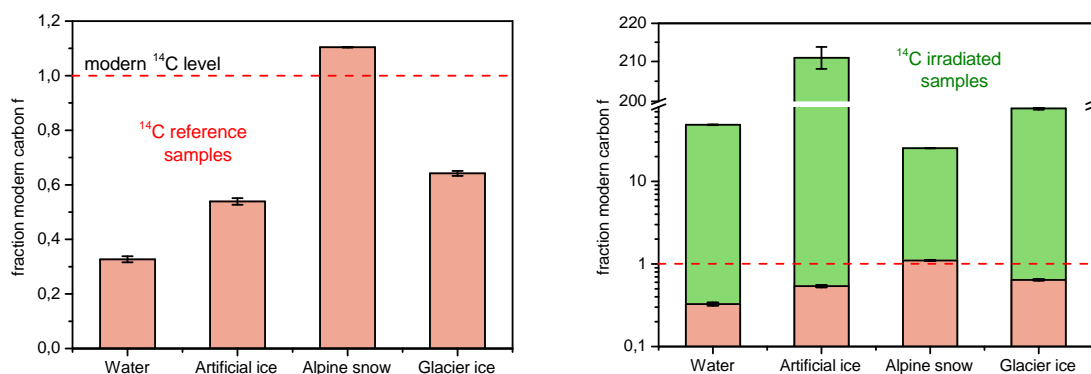


**Fig. 4.6.:** **Left:**  $^{14}\text{C}$  results of the reference samples. All results agree with the expected ranges. **Right:**  $^{14}\text{C}$  results of the irradiated samples (green) together with the reference samples (red). Note the logarithmic scale and the very enriched  $^{14}\text{C}$  contents of all samples.

**Tab. 4.3.:** Relative fractions of  $^{14}\text{C}$ , produced by irradiation that entered the DOC fraction for all irradiated ice samples.

Sample type	$^{14}\text{C}$ produced in DOC [%]
MQ-water	9 - 20
Blank ice	12 - 28
Alpine snow	32 - 72
Glacier ice	11 - 25

The major findings of the whole set of irradiation experiment can be summarised as follows:

1. It could be shown that the incorporation of artificially produced  $^{14}\text{C}$  by neutron irradiation of ice samples into the DOC fraction of organic carbon is possible to significant amounts.
2. The actual amount of the incorporated  $^{14}\text{C}$  is in ice typically ranging from 10-30% depending on the assumed reaction cross section and type of material. The chemical composition of this in situ produced DOC remains however unclear.
3. The amount of in situ  $^{14}\text{C}$  incorporated into the DOC fraction is sufficient to explain the enhanced  $^{14}\text{C}$  values in glacier ice from Colle Gnifetti, but makes establishment of a core chronology based on radiocarbon dating of the DOC fraction impossible.

The artificial neutron fluxes were with  $10^8$  n/s/cm<sup>2</sup> much higher than natural values, which are in the order of  $10^{-2}$  for mid-latitudes and altitudes of ca. 3000 m a.s.l. (Gordon et al., 2004; Cheminet et al., 2012). However, the main goal of this irradiation experiment was to prove the fundamental possibility of incorporation of in situ produced  $^{14}\text{C}$  into the DOC fraction, which

could be shown impressively, and not the realistic reproduction of natural conditions. The natural in situ produced  $^{14}\text{C}$  is mainly output of the reaction  $^{16}\text{O}(n,3\alpha)^{14}\text{C}$ , which is dominating because of the large abundance of  $^{16}\text{O}$ . The naturally produced amount of in situ  $^{14}\text{C}$  is additionally dependent on altitude, ice density, accumulation and mean free path length (see Equation 4.1).

Because of this major bias of the DOC fraction, the DOC should not be used for dating of high Alpine ice samples from archives at high altitudes with low snow accumulation. For such archives, like Colle Gnifetti, the POC fraction is therefore the only option for radiocarbon dating of ice samples.

## 4.2. Principle of the method and state of the art of POC dating

Preparation of ice samples for  $^{14}\text{C}$  analysis of the POC fraction follows certain process steps that allow variations only at distinct points of the sample treatment. The main distinction between different preparation systems lies in the method of particle extraction from the ice sample. Most common is the separation of POC by melting and filtration as for example described in Steier et al. (2006) and Jenk et al. (2007). Another method to extract POC from ice is the sublimation of the solid sample and collection of the residual particles (Biegalski et al., 1998). Sublimation has the advantage of a very good particle recovery and no selection of distinct particle sizes, but on the other hand during sublimation the material of the ice matrix is lost by evaporation. This is not desirable for very rare samples. The focus of this work lies therefore on the melting and filtration technique, which in principle follows the procedure below:

1. Decontamination of solid ice sample
2. Melting of sample and filtration of insoluble particles
3. Removal of inorganic carbon (IC) by acidification of filtered material
4. Combustion of retrieved organic carbon into  $\text{CO}_2$
5. Cleaning and manometric quantification of  $\text{CO}_2$
6. Graphitisation of sample or direct  $\text{CO}_2$  radiocarbon measurement at the Accelerator Mass Spectrometer (AMS)

In any case, the process starts with the surface decontamination of the solid ice to remove any contamination introduced during sampling, packaging and previous handling of the sample. Next, the sample is melted and filtered under a clean atmosphere, where all insoluble particles are collected on a filtration medium. After filtration, the sample is acidified to remove all inorganic carbon, because depending on the origin (mostly carbonates) this carbon fraction can bias the sample age dramatically. After acidification, the remaining organic particles are combusted to  $\text{CO}_2$ , which is then cleaned from residual gases and water vapour before manometric quantification of the actual sample size. The cleaned  $\text{CO}_2$  is then ready to be either graphitised or directly measured at a radiocarbon AMS facility. For details of the AMS measurements see section 2.3.

The largest challenge for ice with very low organic carbon contents in the microgram range, is to remove the surface contamination of the solid ice sample without introducing new contamination during handling of the ice and the following steps. Therefore, all surfaces in contact with

## 4. State of the art and new insights into micro-radiocarbon dating of high Alpine ice samples

the sample must be cleaned thoroughly, best by prebaking at high temperatures (800 °C), to oxidise and remove all organic substances from the surface. This is done mostly for filters and combustion ampoules. Where cleaning via preheating is not possible, materials are used whose surfaces can be cleaned easily by rinsing with ultra pure water. These materials are mainly PFA, glass and stainless steel. For average POC contents of high Alpine ice of ca.  $10\text{-}60 \frac{\mu\text{gC}}{\text{kg}}$ , and typically available sample sizes of a few hundred grams up to 1 kg, the process blank should thus ideally not exceed a total carbon mass of ca.  $1 \mu\text{gC}$ .

### 4.2.1. Operational systems outside the IUP Heidelberg

First pilote studies of the POC filtration method for dating of glacier ice were done by Steier et al. (2006) at the VERA laboratory in Vienna. They yielded a rather high and variable process blank of at least  $7 \mu\text{gC}$  total carbon mass and were thus only applicable for rather large samples of about 1 kg ice for high Alpine samples. In this case block samples from Grenzgletscher (Switzerland) with highly variable POC concentrations of ca.  $30\text{-}200 \frac{\mu\text{gC}}{\text{kg}}$ .

The Paul Scherrer Institute (PSI) in Switzerland then improved the method based on an overall process blank of ca.  $1.5 \mu\text{gC}$  (Jenk et al., 2007) for carbon sample sizes down to ca.  $10 \mu\text{gC}$  (equals less than 1 kg ice for average concentrations). Their system is still operational and being applied for many different ice dating purposes (Jenk et al., 2009; Sigl et al., 2009; Herren et al., 2013; Cao et al., 2013). It uses the decontamination and preparation protocol shown in Fig. 4.7 (Zapf et al., 2013) following the principles of POC extraction stated above.

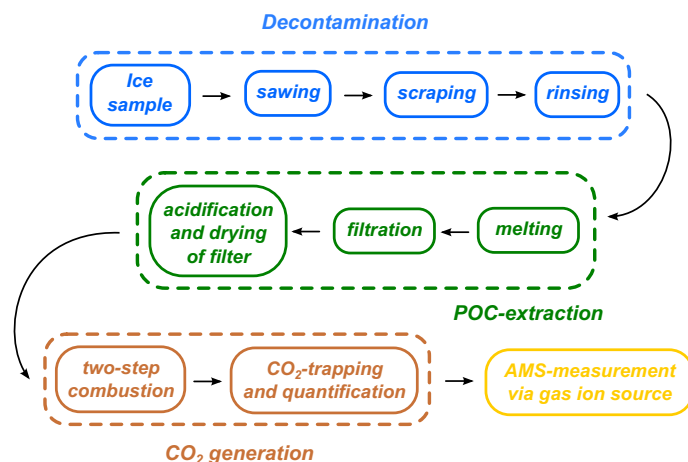


**Fig. 4.7.:** Schematic illustration of the main processing steps for POC extraction from ice samples and radiocarbon dating used at the Paul-Scherrer-Institute (Switzerland).

Both systems (VERA and PSI) use quartz fibre filters as filtration medium and have two main disadvantages where the method improvements of this work will start:

- The whole sample is first completely melted, stored and then filtered, which involves the risk of losing material during filtration by sedimentation and adhesion of POC to the melting pot walls

- After filtration, the filter has to be taken out of the holder for further processing, which holds the risk of material loss, additional contamination of the sample and destruction of the fragile filter tissue during removal from the filter holder

### 4.2.2. First system at the IUP Heidelberg

At the Institute for Environmental Physics in Heidelberg, the first system for POC filtration from ice samples was developed as additional part of a DOC extraction system (see May (2009)) and also used the technique of total melting of the sample followed first by DOC extraction and subsequent filtration on a quartz fibre filter. This also includes the disadvantages already mentioned and additionally inherited a high and variable process blank for ice samples of 6.4  $\mu\text{gC}$  total carbon mass. This high process blank made a reliable application to Alpine ice core samples in the order of 200-500 g of ice with POC concentrations of 20  $\frac{\mu\text{gC}}{\text{kg}}$  on average extremely difficult and uncertain.

As a consequence, all method improvements in the present work aim for reduction of contamination during the sample preparation process. This means keeping the artificially introduced amount of organic carbon (system blank) as low as possible with a simultaneously maximisation of the POC yield from the sample. These method improvements are broadly discussed in the following chapter.



## 5. Methods - Implementation of the gas ion source at the MICADAS-AMS Mannheim

After the description of the gas ion source measurement principle in section 2.3.2, this chapter deals with the implementation and characterisation of the gas ion source measurements and the Gas Inlet System at the MICADAS AMS facility in Mannheim.

### 5.1. Setup of the Gas Inlet System (GIS)

For processing of CO<sub>2</sub> gas samples for <sup>14</sup>C measurement, the ETH Zürich developed a Gas Inlet System (GIS) (Wacker et al., 2013), which is now commercially available and is distributed by the Ionplus AG (Switzerland). Such a system (see Fig. 5.1) was initially set up and adapted for the specific settings at the MICADAS in Mannheim. At the beginning of this work, the ion source of the MICADAS system in Mannheim was already equipped with an inlet for the CO<sub>2</sub>-delivering capillary (ca. 1 m length), which then only needed to be attached to the GIS.

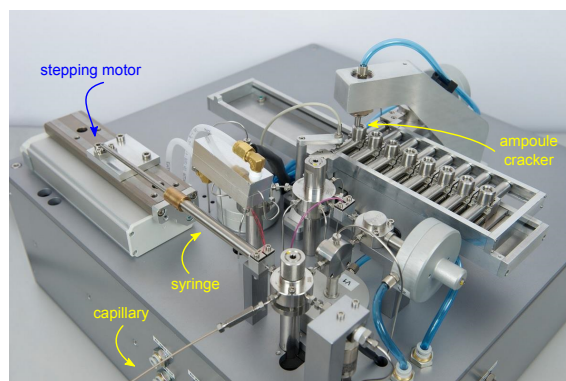
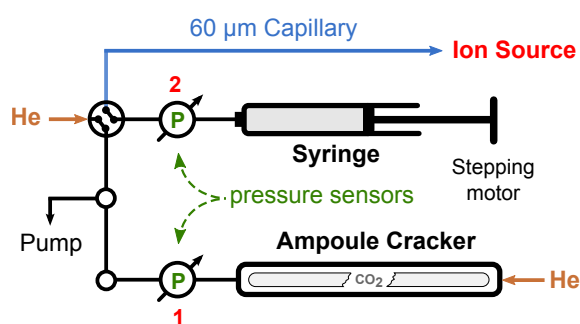


**Fig. 5.1.:** Picture (Ionplus) and schematic view (adapted from Ruff et al. (2007)) of the Gas Inlet System (GIS) built by the Ionplus AG. The sample ampoule is cracked, CO<sub>2</sub> is released and manometrically quantified, mixed with helium to desired pressure in the syringe and pushed into the ion source via the capillary.

The GIS is able to handle discrete CO<sub>2</sub> samples up to 100 µgC from sealed glass tubes (as used during this work) and alternatively the CO<sub>2</sub> output from an elemental analyser, which allows effectively continuous <sup>14</sup>C measurements. Additionally, a carbonate handling system can be attached, which enables CO<sub>2</sub> production and direct <sup>14</sup>C measurement from small carbonate samples. The GIS is controlled by a LabVIEW program, which allows completely automated measurements but also manual operation. The main process steps for <sup>14</sup>C measurements from sealed glass tubes are:

## 5. Methods - Implementation of the gas ion source at the MICADAS-AMS Mannheim

---

1. The sample ampoule (max. 4 x 80 mm) is inserted into the cracker (one cracker magazine has 8 positions) and the cracker is evacuated. At the same time the sample changer of the accelerator moves to a new gas target (see section 2.3.2), which is pre-sputtered for cleaning by purging with a helium flow through the capillary.
2. After evacuation, the sample ampoule is cracked by a pneumatically controlled stamp. The CO<sub>2</sub> is released and quantified manometrically at sensor 1 (Fig. 5.1) in order to calculate the mass of the sample.
3. Depending on the measured sample mass, the position of the syringe is adjusted (max. capacity 100 µgC) and the sample is expanded and purged into the syringe by a helium flow.
4. When the desired pressure (CO<sub>2</sub>-He-mixture) at sensor 2 in the syringe is reached, and the target within the ion source is clean, the 4-port-valve switches and connects the syringe to the capillary, injecting the gas mixture into the ion source.
5. The syringe volume is during the measurement constantly adjusted to maintain the pressure in the capillary, respectively the mass flow, constant. The CO<sub>2</sub>-He-mixture is pushed through the capillary onto the gas target, sputtered and the <sup>14</sup>C-measurement (as described in section 2.3.1) starts.
6. The sample can be measured until all CO<sub>2</sub> was pushed into the ion source (limiting factor for very small samples < 10 µgC) or until the desired accuracy is reached. A 10 µgC sample can typically be measured for ca. 3 minutes.
7. After the end of the measurement, the syringe is cleaned by sequential pumping and flushing with helium while it is moved backwards and forwards. The cracker magazine is moved to the next position and is also evacuated. During evacuation, the sample changer of the MICADAS moves to the next target and pre-sputtering for cleaning starts again.

### 5.2. Characterisation of the system performance

#### 5.2.1. Optimisation of the GIS and ion source settings

Despite the fact that the GIS was already completely mounted and operational when it was installed in Mannheim, several system parameters had to be optimised with respect to:

- Maximisation of the ion current in the AMS for best possible counting statistics and precision at simultaneous high system stability
- Minimisation of contamination and memory effects

#### Caesium regulation

The ion current retrieved from a gas sample mainly depends on the amount of caesium available for sputtering and the mass flow of CO<sub>2</sub> into the ion source. The more caesium is evaporated from the reservoir, the more can be ionised and directed onto the target for sputtering. Nevertheless, too much Cs will lead to high leak currents between the different ion source potentials, sparks and potential clogging of the target. In this regard, balancing the Cs availability (by changing the Cs

temperature) to the amount of CO<sub>2</sub> that reaches the ion source (by adjusting the syringe pressure) is the key to a stable ion production. The best results for the Mannheim MICADAS system have been achieved for reservoir temperatures between 160 °C and 167 °C with very sensitive reactions to 1 °C changes. The temperature is about 20 °C higher than for graphite samples. This is due to the fact that the ionisation efficiency of the sputtered material is much lower for gas samples than for graphite. For every measurement period, the optimal temperature has to be found within the range stated above, because it also depends on the condition of the ion source e.g. the time since last cleaning. The whole system is very sluggish with respect to temperature changes. After the first heating up from 140 °C to ca. 160 °C, it takes about two hours until the first measurable ion currents (above 3 µA) can be observed with gas samples.

### CO<sub>2</sub> mass flow regulation

Besides the availability of Cs, the ionisation behaviour and sensitivity of the ion source strongly depends on the amount of CO<sub>2</sub> deposited on the gas target surface. The CO<sub>2</sub> mass flow into the ion source can be regulated by basically two parameters: The pre-pressure in the syringe and the mixing ratio of He and CO<sub>2</sub>. Therefore, different mixing ratios of CO<sub>2</sub> in helium at different syringe pre-pressures have been tested (see Fig. 5.2) at similar ion source conditions (constant Cs temperature: 160 °C). The x-axis of the plot shows the actual amount of CO<sub>2</sub> as pressure, calculated by multiplication of total syringe pressure with the fraction of CO<sub>2</sub>. The y-axis shows the retrieved LE <sup>12</sup>C<sup>-</sup>-currents for the respective mixtures.

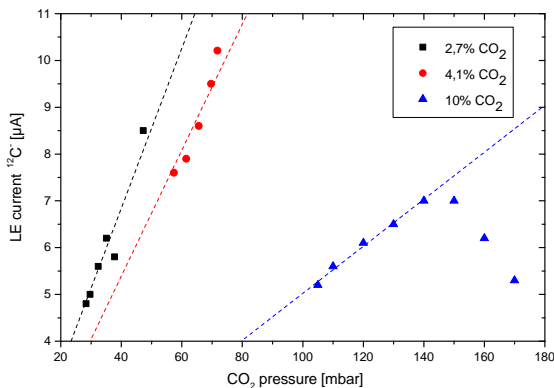


**Fig. 5.2.:** Variation of LE <sup>12</sup>C<sup>-</sup> current dependent on different syringe pressures and CO<sub>2</sub>-He-mixing ratios. The dashed lines are linear fits to the respective datasets. Note the highest current at 4,1% and ca. 10 µA

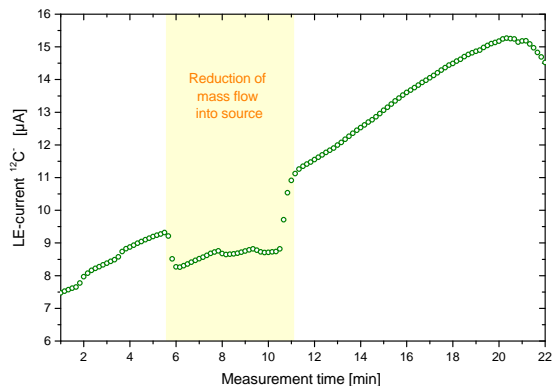


**Fig. 5.3.:** Effect of changing gas pressure on the <sup>12</sup>C ion current in the AMS. Note the distinct drop in current after reducing the mass flow of CO<sub>2</sub> into the source by reducing the syringe pressure

The samples with 2.7 and 4.1% of CO<sub>2</sub> show a typical ion current increase with increasing syringe pressure (mass flow). The ion currents of the sample with 10% CO<sub>2</sub> however drop with increasing pressures above a certain CO<sub>2</sub> pressure. This occurs, when the CO<sub>2</sub> mass flow gets too high for effective sputtering or there is not enough ionised Cs available for sputtering in the ion source. This particularly can happen during the start up phase of the system in the morning.

## 5. Methods - Implementation of the gas ion source at the MICADAS-AMS Mannheim

---

If this happens, the mass flow (pressure) has to be reduced, until the ion current starts to rise again. The highest currents could be achieved for a mixing ratio of 4.1% CO<sub>2</sub> in He and syringe pressures of ca. 1600-1800 mbar, which equals a mass flow of ca. 3.5 μgC/min. In Fig. 5.2, the data has been fitted linearly through zero (dashed lines) and the slope  $m$  of this fit can serve as a measure for the ionisation efficiency (or ion source sensitivity) in μA/mbar CO<sub>2</sub>. For 2.7% CO<sub>2</sub>, this was determined to  $m_{2.7} = (0.171 \pm 0.004)$  μA/mbar and for 4.1% CO<sub>2</sub> the fit yielded  $m_{4.1} = (0.135 \pm 0.002)$  μA/mbar. Therefore, the ionisation efficiencies of the 2.7% and 4.1% mixture do not differ very much. The 4.1 % mixture produced almost double LE currents and should thus be preferred for retrieval of better counting statistics and an overall higher system stability in terms of fractionation processes in the ion source. The slope of the 10% data (fitted only to the increasing part of the data) is with  $m_{10} = (0.044 \pm 0.003)$  μA/mbar about three times lower than the ones of the other mixtures. Therefore the 10% was not considered as an option. Fahrni et al. (2013) state a mass flow of 1.6-2.5 μgC/min, which equals a CO<sub>2</sub> - He mixture of ca. 2.5 % as the best settings for the MICADAS system at the ETH Zürich. During this work, the results achieved with the parameter set described above (4% CO<sub>2</sub> in He, 1600-1800 mbar) have been regarded sufficiently good for stable and reproducible gas measurements, but there is still room for optimisation.

Figure 5.3 illustrates the typical course of a gas measurement at the example of oxalic acid. The ion current starts at ca. 7 μA and rises slowly, the small variations are manual pressure increases. After six minutes, the syringe pressure was dropped on purpose and the ion current drops accordingly. By application of the original mass flow again, the ion current recovers very fast and continues rising to ca. 15 μA over 20 minutes of measurement time. The best currents that could be achieved with this setup so far were about 17 μA. Measurements are usually performed at 8-12 μA, which yielded the highest stability of the system.

### 5.2.2. Standard and blank measurements - reproducibility

For interpretation and isotope fractionation correction (see section 2.2.3) it is necessary to measure standard and blank materials along with the real samples.

#### Oxalic acid II measurements

During this work, oxalic acid gas (OxII) with a <sup>14</sup>C-content of 1.3408 F<sup>14</sup>C and  $\delta^{13}\text{C} = -17.8$  ‰ and blank (<sup>14</sup>C-free) CO<sub>2</sub> gas of mineral origin, used in the conventional <sup>14</sup>C dating laboratory at the IUP have been measured for standard and blank corrections. The gases have been directly expanded into the syringe and were mixed with helium to a 4% ratio. Oxalic acid standards are typically measured to a relative error of ca. 0.8% (20 000 <sup>14</sup>C-counts). For every set of samples, at least two oxalic acid measurements have been performed, ideally one before and after every eight samples (1 cracker magazine) to ensure the stability of the system. The results of all OxII measurements over a course of ca. two years time are shown in Fig. 5.4. The dashed lines mark the expected values for <sup>14</sup>C and  $\delta^{13}\text{C}$  respectively. For the <sup>14</sup>C values, 1σ error bars are shown.

The Oxalic acid results of each measurement period are normalised to the expected value, so Fig. 5.4 shows only the degree of scatter around that fixed literature value (dashed lines). The <sup>14</sup>C results have a very small standard deviation of 0.008, which equals 0.6% of the literature value and is thus smaller than the relative error of each individual measurement. Also no drifts of the OxII results over each measurement period could be observed.

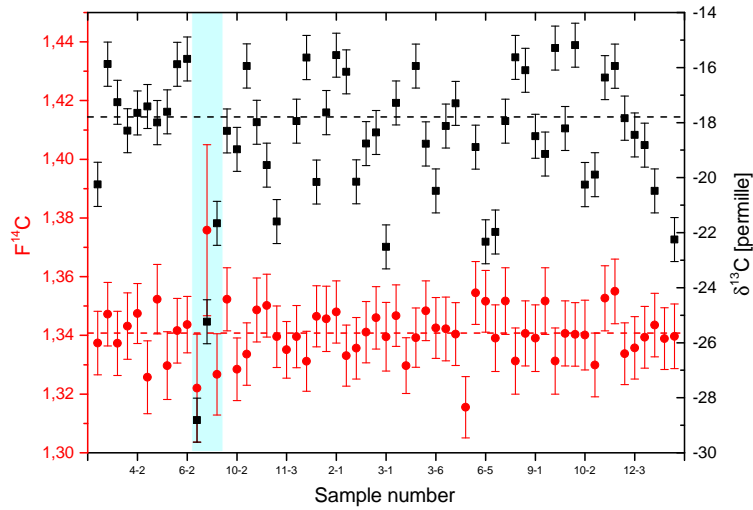


**Fig. 5.4.:** Measurements of standard material (Oxalic acid II) as  $\text{CO}_2$  over the course of two years. The dashed lines mark the expected value. All results measured to ca. 0.8% counting error agree well with the expected values, the blue area marks samples with smaller measurement times and thus larger errors

The  $\delta^{13}\text{C}$  results show a larger scatter, which can be due to fractionation processes within the ion source, but still with an overall relatively good agreement (standard deviation of 2.8) with the expected value. For every period of measurements, the average of all oxalic measurement has been used as reference for the calculation of the sample  $F^{14}\text{C}$ .

Additionally to these oxalic acid standards from the tank, a set of small oxalic acid samples prepared at the IUP Heidelberg have been measured as samples and not as normalised standards. This was done to test the reproducibility of the ampoule cracking procedure, which was used for all ice samples. These samples were chosen in size ranges where the latter ice samples were expected. They have been manometrically quantified in the measuring volume described in section 6.5 and were flame sealed into glass tubes of 4 mm diameter. They have been processed in the GIS along with normal (ice) samples. The results are shown in Fig. 5.5 again with  $1\sigma$  errorbars. Most of the samples hit the expected  $^{14}\text{C}$ -value within  $1\sigma$  uncertainty. Even for the very small samples below  $10\ \mu\text{gC}$ , there is no trend in  $^{14}\text{C}$  values, which excludes a significant blank contribution and thus no bias of the real samples. The mean  $^{14}\text{C}$ -value for all samples is:

$$\overline{\text{Oxa}_{\text{HD}}} = (1.334 \pm 0.03) F^{14}\text{C} \quad (5.1)$$

The depletion in  $\delta^{13}\text{C}$  for very small samples is probably due to fractionation processes within the ion source. This will however not affect the  $^{14}\text{C}$ -results, because the fractionation in  $^{14}\text{C}$  will be corrected accordingly (see section 2.2.3).

## 5. Methods - Implementation of the gas ion source at the MICADAS-AMS Mannheim

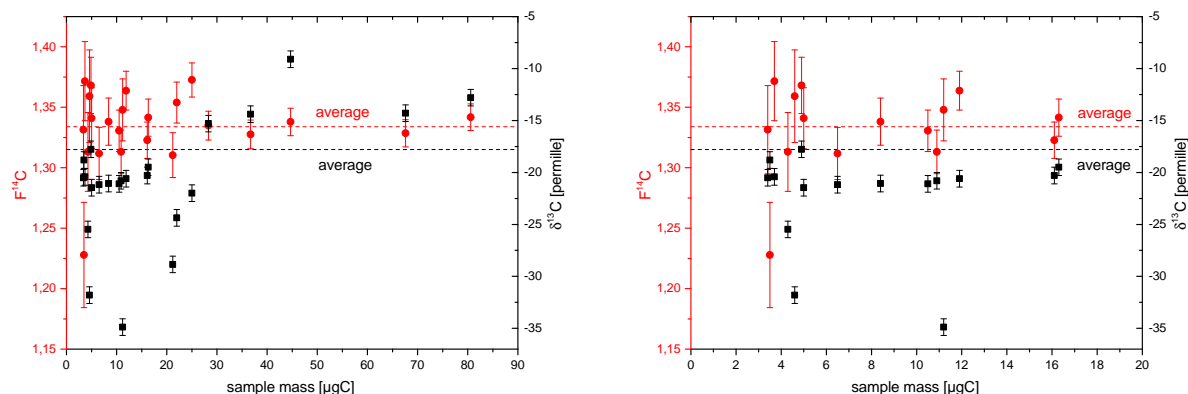


**Fig. 5.5.:** **Left:** Results of small (down to ca. 3  $\mu\text{gC}$ ) oxalic acid gas samples prepared at the IUP. The  $^{14}\text{C}$  results agree reasonably well with the expected value. The depletion in  $\delta^{13}\text{C}$  for the very small samples is due to a fractionation in the ion source at very low ion currents. **Right:** Zoom to the section of smallest sample sizes.

### Blank gas measurements

For the blank correction, similar to the oxalic acid measurements directly from the tank,  $^{14}\text{C}$ -free  $\text{CO}_2$  gas of fossil origin has been measured (4% in He). All measurements were run for ca. nine minutes, which equals the approximate measurement time for the oxalic acid measurements used for standardisation.

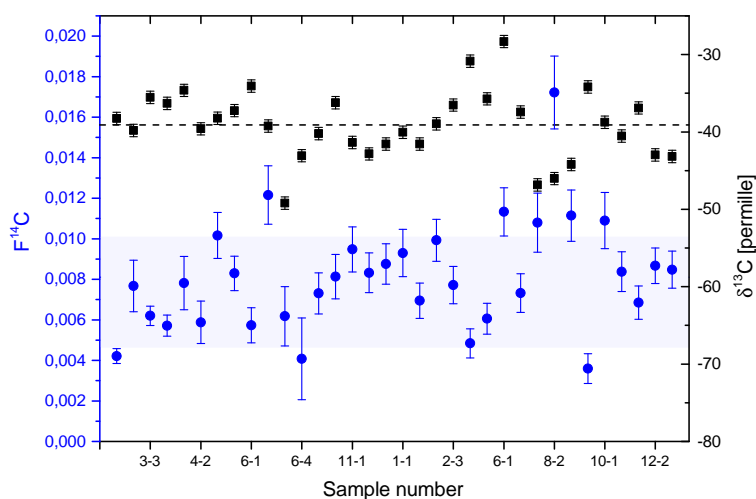


**Fig. 5.6.:** Measurement of blank material (fossil  $\text{CO}_2$ ) over the course of two years. Results are in the range of 35 000 - 40 000 years BP (uncalibrated), which is reasonably good for all measured samples. The dashed lines mark the average values of all measurements, no trend is visible.

## 5.2 Characterisation of the system performance

---

The results for all blank samples (see Fig. 5.6) measured over the course of ca. two years are scattering around an average  $^{14}\text{C}$  content of

$$\overline{\text{Blank}}_{\text{MA}} = (0.0081 \pm 0.0027) \text{ F}^{14}\text{C} \quad (5.2)$$

which results in  $^{14}\text{C}$  ages of 35 000 - 40 000 years BP. This is slightly higher than the blank measurements with graphite samples (in the range of ca. 50 000 yBP), but still low enough for the expected age ranges of the ice samples, which are in the range of several thousand years. They are also comparable to the results found by Fahrni et al. (2013) for the ETH system. The slightly enhanced blanks could likely be due to a small leakage at the valve of the gas tank, which will be fixed for future measurements. The blank results do not show a trend, which implicates, that there is no contamination accumulating in the system over time and thus reliable measurements even of very old samples are possible.

### 5.2.3. Memory effect

To avoid cross contamination between samples, it is crucial to ensure that the sample handling system is cleaned sufficiently. All dimensions of tubing (1/16") and valves are designed for minimal internal volumes to avoid sample losses during manometric quantification and transfer into the syringe. Because of the small diameters of the tubing, pumping alone is not a sufficient way to remove remaining gases from the system. Usually, the cracker and the syringe are pumped and flushed with helium twice after every sample, while the syringe is additionally moved forwards and backwards. This cleaning procedure is done automatically.

To test the effect of just pumping the system without any helium flushing, two oxalic acid and two blank samples have been measured directly after each other without any additional cleaning of the cracker / syringe than just pumping for ca. 3 min. As the results in Table 5.1 show, all  $^{14}\text{C}$  values are within the ranges stated above for the overall mean and there is no cross contamination visible, even without the helium flushing step and despite a large difference in absolute  $^{14}\text{C}$  values of sequential samples. The memory effect should therefore not play a role for the routine measurements.

**Tab. 5.1.:** Sequential measurements of oxalic acid and blank gas to investigate possible cross contamination within the GIS

Sample type	$^{14}\text{C}$ [pmC]
Oxalic acid	$134.83 \pm 1.12$
Blank CO <sub>2</sub>	$0.74 \pm 0.09$
Oxalic acid	$134.64 \pm 1.11$
Blank CO <sub>2</sub>	$0.92 \pm 0.09$

## 5. Methods - Implementation of the gas ion source at the MICADAS-AMS Mannheim

### 5.2.4. Very small samples (< 10 µgC)

The processing of very small samples below 10 µgC can be difficult, but is very important for the  $^{14}\text{C}$  measurement of Alpine ice samples, where the retrieved carbon masses usually are in that range. For these small samples, the danger of material loss during sample transfer from the cracker to the syringe rises. Additionally, the accuracy of the  $\text{CO}_2 / \text{He}$  - ratio declines, because the pressure sensors are not very precise for those very small volumes. The pressure adjustment can be supervised manually, but still most of the time too much He is inserted into the syringe and so the mixing ratio is smaller than 4%. This results in smaller carbon mass flows to the ion source and thus lower currents (see section 5.2.1). For samples below 5 µgC, the ion current can thus drop down to half of the current achieved with normal sized samples. This results in a lower number of  $^{14}\text{C}$  counts and together with a very short measurement time in an increasing statistical error. Samples below 5 µgC often yield less than 1000 counts, with average errors of 3-8%, whereas samples of normal size > 10 µgC usually have a relative error of 1-2%. The smallest sample that could successfully be measured so far, had a mass of 1.1 µgC and was counted to a relative error of 7%.

### 5.2.5. Summary of the Gas Ion Source characteristics

The key settings and characteristic parameters of the gas ion source and Gas Inlet System at the MICADAS-AMS in Mannheim as they have been determined and used during this work are summarised in Table 5.2.

**Tab. 5.2.:** Summary of the characteristic gas ion source system parameters

<b>Process parameter</b>	
Cs reservoir temperature:	160 - 167 °C
$\text{CO}_2$ in Helium, volume ratio	4%
Average carbon mass flow:	3.5 µgC /min
Maximum $^{12}\text{C}^-$ LE current:	17 µA
Average $^{12}\text{C}^-$ LE current (> 10µgC):	8-12 µA
Average $^{12}\text{C}^-$ LE current (< 5µgC):	5-10 µA
Sample size range:	2-100 µgC
Average blank $\text{F}^{14}\text{C}$ :	$\overline{\text{Blank}}_{\text{MA}} = (0.0081 \pm 0.0027)$
Average precision for samples > 10 µgC:	1-2%
Average precision for samples < 10 µgC:	3-7%

With this set of settings and characteristic parameters, the gas ion source can now be used on a routine basis. The largest room for further optimisation is the investigation of the optimal carbon mass flows and  $\text{CO}_2 / \text{He}$  ratios for the feeding of samples into the ion source.

## 6. Methods - Optimisation of the POC extraction system

*The method improvements of POC extraction from ice samples and preparation for  $^{14}\text{C}$  analyses described in this chapter are all dedicated to the achievement of a maximum filtration efficiency and a minimal sample contamination. Therefore the main goal is to achieve a process blank if possible below  $1\ \mu\text{gC}$ . This is crucial to enable reliable  $^{14}\text{C}$  measurements of samples in the mass range below  $10\ \mu\text{gC}$ , typical for high Alpine ice samples.*

### 6.1. General remarks on filtration media for POC separation

One of the key parts of any POC extraction for  $^{14}\text{C}$  measurements is the step of sample filtration. Here, the particles are in a first order separated by size. The main requirements for the filter material are:

- Low organic contamination (blank contribution) of the filter material, cleanable of all organic residues before use (by preheating)
- No disintegration of filter material during combustion and acidification
- Easy to handle
- Small clogging effects

These requirements restrict the possible filter materials to mainly quartz fibre and silver membrane filters. These two filter types largely differ in their filtration principles. (Brock, 1983). Quartz fibre filters are depth filters, made of a mat of overlapping fibres (see Fig. 6.1 left) and thus do not have a technically defined pore size. Here, filtration happens by trapping of particles within the winding pathways of the fibre mat. Also adsorption of particles to fibres is possible (see e.g. Hou et al. (1980)). The pore size is thus defined operational and varies from the manufacturer's declaration of  $2.2\ \mu\text{m}$  for liquids (Whatman, QM-A filters) to experimentally defined pore sizes of down to  $0.3\ \mu\text{m}$  (Kuchiki et al., 2015).

Silver membrane filters have better defined pore sizes (see Fig. 6.1, right), created by etching of the material, which leads to a more sieve-like structure. Here in general a sharper size selection of particle by choice of pore size is possible. The main size separation of particles happens on the surface of the filter, where all particles bigger than the pore size of the filter are retained. This leads however to a fast clogging of the filter pores compared to the quartz fibre filters. For a nominal pore size in the same range, thus the membrane filter will retain smaller particles than the fibre filter (see e.g. Kuchiki et al. (2015)).

## 6. Methods - Optimisation of the POC extraction system

---

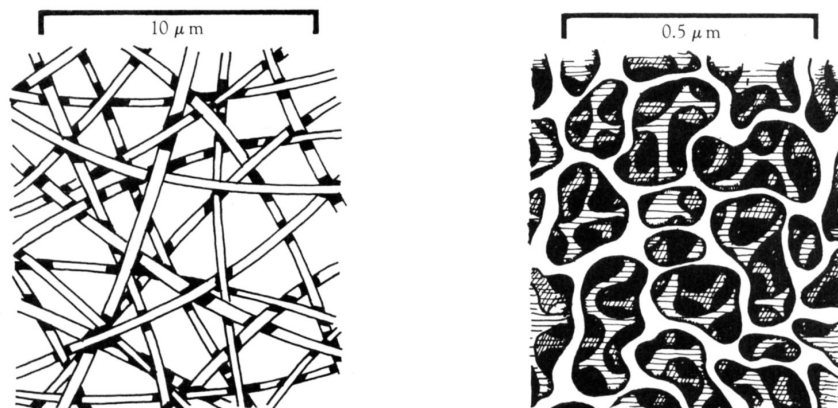


**Fig. 6.1.:** Schematic view of the internal structure of depth filters (e.g. quartz fibre filters, left) and membrane filters (e.g. silver membranes, right). Note the very variable interstices of the fibre filter. Figures taken from Brock (1983)

Both filter types can be preheated to remove organic contaminations (silver: 500 °C, quartz: 800 °C). The silver membrane filters are however much better to handle when wet, where the quartz fibres are very delicate and tend to defibre. For POC filtration of high Alpine ice samples with very low POC concentrations, it is on first order desirable to have a filtration efficiency as high as possible. This would lead to the use of membrane filters with small pore sizes, which however have the drawback of very fast clogging. During this work, both filter types have been in use, depending on the respective filtration requirements. Silver membrane filters with a large pore size for size separation (Sterlitech, silver membrane 13 mm, 5 μm pore size) were used in the so-called offline filtration system. This pore size was chosen to prevent the membranes from clogging and to only collect the large particle fraction (see Section 9.3.1). Quartz fibre filters (Whatman QM-A, nominal pore size 2.2 μm) have been used in the online filtration system REFILOX developed within this work, for collection of a broad cross section of particle sizes. Both systems will be described and characterised in the following.

### 6.2. Pre-existing offline filtration system at the IUP Heidelberg

In this section the already existing POC filtration system at the IUP Heidelberg is described shortly. This system was developed in advance of this work (Hoffmann, 2010) and provides the basis for all method improvements achieved within this study.

The filtration unit of this system is schematically shown in Fig. 6.2. It mainly consists of a 2l PFA (perfluoroether) bottle, where the ice sample is inserted through the inlet. At the outlet of the bottle, a filter holder containing a silver membrane filter is mounted. Here, in contrast to the early system used by May (2009) (see Section 4.2.2), the meltwater of the sample is directly filtered after melting under a clean atmosphere. This avoids the step of intermediate storage, which minimises potential losses of sample material by adhesion to the walls and sedimentation. After filtration, the filter has to be taken out of the holder and is inserted into a glass ampoule for combustion (with O<sub>2</sub>) followed by cleaning and manometric quantification (see Section 6.5).

This step holds the risk of additional contamination during handling of the filter, together with potential losses of material during removal and insertion of the filter into the glass tube particularly. Another disadvantage of the offline system is the combustion of the sample in a sealed glass tube, which allows only one combustion temperature to be applied and therefore no thermal separation of different carbon fractions (see Section 6.6).

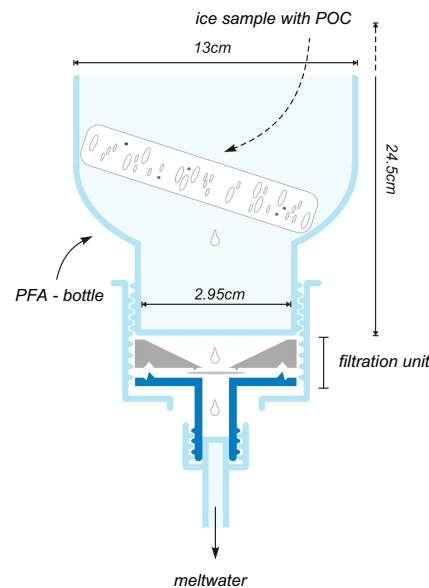


**Fig. 6.2.:** Offline POC filtration system for direct filtration of meltwater and silver membrane filters still in use at the IUP. the sketch only shows the lowest part of the melting vessel (a 2l closed PFA-bottle) and the filtration unit.

This so-called offline filtration system was still in use during this work, the characterisation is discussed in Section 6.3.2 .

### 6.3. Process blank reduction

At the starting point of this work, the offline system mentioned above had a major problem with high and variable contamination (ca. 6-30  $\mu\text{gC}$ ) due to an insufficient cleaning method for the solid ice samples (Hoffmann, 2010). The main goal of all POC extraction system optimisation measures are therefore:

1. Reduction and stabilisation of the blank
2. Increasing of the carbon extraction efficiency

Blank in this context means process blank. This describes the amount of particulate organic carbon that was not originally part of the ice sample and has been introduced by contact with organically contaminated surfaces and lab air. Sources for such contamination can be summarised to:

## 6. Methods - Optimisation of the POC extraction system

---

### Primary contaminations

Contaminations, already present in the sample, when preparation in the lab starts

- Use of organic drilling liquids (e.g kerosene), at the ice core drilling process
- Inscriptions on the ice surface, often done by pencil (graphite)
- Surface contamination of the sample with textile fibres (from gloves) at initial handling and packing of the sample in the field
- Surface contamination introduced by earlier analyses of the sample

### Secondary contaminations

Possible sources for contaminations during the sample preparation and processing

- Sample contamination during handling and cutting of the ice in the cold room (textile fibres from gloves and clothes, dirt on the saw blade)
- Adsorption of air dust particles onto the surface of the ice sample
- Contact of the sample with possibly contaminated surfaces (transport box, melting pot, filtration system)
- Contamination by impure rinsing liquids for vessel cleaning (ultra pure water - MQ) and acid
- Intrinsic contamination of the filter

For high Alpine ice samples, where carbon sample sizes are often limited to  $< 10 \mu\text{gC}$ , the overall aim for the process blank is thus to keep it ideally below  $1 \mu\text{gC}$ . This limit is set to ensure that the blank does not influence the sample mass by more than 10%.

#### 6.3.1. Blank reduction - the problem of clean ice

The best method to determine the process blank of the whole ice sample preparation system is to run an artificially created or natural ice sample, which is evidently POC free (e.g. Antarctic ice), through the sample preparation process and measure the carbon mass that was introduced on the way. A major problem is here to guarantee the initial purity of the ice, which is crucial to finally decide if the decontamination routine was successful or not. Tests revealed that it is not straight forward to create particle free (organic or inorganic) ice. Just freezing ultra pure water (further called MQ, created by a PURELAB ultra analytic system,  $18.2 \text{ M}\Omega\text{-cm}$ , 1-2 ppb TOC (ELGA, 2016)) in PE-foil or other materials yielded absolute blank masses of  $2.7\text{-}7.1 \mu\text{gC}$ , which equals  $8\text{-}25 \frac{\mu\text{gC}}{\text{kg}}$  (measured with the offline filtration system). The data can be found in Table A.3 in Appendix A.2.

Based on these high and variable results, it was therefore attempted to create particle free ice on the basic principle of slow freezing of water by constant movement. This method has been used for growth of single ice crystals for many years (Bridgman method, see e.g. Higashi (1974); Thibert and Dominé (1997)). Slow freezing of water leads to a separation of solutes and particles in the liquid phase from an impurity free solid ice crystal (Halde, 1980; Shafique et al., 2012). To

track the particle accumulation in the blank ice tests within this work, a water sample in PE-foil was spiked with a UV-fluorescent powder, consisting of plastic particles in the size range of a few micrometers. The water was frozen on a lab shaker at  $-20\text{ }^{\circ}\text{C}$  for two days. During this slow freezing, the particles have enough time to move ahead of the freezing front and accumulate in the centre of the block, where a large air bubble forms (Fig. 6.3, a not shaken PE (polyethylene) foil sample for comparison). The so collected particles can be cut out easily and the remaining ice block is completely particle and thus POC free. This routine (without particle spiking) has been applied for all blank ice samples discussed in this work.



**Fig. 6.3.:** **Left:** MQ-water frozen in PE-foil spiked with fluorescent powder. Most of the particles accumulate in the middle, where the water freezes last, but there is also still a fraction homogeneously distributed over the complete ice block. **Right:** MQ-water frozen in PE-foil spiked with fluorescent powder and frozen on a lab shaker. By shaking, freezing is so slow that all particles have time to accumulate in the middle of the sample and can be cut out. The rest of the ice is completely particle free (pictures taken from Leinfelder (2012))

### 6.3.2. Improvement of the decontamination routine

Past experiences (Hoffmann, 2010) showed that decontamination of the solid ice sample and the handling until its insertion into the melting vessel is the most critical part where contamination occurs. Therefore, the decontamination routine was adapted to the routines used for analyses of DOC and volatile organic species in high Alpine and Antarctic ice samples, which are even more prone to contamination (Preunkert et al., 2011; De Angelis et al., 2012). The decontamination routine includes the following steps:

- Sawing of the ice sample to remove larger surface contaminations (e.g. writings, drilling liquid)
- Scraping of the sample surface with a ceramic knife to remove sawing powder from the bubbles
- Tempering of ice sample to  $0\text{ }^{\circ}\text{C}$  to avoid cracking of the sample
- Washing of the sample surface with MQ-water

## 6. Methods - Optimisation of the POC extraction system

---

Washing of the sample and the additional use of protective clothing to avoid the deposition of textile fibres on the ice sample and filter proved to be the most important improvements in terms of blank reduction in the new decontamination routine. For a better overview, the major changes in the ice sample preparation routine are summarised in Table 6.1. A more detailed description of the decontamination routine can be found in Appendix A.2.2.

**Tab. 6.1.:** Comparison of the major elements of the old and new ice sample decontamination routine

Preparation step	Old routine	New routine
<b>Ice sample handling</b>	latex gloves no protective clothing, samples moved by hand	latex gloves and protective clothing, ice samples only touched by forceps after cutting
<b>Cutting of sample</b>	electric band saw	electric band saw
<b>Cutting powder removal</b>	none	scraping with ceramic knife under laminar flow
<b>Tempering</b>	30 min. in PFA box	30 min. in PFA box
<b>Washing</b>	handheld under MQ-water	washing each side in MQ-water stream, held by forceps

The combination of all those cleaning steps leads to an average mass loss of the original sample of ca. 20-40% from cutting to melting and is still in the range of the values found by May (2009), although the scraping step was added. This loss has to be calculated on top of the required sample mass, when samples are selected. With this improved decontamination routine, a reliable and reproducible procedure was found that was applied to all ice samples during this work. The discussion of the achieved POC blank values can be found in Section 6.6.1.

### 6.4. Development and setup of the online cleaning - filtration - combustion unit REFILOX

Within this work, the existing offline POC filtration unit briefly described in Section 6.2 (for details see Hoffmann (2010)) was complemented by a new, completely independent system, whose development comprised a major part of the presented work.

The main reasons to build this new setup in addition to the already existing one can be summarised in the following aims:

1. Keep the danger of sample contamination and thus the process blank as low as possible by construction of a setup that unifies the processes of cleaning, filtration and combustion in one closed system
2. Improve the filtration efficiency and reduce the potential sample losses and contamination by avoiding the removal of the filter after filtration for combustion. Removing of the filter

## 6.4 Development and setup of the online cleaning - filtration - combustion unit REFILOX

after filtration holds the risk of contamination by adsorption of DOC onto the wet surface, which has been found to be potentially as high as  $0.2 \mu\text{gC}/\text{min}$  (Preunkert et al., 2011).

3. Develop a setup that allows fast quantification of the POC content of a sample without the time consuming combustion and cleaning process of the offline system, thus speeding up the whole process
4. Build a setup that allows stepwise heating and makes combustion at different temperatures for the same sample possible, which can be desirable for thermal separation of organic fractions (see Section 6.7.1)

This new online setup called REFILOX (REinigungs-FILtrations-OXidations-Einheit) is completely home-made and will now be described and characterised in detail.

### 6.4.1. Description of the system components

#### Technical prerequisites

Out of the scientific aims stated above, some technical demands on the different parts of the system arise, which determined the following choice of the single components:

- Use of inert and easy to clean materials (PFA, glass, stainless steel)
- Airtight filtration unit to avoid entering of ambient air during the combustion process
- Easy access for cleaning of the whole setup

#### Melting vessel

The melting vessel for the ice samples is a 2l PFA standard bottle upside down (PFA: perfluoroalkoxy alkanes (special type of Teflon)), which provides a very hydrophobic inner surface that allows an almost traceless runoff of the meltwater. This material was preferred over glass, because glass surfaces are much harder to clean, especially from black carbon (Lim et al., 2014). Additionally, PFA allows the application of larger air pressures without breaking the vessel. The ice samples have to be inserted through the bottleneck and are thus restricted to a maximum diameter of 5.4 cm or an edge length of 3.8 cm for rectangular samples. At the bottom of the bottle, there are two inserts for adding of hydrochloric acid and application of a synthetic air (20%  $\text{O}_2$  / 80%  $\text{N}_2$ , free of trace gases) over pressure.

#### Filtration unit

The major part of the filtration unit is a quartz glass tube with a sealed-in quartz frit (porosity 2). This quartz tube is connected to a CF 16 vacuum flange (VACOM) via a glued glass-metal-transfer on both sides. On top of the frit, by use of a tweezer, a quartz fibre filter (9 mm diameter) can be applied, which is then fixed by an inner quartz tube. This tube is loose and pushes down onto the filter by the pressure of a spiral spring, which itself is fixed by downward push of the flange seal. The meltwater coming down from the bottle is introduced through a stainless steel water duct, which is connected to the upper flange and allows directing of the water drops straight onto the filter without touching the copper seals of the flange (see Fig. 6.4 right). Pictures of the REFILOX filtration system can be found in Fig. A.5 in Appendix A.2.

## 6. Methods - Optimisation of the POC extraction system

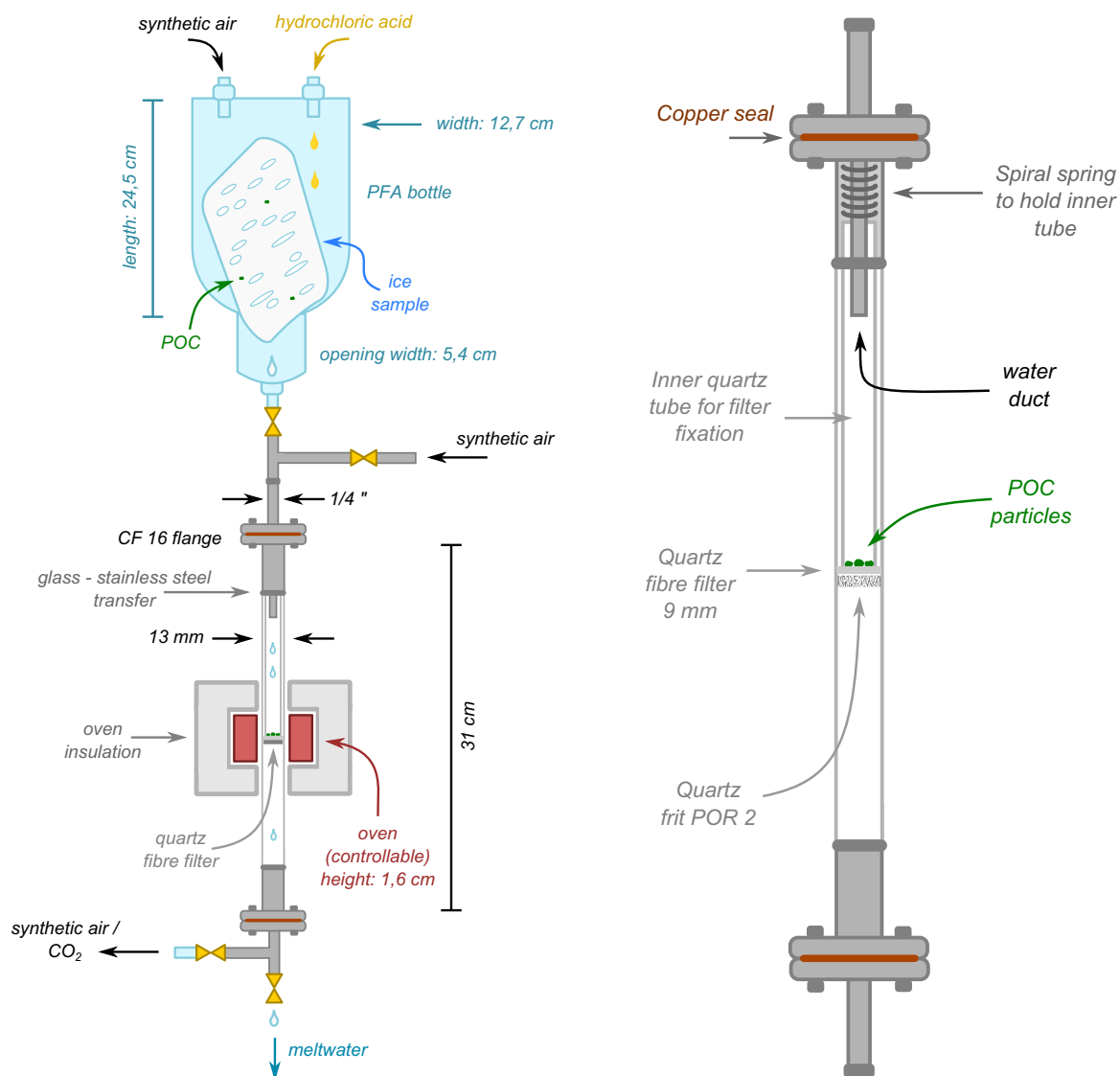


**Fig. 6.4.:** Schematic views of the main parts of REFILOX. **Left:** Overview of the filtration combustion unit with all major components. The oven is mobile, it can be attached and removed as required. The filtration part of the system is airtight. **Right:** Detailed view of the inner part of the filtration system. The filter is placed on top of a fixed quartz frit and pressed down by the inner glass tube, which itself is fixed by the pressure of a spiral spring. Pictures of the system are shown in Fig. A.5 in Appendix A.2.

### Heating system

The oven unit was developed and custom built by the workshop of the IUP (Leinfelder, 2012). It consists of two half-shells made of tool steel, that can be clipped around the filter section of the quartz tube and fit tightly onto the tube for maximum heat transfer. The two steel blocks are heated by four glowplugs and each has a separate temperature control. The oven temperature

can be chosen manually and is then regulated automatically by adaption of current and voltage between ca. 50 and 950 °C with an accuracy of about 5 °C. The oven unit is isolated by an outer shell of ceramic that is clipped around the heated parts to keep the temperature on the inside as stable as possible.

### Connecting units

All connections in the system, apart from the two CF-flanges, consist of Swagelok tube fittings and are made of stainless steel. The connecting valves to the bottle, the air inlet and outlet and the meltwater outlet are Swagelok stainless steel ball valves. When all valves are closed (see Fig. 6.4 left), the center of the system, where the filter is located and the combustion takes place, is therefore vacuum tight.

## 6.5. Sample handling in the REFILOX system

The whole POC sample preparation for  $^{14}\text{C}$ -dating involves many different steps and will be now explained. A schematic view of the individual processing steps is shown below.

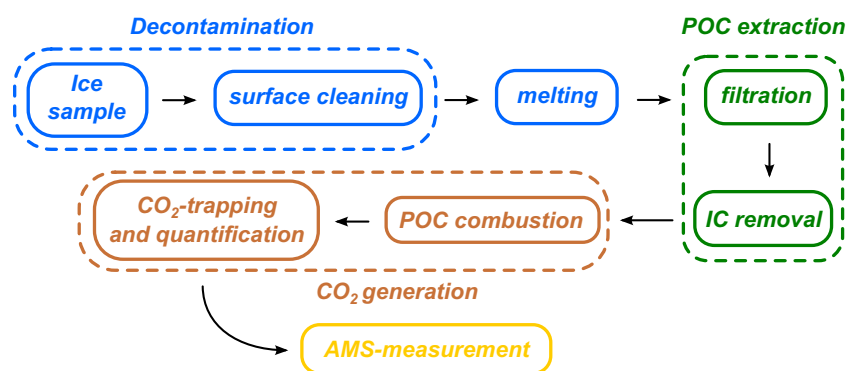


**Fig. 6.5.:** Schematic view of the sample processing steps for POC extraction

Sample preparation starts with the sawing and surface decontamination of the solid ice sample, which proved to be the most critical part of the preparation procedure in terms of process blank. A schematic overview over the whole POC extraction system including the vacuum line for cleaning and quantification is shown in Fig. 6.7.

### Cleaning of the system

A very important part before and after the processing of an ice sample is the cleaning of the whole system. The vacuum line connected to the REFILOX (see Fig. 6.7) is pumped (down to a minimal pressure of ca.  $2 \cdot 10^{-6}$  mbar). The melting pot is rinsed three times with a 5% solution of ammonia and MQ-water. All stainless steel connections between the melting pot and the filtration unit and the inner quartz tube are cleaned separately in an ultrasonic bath for 10 min. The filtration unit is wiped with fibre free tissues and ammonia and rinsed with an inorganic alkaline cleaner (Roth, RBS 50). A new quartz filter is inserted to the tube and after re-assembly of the whole system together with the PFA-bottle on top, it is rinsed first with HCL

## 6. Methods - Optimisation of the POC extraction system

(0.2M) and second with RBS 50. After the cleaning solutions, is flushed with ca. 4l of MQ-water to wash out remaining contaminations.

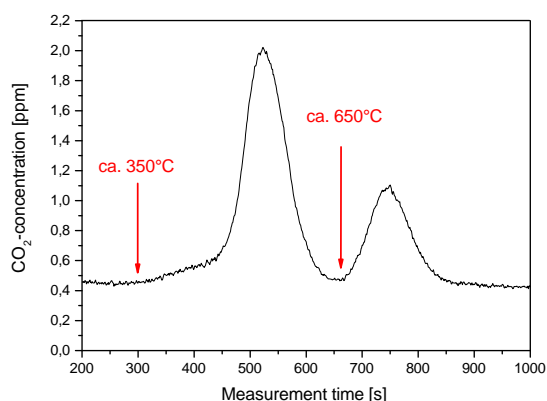


**Fig. 6.6.:** Pre-heating of the quartz filter at 900 °C to remove intrinsic and by rinsing accumulated contamination. Typically two combustion peaks arise, the first starting at ca. 350 °C and the second at ca. 600 °C.

Then, valves 1 and two are closed, the system is purged with synthetic air and the CO<sub>2</sub> content of the air is monitored online by a infrared CO<sub>2</sub> detector. The oven is put around the quartz tube, and when the CO<sub>2</sub> concentration in the purging gas drops below ca. 0.5 ppm, heating to 900 °C starts. During the course of heating, usually two peaks evolve. The first one starting at ca. 350 °C and the second around 650 °C. The two peaks represent different organic carbon fractions, this will be discussed in detail in Section 6.7.1. For the particular measurement shown in Fig. 6.6, the sum of the combusted carbon was ca. 4 µgC, which is quite characteristic for a cleaning step. When the peak has declined, the filter is cleaned from all carbon contamination and prepared for the next sample. This cleaning procedure has been applied before every sample and proved to be effective enough to avoid any memory effects.

### Melting of sample

After surface decontamination, the ice pieces are placed inside the melting vessel in a laminar flow box. The bottle is immediately closed with a screw cap and placed upside down on top of the filtration unit. It is attached to the filtration unit via a screw connection. A stream of synthetic air is connected to the bottle (1-1.5 bar), to press the evolving meltwater directly through the filter. The melting process is sped up by illumination of the bottle with an infrared lamp. Still, 500g ice take about 2-2.5 hours to melt completely.

### Inorganic carbon (IC) removal and drying of filter

After the ice is completely melted, a few drops of hydrochloric acid (0.2 M) are applied onto the filter (see Fig. 6.7). This serves to remove all inorganic carbon (IC, mostly carbonates) from the sample. After acidification, the oven is attached to the quartz tube and set to 75 °C to speed up the reaction and dry the filter. Simultaneously, the top and bottom valve of REFILOX are closed (1 and 2 in Fig. 6.7), to shut the system from ambient air and the filtration system is purged with a stream of synthetic air (400 ml/min). This stream is led through a water trap cooled down to -78 °C by a acetone - dry ice - mixture and a flow controller to the CO<sub>2</sub> detector.

This detector monitors the CO<sub>2</sub> concentration, which can be watched online. When the measured CO<sub>2</sub> content of the gas stream drops below ca. 0.2 ppm, the system is considered to be clean and combustion can start. This purging process usually takes about 45 min.

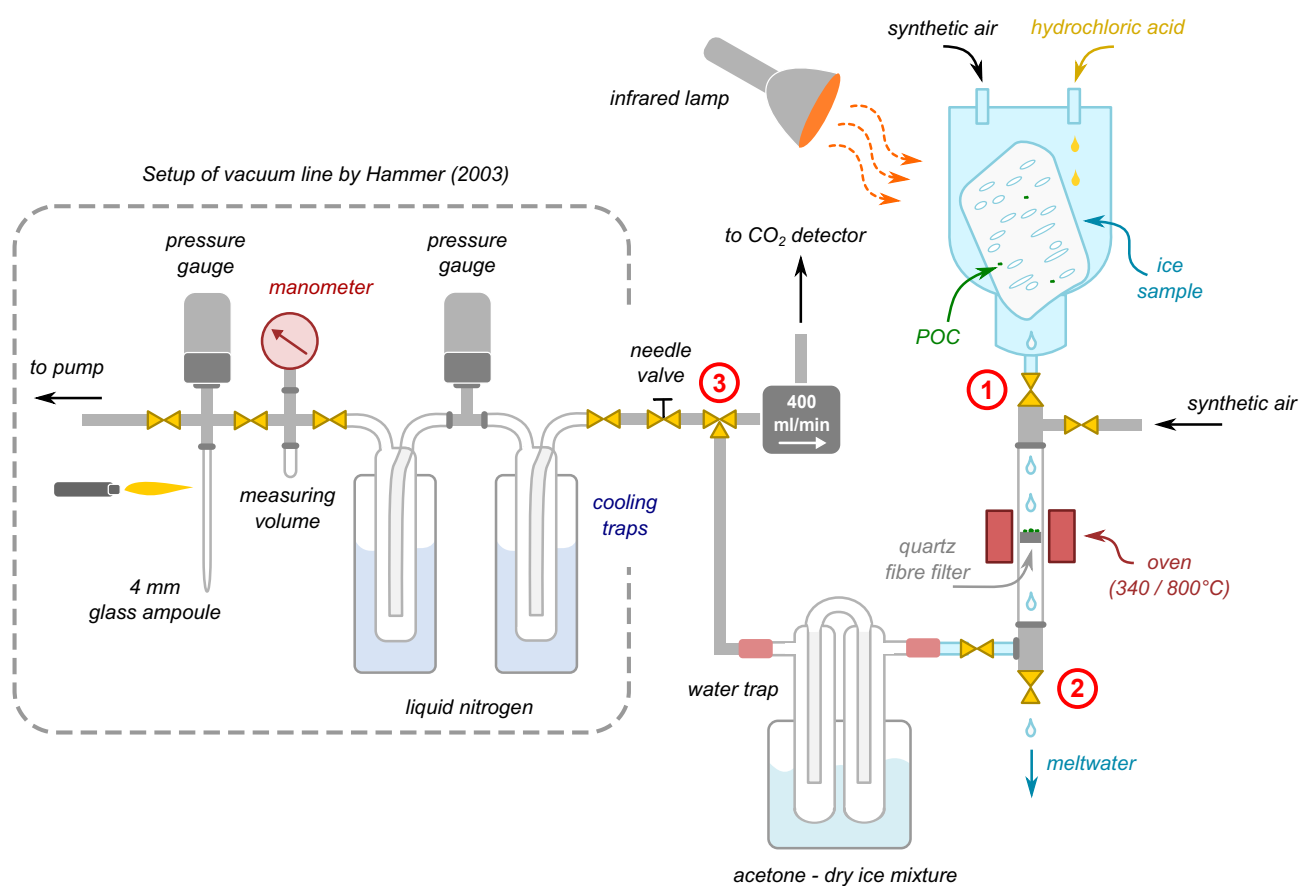


**Fig. 6.7.:** Schematic overview over the complete POC extraction and cleaning system. The process starts on the right with melting and filtration of the ice sample in the REFILOX. After filtration, the sample is acidified and combusted to CO<sub>2</sub>, which is purged out with synthetic air. The CO<sub>2</sub> is then collected in the cooling traps under liquid nitrogen temperature at ca. 20 mbar total pressure to avoid condensation of O<sub>2</sub>. After cleaning of residual gases and manometric quantification, the CO<sub>2</sub> is flame sealed in a 4 mm glass ampoule and ready for AMS-measurement. The setup of the vacuum line was not part of this work, a description and characterisation can be found in Hammer (2003) and May (2005).

### POC combustion

Before the heating starts, the pressure in the filtration system is reduced to 800 mbar by pumping shortly through the vacuum line. This is done to avoid large over pressures in the quartz tube during the high temperatures of combustion. After the pressure reduction, valves 1 and 2 are closed and thus the quartz tube functions as a combustion ampoule. The desired combustion temperature is set and the oven heats up, which takes between 3 and 10 minutes maximum for a maximum temperature of 900 °C. The sample is combusted for 30 minutes, then the CO<sub>2</sub> trapping starts.

## 6. Methods - Optimisation of the POC extraction system

---

### CO<sub>2</sub> trapping and quantification

After the combustion, both cooling traps in the vacuum line are cooled with liquid nitrogen, valve 1 and 2 are opened and the CO<sub>2</sub> created from the combustion of the POC is purged into the vacuum line, which is continuously pumped, while CO<sub>2</sub> is caught in the traps. The gas flow is regulated by a needle valve to make sure that the pressure in the traps does not exceed 200 mbar, when O<sub>2</sub> would start to condensate too.

This purging setup is kept for 15 min. to make sure that all remaining CO<sub>2</sub> is washed out from the REFILOX. With an internal volume of 0.38 l of the gas system and a flow rate through the needle valve of ca. 0.5 l/min this is 20 times the internal volume and should thus be sufficient. After the 15 minutes of CO<sub>2</sub> collection, the valve between REFILOX and the vacuum line is shut and the residual gases that do not freeze (mostly N<sub>2</sub> and O<sub>2</sub>) are pumped away.

Now, by thawing and cooling of the traps in dry ice again, the sample is cleaned from water vapour and moved by cryogenic pumping to the measuring volume (3.265 ml), where it is quantified manometrically. The calculations for CO<sub>2</sub> quantification can be found in Hammer (2003) and also in Appendix A.2.5.

After quantification, the gas is further cryogenically pumped to a 4 mm glass ampoule, flame sealed and then ready for AMS-measurement. For detailed descriptions and characterisations of the vacuum line, whose setup was not part of this work, see Hammer (2003) and May (2005).

### 6.6. Characterisation of the two POC extraction systems (offline and REFILOX)

To assure the reliability and reproducibility of the whole POC extraction process, it is necessary to test the system with standard and blank samples of known mass and <sup>14</sup>C content.

#### 6.6.1. Standard and blank material measurements

##### General blank correction

The process background of organic carbon contamination influences the measured radiocarbon value of the sample. This influence can be expressed as:

$$F_m \cdot m_m = F_s \cdot m_s + F_b \cdot m_b \quad (6.1)$$

With  $F_m$  and  $m_m$  as the measured <sup>14</sup>C content and mass of the sample.  $F_s$  and  $m_s$  denote the real values of the sample, which are biased by the blank mass  $m_b$  and its <sup>14</sup>C content  $F_b$ . The actual sample mass  $m_s$  can be substituted by the measured and the blank mass:

$$m_s = m_m - m_b$$

The true <sup>14</sup>C-value of the sample can then be denoted as:

$$F_s = \frac{F_m \cdot m_m - F_b \cdot m_b}{m_m - m_b} \quad (6.2)$$

This relation (6.2) has been used to correct all measured radiocarbon results for blank influences during this work. As discussed in Section 6.3.1, the ideal blank mass determination is done by running a clean ice sample through the whole sample preparation and POC extraction process and measure the carbon mass that was introduced during the process.

### Blank measurements in the offline system

A fast method to get a first guess of the process blank is the use of liquid MQ-water as a sample instead of blank ice, of which production is rather time consuming. The major disadvantage of this method is that the whole process of solid ice decontamination is not included in the result. Wherever possible, the blank determination should thus be done by use of blank ice samples. In the offline filtration system (shortly described in Section 6.2), in which silver membrane filters with a nominal pore size of 5  $\mu\text{m}$  are used and in which a separate combustion at 800  $^{\circ}\text{C}$  with pure  $\text{O}_2$  is done, eight blank ice samples have been measured over the course of ca. one year. Seven artificial and one natural holocene Antarctic ice. The results are shown in Fig. 6.8. All of these samples have been pretreated according to the improved decontamination routine described in Section 6.3.2.

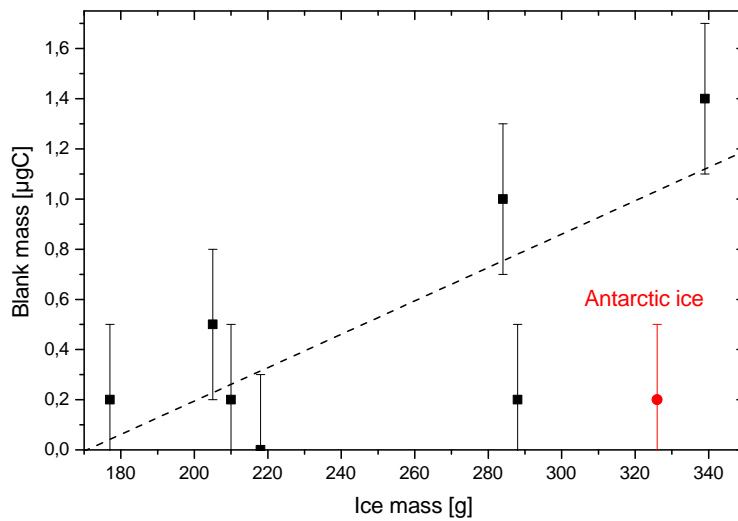


**Fig. 6.8.:** Artificial blank ice measurements in the offline filtration system together with one natural Antarctic sample. Note the linear correlation of the blank ice samples and the low carbon mass retrieved from the Antarctic sample

The average carbon mass of all measurements (data summarised in Table A.4 in Appendix A.2) is:

$$\overline{m}_b(\text{offline}) = (0.5 \pm 0.4) \mu\text{gC} \quad (6.3)$$

This equals an average POC content of  $1.7 \frac{\mu\text{gC}}{\text{kg}}$ . This result shows a carbon blank reduction for the offline system of a factor of almost ten compared to the values determined by May (2009) and Hoffmann (2010) and is a big success for the processing of small samples in the order of less than 10  $\mu\text{gC}$ .

The blank masses in Fig. 6.8 follow a weak linear trend, with a slope of 0.006  $\mu\text{gC/g}$ . The only natural Antarctic ice sample however yielded a very low POC mass of 0.2  $\mu\text{gC}$  or  $0.69 \frac{\mu\text{gC}}{\text{kg}}$ , even with a comparably high processed ice mass of 326 g. This value fits perfectly into the range of POC (WinOC) concentrations observed in Antarctic ice samples  $(0.83 \pm 0.44) \frac{\mu\text{gC}}{\text{kg}}$  (Hagler et al., 2007; Legrand et al., 2013a) and implies that this sample was not influenced by any blank. The

## 6. Methods - Optimisation of the POC extraction system

---

mass dependence of all other samples could therefore be regarded as an intrinsic contamination of the MQ-water and not to be caused by insufficient decontamination. However, it is too uncertain to assume the complete absence of a sample contamination based on only one result. Therefore, the average blank mass stated above is regarded as an upper limit and used for correction.

Unfortunately, it was not possible to measure the  $^{14}\text{C}$  content of these blank ice samples directly, just because the absolute carbon masses were too small. Thus, for blank correction the average  $^{14}\text{C}$  value of the blank samples measured with the old decontamination routine (Hoffmann, 2010) was used for correction as the best guess:

$$\overline{F_b}(\text{offline}) = (0.523 \pm 0.12) \quad (6.4)$$

### Blank ice measurements in the online system REFILOX

For the REFILOX system, a differentiation has to be made between process blanks for different combustion temperatures. The temperatures used for ice samples during this work were 340 °C and 800 °C. With this sample preparation system, the focus of blank measurements was on filtration of liquid MQ-water samples. This was mainly due to the fact, that the results with the offline system proved the new ice decontamination routine to be successful. It was therefore considered to be sufficient to test the new filtration system mainly with MQ-water samples, which is much faster than the blank ice measurements. The only two blank ice samples that have been processed so far in the REFILOX system gave the following results (combusted completely at 800 °C):

**Tab. 6.2.:** Overview of blank ice measurements done with the REFILOX

Name	Type	Processing date	Ice mass [g]	POC mass [ $\mu\text{gC}$ ]
Blank REFILOX ice 1	blank ice	13.10.14	335	$0.5 \pm 0.3$
Blank REFILOX ice 2	blank ice	5.3.15	330	$2.5 \pm 0.3$

This gives a nominal average of

$$\overline{m_b}(\text{online}, \text{ice}) = (1.5 \pm 1.0) \mu\text{gC} \quad (6.5)$$

which is considered rather an upper limit, because the second sample has been measured directly after a larger reconstruction of the gas tubing system and could be influenced by some residual contamination. The second sample was large enough for  $^{14}\text{C}$  measurement and yielded a value of

$$F_b(\text{online}, \text{ice}) = (0.574 \pm 0.030) \quad (6.6)$$

Additionally to the blank ice measurements, MQ-water blanks have been measured on a routine base between all ice samples, to guarantee that the cleaning of the filtration system was successful. In each case, ca. 500 ml MQ water have been filtered from the melting vessel, treated from there accordingly to the routine in Section 6.5 and were combusted in basically two different ways:

1. total combustion of whole sample at 800 °C
2. stepwise combustion first at 340 °C second at 800 °C

## 6.6 Characterisation of the two POC extraction systems (offline and REFILOX)

### MQ water total combustion at 800 °C in REFILOX

The results for the total combustion procedure can be found in Table A.5 in Appendix A.2. The average value for the 9 samples processed with the total combustion method is:

$$\overline{m}_b(\text{online, total}) = (1.5 \pm 0.5) \mu\text{gC} \quad (6.7)$$

equalling an average POC concentration of  $3 \frac{\mu\text{gC}}{\text{kg}}$ , thus only slightly higher than the purity specifications of the MQ-water (1-2 ppb TOC). This is also slightly enhanced compared to the ice blank of the offline system, but still in the desired range of about  $1 \mu\text{gC}$ . For one sample, a  $^{14}\text{C}$  measurement was possible and yielded a value of

$$\overline{F}_b(\text{online, total}) = (0.272 \pm 0.031) \quad (6.8)$$

which is lower than the result for the blank ice. This could be explained by omitting the step of ice sample handling, which can introduce a fraction of modern carbon. This fraction is not present in the processing of only MQ-water.

### MQ water only 340 °C fraction in REFILOX

For the first step (340 °C) of the two step combustion, only one sample out of 12 yielded a carbon mass that was large enough to be detected with  $0.5 \mu\text{gC}$ . The blank contribution of the 340 °C fraction was therefore considered to be negligible, which is a very good result.

### MQ water only 800 °C fraction in REFILOX

For the second combustion temperature step, out of 12 sample an average blank mass of

$$\overline{m}_b(\text{online, 800}) = (1.7 \pm 1.2) \mu\text{gC} \quad (6.9)$$

was retrieved. The results for the 800 °C fraction are summarised in Table A.6 in Appendix A.2. Again, only one sample could be measured for  $^{14}\text{C}$  and yielded:

$$F_b(\text{online, 800}) = (0.299 \pm 0.027) \quad (6.10)$$

Both values, mass and  $^{14}\text{C}$  content, are in good agreement with the total combustion results and thus also indicate, that the majority of the blank mass only combusts at 800°C and has almost no influence at the lower temperatures. This is an interesting finding and will become very important, when it comes to the interpretation of results.

For blank correction of the results however, only the blank mass and  $^{14}\text{C}$  result of the blank ice samples are used. This is done, because as stated above only those sample represent the whole sample preparation process.

### Standard material measurements

Processing of standard material with known carbon mass and  $^{14}\text{C}$  content together with the blanks provides important information to investigate the reliability and reproducibility of the  $^{14}\text{C}$  results. Standard materials that have been used during this work are cellulose (IAEA standard material C3 (Rozanski et al., 1992)) with a  $^{14}\text{C}$ - content of  $F_{\text{cell}} = 1.2941$ , oxalic acid (Ox II, SRM 4990 C (Mann, 1983)) with  $F_{\text{Oxa}} = 1.3408$  and brown coal, which should be in the range of 25 000 -

## 6. Methods - Optimisation of the POC extraction system

45 000 yBP according to Lowe (1989). To investigate any influences of the process blank on the radiocarbon results of these materials (and therefore also the real ice samples), it would be best to run them through the whole ice sample preparation process. Unfortunately, it was not possible to produce clean standard ice samples with a homogeneous distribution of standard material. This is due to the fact that particles (and solutes) are pushed ahead of the freezing front ((Halde, 1980; Shafique et al., 2012)) which was utilised in Section 6.3.1 to produce blank ice. The standard material measurements therefore only represent the process from combustion to  $^{14}\text{C}$  measurement but not the ice sample preparation.

### Offline filtration system

For the offline filtration system, the standard materials have been prepared in the mass range of the real ice POC samples. They were inserted directly into a preheated glass ampoule together with a piece of silver wire, which binds sulphur and halogen compounds. The ampoule was filled with pure  $\text{O}_2$ , flame sealed and heated to  $800\text{ }^\circ\text{C}$  for 6 hours. After that, the  $\text{CO}_2$  samples have been cleaned, quantified and processed as described in Section 6.5. Table 6.3 gives an overview of the  $^{14}\text{C}$  results of the different materials and the results for the cellulose are shown in Fig. 6.9.

**Tab. 6.3.:** Overview of standard material  $^{14}\text{C}$  results, combusted like ice POC samples in the offline filtration system

Material type	Sample mass [ $\mu\text{gC}$ ]	$^{14}\text{C}$ -content [ $\text{F}^{14}\text{C}$ ]	$\sigma\text{F}^{14}\text{C}$
Cellulose	17.4	1.178	0.038
Cellulose	12.9	1.269	0.018
Cellulose	9.7	1.292	0.0190
Cellulose	16.3	1.265	0.014
Cellulose	10.6	1.315	0.014
Cellulose	56	1.292	0.011
Oxalic acid	16.8	1.315	0.024
Oxalic acid	13.5	1.311	0.020
Brown coal	31.4	below blank	-
Brown coal	15.5	0.004	0.002
Brown coal	16	0.006	0.002

The error-weighted  $^{14}\text{C}$ -average of all cellulose samples is:

$$\overline{f_{\text{Cell}}(\text{offline})} = (1.286 \pm 0.020) \quad (6.11)$$

This average hits the expected value within the error range and no trend to a blank bias is visible, even for the small samples. The one outlier (see Fig. 6.9) gave only a third of the ion current during the measurement compared to the other measurements of that batch. It was therefore regarded to be contaminated with residual gases and was not considered in the average. The two oxalic acid measurements are slightly too low in  $^{14}\text{C}$ , but still hit the expected value of 1.341 within  $2\sigma$ . For the brown coal, one was measured even below the system blank of the gas ion source. The other two gave  $^{14}\text{C}$  ages of ca. 25 000 - 30 000 years with very large statistical errors of 20-30 %, which is due to the very low number of  $^{14}\text{C}$  counts. For the expected age range of the

## 6.6 Characterisation of the two POC extraction systems (offline and REFILOX)

ice samples of probably up to 10 000 years, this blank is sufficiently low to distinguish any of the ice samples from background. It also agrees with the expected values stated in Lowe (1989).

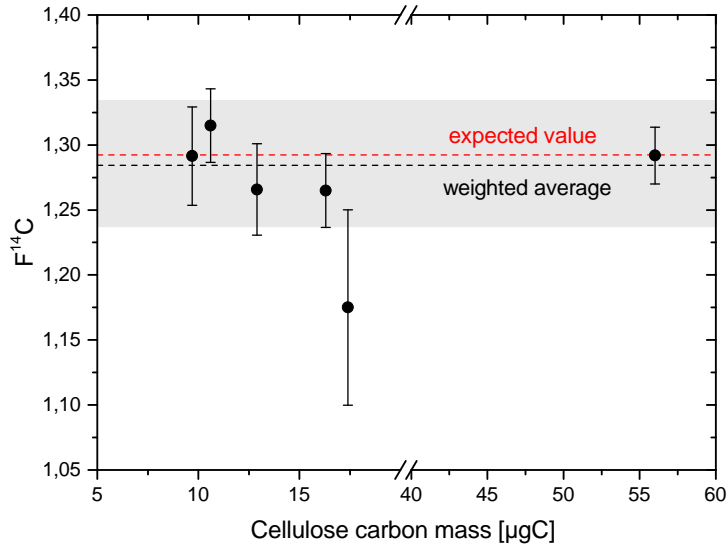


**Fig. 6.9.:** Results of the cellulose <sup>14</sup>C measurements processed in the offline filtration system. The error bars denote the 2σ range. Within this range, all results except one hit the expected value (red line) and so does the weighted average (black line) within error. The outlier was not considered in the average.

Overall, the standard material measurements made with the offline filtration system gave excellent results, even the very small samples of ≈ 10 µgC showed no influence of any contamination. The preparation of even smaller samples was not possible because of limits of the balance and manageability of such small amounts of sample material.

### Online filtration system REFILOX

In the REFILOX system, the same type of standard samples has been used as for the offline system. The samples have been weighed and were inserted directly into the quartz tube on top of a pre-cleaned filter. Combustion was done at 800 °C total for all samples. <sup>14</sup>C results are summarised in Table 6.4. Sample masses are in total slightly bigger than for the offline system, which results from the more difficult insertion to the tube. Very small samples often get statically charged, stick to the walls of the tube and can thus not be combusted. The error-weighted average of all cellulose samples is:

$$\overline{F_{Cell}}(online) = (1.281 \pm 0.029) \quad (6.12)$$

Within the error range, this is in good agreement with the expectation and the results from the offline system (see Fig. 6.10). Only the smallest sample shows a weak bias towards a lower <sup>14</sup>C content.

## 6. Methods - Optimisation of the POC extraction system

**Tab. 6.4.:** Overview of standard material  $^{14}\text{C}$  results, combusted like ice POC samples in the online filtration system REFILOX

Material type	Sample mass [ $\mu\text{gC}$ ]	$^{14}\text{C}$ content [ $F^{14}\text{C}$ ]	$\sigma F^{14}\text{C}$
Cellulose	7.8	1.245	0.022
Cellulose	28	1.265	0.011
Cellulose	46.6	1.284	0.014
Cellulose	36.9	1.301	0.013
Cellulose	19.1	1.318	0.020
Oxalic acid	34.8	1.347	0.014
Brown coal	38	0.004	0.002

This could be due to a small blank influence. If the result is corrected according to equation 6.2 with a blank mass of only  $0.3 \mu\text{gC}$  and the blank  $^{14}\text{C}$  content from equation 6.6, the result is already shifted to  $F=1.272$  and lies perfectly within the error range of the average. The oxalic acid result hits the literature value almost perfectly and the brown coal is in the same range as for the offline system. The combustion process at  $800 \text{ }^\circ\text{C}$  of the online REFILOX system shows no significant systematical biases of the  $^{14}\text{C}$  results, at least for samples larger than  $10 \mu\text{gC}$ . Another type of system calibration with aerosol samples of known  $^{14}\text{C}$  content will be discussed in Section 6.7.1.

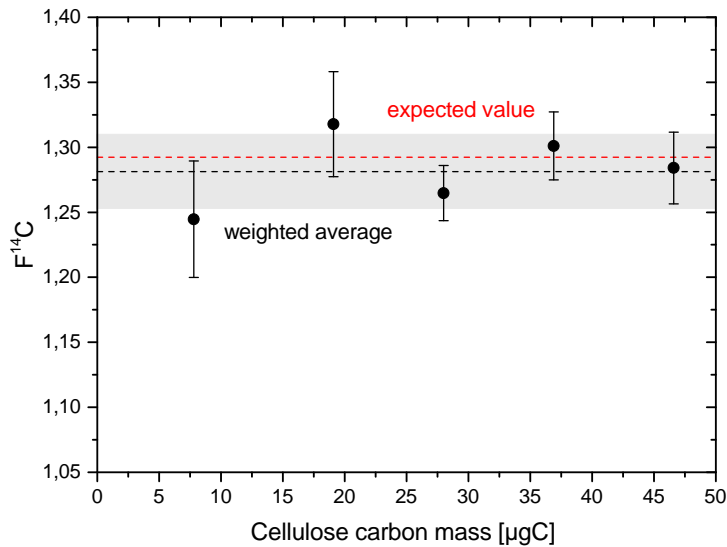


**Fig. 6.10.:** Results of the cellulose measurements in the REFILOX filtration system. The error bars denote the  $2\sigma$  range. Within this range, all results except one hit the expected value (red line) and so does the weighted average (black line) within error.

### 6.6.2. Extraction and combustion efficiency

Another important parameter of the system characterisation is the efficiency of POC extraction from an ice sample and the subsequent combustion into CO<sub>2</sub>. As discussed in Section 6.6.1, it was not possible to produce artificial standard ice samples. The POC filtration efficiency can therefore not be quantified and only be assessed qualitatively. Both used filter materials do not retain 100 % of all particles. On top of that, within the offline system always leftovers of particles have been discovered on the filter holder when the filter was taken out. Additionally, the folding and insertion into the combustion tube involves the danger of material loss to the tweezers and the walls of the tube. By omitting that step in the online system, apart from the use of different filter materials, this risk of material loss is avoided and the overall recovery of POC should be larger than for the offline system. The combustion and CO<sub>2</sub> extraction efficiency was determined by the standard material measurements. For each material, the theoretical carbon content was calculated. After combustion and CO<sub>2</sub> quantification, the ratio of weighed carbon and extracted carbon was computed.

For the offline system, the combustion efficiencies ranged from ca. 50% to more than 90% and for the online system from 65% to 90%. The smaller samples tended to yield a worse efficiency than the larger samples (see Fig. 6.11).

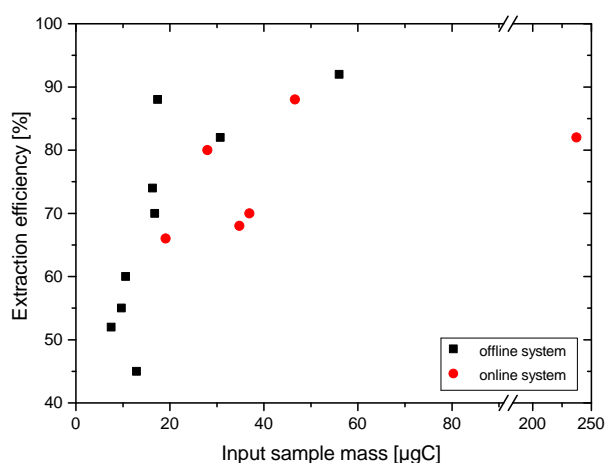


**Fig. 6.11.:** Carbon extraction efficiencies for different input sample masses in both combustion systems. Note that the efficiencies for larger samples are better than for very small samples.

At first glance, this seems to be contra intuitive, if the combustion efficiency was only constrained by the available amount of oxygen. The effect is however mainly caused by:

- Limited accuracy of the balance (5 µg)
- Difficult handling of very small samples
- Easy loss of sample material to combustion tube walls at sample insertion

## 6. Methods - Optimisation of the POC extraction system

---

All these factors, especially the sample losses, are relatively a more serious problem for small samples than for large ones. The bad extraction efficiencies of the small samples are therefore attributed to these uncertainty factors, which probably will not play a role for the real ice samples. The high efficiencies (80-90%) of the largest samples are thus taken as an indicator for an efficient combustion process. Overall, 70% efficiency were assumed as an average combustion efficiency for both systems.

### 6.6.3. Memory effect

The term memory effect describes a carryover of material from one sample to the next due to insufficient cleaning of the system, which results in a bias of the result. To make sure that this effect is not a problem in the whole sample preparation process, a (MQ-water) process blank was always run in between two ice samples. Even after large samples, no systematic enhancement of the blank values could be observed, which means that the cleaning process is sufficient and reliable and memory effects are not a problem for both systems.

### 6.6.4. Error estimation and consequences for the minimum sample mass

After characterisation and evaluation of the extraction system performance, now the consequences for the accuracy of  $^{14}\text{C}$  results will be assessed. All  $^{14}\text{C}$  results will be corrected according to equation 6.2. The uncertainty of the corrected  $^{14}\text{C}$  result  $F_s$  of the sample is then calculated by error propagation to:

$$\sigma_{F_s} = \sqrt{\sigma_{F_m}^2 \cdot \left(\frac{\partial F_s}{\partial F_m}\right)^2 + \sigma_{m_m}^2 \cdot \left(\frac{\partial F_s}{\partial m_m}\right)^2 + \sigma_{F_b}^2 \cdot \left(\frac{\partial F_s}{\partial F_b}\right)^2 + \sigma_{m_b}^2 \cdot \left(\frac{\partial F_s}{\partial m_b}\right)^2} \quad (6.13)$$

with the single components:

$$\frac{\partial F_s}{\partial F_m} = \frac{m_m^2 - m_m \cdot m_b}{(m_m - m_b)^2}$$

$$\frac{\partial F_s}{\partial m_m} = \frac{F_b \cdot m_b - F_m \cdot m_m}{(m_m - m_b)^2}$$

$$\frac{\partial F_s}{\partial F_b} = \frac{m_b^2 - m_b \cdot m_m}{(m_m - m_b)^2}$$

$$\frac{\partial F_s}{\partial m_b} = \frac{2F_b \cdot m_b - F_m \cdot m_m - F_b \cdot m_m}{(m_m - m_b)^2}$$

The errors of  $F_b$  (the ice blank  $F^{14}\text{C}$ ) and  $m_b$  (the blank mass) have been determined in Section 6.6.1. The error of the measured  $^{14}\text{C}$   $F_m$  is the statistical error of the  $^{14}\text{C}$  measurement and the error of the measured carbon mass  $m_m$  results from the uncertainty of the manometric quantification. For an accuracy of the manometer of ca. 0.2 mbar this can be set to 0.3  $\mu\text{gC}$  for samples smaller than 30  $\mu\text{gC}$ . A detailed calculation of the manometric quantification can be found in Hammer (2003) and in Appendix A.2.5.

## 6.6 Characterisation of the two POC extraction systems (offline and REFILOX)

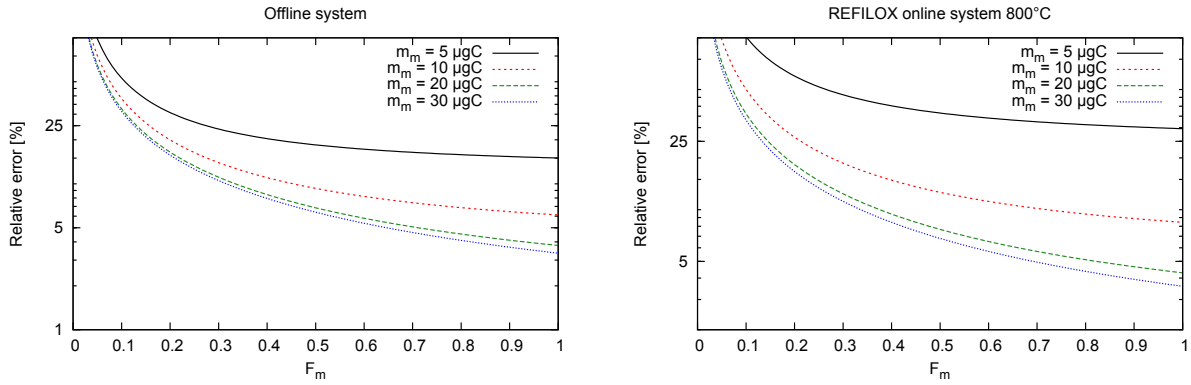


**Fig. 6.12.:** Relative errors of the  $^{14}\text{C}$ -results depending on the measured  $F_m$

If  $m_m$  is set as a parameter and  $\sigma F_m$  is estimated to be on average about 3%, equation 6.13 only depends on  $F_m$ . The resulting relative measurement error depending on  $F_m$  is illustrated in Fig. 6.12. To get a  $^{14}\text{C}$  result with a relative error below 10%, for the offline system the sample should thus not be smaller 10 $\mu\text{gC}$ , for the expected age ranges mostly above  $F=0.2$ . This results in ca. 500 g of ice needed for reliable dating, assuming an average POC content in high Alpine samples of 20  $\mu\text{gC}$  per kg.

In the online system, the sample should not be smaller than 10-20  $\mu\text{gC}$ , resulting in a required ice mass of 500-1000 g. Note that this calculation was done for the total combustion at 800°C. For the 340 °C fraction, the blank mass was below detection limit and thus the measurement error is mainly dominated by the AMS-measurement and the minimal sample size measurable with the gas ion source. It has been technically possible to measure samples down to 2  $\mu\text{gC}$ , so based on this, the minimal required ice mass for the 340 °C fraction would be about 100 g of glacier ice.

### 6.6.5. Summary of the technical improvements in the REFILOX system

The offline and the online system differ in many points, the main differences are summarised in Table 6.5. Compared to the offline system, the new REFILOX setup has many advantages but also a few drawbacks. The largest advantage of the new setup lies in the direct combination of the pre-cleaning of the filter, the filtration and combustion process in one closed system. The large risk of contamination and loss of material, if the filter has to be taken out of the holder after filtration is thus minimised. Also a possible contamination of a new filter at insertion is avoided, because the filter can be preheated directly before use. Another large advantage is the adjustability of the combustion temperature, which enables stepwise combustion and is not possible for the offline setup. The benefit of this stepwise combustion will be addressed in the following section. Overall, the technical goals for the new setup have been widely achieved. A drawback of the REFILOX is however the cleaning of its components. Especially the quartz tube with the glass-metal-transfers is very delicate. Usually, glass and metal parts are cleaned in an ultrasonic bath, which is not possible for those transfers. This complicated cleaning is pictured in the slightly enhanced process blank of the REFILOX compared to the offline system.

## 6. Methods - Optimisation of the POC extraction system

**Tab. 6.5.:** Comparison of different technical setups, advantages and disadvantages of the offline and online POC extraction system

Process component	offline system	REFILOX
<b>Filter material</b>	only silver membrane	only quartz fibre
<b>Filter cleaning</b>	preheating outside filter holder	preheating directly in filtration system
<b>POC combustion</b>	filter combustion in separate glass ampoule, has to be taken out of holder after filtration	direct combustion of material on filter surface, filter stays in holder, closed system
<b>Combustion temperature</b>	fixed to one temperature (800 °C)	variable between 50 °C and 950 °C
<b>Setup cleaning</b>	all components can be taken apart and cleaned separately	no separate cleaning of all components possible, delicate glassware

The cleaning of that crucial part is thus restricted to wiping and rinsing and has to be done very carefully. This particularly comes into play, when a large sample has been processed and a lot of residual material has to be cleaned from the middle of the tube. During this work, both filtration systems (offline and REFILOX) have been used, considering their respective advantages.

### 6.6.6. Summary of the main findings of the system characterisation

The main findings and parameters of the whole system characterisation, blank and standard measurements are summarised in Table 6.6. The most impressive finding in the whole system characterisation process was, that the blank mass at the 340 °C fraction in the online system was below detection limit, what becomes very important for the real ice samples later on. The blank mass results show a major improvement compared to earlier IUP systems, with a reduction of a factor of four to ten, which is a large success. The <sup>14</sup>C results of the standard material measurements show no significant influence of blank contamination. Even samples below 10 µgC are not influenced by blank contamination, which is very promising for further measurements. As a summary, the overarching goals of the POC extraction system optimisation have been satisfyingly reached.

## 6.7 Calibration of REFILOX combustion temperatures

**Tab. 6.6.:** Summary of the main characteristic system parameters.

Process parameter	offline system	REFILOX
<b>Process blank mass</b> [ $\mu\text{gC}$ ]	blank ice 800 °C: $\overline{m_b} = (0.5 \pm 0.4) \mu\text{gC}$	blank ice 800 °C: $\overline{m_b} = (1.5 \pm 1.0) \mu\text{gC}$ MQ-water 340°C: below detection limit
<b>Process blank</b> $^{14}\text{C}$	blank ice: $\overline{F_b} = (0.523 \pm 0.12)$	blank ice: $F_b = (0.5735 \pm 0.0300)$
<b>Standard material Cellulose</b> $^{14}\text{C}$	$\overline{F_{Cell}} = (1.2844 \pm 0.0489)$	$\overline{F_{Cell}} = (1.2813 \pm 0.0289)$
<b>Combustion efficiency</b>	50-90% for Cellulose and OxII	70-80% for Cellulose and OxII
<b>Minimal sample size:</b>	10 $\mu\text{gC} \rightarrow$ 500g ice	800 °C: 10-20 $\mu\text{gC} \rightarrow$ 500-1000g ice 340 °C: 2 $\mu\text{gC} \rightarrow$ 100g ice

## 6.7. Calibration of REFILOX combustion temperatures

Because of the potentially  $^{14}\text{C}$  age biasing effects, which will be discussed in Section 7.3, a strategy must be developed to avoid the influence of these materials in high Alpine ice samples (for example from Colle Gnifetti or Grenzgletscher). Especially where no macroscopic selection of the dated POC is possible. Different organic carbon fractions combust at different temperatures. This characteristic feature has been used to separate OC and EC fractions of modern aerosol samples for long years (see e.g. Pio et al. (1994); Szidat et al. (2004b); Pio et al. (2007)). The EC fractions of these samples often originate from fossil fuel burning (Suess effect) and are therefore strongly depleted in  $^{14}\text{C}$  (see e.g. Szidat et al. (2004a)). So far, POC combustion from Alpine ice samples at the IUP has only been carried out at one very high temperature (800 °C) where all organic carbon is oxidised to  $\text{CO}_2$ . This was done under the assumption, that for pre-industrial times EC from fossil fuel should not be relevant and the age offset from EC of biomass burning compared to the living biosphere is negligible. Because of the overall very small sample sizes, it was therefore decided to combust and collect all particulate organic material together.

Based on the results of the age bias investigations of different materials (e.g. Saharan dust and soil components) retrieved within this study (see Section 7.3), this assumption is probably not true. Indications for an age biasing influence of Saharan dust in the EC combustion (but not in the OC) fraction have also been for example discussed in Jenk et al. (2006) and Sigl et al. (2009), but with no final conclusion on the biasing effect. They only derive the suggestion to preventively avoid the EC fraction for dating purposes of ice samples, by adapting the combustion temperature to 340 °C.

During this study, it was therefore envisaged, to find the best way for separation of the age biased carbon fractions from the non-biased fractions by selectively combusting only the primary biogenic particles. To test and calibrate the REFILOX system with regard to this selective combustion, aerosol samples with known OC and EC composition have been processed and  $^{14}\text{C}$  dated.

## 6. Methods - Optimisation of the POC extraction system

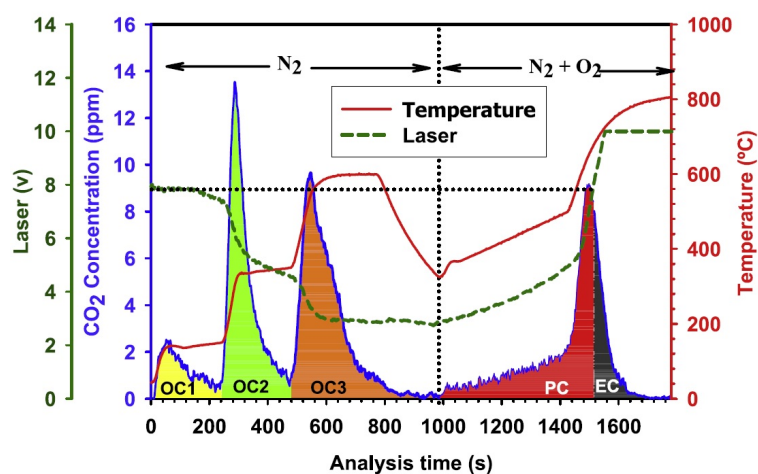


**Fig. 6.13.:** Thermogram of the method for carbon fraction separation used in the CARBOSOL project. The total organic fraction is subdivided into five subfractions OC1, OC2, OC3, PC and EC by heating in an inert atmosphere before combustion with O<sub>2</sub> (Pio et al., 2007).

In the years 2002-2004, an European programme, which aimed to characterise the present and retrospective composition of organic aerosol over Europe (CARBOSOL) has been conducted (Legrand and Puxbaum, 2007) under strong participation of the IUP Heidelberg. During the course of this project, aerosol has been sampled on air filters along a transect across Europe and has been analysed. The samples were characterised for composition (inorganic and organic species) as well as <sup>14</sup>C signature (May et al., 2009). Some of these aerosol filters were still available and have been used during this work to investigate the best combustion temperature for POC samples from ice.

Most studies which aim to measure OC / EC fractions, use a thermo-optical method, where the separation of different carbon fractions is achieved by stepwise heating under inert and oxidising atmospheres by simultaneous supervision of the optical filter reflectance (see e.g. Huntzicker et al. (1982); Zhang et al. (2012)). Apart from these thermo-optical methods, also two and three step combustion systems are used to separate OC and EC fractions (see e.g. Cachier et al. (1989); Szidat et al. (2004b)). Within the CARBOSOL project, the separation of OC and EC was done by a thermo-optical method (Pio et al., 1994), which allows separation of the carbonaceous species into five subfractions (see Fig. 6.13) with the following characteristics:

- **OC1:** T = 170 °C N<sub>2</sub> atmosphere, including volatile organic compounds
- **OC2:** T = 340 °C N<sub>2</sub> atmosphere, including non polar organic species (e.g. alkanes, fat)
- **OC3:** T = 600 °C N<sub>2</sub> atmosphere, including polar species (e.g. HULIS)
- **PC:** T = 340-500 °C N<sub>2</sub> + O<sub>2</sub> atmosphere, including organic carbon, which pyrolysed under the inert atmosphere and high temperatures (e.g. HULIS, Levoglucosan)
- **EC:** T = 500-600 °C N<sub>2</sub> + O<sub>2</sub> atmosphere, including initially present elemental carbon (soot)

The REFILOX is not capable of reproducing this whole process. Therefore, a simplified 3-step heating procedure (340 °C, 380 °C and 800 °C) similar to Szidat et al. (2004a) has been applied with the aim to attribute the carbon fractions stated above to these temperature steps. For comparison of the  $^{14}\text{C}$  results, also data measured by May et al. (2009) of CARBOSOL filter samples was available. This data however only includes  $^{14}\text{C}$  values of the total organic carbon but no evaluation of the single fractions. They will however serve as a reference.

### 6.7.1. Analyses of CARBOSOL aerosol samples processed in REFILOX

For the systematic investigation of  $^{14}\text{C}$  signatures of different organic carbon fractions, aerosol filters from three CARBOSOL sampling sites (Legrand and Puxbaum, 2007), Sonnblick observatory 3106 m a.s.l. (SBO), Schauinsland 1205 m a.s.l. (SIL) and Aveiro (AVE) have been selected:

- SBO 32: Summer, average dust contents, best reference for high Alpine glacier sites
- SIL 02/08: Winter, high influences of fossil fuel burning
- SIL 3/24: Summer, high contribution of biogenic carbon
- SIL 3/28: Summer, probably influenced by Saharan dust
- AVE 03: Summer, influenced by fossil fuel burning
- AVE 31: Winter, high influences of biomass burning

A piece of 10 mm diameter has been cut out from each aerosol filter. It was acidified in acid vapour (HCl, 0.2M) prior to combustion following the protocol used in the CARBOSOL project (May et al., 2009). The filter piece was inserted into the REFILOX and the combustion and  $\text{CO}_2$  collection has been carried out according to the procedure described in Section 6.5. Three temperature steps have been applied: 340 °C 380 °C and 800 °C, each for 40 minutes, trying to achieve a similar OC / EC separation as reported by Cachier et al. (1989) and Szidat et al. (2004a). The carbon concentrations retrieved from the filters are reported in Table 6.7. They are given in the unit [ $\mu\text{gC}/\text{m}^3$ ], to make the values comparable with the CARBOSOL results. A combustion efficiency of 70% for the REFILOX has been assumed (see Section 6.6.2) and was included in the calculation.

## 6. Methods - Optimisation of the POC extraction system

**Tab. 6.7.:** Extracted carbon contents at different temperature steps of CARBOSOL filters processed in REFILOX referred to  $\text{m}^3$  of air. The results are shown in comparison to the carbon masses extracted during the CARBOSOL project.

Sample name	TC CARBOSOL [ $\mu\text{gC}/\text{m}^3$ ]	TC REFILOX [ $\mu\text{gC}/\text{m}^3$ ]	OC1+OC2 CARBOSOL [ $\mu\text{gC}/\text{m}^3$ ]	EC+PC+OC3 CARBOSOL [ $\mu\text{gC}/\text{m}^3$ ]	REFILOX (380°C+800°C) [ $\mu\text{gC}/\text{m}^3$ ]	EC CARBOSOL [ $\mu\text{gC}/\text{m}^3$ ]
SBO 32-340°C		0.57	0.60			
SBO 32-380°C		0.32				
SBO 32-800°C		0.83		1.31	1.15	0.13
SBO 32-sum	1.91	1.72				
SIL-02/08-340°C		0.27	0.14			
SIL-02/08-380°C		0.19				
SIL-02/08-800°C		0.36		0.72	0.55	0.23
SIL-02/08-sum	0.87	0.82				
SIL-03/24-340°C		1.62	1.05			
SIL-03/24-380°C		0.64				
SIL-03/24-800°C		2.30		3.02	2.94	0.35
SIL-03/24-sum	4.07	4.56				
SIL-03/28-340°C		1.32	1.04			
SIL-03/28-380°C		0.94				
SIL-03/28-800°C		1.92		2.86	2.95	0.26
SIL-03/28-sum	3.99	4.37				
AVE 31-340°C		7.37	4.55			
AVE 31-380°C		6.37				
AVE 31-800°C		2.76		14.35	9.13	1.94
AVE 31-sum	18.90	16.50				
AVE 03-340°C		1.32	1.01			
AVE 03-380°C		1.07				
AVE 03-800°C		3.25		3.37	4.32	0.52
AVE 03-sum	4.37	5.64				

### 6.7.2. Comparison of extracted carbon fractions for REFILOX and CARBOSOL

In the following, relations between the different carbon fraction retrieved via REFILOX and the CARBOSOL method are investigated. In Fig. 6.14, the extracted carbon concentrations for all processed filters and different compared fractions are shown. The ratios of several carbon fraction for each single filter are reported in Table A.7 in Appendix A.2.

#### Total carbon (TC)

The total carbon masses retrieved with the thermo-optical method and the REFILOX system correspond very well. A linear fit of the measured TC values in Fig. 6.14 yields a slope of  $(0.91 \pm 0.05)$ . This means that almost 100% of the CARBOSOL TC mass has been recovered by the REFILOX system. The slight variation can be caused on one hand by the principal differences in the method and on the other hand by the assumed 70% combustion efficiency in the REFILOX. It is striking that both total carbon masses are on average almost equal despite the fundamental differences in the extraction system.

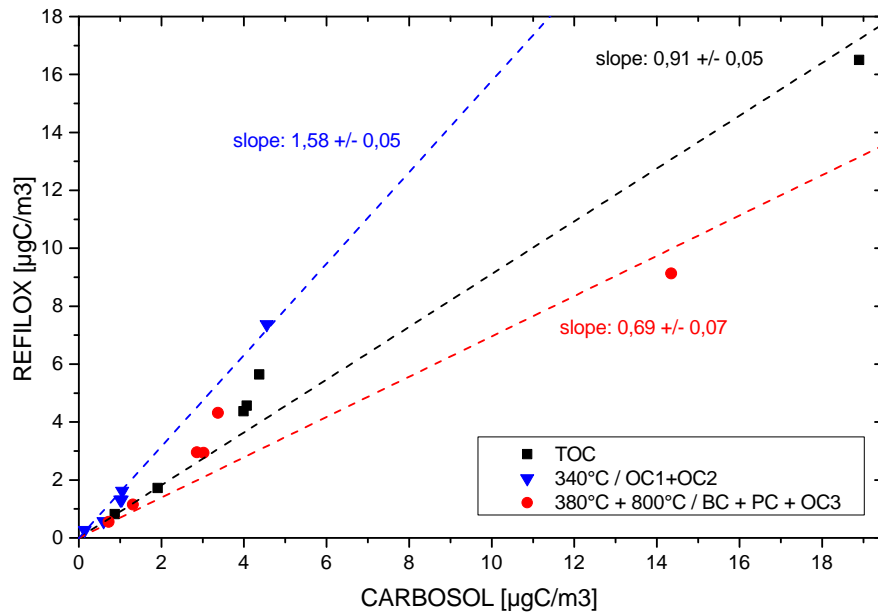


**Fig. 6.14.:** Comparison of the retrieved carbon concentrations for the CARBOSOL system and the REFILOX for total carbon content and the 380 °C + 800 °C fraction of REFILOX.

#### REFILOX 340 °C fraction

A comparison of the REFILOX 340 °C fraction with the sum of the OC1 and OC2 fractions via a linear fit (see Fig. 6.14) yields a slope of  $(1.58 \pm 0.05)$ . Thus, the REFILOX extracts on the 340 °C fraction more than the sum of OC1 and OC2. According to the applied temperatures in the thermogram (Fig. 6.13), this additional carbon fraction should likely consist of a certain amount of PC, combusting at very low temperatures and possibly also a fraction of OC3. A quantitative apportionment would be on the basis of only seven samples however highly speculative.

## 6. Methods - Optimisation of the POC extraction system

---

### REFILOX 380 °C and 800 °C fraction

Comparing the sum of the 380 °C and the 800 °C fraction of REFILOX to the EC, PC and OC3 fractions of the thermo-optical method correlating in combustion temperature, this yields a slope of  $(0.69 \pm 0.07)$  in a linear fit. The REFILOX does therefore retrieve less carbon than the CARBOSOL method. This missing fraction was in the REFILOX combustion very likely incorporated in the excess of the 340 °C fraction compared to OC1 and OC2. Again, the variable missing fraction is attributed to OC3 and mostly PC, combusting at temperatures below 380 °C. This effect is most prominent for the sample AVE 31, where the 340 °C fraction of REFILOX was 1.6 times higher than OC1+OC2 and for the sum of 380 °C and 800 °C only 63 % of the CARBOSOL EC+PC+OC3 was reached. AVE 31 is known to be highly influenced by levoglucosan, a product of biomass burning, which is attributed to the PC fraction in the thermo-optical method. This finding is also backed up by comparison of only the 800 °C fraction of REFILOX with the according EC fraction of the CARBOSOL method. The REFILOX 800 °C fraction (including parts of PC and OC3) is up to seven times higher than the CARBOSOL EC. Especially interesting is in this context the direct comparison of the samples SIL 3/24 and SIL 3/28. Both summer samples, but SIL 3/28 probably influenced by a Saharan dust event. This sample shows the overall highest ratio of EC fractions measured in CARBOSOL and REFILOX, which is also 12% higher than the one of SIL 3/24. This finding could support the hypothesis, that Saharan dust mainly biases the high temperature (EC) fraction, which was suggested by Jenk et al. (2006). This hypothesis is however so far only based on the result of one sample and needs further investigation. The main conclusions drawn from the analyses of the extracted carbon masses are therefore:

- Overall very good agreement in TC masses retrieved with the CARBOSOL and REFILOX method (90% REFILOX recovery).
- The 340°C carbon mass in REFILOX is slightly higher than OC1+OC2 in CARBOSOL, likely due to small incorporations of OC3 and PC.
- Most of the OC3 and PC fraction are incorporated together with EC into the 800 °C fraction of REFILOX, thus very likely also organic substances from soils and dust.
- The REFILOX 340°C carbon fraction should therefore be the best option to extract primarily biogenic carbon, which should have the smallest age bias.

### 6.7.3. Assessment of the $^{14}\text{C}$ values measured for the REFILOX fractions

After the comparison of carbon concentrations measured with the CARBOSOL and REFILOX system, now the  $^{14}\text{C}$  content of the different fractions is investigated. The conclusion that the least age biased material should be combusted in the 340 °C fraction of the REFILOX system was investigated by  $^{14}\text{C}$  measurements of the single carbon fractions. All  $^{14}\text{C}$  measurements have been carried out at the MICADAS AMS in Mannheim via the gas ion source, because of the overall small sample sizes below 100  $\mu\text{gC}$ . The results of these  $^{14}\text{C}$  measurements together with the total TC  $^{14}\text{C}$  results measured by May et al. (2009) are given in Table 6.8. The 380 °C fraction of sample SBO-32 was too small to be measured. Additional to the single fractions, one sample from SIL-3/28 has been combusted completely at 800 °C, to investigate if this can reproduce the average of all other fractions  $F_{\text{sum}}$  calculated according to:

$$F_{\text{sum}} = \frac{F_{340} \cdot m_{340} + F_{380} \cdot m_{380} + F_{800} \cdot m_{800}}{m_{340} + m_{380} + m_{800}} \quad (6.14)$$

## 6.7 Calibration of REFILOX combustion temperatures

With the respective  $^{14}\text{C}$  values  $F$  and the carbon masses  $m$  for each temperature fraction. The results of the sample SBO 32 and SIL 3/28 are exemplarily shown in Fig. 6.15 and 6.16, all other results are shown in Appendix A.2. For SIL 3/28 also a measurement of May et al. (2009) was available and SBO 32 is the best representative for high Alpine conditions. The first striking observation is that there is a large difference in  $^{14}\text{C}$  values for the different combustion temperatures in all samples, even between the 340 °C and the 380 °C fraction. The samples systematically show the youngest results at the 340 °C and get older to higher combustion temperatures. This was expected based on earlier aerosol  $^{14}\text{C}$  investigations (Szidat et al., 2004a), because the fossil black carbon fraction is known to be mostly combusted at that high temperature fraction.

**Tab. 6.8.:**  $^{14}\text{C}$  results of all carbon fractions extracted from CARBOSOL aerosol filters processed in the REFILOX system. Additionally, as a reference the bulk TC  $^{14}\text{C}$  results measured by May et al. (2009) are given.

Sample name	$F^{14}\text{C}$	$\sigma F$	Average $F^{14}\text{C}$	May (2009) $F^{14}\text{C}$
SBO 32-340°C	0.902	0.027	$0.818 \pm 0.025$	SBO summer average $0.794 \pm 0.018$
SBO 32-380°C	0.875	0.033		
SBO 32-800°C	0.751	0.019		
SIL-02/08-340°C	1.044	0.023	$0.753 \pm 0.091$	SIL winter average $0.731 \pm 0.006$
SIL-02/08-380°C	0.883	0.028		
SIL-02/08-800°C	0.453	0.016		
SIL-03/24-340°C	0.933	0.011	$0.804 \pm 0.038$	SIL summer average $0.856 \pm 0.006$
SIL-03/24-380°C	0.915	0.016		
SIL-03/24-800°C	0.679	0.008		
SIL-03/28-340°C	0.939	0.009	$0.782 \pm 0.050$	SIL 3/28 by May et al. (2009) $0.820 \pm 0.005$
SIL-03/28-380°C	0.870	0.012		
SIL-03/28-800°C	0.615	0.007		
AVE 31-340°C	1.024	0.010	$0.893 \pm 0.078$	AVE winter average $0.921 \pm 0.009$
AVE 31-380°C	0.857	0.008		
AVE 31-800°C	0.637	0.009		
AVE 03-340°C	1.011	0.017	$0.747 \pm 0.040$	AVE summer average $0.772 \pm 0.006$
AVE 03-380°C	0.804	0.019		
AVE 03-800°C	0.620	0.009		

The hypothesis of high temperature fractions being most influenced by fossil fuel EC is also backed up by the sample SBO 32, which shows the highest  $^{14}\text{C}$  content in the 800 °C fraction compared to all others. Sonnblick observatory at 3106 m a.s.l. should be least influenced by anthropogenic fossil fuel emissions, which is thus pictured in the result.

The second observation is that even the youngest results on the 340 °C fraction are 4-16% lower than the expected atmospheric value of ca.  $F=1.08-1.09$  for the years 2002-2004 (Levin et al., 2010). This is probably due to the fact that a certain amount of organic species (6-19% of the sample mass) derived from fossil fuel burning combusts at very low temperatures. It thus contributes to the low combusting organic species, which are mainly derived from the living biosphere. Overall the averaged values of the samples show a very good agreement with the seasonal averages

## 6. Methods - Optimisation of the POC extraction system

for the respective sites found by May et al. (2009) with a maximum deviation of 5% from these reference values. This means, that the combustion and CO<sub>2</sub> collection of the single fractions did not lead to any isotope fractionation processes, which would have biased the average.

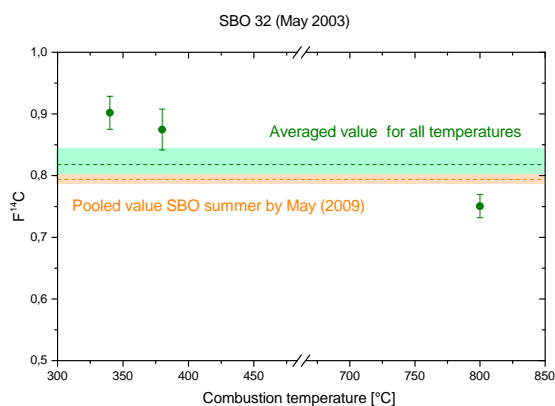


**Fig. 6.15.:** <sup>14</sup>C results for the different temperature carbon fractions of sample SBO-32.

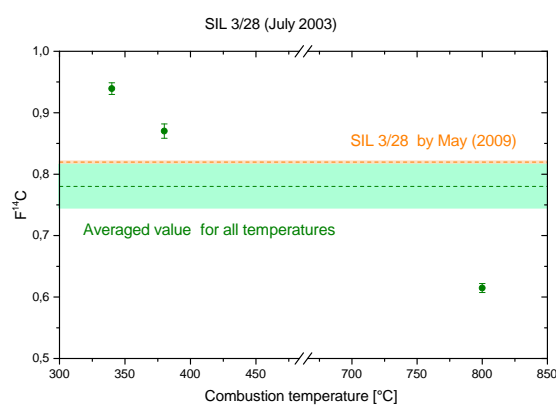


**Fig. 6.16.:** <sup>14</sup>C results for the different temperature carbon fractions of sample SIL-3/28.

### 6.7.4. Conclusions on the optimal POC combustion procedure

As a summary of all CARBOSOL aerosol filter analyses, it can be stated that the separation of the main organic carbon fractions within the REFILOX filtration and combustion system was very successful. It could be shown, that the OC1 and OC2 carbon fractions, which are the ones mainly consisting of relative volatile emissions mainly derived from from the living biosphere, can be extracted at a combustion temperature of 340 °C. Soil and Saharan dust organic matter like HULIS (part of OC3 and PC) probably contributes to the high combustion temperature fraction at 800 °C together with the main fossil fuel contribution. This fossil fuel contribution should not be present in pre-industrial samples. The <sup>14</sup>C analyses of the single fractions retrieved via the REFILOX system showed a large trend in <sup>14</sup>C depletion with increasing combustion temperature. The lowest temperature yields the best agreement with the expected atmospheric value. Therefore, this fraction should primarily be used for POC dating of ice samples, because it has the smallest biases to older ages and will give the best representation of the real ice age. Nevertheless, POC retrieved ice ages should be regarded as an upper limit.

## 7. Results - Systematical investigation of $^{14}\text{C}$ age biasing effects in glacier ice

### 7.1. Introductory remarks

Incorporation of aged organic material (see Section 3.2) into the POC fraction of glacier ice can lead to large biases of the measured  $^{14}\text{C}$  ages. Systematic information on possible  $^{14}\text{C}$  age ranges of these materials is however sparse. For pre-industrial Alpine ice samples, so far only Jenk et al. (2006) reported a likely influence of Saharan dust, shifting the  $^{14}\text{C}$  age of an ice samples to higher values than expected. It was therefore envisaged to investigate  $^{14}\text{C}$  ages of typical materials contributing to the POC in glacier ice, namely Saharan dust, cryoconite and basal sediment. Cryoconite is windblown material of organic and mineral origin, which accumulates on the glacier surface. It can form water filled holes due to the low albedo of the dark material and subsequent punctual surface melting (Wharton et al., 1985).



**Fig. 7.1.:** Map of the sampling sites for investigations of POC  $^{14}\text{C}$  age biasing effects of Saharan dust, cryoconite and sediment

The main questions that will be addressed in this context are:

1. What are the typical  $^{14}\text{C}$  age ranges of Saharan dust, cryoconite and basal sediment incorporated in glacier ice?
2. Is it possible to detect common age features, which could help for data interpretation and evaluation of micro POC  $^{14}\text{C}$  ice sample ages?

## 7. Results - Systematical investigation of $^{14}\text{C}$ age biasing effects in glacier ice

Under close collaboration with colleagues from Innsbruck and Trieste, it was possible to assemble a collection of macroscopic material samples from selected sites all over the Alps (see Fig. 7.1). These samples span a large range of type and composition. Starting with material collected on the surface of the glaciers (Jamtalferner, Venediger- and Sulzbachkees, Grenzgletscher) over macroscopic incorporations to the ice matrix easy identifiable and accessible in glacier caves (Stubai glacier) and ice caves (Vasto ice cave), to microscopic POC samples retrieved from ice and snow block samples (Grenzgletscher, Colle Gnifetti).

In the following, the  $^{14}\text{C}$  results of these samples are presented according to the sampling sites, followed by a general conclusion on potential  $^{14}\text{C}$  age biasing effects of the respective materials.

### 7.2. Site descriptions and presentation of radiocarbon results

#### 7.2.1. Jamtalferner (Austria) - surface cryoconite and sediment samples

The main study area for collection of sediment and cryoconite samples was Jamtalferner glacier located at the Silvretta mountain range in Austria, directly at the Swiss border. This glacier was chosen on one hand because of easy accessibility (by car and foot) and on the other hand, because it is retreating very fast (see e.g. Fischer (2013)) and uncovers more basal sediment each year. It also produces a lot of cryoconite holes every summer, because of the comparably low altitude (ca. 2430-3160 m a.s.l.) and significant surface melting during the summer season.



**Fig. 7.2.:** Aerial view of the Jamtalferner (Austria) 2013 from the south, with the sampling sites for sediment and cryoconite. Picture provided by Andrea Fischer (Innsbruck).

A view of the whole sampling area is given in Fig. 7.2. During the summer seasons 2012-14, five sediment samples, four cryoconite samples and one Saharan dust sample fresh from the surface have been collected and radiocarbon dated (see Table 7.1). Two exemplary pictures of the sampling are shown in Fig. 7.3 and 7.4.

## 7.2 Site descriptions and presentation of radiocarbon results



**Fig. 7.3.:** Sampling location of Jam 2-2 sed. The greyish and sandy sediment became ice free in the year of sampling and immediately a patch of grass grew there. Picture by Andrea Fischer.



**Fig. 7.4.:** Sampling site of Jam 1-1 sed. The sample was very wet, rather dark and smelly, which indicates microbial activity (Hoover and Pikuta, 2012) Picture by Andrea Fischer.

All samples have been stored in glass bottles and kept frozen as long as possible, but not during transports. They have all been pretreated according to the standard protocol used for sediment samples in the Klaus-Tschira-Lab Mannheim (see Appendix A.3) and were graphitised for  $^{14}\text{C}$  measurement. Only the samples Jam 1-3 sed, Jam F-2 sed and Jam M-1 sed have not been graphitised, but were combusted at the IUP Heidelberg and measured via the gas ion source, because of their small carbon masses. The Saharan dust sample was processed in the offline filtration system and blank corrected accordingly.

**Tab. 7.1.:** Sample parameters and  $^{14}\text{C}$  results of sediment (ending: sed) and cryoconite samples (ending: cryo) and one surface Saharan dust fall collected at Jamtalferner.

Sample name	Sample mass [mgC]	%C <sub>mass</sub>	F $^{14}\text{C}$	$\Delta\text{F}$	$^{14}\text{C}$ age [yBP]	Error [yBP]	$\delta^{13}\text{C}$ [‰]
Jam 1-1 sed	0.226	0.2	0.856	0.002	1247	22	-26.5
Jam 1-2 sed	0.985	0.7	0.928	0.002	602	19	-22.9
Jam 2-2 sed	0.436	0.1	0.444	0.003	6514	50	-36.6
Jam F-2 sed	0.016		0.124	0.005	16749	308	-36.7
Jam M-1 sed	0.093		0.365	0.004	8090	95	-23.5
Jam 2-1 cryo	3.313	5.3	0.796	0.002	1833	17	-19.9
Jam S-1 cryo	1.422	1.3	0.802	0.002	1774	24	-22.9
Jam H-1 cryo	1.655	1.7	0.828	0.002	1517	24	-21.0
Jam H-2 cryo	1.125	0.5	0.740	0.002	2415	26	-19.7
Sahara 7-A	42.2 $\mu\text{gC}$		0.61	0.015	3973	199	-19.3

All sediment samples showed carbon contents below 1% of the sample mass, which is quite typical for soil with low organic content. The  $\delta^{13}\text{C}$  values indicate average organic material (see Table 2.1), the very low values of Jam 2-2 sed and Jam F-2 sed are due to the small sample sizes.

## 7. Results - Systematical investigation of $^{14}\text{C}$ age biasing effects in glacier ice

### 7.2.2. Grenzgletscher (Swiss Alps) - surface cryoconite and Saharan dust samples from ice blocks

The Grenzgletscher originates in the summit region of the Monte Rosa Massif at the Swiss Italian border, namely at the Colle Gnifetti, where the ice cores discussed later in this work have been drilled.

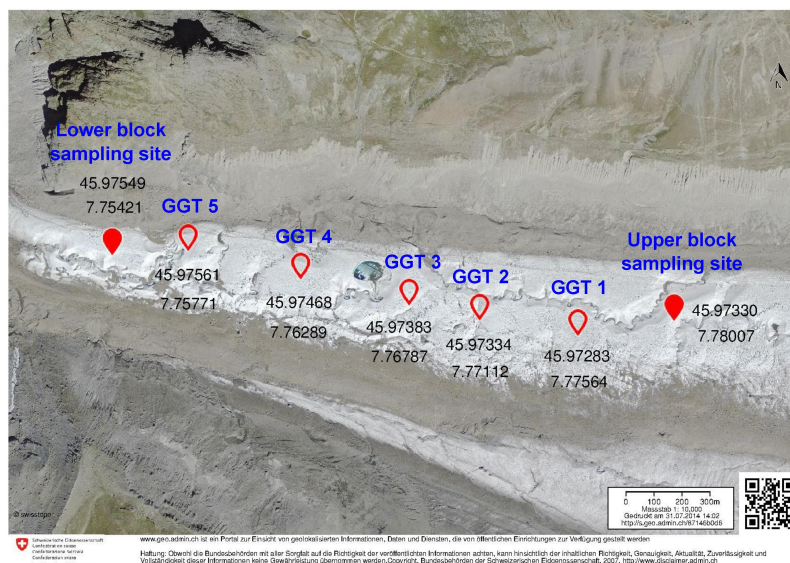


**Fig. 7.5.:** Map of the Grenzgletscher sampling area downstream of the glacier in the ablation zone. The sampling sites for cryoconite are marked in blue.

It is a polythermal glacier, which means that the ice is cold at the base and has a temperate section on top of that cold basal ice in the mid altitudes (Steier et al., 2006). This flow characteristic leads to the resurfacing of old, cold ice in the tongue area (Haeberli, 1975), which was formed at very high altitudes (For a more detailed description see Appendix A.3). No measurable amounts of  $^{210}\text{Pb}$  could be detected within the ice (Steier et al., 2006), which implies, that it is older than ca. 150 years and therefore pre-industrial. In summer 2014, a large ice block sampling campaign has been carried out at the ablation zone of Grenzgletscher, at two main sites, shown in Fig. 7.5.

Overall, 27 blocks have been extracted from the upper (2460 m a.s.l.) and lower (2300 m a.s.l.) sampling site by use of a chainsaw and shipped frozen to the IUP Heidelberg. Two blocks (15R and Dust S, see Table 7.2) from the upper site were by the characteristic yellow / red colour identified to have a large Saharan dust content.

Additionally, along a transect between the two major block sampling sites, five cryoconite samples (ending cryo in Table 7.2) have been collected from water-filled holes. They were stored in glass bottles in the freezer until sample preparation. The cryoconite samples have been pretreated like sediment samples (see protocol in Appendix A.3) and were graphitised for AMS measurement. Some of the ice samples have been processed in The REFILOX (total combustion at 800 °C) and some in the offline system. All have been blank corrected accordingly and  $^{14}\text{C}$  dated via the gas ion source.

## 7.2 Site descriptions and presentation of radiocarbon results

**Tab. 7.2.:** Sample parameters and POC  $^{14}\text{C}$  results of Saharan dust, clean ice and cryoconite samples from Grenzgletscher (Swiss Alps). The samples with ending REFILOX have been processed in the REFILOX system, the ones with ending Offline in the offline filtration system. Carbon concentrations are given in  $\frac{\mu\text{gC}}{\text{kg}}$  for the ice samples and mass % for the cryoconite samples

Sample name	Sample mass [mgC] / [ $\mu\text{gC}$ ]	C conc. [ $\frac{\mu\text{gC}}{\text{kg}}$ ] / [%]	F $^{14}\text{C}$	$\Delta\text{F}$	$^{14}\text{C}$ age [yBP]	Error [yBP]	$\delta^{13}\text{C}$ [‰]
4-1 REFILOX	4	11	0.342	0.187	8620	1502	-34.2
4-1 Offline	3.5	9	0.862	0.187	1192	1506	-22.9
4-2 Offline	3.3	5	0.694	0.176	2929	1412	-24.2
16-1 REFILOX	3.8	14	0.609	0.26	3980	2087	-28.7
16-2 REFILOX	3.3	9	0.827	0.393	1529	3161	-27.7
16-3 Offline	3.0	7	0.7	0.201	2863	1616	-26.4
15 REFILOX	6.3	22	0.778	0.143	2019	1148	-15.8
Dust Offline	13.5	67	0.745	0.041	2368	329	-19.9
GGT-1 cryo	1.025	1.0%	0.933	0.003	556	23	-18.3
GGT-2 cryo	0.870	0.8%	0.940	0.003	494	23	-18.6
GGT-3 cryo	0.899	0.9%	0.923	0.002	642	23	-19.2
GGT-4 cryo	0.411	0.4%	0.838	0.002	1420	25	-19.7
GGT-5 cryo	0.427	0.2%	0.772	0.002	2076	27	-21.2

### 7.2.3. Stubai glacier cave (Austria) - sediment, cryoconite, Saharan dust and macroscopic organic material

Stubai glacier cave is an artificial cave, carved along bedrock in the tongue of Schaufelferner (Stubai glacier) near Innsbruck (Austria). The glacier is located at an altitude of 1750-3210 m a.s.l. and is therefore temperate, but nevertheless shows regions of bedrock permafrost (Andrea Fischer (Innsbruck), pers. comm.).

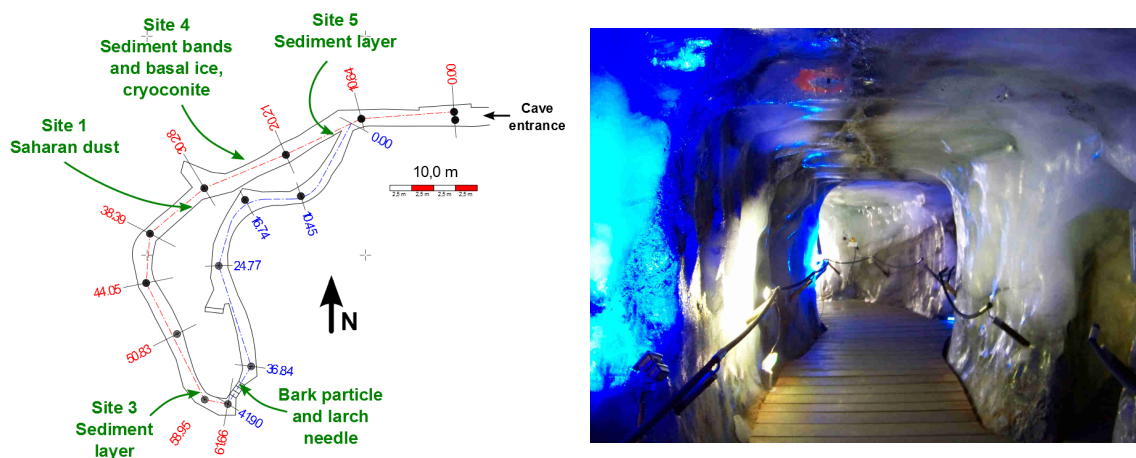


**Fig. 7.6.:** Left: Map of the cave with the sampling sites. Right: View inside Stubai glacier cave. Note the distinct layering visible in the walls.

## 7. Results - Systematical investigation of $^{14}\text{C}$ age biasing effects in glacier ice

At the position of the cave, the glacier diverges trapezoidal around a rock feature, where the cable car station Eisgrat is located. Thus the flow velocity is not larger than ca. 0.5 m/year and the layers are strongly tilted (ca.  $45^\circ$ ). The cave was mainly laid out for touristic purposes, but now allows easy access to basal glacier ice without ice core drilling. Fig. 7.6 shows a view into the cave. The cave walls reveal a large variety of different material incorporated into the layering of the glacier. During April and September 2014, nine samples (see table 7.3) of macroscopic material have been extracted directly from the ice walls of the tunnels by use of ice screws.

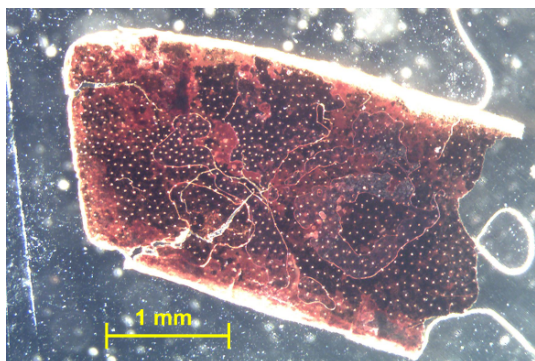


**Fig. 7.7.:** Microscope image of the bark particle extracted from the wall of Stubai glacier cave for  $^{14}\text{C}$  dating. Note the scale.



**Fig. 7.8.:** Saharan dustband in the wall of the glacier cave, which was sampled for POC  $^{14}\text{C}$  dating. Picture by Andrea Fischer.

**Tab. 7.3.:** Samples extracted from the walls of Stubai glacier cave, Austria, their masses and  $^{14}\text{C}$  results. Stubai 1 is from a Saharan dust horizon, Stubai 3-5 are taken from sediment bands, Stubai cryo is probably old cryoconite and the last two are biological remnants (bark and a larch needle).

Sample name	Sample mass [mgC] / [ $\mu\text{gC}$ ]	F $^{14}\text{C}$	$\Delta\text{F}$	$^{14}\text{C}$ age [yBP]	Error [yBP]	$\delta^{13}\text{C}$ [‰]
Stubai 1 Sahara	84.6	0.738	0.008	2442	85	-24.3
Stubai 4 middle	12.4	0.165	0.006	14 500	311	-30
Stubai 4 basal	19	0.073	0.003	21 072	368	-31.8
Stubai 4 sed basal	34	0.058	0.002	22 866	310	-25.2
Stubai 3	7.5	0.135	0.007	16 106	409	-29.3
Stubai 5	16.9	0.181	0.005	13 713	204	-29.3
Stubai bark	25.9	0.960	0.009	325	74	-21.2
Stubai larch needle	14.8	0.942	0.013	484	108	-21.9

The samples include: A saharan dust band (Stubai 1, see Fig. 7.8), several sediment bands (Stubai 3-5, see e.g. Fig. 7.9), a sample probably containing enclosed cryoconite (Stubai cryo) and two particles of clearly biological origin. A bark particle (Fig. 7.7) and a larch needle.



**Fig. 7.9.:** Exemplary sediment band sampled for POC  $^{14}\text{C}$  dating with ice screws. Picture by Andrea Fischer.

Although the samples were not large enough for graphitisation, they have been pretreated at the IUP Heidelberg according to the protocol used for sediments stated above and were combusted completely at  $800\text{ }^{\circ}\text{C}$ . All have been measured for  $^{14}\text{C}$  via the gas ion source.

### 7.2.4. Vasto ice cave (Italy) - Saharan dust

Vasto ice cave is located in the Eastern Alps in the Monte Canin massif at an altitude of ca. 2200 m a.s.l. (Colucci, 2013). It is a karst area, and some of the rock caves host large perennial ice bodies. The original formation of these ice bodies is up to now not entirely clear, but for Vasto ice cave it is assured that nowadays there are wind blown material inputs as well as direct snow accumulation.

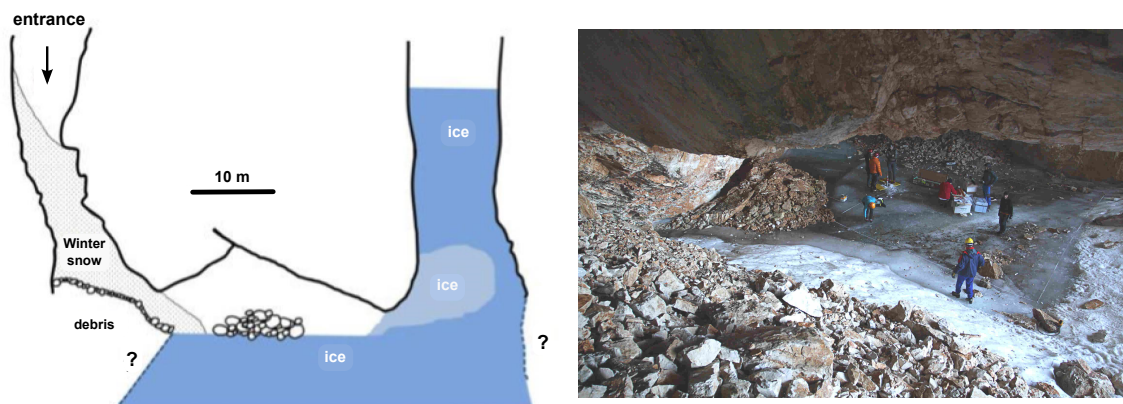


**Fig. 7.10.:** **Left:** Vertical section through Vasto ice cave. The entrance is only open during summer, when the winter snow accumulated in the entrance shaft is gone (Figure taken from Colucci et al. (2014)). **Right:** The cave interior and the ice surface during core drilling. (Picture provided by Jacopo Pasotti).

## 7. Results - Systematical investigation of $^{14}\text{C}$ age biasing effects in glacier ice

After a ground penetrating radar survey in 2012 ((Colucci et al., 2014)), in fall 2014 a ca. 7.8 m long ice core has been drilled from the main ice body (Forte et al., 2014). A map of Vasto ice cave and a picture from the drilling is shown in Fig. 7.10. From the core, six depths (core depth D in Table 7.4), where macroscopic material was visible have been sampled for POC  $^{14}\text{C}$  dating. Part of the layer was consisting of very dark material, which had a large carbonate content and therefore must be considered to contain sediment from the surrounding carbonate rocks. The other layers showed a very red colour typical for Saharan dust, which also can be observed as surface dust falls in that region.

**Tab. 7.4.:** Overview of the ice samples (masses and  $^{14}\text{C}$  results) prepared from an ice core from Vasto ice cave (Italy). The first two samples have been pretreated like sediment, the others were filtered in the offline system.

Sample name	Core depth D [cm]	Sample mass [ $\mu\text{gC}$ ]	$\text{F}^{14}\text{C}$	$\Delta\text{F}$	$^{14}\text{C}$ age [yBP]	Error [yBP]	$\delta^{13}\text{C}$ [‰]
Can 2A	70	58.8	0.861	0.009	1199	85	-16.2
Can 2B	70	62.2	0.704	0.007	2819	83	-26.4
Can 11A	500	65.5	0.713	0.007	2721	84	-26.9
Can 13-A	490	39.7	0.835	0.008	1452	79	-27.6
Can 15-A	515	11.0	0.832	0.015	1481	142	-31.4
Can 16-A	530	30.1	0.794	0.008	1852	81	-25.5

Samples 2A and 2B were large enough to be treated directly like sediment samples. All others have been processed in the offline filtration system and their  $^{14}\text{C}$  results have been blank corrected according to the values in Table 6.6. All samples have been  $^{14}\text{C}$  dated via the gas ion source.

### 7.3. Discussion of radiocarbon results

In this section, the  $^{14}\text{C}$  ages of macroscopic sediment, cryoconite and Saharan dust samples from different locations described above are analysed for age biases and common features. The aim is to draw some conclusions for the interpretation of  $^{14}\text{C}$  dates derived from micro scale POC analyses of Alpine ice samples.

#### 7.3.1. Saharan dust

The  $^{14}\text{C}$  ages of the Saharan dust samples from all sites are shown together in Fig. 7.11. They are complemented by three snow samples from the high Alpine glacier saddle of Colle Gnifetti (detailed site description in Chapter 9), whose sample parameters and results can be found in Table A.10 in Appendix A.3. The samples S4 and S4-2 are from one snow block, taken directly below the fresh snow surface in Summer 2013 and the sample S6 from ca. 2 m depth. Additionally, a firn sample from 1977 A.D. was measured, containing a large Saharan dust fall (Wagenbach and Geis, 1989). The results of all dust samples collected at present day (Colle Gnifetti and Jamtalferner) have been according to Equation 6.2 corrected for a assumed fossil fuel contribution of 7% of total POC mass (based on results for high Alpine modern aerosol by Gelencsér et al. (2007)). These corrected values are marked in grey in Fig. 7.11.

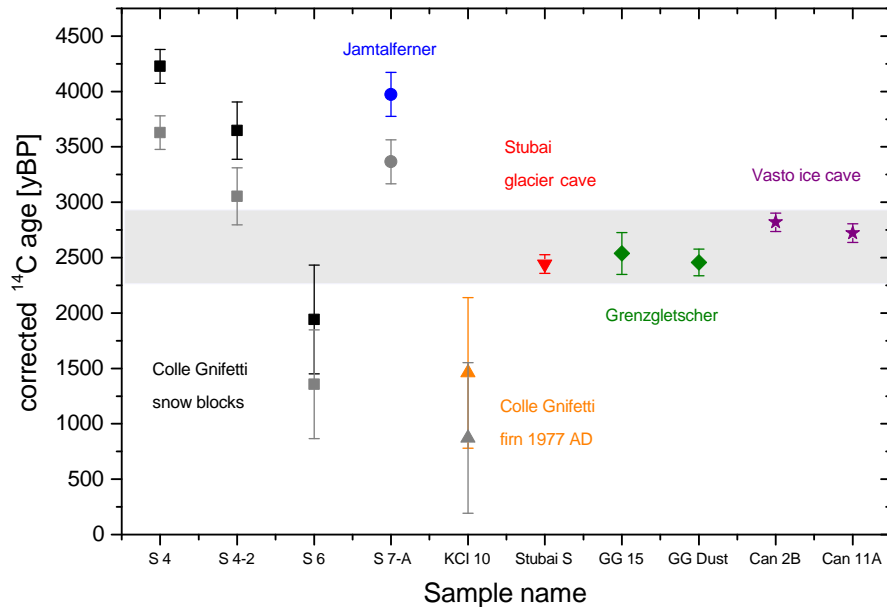


**Fig. 7.11.:**  $^{14}\text{C}$  ages of snow and ice samples clearly containing Saharan dust from sampling sites all over the European Alps. The grey symbols denote the modern dust sample results after correction of a 7% mass contribution of fossil fuel EC. Note the very narrow age range for the pre-industrial samples from Stubai glacier cave, Grenzgletscher and Vasto ice cave.

The most striking observation is that all samples collected from the ice matrix of the pre-industrial sites (Stubai glacier cave, Grenzgletscher, Vasto ice cave), separated by hundreds of km distance and very different ice body characteristics (and ages) agree extremely well, almost within  $1\sigma$  error range. This implies, that in these samples a characteristic POC  $^{14}\text{C}$  signature of Saharan dust has been recorded. This could possibly hint to a similar source region in the north west of the African continent (Aymoz et al., 2004; Sodemann et al., 2006; Thevenon et al., 2012). The POC  $^{14}\text{C}$  ages of these samples are in a range of:

#### Pre-industrial Saharan dust POC $^{14}\text{C}$ age: 2200 - 2800 yBP

This range is marked by the grey bar in Fig 7.11. This finding agrees quite well with the only other direct  $^{14}\text{C}$  measurement of Saharan dust reported so far by Eglinton et al. (2002) over the Atlantic ocean, where ages between 1200 and 2000 yBP have been measured.

All samples from Colle Gnifetti snow, which should represent a modern  $^{14}\text{C}$ -age without a dust bias, are dated within a range of ca. 1500-4500 years BP. The deepest sample from ca. 2 m depth (S6) showing the youngest age. There are probably several reasons for these high  $^{14}\text{C}$  ages:

- Incomplete decontamination of the very porous snow samples, therefore possibly higher and unknown blank contribution.
- Insufficient correction of fossil fuel contribution, which could be enhanced during summer, where the nearby hut is using a diesel generator for power supply.

## 7. Results - Systematical investigation of $^{14}\text{C}$ age biasing effects in glacier ice

Also the firn sample from 1977 shows an age of about 1500 yBP and not an over modern  $^{14}\text{C}$  signature of  $F=1.37$  (Levin et al., 2010), which would be expected from an atmospheric sample archived during the bomb peak period. If this sample is hypothetically corrected to  $F=1.37$  (Eq. 6.2), under assumption of a Saharan dust age of 2500 yBP, this would result in a contribution of 67% mass of dust to the total POC of the sample, which is regarded to be not unrealistic by the optical appearance of the sample material. About the same contribution, 62% is calculated for the snow sample S6. For the snow samples S4 and S4-2, as well as for the surface sample from Jamtalferner however, this correction does not work, because they are already older than the assumed Saharan dust age. Here, it is concluded that the fossil fuel correction of 7% was probably too low and not representing the real conditions. The uncertainty of this correction is a major problem for all samples from the industrial period.

### Vasto ice cave and Grenzgletscher - examples for dating problems caused by dust biases

An impressive example of the  $^{14}\text{C}$  age biasing abilities of Saharan dust, put into the context of a glaciological investigation, is the dating of the ice core samples from Vasto ice cave. The uncalibrated results of all  $^{14}\text{C}$  dated POC samples are shown in Fig. 7.12. It is striking that four samples show a reasonably increasing age with core depth, while two are showing much larger ages, with deviations of up to 1500 years. These two samples (2B and 11A) were taken directly adjacent in depth to 2A and 13A. They were the ones with the characteristic red colouring of Saharan dust. In this case, the biased samples could be optically identified. If the POC concentrations are very low and optical identification of these horizons is no longer possible, the distinction of dust biased outliers, especially in older age ranges can be very difficult.

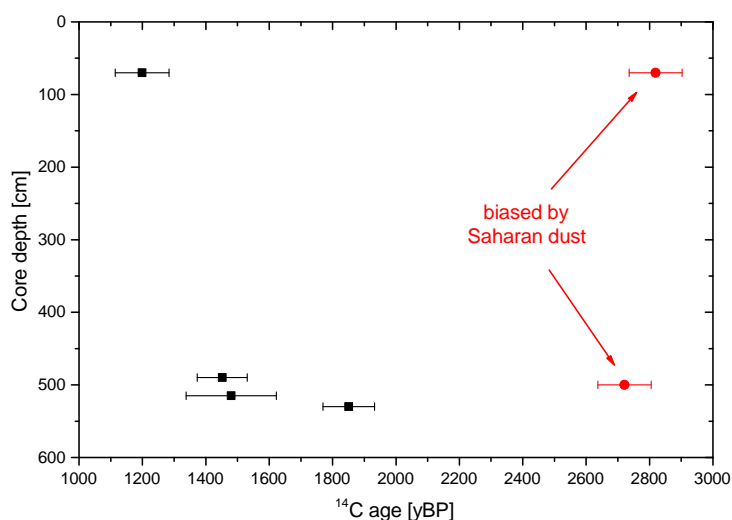


**Fig. 7.12.:** POC  $^{14}\text{C}$  dating results for samples from an ice core drilled in Vasto ice cave (Italy). Note the two very high ages produced by obvious Saharan dust input directly adjacent to unbiased samples.

An example, where this macroscopic distinction is not possible and thus more representative for the real problems when it comes to dating of high Alpine ice samples, is the POC  $^{14}\text{C}$  dating of

block samples from Grenzgletscher (Swiss Alps) collected in summer 2014. All ice block samples had a very white and bubble rich appearance and no incorporated macroscopic material. Out of the total 27 ice blocks, only three yielded high enough POC concentrations for  $^{14}\text{C}$  dating so far.

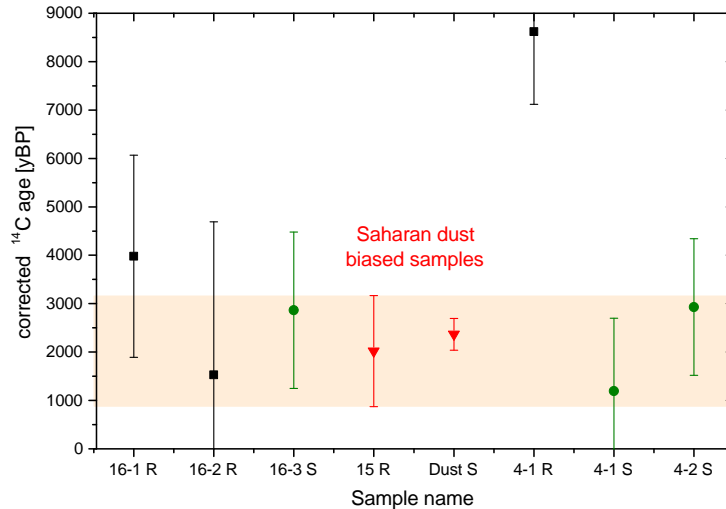


**Fig. 7.13.:** POC  $^{14}\text{C}$  ages of all measurable Grenzgletscher ice blocks. The large errorbars result from the very small sample masses. Note the coincidence of the dust biased and not dust biased sample ages (shaded area).

All samples have been  $^{14}\text{C}$  dated via the gas ion source, with rather large errors because of the very small sample masses below  $5 \mu\text{gC}$ . All yielded very low POC contents of  $5\text{--}14 \frac{\mu\text{gC}}{\text{kg}}$  and were thus really at the lower limit of feasibility. The  $^{14}\text{C}$  ages of the ones large enough to be dated are shown in Fig. 7.13. Remarkably, the two obviously dust biased samples show no large age difference compared to the other samples, apart from one outlier. The question is now: is this agreement a coincidence? Do the non-biased results represent the ice age, as they are in about the same ranges as the results found by Steier et al. (2006), which were also retrieved by POC  $^{14}\text{C}$  dating and scattering around 2000 yBP? Or are all samples biased by small amounts of Saharan dust, which is just not obviously visible. From the  $^{14}\text{C}$  data alone, this question can not be answered. Thus the Grenzgletscher samples are an impressive example for the limitations of the POC  $^{14}\text{C}$  dating method of ice, when it comes to microscopic material sizes.

### Conclusion of the Saharan dust investigations

As a conclusion, the Saharan dust POC  $^{14}\text{C}$  ages of different sample types and a large variation of sampling sites show overall age ranges from ca. 1000 - 4000 yBP with a mean around 2500 y BP for pre-industrial samples. Saharan dust must therefore considered to have a large potential of age biasing effects for POC  $^{14}\text{C}$  dating of Alpine ice samples. Therefore, such dust must be avoided at the sample selection, where it is obvious. Where it can not obviously be excluded by colour, it should be tried to separate it from the residual organic material by other methods. Apart from the separation by application of different combustion temperatures discussed in Section 6.7.1, this could potentially also be achieved by a size separation. Saharan dust reaching the Alpine glaciers by long range transport mainly consists of clay minerals with particle sizes below  $2 \mu\text{m}$

## 7. Results - Systematical investigation of $^{14}\text{C}$ age biasing effects in glacier ice

(Tomadin et al., 1996). In soil, degrading organic (humified) substances are able to build very stable aggregates with these clay minerals (Scheffer and Schachtschabel, 2010), which prevents them from further degradation and allows ageing of the material. It is therefore assumed, that the high  $^{14}\text{C}$  ages found for Saharan dust samples are mainly caused by these aged substances transported along with clay minerals.

### 7.3.2. Cryoconite

The  $^{14}\text{C}$  results of all cryoconite samples collected from the sites described above are shown in Fig. 7.14. They are complemented by three samples from Venedigerkees and Sulzbacherkees, parts of the Obersulzbach glacier below the peak of Grossvenediger, Austria (for glaciological features see Fischer et al. (2014)). For comparison with some non-Alpine cryoconite, also three samples from the Karakoram glaciers (provided by Christoph Mayer (Munich)) have been radiocarbon dated. Sample parameters and  $^{14}\text{C}$  results of these additional samples can be found in Table A.3.4 in Appendix A.3.

The first thing to notice is that most of the Alpine samples reveal ages in the same ranges as the Saharan dust samples around 1500-2500 years BP. This is probably not due to a significant input of Saharan dust, but caused by the diversity of material that makes up the cryoconite, containing sediment, soot and microbes (see e.g. MacDonnel and Fitzsimons (2008); Langford et al. (2010); Xu et al. (2010)).

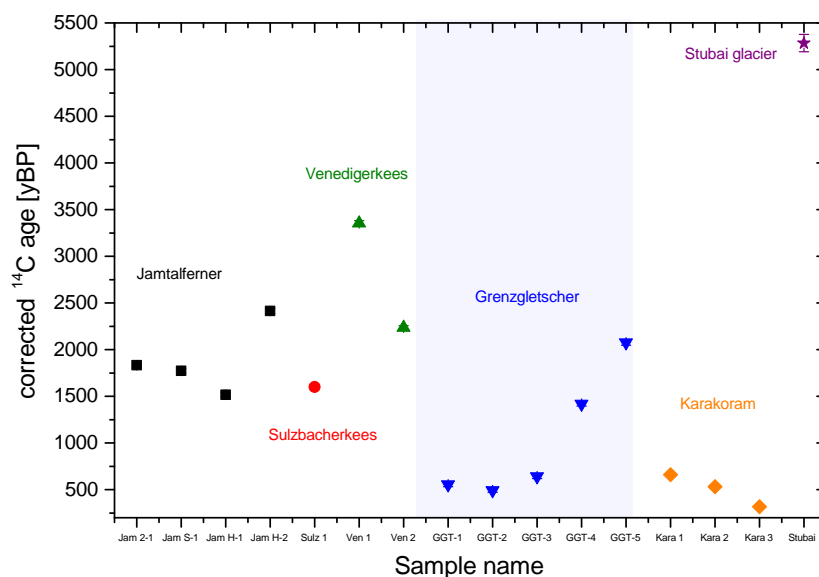


**Fig. 7.14.:** Overview of all cryoconite  $^{14}\text{C}$  results. Note the gradual age increase of the Grenzgletscher (GGT) samples.

The samples from the Austrian glaciers were all very black and smelly, which on one hand indicates a high soot content and on the other a high living microbial activity. These qualities are contradicting elements in terms of  $^{14}\text{C}$  age, assuming the soot in modern times mainly originating from fossil fuel combustion. Only the sample from Stubai glacier cave has with ca. 5000 yBP a much higher age. This sample has been identified as cryoconite mainly because of its very dark

colour. It was also incorporated in the ice matrix and no surface sample. Therefore it is likely also influenced by sediment and does not show as much microbial activity metabolising modern carbon with young  $^{14}\text{C}$  ages than the other samples.

The cryoconite samples collected at Grenzgletscher show a gradually increasing age downstream (see Fig. 7.5 for sampling sites), which is intriguing at first glance because it follows in principle the expected age increase of the glacier surface ice. But this would mean, that the major part of the organic material would have originated from the glacier interior and this is just not plausible. A more realistic scenario is a difference in the source of the particles within the cryoconite holes. All Alpine samples show  $\delta^{13}\text{C}$  values around  $-20\text{‰}$ , which indicates average organic values and no large influence of fossil contributions and thus the age differences are likely to be caused by different origins of the sediment material accumulating in the holes. The ages of the Karakoram samples are overall younger than the Alpine samples, but still show  $^{14}\text{C}$  ages up to 600 years BP. They have a much higher  $\delta^{13}\text{C}$  values of about  $-14\text{‰}$  clearly indicating the influence of C4 plant material and no large contributions of fossil fuel.

Overall, as appreciated from the possible composition, cryoconite also can have large reservoir  $^{14}\text{C}$  ages even if sampled from fresh, active, water filled holes. If these holes are covered again with ice and are slowly subducted into the glacier ice, this cryoconite material can later be taken mistakenly for atmospheric aerosol. In such a case, the POC  $^{14}\text{C}$  ice age will be biased to ages too old and not representing the surrounding ice. With a large age range from ca. 400 yBP to more than 3000 yBP the quantification of this cryoconite influence is difficult, but nevertheless it is a first order of magnitude. Therefore, wherever it is possible to identify old cryoconite within a glacier ice sample for POC  $^{14}\text{C}$  dating, for example by high concentrations of microbes, these sections should be avoided.

### 7.3.3. Sediment

The  $^{14}\text{C}$  ages of the surface sediment samples collected at Jamtalferner and from the walls of Stubai glacier cave are shown in Fig. 7.15. The sediment samples collected at Jamtalferner show an overall very large age range starting at a  $^{14}\text{C}$  age of ca. 600 yBP going up to almost 17 000 years. The youngest samples Jam 1-1 sed (see Fig 7.4) and Jam 1-2 sed were sandy, but had a very black appearance and were smelling like rotten organic material. This is an indicator for microbial activity (see e.g. Hoover and Pikuta (2012)) and thus probably the reason for the comparably young ages. The other three sediment samples that have been collected from patches, which were ice free for at least one season showed very high  $^{14}\text{C}$  ages. The highest age with ca. 16 800 years BP, and therefore almost within the last glacial maximum, was shown by the sample from the highest altitude in the accumulation zone, Jam F-2. This is a significant result and could hint to the possible age range of glacier formation onset, which has to remain however highly speculative only based on the present sparse data. Also the other two samples collected from an old side moraine (Jam M-1) and from a freshly ice free patch a little lower than the oldest sample (Jam 2-2) showed with ca. 6500 yBP and 8000 y BP very high ages compared to all Saharan dust and cryoconite results.

The samples taken from different dust bands in the walls and basal sediment of Stubai glacier cave show even higher  $^{14}\text{C}$  ages of up to almost 23 000 yBP measured for the basal sediment. This impressively shows, that basal glacier sediment is able to conserve very old organic material,

## 7. Results - Systematical investigation of $^{14}\text{C}$ age biasing effects in glacier ice

which then does not represent the surrounding ice age, when folded into the glacier.

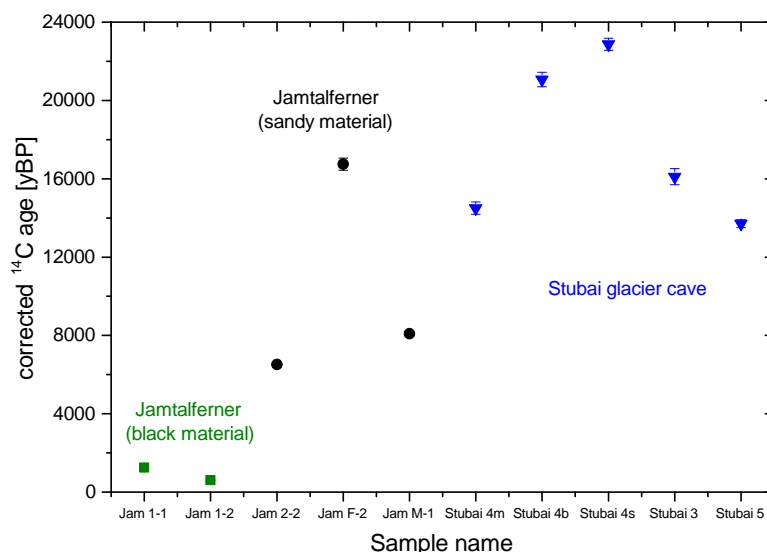


**Fig. 7.15.:** Overview of all sediment  $^{14}\text{C}$  results. The two samples from Jamtalferner marked in green (black material) are very young compared to all other samples. They showed clear indications of living bacterial activity, which is likely the case for the comparably young  $^{14}\text{C}$  ages

As a conclusion, if this openly available very old sediment material is mobilised by wind and transported onto the glacier surface, it can have a significant age biasing effect, when dated as POC later within glacier ice. Therefore, obviously sediment rich layers should not be chosen for POC  $^{14}\text{C}$  dating of ice samples under all circumstances.

### 7.4. General implications for interpretation of POC derived radiocarbon ice ages

Within this study of potentially age biasing effects on the POC  $^{14}\text{C}$  dating of ice samples, for the first time Alpine Saharan dust, cryoconite and sediment samples have been investigated systematically together for their intrinsic  $^{14}\text{C}$  ages and influences on the POC fraction in glacier ice. The averaged  $^{14}\text{C}$  age ranges found for these materials collected from various sites all over the European Alps are summarised in Table 7.5. The overall large intrinsic reservoir ages imply that the incorporation of these materials into POC samples for ice dating should be avoided by all means.

This is most impressively shown at the example of Stubai glacier cave, where Saharan dust, sediment and macroscopic biological remnants could be studied in the ice walls in close vicinity of only a few meters. The macroscopic bark particle and the larch needle were dated to  $^{14}\text{C}$  ages of 325 and 484 yBP and meet within  $1\sigma$  error range. Unfortunately, this is the age range, where calibration with the atmospheric  $^{14}\text{C}$  curve is not possible, but still this age range can serve as a best guess for the representation of the actual glacier ice age. Only because of the lucky finding of

## 7.4 General implications for interpretation of POC derived radiocarbon ice ages

---

these macroscopic biological particles, it was possible to judge the POC  $^{14}\text{C}$  ages from the other layers in the right way as biased by aged material.

**Tab. 7.5.:** Summary of the characteristic  $^{14}\text{C}$  ages of different materials in Alpine glacier ice samples

Material	$^{14}\text{C}$ age range [yBP]
Saharan dust (pre-industrial)	2200 - 2800
Cryoconite (modern)	500 - 3500
Sediment	600 - 22 000

Where no macroscopic organic particles can be found in the ice and also an identification of Saharan dust or sediment layers is not possible in a sample (see e.g. the example of Grenzgletscher), other methods must be applied to exclude the potentially biased materials. This can be done e.g. by size, which could be possible for Saharan dust, or by combustion temperature, which was demonstrated by the analyses of aerosol samples (see section 6.7.1). The main conclusion drawn from these results is that for sampling sites, where the microscopic fraction is the only one that can be dated, the estimation of a glacier ice age is therefore limited. Because of the tendency of biases to very old ages, POC  $^{14}\text{C}$  ages should be regarded as an upper age limit in most cases.



## 8. Results - POC based $^{14}\text{C}$ dating of selected small Alpine glacier caps

### 8.1. Cold Alpine ice patches

Small Alpine glacier caps and ice patches at altitudes below 3500-4000 m a.s.l., where under normal conditions no cold ice bodies can be found (Wagenbach et al., 2012) have recently come into focus again (see e.g. Haeberli et al. (2004); Haeberli (2005)). Some of these ice patches, like Titlis glacier (Switzerland), were found to be still cold at the base, frozen to bedrock and very stagnant (Lorrain and Haeberli, 1990). This characteristic offers the possibility of potentially old, undisturbed basal ice being conserved. The age of this ice could then provide valuable information about the time of glacier formation onset. At present, a new project ((C)old ice AT) to investigate such ice bodies is in progress, led by colleagues from the University an Institute of Mountain Research, Innsbruck. During a pilote study connected with this project at Titlis glacier, it was possible to retrieve some basal ice samples for a first application of POC  $^{14}\text{C}$  dating. Another research target within this project about cold ice patches is Vadret dal Corvatsch (Switzerland), where the glacier base is still cold as well (Hager, 2002) and already an ice core has been drilled in 2007. Here, it was envisaged to apply the improved POC  $^{14}\text{C}$  method of this work to back up earlier measurements of May (2009), which showed a very large measurement error.

### 8.2. Site descriptions

#### 8.2.1. Titlis glacier cave, Swiss Alps

Titlis glacier cave is an artificial cave carved out along the bedrock of Titlis glacier at the summit of Chli Titlis (near Engelberg, Swiss Alps) at an altitude of 3020 m a.s.l. The cave has already been constructed more than 25 years ago for touristic purposes and allows easy access to the basal ice of the glacier along bedrock. A schematic outline of the cave and a view inside the tunnel are shown in Fig. 8.1 and 8.2. The glacier has a maximum thickness in this area of ca. 20 m, but especially in the entrance part of the cave this is nowadays probably rather in the order of 6-8m (Bergbahn Titlis pers. comm.). The walls of the cave show a very distinct layering including very dark layers and especially near bedrock very much sediment-like material.

In 2014 and 2015, two reconnaissance campaigns have been realised, together with new measurements of the englacial temperature. The basal ice temperature in August 2015 was still about  $-1\text{ }^{\circ}\text{C}$ , so after 25 years (see Lorrain and Haeberli (1990)), the glacier cap can still be considered to be cold and frozen to bedrock despite substantial surface melting. In total three spots in the cave walls have been sampled for ice blocks with a chainsaw. Two profiles were cut out near the entrance of the cave, probably close to the spot where also Lorrain and Haeberli took samples for water isotope analyses 25 years ago. The third spot was about 20 m deeper in the cave.

## 8. Results - POC based $^{14}\text{C}$ dating of selected small Alpine glacier caps

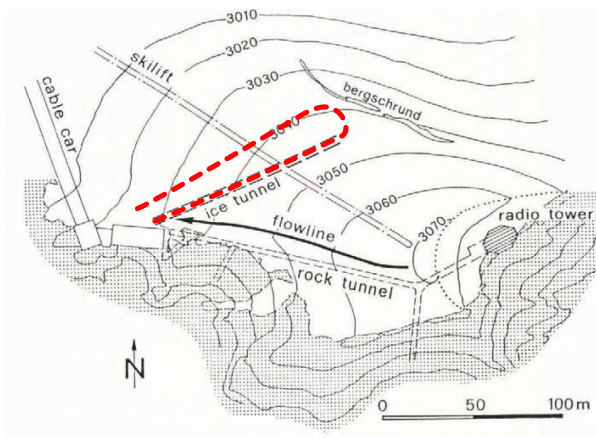


**Fig. 8.1.:** Schematic view of the outline of the ice tunnel at the summit of Chli Titlis. Today the cave is extended to a U-shape, roughly marked in red. Adapted from Lorrain and Haeberli (1990).

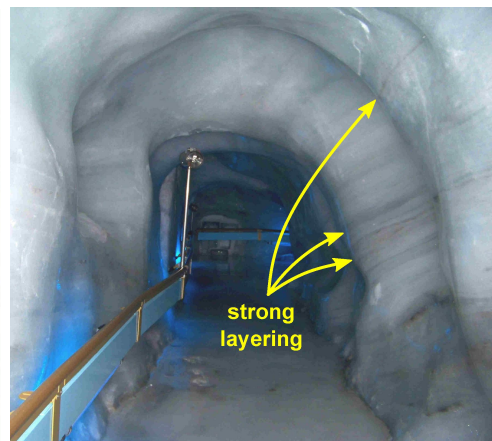


**Fig. 8.2.:** View into the ice tunnel at Titlis glacier (2015). A level floor has been constructed by freezing water. Note the distinct layering visible in the walls.

Pictures of the three sampling sites can be found in Fig. A.11 in Appendix A.4, sketches of the sampling sites are shown in Fig. 8.5 and 8.6. All profiles were cut down to bedrock, where the deepest part of the first profile from 2014 showed a section of very clear, bubble free ice. The origin of that section is up to now not entirely clear, but crystal fabric investigations showed strong signs of meltwater influences (pers. comm. Johanna Kerch). This clear ice section was not present in the other two profiles.

### 8.2.2. Vadret dal Corvatsch (Piz Murtel), Swiss Alps

Vadret dal Corvatsch is a small glacier cap on top of Piz Murtel (3433 m a.s.l.) in the Upper Engadin, Switzerland. Pictures of the glacier cap in 1998 during a strong melting event and 2007 are shown in Fig 8.3 and 8.4, with a strong layering visible at the flank. A more detailed description of the glaciological settings can be found in Haeberli et al. (2004) and May (2009).

In winter 2007, in cooperation with the University of Zürich, an ice core (VCL) has been drilled to bedrock, about 100 m below the peak (see Fig. 8.4). Along many other ice impurity investigations (see e.g. Rau (2008)),  $^{14}\text{C}$  measurements of DOC and POC over the whole core length have been carried out by May (2009). The POC  $^{14}\text{C}$  results indicate a basal ice age of ca. 7500 yBP, but exhibit very large errors of up to 100% for most data points.



**Fig. 8.3.:** Crest of Vadret dal Corvatsch in summer 1998 (picture by Martin Hölzle), strong melting revealed the glacier ice surface



**Fig. 8.4.:** Vadret dal Corvatsch in winter 2007. The VCL core drilling site is marked. Picture by Barbara May

### 8.3. Presentation of radiocarbon results

For Titlis glacier cave five different ice blocks, extracted from the cave walls by chainsaw, have been POC  $^{14}\text{C}$  dated. Three samples were processed in the REFILOX and four in the offline (ending-S in Table 8.1) system.

**Tab. 8.1.:** POC  $^{14}\text{C}$  dating results for the samples from Titlis glacier cave and the one sample from the VCL core. The Titlis samples with ending -S have been processed in the offline filtration system, the others in the REFILOX, also the VCL sample. The VCL samples are complemented by the results of May (2009) for the sample VCL 38.

Sample name	POC [ $\mu\text{gC}$ ]	$\text{F}^{14}\text{C}_{corr}$	$^{14}\text{C age}_{corr}$ [yBP]	$^{14}\text{C age}_{cal}$ [yBP]	$\delta^{13}\text{C}$ [‰]
Titlis 1-2-S	96.5	$0.848 \pm 0.008$	$1323 \pm 73$	1180-1305	-22.2
Titlis 1-9-S	47.7	$0.702 \pm 0.007$	$2848 \pm 78$	2861-3070	-25.3
Titlis 2-3-S	89.7	$0.551 \pm 0.007$	$4784 \pm 97$		-25.8
Titlis 2-3-340	43.6	$0.610 \pm 0.009$	$3974 \pm 125$	4237-4615	-29.2
Titlis 2-3-800	29.7	$0.490 \pm 0.011$	$5735 \pm 187$		-29,9
Titlis 2-3 average		$0.561 \pm 0.010$	$4687 \pm 106$		
Titlis 2-6-340	20.1	$0.754 \pm 0.009$	$2270 \pm 99$	2122-2378	-32,8
Titlis 3-5-S	56.2	$0.568 \pm 0.006$	$4539 \pm 89$	5047-5319	-25,8
VCL 38-total this work	26.2	$0.904 \pm 0.009$	$807 \pm 79$	$811 \pm 78$	-26.4
VCL 38 (May, 2009)	7.8	$0.990 \pm 0.050$	$80 \pm 404$	$408 \pm 408$	-28.7
VCL 38-CFA (May, 2009)	7.9	$0.920 \pm 0.102$	$667 \pm 887$	$727 \pm 717$	-13.1

## 8. Results - POC based $^{14}\text{C}$ dating of selected small Alpine glacier caps

All samples showed very high contents of visible material, dark bands in the ice and a lot of small stones and sediment material in the section closest to bedrock. Even though it was tried to avoid the visible dark layers and sediment contaminated parts, all Titlis samples exhibited a thick layer of very black material on the filter surface after filtration. From the VCL core, only one sample could be dated during this work, because the available core material was very limited. All results together with two results from VCL measured by May (2009) are shown in Table 8.1 All samples have been  $^{14}\text{C}$  dated via the gas ion source at the MICADAS AMS in Mannheim with an average statistical error of 1-2 %.

### 8.3.1. Discussion of radiocarbon results

#### Titlis glacier cave

The Titlis samples showed overall very large POC concentrations starting at  $500 \frac{\mu\text{gC}}{\text{kg}}$  of up to almost  $4 \text{ mgC/kg}$  ice. Even in samples, which had no large obvious material inclusions. This is remarkable and has not been observed in any other Alpine ice samples during this work. By the optical appearance and together with the lessons learned from the analyses of potentially age biasing materials, they could probably have a large contribution of old cryoconite. To confirm this, chemical and biological analysis of the material composition would be needed, which are planned, but have not been carried out so far. Also the VCL sample had a high POC content of  $187 \frac{\mu\text{gC}}{\text{kg}}$  and the material collected on the filter had very similar optical appearance as the Titlis samples. This must however up to now be considered as coincidence, until further analyses of the material.

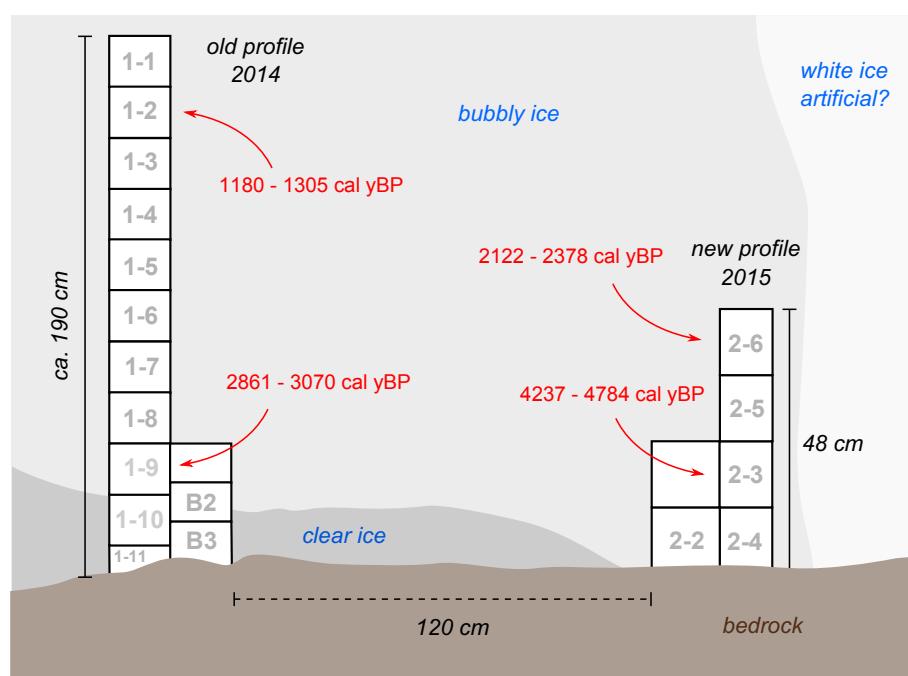


**Fig. 8.5.:** Schematic view of sampling site one (2014) and two (2015) with the calibrated  $^{14}\text{C}$  ages shown in red.

All radiocarbon ages have been calibrated using OxCal 4.2 and the calibrated ages within  $1\sigma$  range are shown in Fig. 8.5 and 8.6. For block 2-3, which has been processed both in the offline filtration ( $5\ \mu$  silver membrane filter) system and the REFILOX, only the result of the  $340\ ^\circ\text{C}$  fraction has been calibrated. This fraction will according to section 6.7.1 give the best representation of actual ice age. In this context it is worth to notice that the average uncalibrated  $^{14}\text{C}$  age of both REFILOX temperature fractions (calculated according to eq. 6.14) with  $(4687 \pm 106)$  yBP almost exactly hits the result of the offline filtration system combusted completely at  $800\ ^\circ\text{C}$ . This indicates a high comparability between both systems.

The conventional  $^{14}\text{C}$  ages of the basal blocks 2-3 and 3-5 differ about 400 years on average. This difference in the calibrated ages shown in Fig. 8.5 and 8.6 is due to the fact, that for block 2-3 only the  $340\ ^\circ\text{C}$  result has been calibrated. If the averaged uncalibrated  $^{14}\text{C}$  age for both temperature fractions of block 2-3,  $(4687 \pm 106)$  is compared to the  $^{14}\text{C}$  age of block 3-5, both values meet in the one sigma range. Therefore they agree extremely well. Considering the findings about the optimal combustion temperature, the calibrated age of block 2-3 will however give a better estimation of the real ice age.

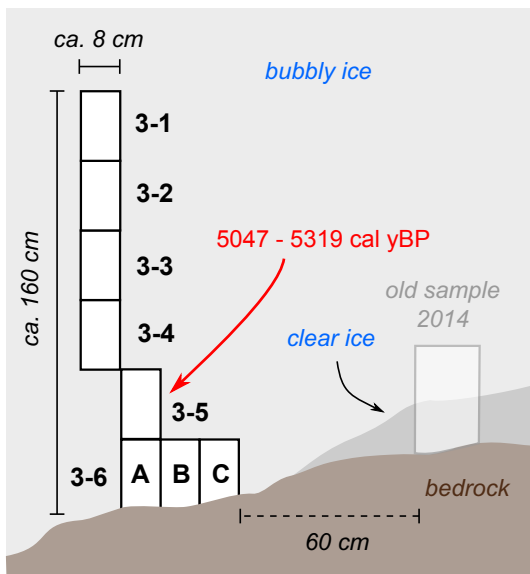


**Fig. 8.6.:** Schematic view of sampling site 3. The calibrated age of block 3-5 in red

Block 1-9 from the 2014 profile showed a  $^{14}\text{C}$  age significantly younger. This could possibly be caused by the close proximity to the clear ice layer, which was probably melted at some point. Thus it may be influenced by younger material penetrating the ice in the past. This needs however to be backed up by further analyses of adjacent blocks. The blocks recovered from higher positions in the wall (2-6 and 1-2) show ages gradually getting younger with higher block positions, which is reasonable, if the layers of the glacier have formed chronologically and have not been folded or mixed in another way. An age step from the basal ca. 5000 yBP to ca. 1200 yBP only two meters above is nevertheless significant. The course of  $^{14}\text{C}$  ages over the upper part of the wall thus also needs to be investigated by additional  $^{14}\text{C}$  measurements of other block samples.

With the knowledge derived from the analyses of potentially age biasing materials, all Titlis  $^{14}\text{C}$  ages should be regarded as upper age limits. This is due to the remaining possibility of age biases caused by incorporated old cryoconite or sediment material, which would lead to a systematic overestimation of the sample age. As a hypothesis based on the present data, the maximum age of the basal ice of Titlis glacier can thus be estimated to be likely not older than 4237-4784 years BP (calibrated age of  $340\ ^\circ\text{C}$  fraction of block 2-3).

The dating of samples from Titlis glacier cave can thus be treated as a successful application of the POC dating method, where the problems of very small sample sizes were not present and there is no reason to question the retrieved  $^{14}\text{C}$  results from a methodological point of view.

## 8. Results - POC based $^{14}\text{C}$ dating of selected small Alpine glacier caps

---

However, for a more detailed interpretation of the results in terms of glacier age and onset of formation, chemical and biological analyses of the dated material are necessary.

### Vadret dal Corvatsch

The main purpose for analyses of a VCL core sample additionally to the samples measured by May (2009), was to narrow down the large errors applying the improved POC extraction method and confirm the basal ages. The sample VCL 38 processed in the REFILOX system (total combustion at 800 °C, to ensure comparability) within this work indeed shows a relative measurement error of ca. 1%, which is five to ten times lower than the ones retrieved by May (2009). In that study, two samples out of VCL 38 were filtered, the first one directly (quartz fibre filter, 800 °C) and the second in succession of the continuous flow analyses (CFA). The error of this second sample is thus almost double of the one directly filtered, because the CFA measurement produces a higher blank contribution in the POC. The massive error reduction of the sample processed during this study is due to the major improvements of methodology and blank reduction reported in Chapter 6. The absolute age retrieved in this study agrees within error almost with the former results. The result is an important contribution to the confirmation of basal ice ages at Vadret dal Corvatsch and it is envisioned to continue the POC dating in more sections of the core, where the old results show the largest errors.

The two examples of Titlis glacier cave and Vadret dal Corvatsch show the capability of the new POC  $^{14}\text{C}$  measurement method. However, the POC dating of these ice samples was not additionally complicated by very small sample sizes. This is the case for samples from Colle Gnifetti, which will be discussed in the following Chapter.

## 9. Results - POC based $^{14}\text{C}$ dating of a new ice core from the high Alpine firn saddle Colle Gnifetti (Swiss Alps)

### 9.1. Glaciological site description, available ice cores and dating challenges

#### 9.1.1. Glaciological characteristics of Colle Gnifetti

Colle Gnifetti is a cold firn saddle in the summit regions of the Monte Rosa Massif, Swiss Alps (see Fig. 9.1). It has a distinctive saddle geometry of only a few hundred meters spatial extension between the peaks of Zumsteinspitze in the north west and Signalkuppe in the south east. To the east, the saddle is confined by a steep, overhanging ice cliff, to the west it flows down the mountain flank and forms the catchment area of Grenzgletscher (see Fig. 9.2).

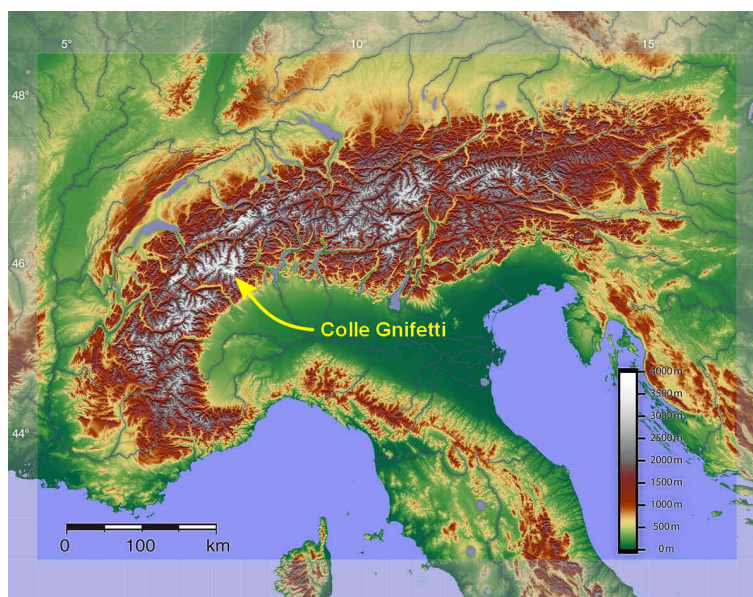


**Fig. 9.1.:** Location of Colle Gnifetti in the European Alps. Adapted from Wagenbach et al. (2012).

The Colle Gnifetti is located at an altitude of 4450 m a.s.l., which is high enough to guarantee perennial air, firn and ice temperatures below  $0\text{ }^{\circ}\text{C}$  (Haeberli and Funk, 1991; Hoelzle et al., 2011) and therefore makes it a so called cold or non-temperate glacier. These low englacial temperatures are a main prerequisite for the capability of a glacier body to serve as a stratigraphic climate archive. Only by the complete preservation of precipitation without loss or mixing of material

## 9. Results - POC based $^{14}\text{C}$ dating of a new ice core from the high Alpine firn saddle Colle Gnifetti (Swiss Alps)

during melt events, a continuous archiving of climate signals is possible (see e.g. Wagenbach et al. (2012)). Colle Gnifetti however has due to its exposed location a very complex and variable accumulation regime, with very low net accumulation rates rarely exceeding 1 m w.e./year (see e.g. Haeberli et al. (1983); Haeberli and Alean (1985); Lüthi (2000)). Especially on the southern flank, where all ice cores discussed in this study were drilled, the net accumulation is typically below 0.5 m w.e./year.

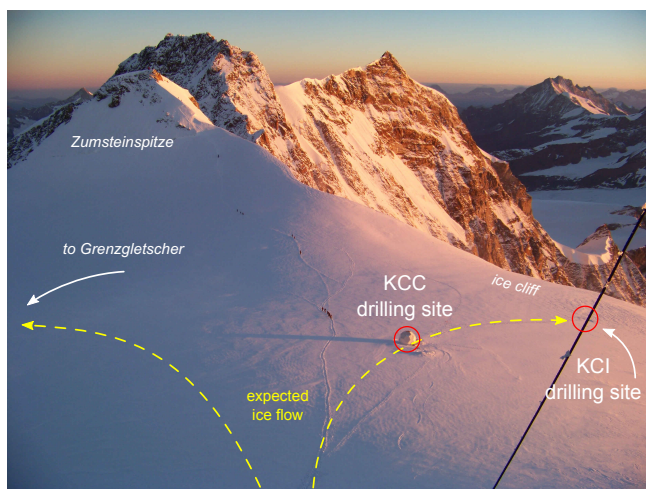


**Fig. 9.2.:** View of the saddle of Colle Gnifetti from the top of Signalkuppe in the south east. Note the locations of the cores KCC and KCI on the same flow line. The picture was taken during the 2013 drilling campaign.

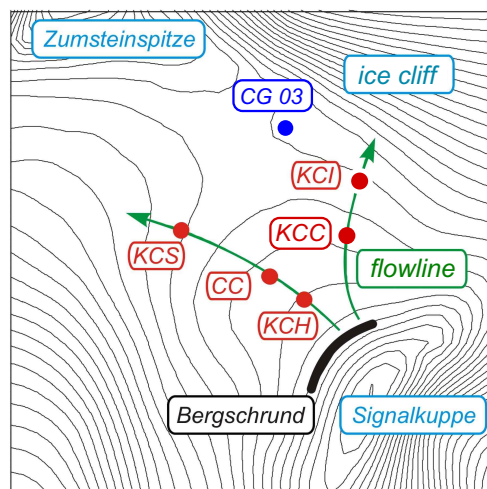


**Fig. 9.3.:** Schematic view of all deep ice core positions and names, where drilling was led by the IUP Heidelberg (red) and the core CG03 drilled by the Paul Scherrer Institute.

Together with the small total thickness of the glacier body in the order of 100 m (Wagenbach et al., 2012), this leads to a rapid layer thinning with depth (Bohleber et al., 2013), but also basal ages of more than 1000 years BP can be expected (Wagenbach et al., 2012). This makes the Colle Gnifetti until now a unique climate archive in the European Alps. The main glaciological characteristics of Colle Gnifetti can be summarised to:

- glacier body frozen to bedrock, basal temperature in 2014:  $-12.4\text{ }^{\circ}\text{C}$  (pers. comm. Martin Hölzle)
- due to wind erosion, only ca. 10% of annual precipitation is preserved with strong bias to wet summer snow, no closed system in terms of precipitation (Wagenbach et al., 2012).
- overall low and spatially highly variable net snow accumulation, ca.  $0.15 - 1.2 \frac{\text{m.w.e.}}{\text{a}}$  (Bohleber et al., 2013))
- total loss of annual precipitation by wind erosion over the ice cliff is possible
- low net accumulation together with small glacier thickness (60-140 m) leads to rapid layer thinning with depth, but also high expected basal ice ages

9.1.2. Colle Gnifetti ice core material and data available for this study

So far, five deep ice cores have been drilled at Colle Gnifetti under the lead of the IUP Heidelberg, the first in 1982 and the last in 2013. The core positions, mainly located on two divergent flow lines, are shown in Fig. 9.2 and 9.3. An overview of all key parameters of the ice cores drilled under the lead of IUP together with the characteristics of the core CG03, drilled by the Paul-Scherrer-Institute, Switzerland (PSI), is given in Table 9.1. The core CG03 was included, because it will be used for data comparison in section 9.5. For the IUP cores, CC, KCS and probably KCC reached bedrock, indicated by the appearance of yellow silt in the KCS (Keck, 2001) and small stones as well as a strong change in the microstructural characteristics induced by a large load of mineral dust (pers. comm. Johanna Kerch) in the KCC. This work mainly focuses on the latest core, KCC.

**Tab. 9.1.:** Key parameters of all deep Colle Gnifetti ice cores drilled under the lead of the IUP Heidelberg, together with the core CG03 drilled by the Paul-Scherrer-Institute (PSI). The firn ice transition is defined by a density of  $0.83 \frac{\text{g}}{\text{cm}^3}$  for all cores without KCC. Table adapted from Bohleber (2008).

Name	CC	KCS	KCH	KCI	KCC	CG03
Depth absolute [m]	64.10	100	60.30	61.84	71.81	80.18
Depth [m.w.e]	49.85	78.65	45.02	48.44	53.77	62.79
Year of drilling	1982	1995	1995	2005	2013	2003
Accumulation [m.w.e./a]	0.22	0.51	0.23	0.14	0.22	0.46
Firn-ice-transition [m.w.e.]	20	28	22	17	21	no data

This core was drilled in August 2013 in close collaboration with the Institute for Climate and Environmental Physics in Bern and the Climate Change Institute of the University of Maine.

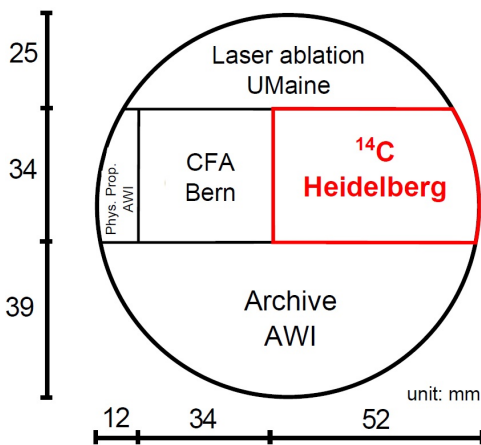


**Fig. 9.4.:** Cutting plan of the KCC ice core and method attribution of the aliquots.

The drilling site was chosen to complement the KCI core on the eastern, low accumulation flank of Colle Gnifetti. The core is with almost 72 m total length the second longest of the IUP cores and of very good quality. It was dedicated to the application of several state of the art ice core investigation methods, to create the optimal set of parameters for the retrieval and interpretation of climate signals. These methods include high resolution continuous flow analysis (CFA) for dust, chemical composition and water isotope analyses and, for the first time, Laser ablation ICP-MS for high resolution impurity measurements.

## 9. Results - POC based $^{14}\text{C}$ dating of a new ice core from the high Alpine firn saddle Colle Gnifetti (Swiss Alps)

---

Together with a 3D flow model, this dataset is the most comprehensive pool of information retrieved from one single Colle Gnifetti ice core so far.

### 9.1.3. Challenges in Colle Gnifetti ice core dating and previous $^{14}\text{C}$ dating attempts

High basal ice ages can only be achieved by a rapid layer thinning with depth (and the glacier being frozen to bedrock), which in turn leads to a very non-linear age-depth relationship. This, together with the highly variable accumulation rate with potentially missing annual layers, makes the development of a core chronology a large challenge. The chronologies of all IUP Colle Gnifetti ice cores are so far based on the identification of absolute time markers (like the bomb peak at 1963 A.D. or well documented Saharan dust events), annual layer counting (based on CFA data) and age depth models (see Schäfer (1995); Armbruster (2000), Keck (2001) and Bohleber (2008)). For the new KCC core, the following dating methods have been applied so far (pers. comm. Pascal Bohleber):

- Identification of absolute time markers: Bomb peak: depth of 11.18 m w.e. (20.84 m abs.); large Saharan dust falls in 1977 AD and in 1901 AD (pers. comm. Pascal Bohleber)
- CFA (setup by University of Bern (Röthlisberger et al., 2000; Kaufmann et al., 2008)) based annual layer counting ( $\text{NH}_4$  signal), depth resolution ca. 0.5 cm
- Laser ablation ICP-MS based annual layer counting (Ca and Na signal), depth resolution ca. 100  $\mu\text{m}$  (for method see Sneed et al. (2015))

The resulting preliminary working chronology was not developed within this study, but will be discussed with respect to the  $^{14}\text{C}$  data in Section 9.3. All conventional cm-resolution counting methods and absolute time markers are however restricted in reliability to the last few hundred years, because potentially missing annual layers and multi-year-cycles can occur with increasing depth (Bohleber, 2008). These effects introduce a cumulative age error, which is estimated to at least 10%. The high resolution laser ICP-MS technique can only reduce but not eliminate this error. There are many possible sources of uncertainty, which are not yet completely evaluated. The most important sources of these uncertainties are:

- No absolute age markers available so far in the lower half of the core, thus increasing cumulative counting error with depth.
- Potential discontinuities in glacier flow, which do not have to be visible in the structure of the ice, causing discontinuities in layering.
- Laser ICP-MS layer counting has been performed based on the calcium and sodium signal, which has a ca. four times lower seasonal amplitude than the usually used ammonium (Preunkert et al., 2000).

The assessment of the dating uncertainty of the annual layer counting chronology was however out of the scope of this work, and the chronology will thus be treated as the best working hypothesis available so far.

For the deep and oldest parts of the cores, thus  $^{14}\text{C}$  dating is the only option to extract direct and absolute age information from the ice, which is the main goal of this study.

## 9.2 Sample selection, presentation of radiocarbon results and blank correction

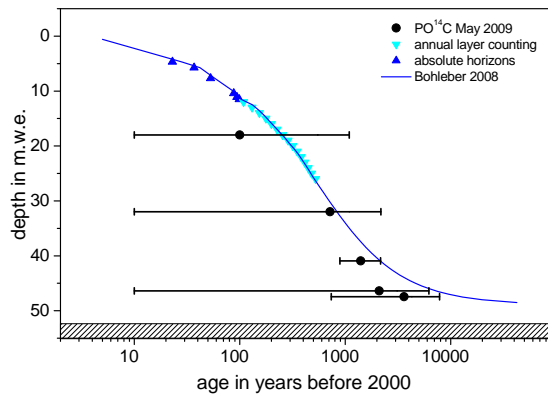


**Fig. 9.5.:** POC  $^{14}\text{C}$  dating attempts of the KCI core by May (2009) together with absolute time markers, annual layer counting and a simple flow model (Bohleber, 2008). Note the very large age uncertainties of the  $^{14}\text{C}$  data.

The first attempt of  $^{14}\text{C}$  dating of Colle Gnifetti ice cores at the IUP was carried out by May (2009). Because dating via analyses of the DOC fraction was not possible due to in situ  $^{14}\text{C}$  production (see chapter 4), the only radiocarbon dates available so far are based on POC analyses. Their major drawback of these  $^{14}\text{C}$  dates are very large uncertainties (see Fig. 9.5 for data from the KCI ice core), mainly due to a very high and variable process blank.

Within this work, large methodological improvements, mainly a massive blank reduction, resulting in much smaller measurement errors, have been made (see chapter 6). Compared to the errors reported in May (2009) (40-100%), the errors for the most important samples (340°C fraction) could be reduced within this work by a factor of ten or more.

Together with a better understanding of possible reservoir effects in the POC fraction, these improvements form a solid base for a new attempt of POC radiocarbon dating of Colle Gnifetti ice cores, namely the KCC.

## 9.2. Sample selection, presentation of radiocarbon results and blank correction

For the POC  $^{14}\text{C}$  dating of the new KCC ice core from Colle Gnifetti, samples from 16 different core depths have been selected in two sets, one using the offline filtration system and silver membrane filters, the other using the REFILOX system and quartz fibre filters (see Table 9.2). The main sample selection criteria were:

- The samples should be taken below the firn ice transition (21 m w.e.) to ensure that the decontamination routine can be applied successfully.
- The samples should be expected to be older than about 400 years based on the existing chronology, to avoid the anthropogenic biased industrial period and the age range where  $^{14}\text{C}$  ages can not be calibrated unambiguously (see section 2.2.4).
- Significant high dust and conductivity contents should be avoided to minimise age biasing effects (see section 7.3) together with large variations in the  $\delta^{18}\text{O}$  signal, which could hint to changes in the accumulation regime larger or climatic effects.
- An age range where the error of the annual layer counting chronology is still far below the  $^{14}\text{C}$  dating error should be covered to verify this chronology, together with samples from the very basal section of the core where all other dating methods fail.

## 9. Results - POC based $^{14}\text{C}$ dating of a new ice core from the high Alpine firn saddle Colle Gnifetti (Swiss Alps)

**Tab. 9.2.:** Key sample parameters and POC  $^{14}\text{C}$  results of all samples from KCC ice core. Samples with ending -S have been processed using silver membrane filters in the offline filtration system, samples with ending -R in the REFILOX.  $M_{ice}$  denotes the sample ice mass and  $m_{corr}$  the blank corrected carbon mass. The  $^{14}\text{C}$  values measured in the  $800^\circ\text{C}$  fraction of the REFILOX samples and the samples pretreated in the offline system haven been blank corrected. All  $^{14}\text{C}$  results are reported as fraction modern carbon  $F^{14}\text{C}$ .

Sample name	Depth [m w.e.]	$M_{ice}$ [g]	$m_{corr}$ [ $\mu\text{gC}$ ]	POC [ $\frac{\mu\text{gC}}{\text{kg}}$ ]	$F^{14}\text{C}_{corr}$	$\sigma F^{14}\text{C}$
KCC 61/62-S	35.00 $\pm$ 0.27	360	4.1	11	0.838	0.153
KCC 68-S	38.14 $\pm$ 0.19	290	4.5	16	0.908	0.145
KCC 69-340-R	38.46 $\pm$ 0.16	304	3.2	22	0.914	0.029
KCC 69-800-R	38.46 $\pm$ 0.16	304	3.5		0.624	0.253
KCC 70/71-340-R	39.21 $\pm$ 0.23	386	1.1	18	0.955	0.050
KCC 70/71-800-R	39.21 $\pm$ 0.23	386	5.9		-	-
KCC 71/72-S	39.64 $\pm$ 0.23	355	5.4	16	0.808	0.111
KCC 75/76-340-R	41.33 $\pm$ 0.23	438	5.9	32	0.875	0.052
KCC 75/76-800-R	41.33 $\pm$ 0.23	438	8.0		0.340	0.115
KCC 77a/b-S	42.17 $\pm$ 0.18	284	2.7	10	0.947	0.275
KCC 81/82a-S	44.19 $\pm$ 0.23	340	5.4	16	0.948	0.143
KCC 83/84-1-R	45.12 $\pm$ 0.27	460	1.9	10	0.942	0.018
KCC 83/84-2-R	45.12 $\pm$ 0.27	460	2.7		0.490	0.397
KCC 84-S	45.69 $\pm$ 0.14	290	2.2	8	0.826	0.321
KCC 86-340-R	46.33 $\pm$ 0.23	404	6.6	29	0.933	0.062
KCC 86-800-R	46.33 $\pm$ 0.23	404	5.0		0.654	0.247
KCC 88/89-S	47.84 $\pm$ 0.23	378	6.0	16	0.903	0.107
KCC 89/90-340-R	48.38 $\pm$ 0.23	400	5.3	26	0.905	0.048
KCC 89/90-800-R	48.38 $\pm$ 0.23	400	5.0		0.294	0.175
KCC 94-340-R	50.5 $\pm$ 0.18	277	7.9	50	0.848	0.067
KCC 94-800-R	50.5 $\pm$ 0.18	277	5.1		0.653	0.242
KCC 97 a/b 340-R	51.9 $\pm$ 0.18	280	8.3	53	0.801	0.014
KCC 97 a/b 800-R	51.9 $\pm$ 0.18	280	6.4		0.409	0.155
KCC 100-340-R	53.3 $\pm$ 0.16	250	10.6	92	0.688	0.015
KCC 100-800-R	53.3 $\pm$ 0.16	250	12.5		0.354	0.075
KCI 53-340-R	33.9 $\pm$ 0.18	656	7.4	22	0.921	0.029
KCI 53-800-R	33.9 $\pm$ 0.18	656	7.3		0.566	0.144
KCI 59-340-R	38.5 $\pm$ 0.18	388	5.4	40	0.854	0.019
KCI 59-800-R	38.5 $\pm$ 0.18	388	10.1		0.282	0.078

Additionally, two samples from the KCI core have been selected for inter-core age comparison. Based on the insights from the blank measurements and error estimations in chapter 6, samples of about 500 g ice mass were targeted. However, compromises between comfortable sample sizes and depth average had to be made with prevention of large dust peaks. Thus, the depth ranges varied between 30 and 60 cm with sample masses after decontamination between 250 and 460 g of ice.

The dust and  $\text{NH}_4^+$  signal were chosen as the best indicators for the amount of expected organic material (see Section 2.1.1). The integrated dust content of a sample, which includes inorganic and organic particles shows a strong linear dependence (see appendix, section A.5.1) with a correlation coefficient of  $R=0.9$  with the sample POC mass in the  $340^\circ\text{C}$  combustion

## 9.2 Sample selection, presentation of radiocarbon results and blank correction

---

fraction. Therefore, even though very large and distinct spikes in the dust signal were avoided, it was tried to choose sampling ranges of average instead of very low dust contents to guarantee measurable POC contents within the samples. Higher dust values indicate summer samples, which also contain more  $\text{NH}_4$  indicating organic material (Preunkert and Legrand, 2001) than the very low concentration winter samples and thus should also yield higher POC masses.

The results produced with the offline system using silver membrane filters (5  $\mu\text{m}$  pore size) and the REFILOX 800°C  $\text{F}^{14}\text{C}$  results have been blank corrected, according to the blank mass  $\overline{m}_b$  and blank  $\text{F}^{14}\text{C}$  value  $\overline{F}_b$  reported in table 6.6:

$$\begin{aligned}\overline{m}_b(\text{REFILOX}) &= (1.5 \pm 1.0) & \overline{F}_b(\text{REFILOX}) &= (0.574 \pm 0.03) \\ \overline{m}_b(\text{silver}) &= (0.5 \pm 0.4) & \overline{F}_b(\text{silver}) &= (0.523 \pm 0.12)\end{aligned}$$

And by use of relation 6.2:

$$F_s = \frac{F_m \cdot m_m - F_b \cdot m_b}{m_m - m_b}$$

The results for the 340 °C fraction of the REFILOX samples have not been blank corrected, because the blank was below detection limit. The results reported in table 9.2 are the base for all latter calculations.

### 9.2.1. Overview of the POC $^{14}\text{C}$ results

In a first set of measurements, samples from seven different core depths below the firn-ice-transition have been selected and were processed in the offline filtration system using silver membrane filters with a pore size of 5  $\mu\text{m}$ . All POC samples have been combusted completely at 800 °C and were  $^{14}\text{C}$  dated via the gas ion source. The results are shown in Fig. 9.6. The blank corrected  $^{14}\text{C}$  ages together with the uncorrected raw data is shown. The large error bars of the blank corrected values result from the rather high uncertainty (23%) of the blank  $\text{F}^{14}\text{C}$  for the offline filtration system. Blank correction shifts the results to younger ages, but there is no trend in both datasets, corrected and uncorrected results.

In the second set of measurements, samples from 9 different core depths have been processed in the REFILOX system using the two-step combustion at 340 °C and 800 °C. The uncalibrated  $^{14}\text{C}$  ages of both combustion fractions are shown in Fig 9.7. The results of the low combustion temperature show a gradual age increase with depth, while the high temperature results are on average almost 4000 years older and show a large scatter. The big error bars result again from the large uncertainties of the blank mass and blank  $\text{F}^{14}\text{C}$ .

## 9. Results - POC based $^{14}\text{C}$ dating of a new ice core from the high Alpine firn saddle Colle Gnifetti (Swiss Alps)

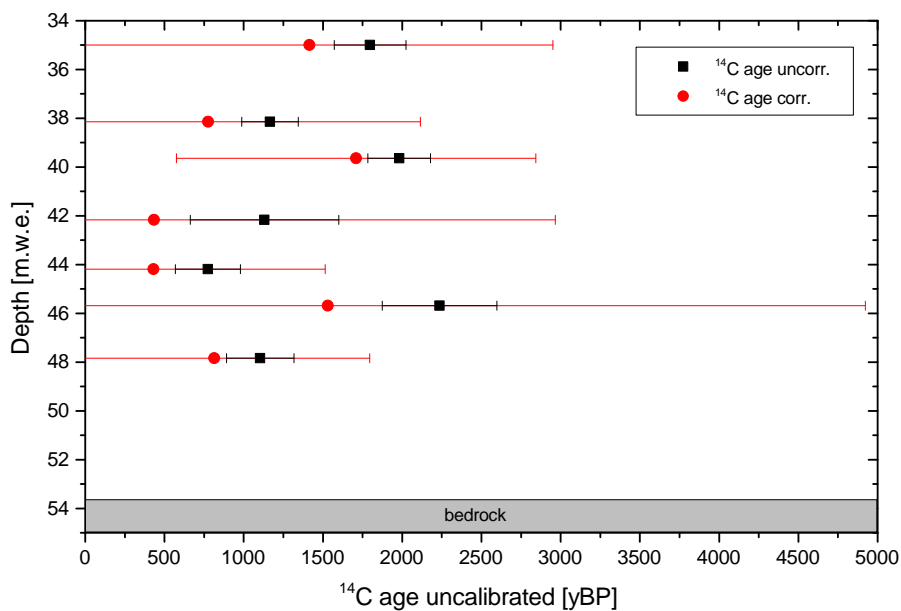


**Fig. 9.6.:** Uncalibrated POC  $^{14}\text{C}$  ages of samples processed in the offline filtration system using silver membrane filters ( $5\ \mu\text{m}$  poresize). No age increase with core depth is discernible.

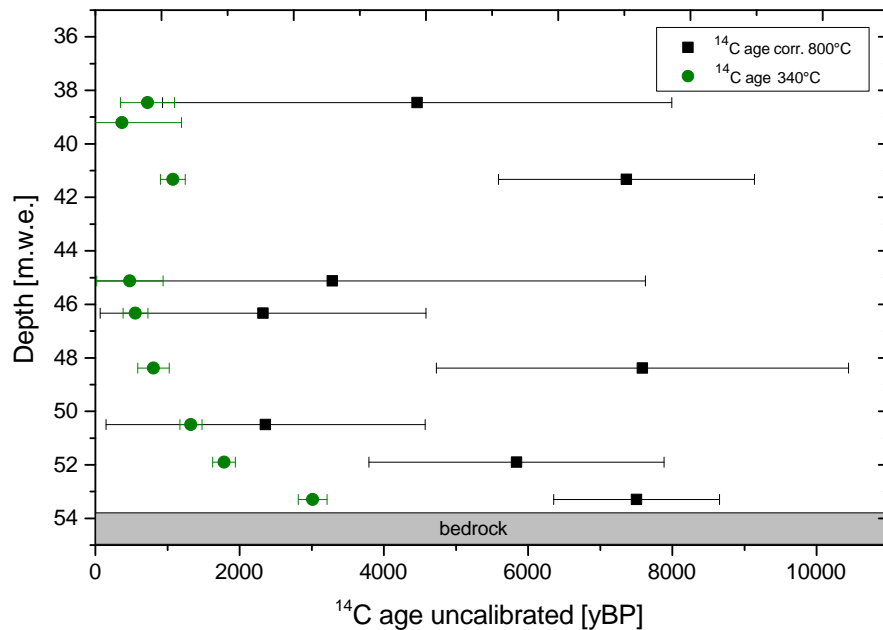


**Fig. 9.7.:** Uncalibrated  $^{14}\text{C}$  ages of the  $340\ ^\circ\text{C}$  (green) and  $800\ ^\circ\text{C}$  (black) fractions. The large errorbars of the  $800\ ^\circ\text{C}$  results are caused by the blank correction. Note the large age offset between both fractions.

## 9.3. Discussion of POC <sup>14</sup>C results

### 9.3.1. First dating attempt applying silver membrane filters and the offline system

For the Colle Gnifetti, the largest source for deposition of already aged POC material is long distance transport of soil material (e.g. Saharan dust (Wagenbach et al., 1996)). Long range transported Saharan dust mainly consists of particles within the clay mineral fraction ( $< 2 \mu\text{m}$ ), which was for example shown in Tomadin et al. (1996). In a first POC <sup>14</sup>C dating attempt of the KCC ice core it was therefore envisaged to remove this potentially age biased organic particle fraction by size selection under use of a silver membrane filter with  $5 \mu\text{m}$  nominal pore size and not by application of different combustion temperatures. This was done because the overall expected carbon sample sizes are with  $< 10 \mu\text{gC}$  already in the lower range of measurability and a further subsection of the POC fractions could lead to very high dating errors because of the bad counting statistics and large influences of the blank correction. An influence of any fossil fuel POC combusting on the high temperature fraction can be excluded for pre-industrial ice samples. However, the <sup>14</sup>C results of these samples, shown in Fig. 9.6 show a large scatter between 500 and 2500 years BP with no trend in the dataset. Not even an overall increase of <sup>14</sup>C ages with core depth, which should be a general criterion. Also the blank correction does not change this observation, apart from largely increasing error bars.

Based on these results, it was decided that the size separation of age biased material by choice of a filter with a larger pore size is not successful, probably due to partial clogging of the pores, which then also allows retention of smaller particles and no sharp size selection.

### 9.3.2. General findings for POC <sup>14</sup>C results retrieved via the REFILOX system

The second set of samples from KCC was processed in the REFILOX system under application of the two-step combustion method despite the initially expected smaller sample sizes.

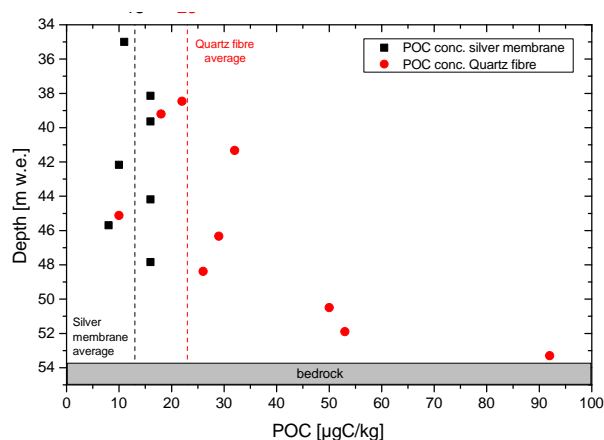


**Fig. 9.8.:** Comparison of retrieved POC concentrations for the offline filtration system and the REFILOX. The respective averages are marked by the dashed lines. Note the strong increase in the basal core section.

Comparing the retrieved POC concentrations from the silver filter method and the quartz filter method (see Fig. 9.8), it is however obvious, that for the quartz filters in the comparable depth section (excluding the three deepest samples) the average retrieved POC concentration is with ca.  $23 \frac{\mu\text{gC}}{\text{kg}}$  almost twice as large as the one of the silver membrane filters ( $13 \frac{\mu\text{gC}}{\text{kg}}$ ) but still very low. This is on one hand probably due to the nominally smaller pore size of the quartz filter ( $0.3 \mu\text{m}$ ) and thus the higher filtration efficiency and on the other hand the result of small material losses during the silver filter handling as described in Chapter 6. Another striking finding is the strong increase of POC content near bedrock to a factor of four of the average value. This is probably caused by incorporation of basal sediment into the ice matrix (indicated by blurring of the ice) inheriting a higher organic content.

## 9. Results - POC based $^{14}\text{C}$ dating of a new ice core from the high Alpine firn saddle Colle Gnifetti (Swiss Alps)

The uncalibrated  $^{14}\text{C}$  results shown in Fig. 9.7 show a gradual increase of age with core depth in the 340 °C fraction, which is not visible in the 800 °C fraction. The high temperature results are scattering around an average age of ca. 5000 y BP. Based on the results of the CARBOSOL aerosol filter analyses, it was expected to see a principle bias to older ages in the high temperature fractions, because on this fraction potentially aged organic matter combusts (see Section 6.7.1). On the other hand, the lower temperature fraction should mainly consist of organic material originating from the recent biosphere and thus give the best representation of the glacier ice age. Therefore, only the 340 °C fraction is considered in the following discussions.

### 9.3.3. Assessment of determined radiocarbon ages with respect to expected dating scenarios

For a better evaluation of the  $^{14}\text{C}$  results retrieved via the 340 °C fraction, a comparison of the  $^{14}\text{C}$  ages with the independently determined dating scenario based on annual layer counting and a preliminary flow model was done. Therefore, the measured  $^{14}\text{C}$  ages have been calibrated using OxCal 4.2 (see Section 2.2.4). The calibrated ages with  $1\sigma$  error bars are shown together with the annual layer counting chronology in Fig. 9.9. The data can be found in Appendix A.5.2.

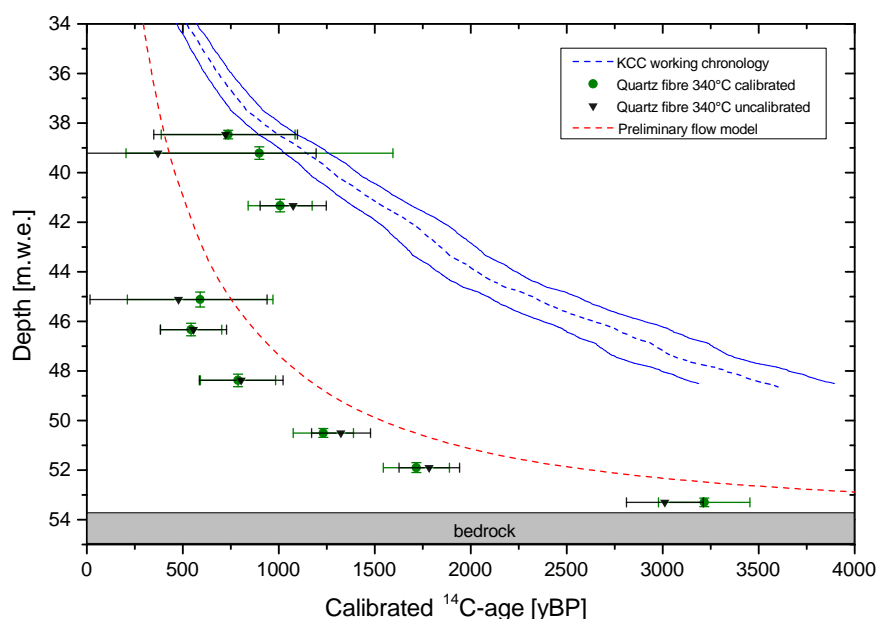


**Fig. 9.9.:** Calibrated  $^{14}\text{C}$  ages of the 340°C POC fraction together with two dating scenarios based on combined CFA and laser ablation annual layer counting (blue) with a 10% error range and a preliminary age-depth model. The  $^{14}\text{C}$  results seem to follow the course of the model. At present state, the model uses however glaciologically unrealistic assumptions. Note the systematical offset between the  $^{14}\text{C}$  ages and the counted chronology.

The main findings of this comparison can be summarised to:

- The samples within the bottom 10 meters of the core show a fast age increase of ca. 2500 years from  $(543 \pm 160)$  to  $(3216 \pm 283)$  yBP with depth.
- A large systematical offset between the  $^{14}\text{C}$  ages and the layer counting chronology is apparent. In the bottom 10 m of the core, the deviation is more than 2500 yBP.
- The  $^{14}\text{C}$  results seem to follow the course of the preliminary age depth model (pers. comm. Carlo Licciulli), with a constant age offset of ca. 250 years. This model uses however at present state too high vertical velocities resulting in largely overestimated accumulation rates of more than 1 m w.e.. It is thus up to now not representing realistic glaciological conditions.
- The three samples above 43 m w.e. however seem to follow a different course with an age increase from 736 - 1007 yBP over 4 meters of depth.
- Sample KCC 70/71 at a depth of 39.21 m w.e. shows a very large error, which is due to the very small sample size of 1.1  $\mu\text{gC}$  and was the smallest sample measured via the gas ion source so far.
- Disregarding the sample KCC 70/71 with the large error, especially sample KCC 75/76 at 41.33 m w.e. seems to be biased within the course of the  $^{14}\text{C}$  ages to a higher value.

One reason for this apparent offset of sample KCC 75/76 could be the location of the sample right above the 4th largest dust peak of the whole core (see Fig. 9.10, a picture of the sample is shown in Appendix A.5.3).

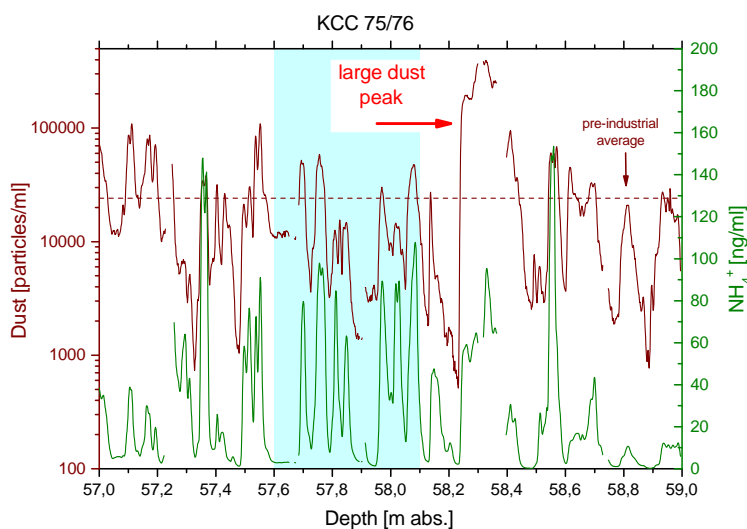


**Fig. 9.10.:** CFA data (dust and  $\text{NH}_4$ ) for sample selection (pers. comm. Tobias Erhardt, Bern). The blue box marks the depth range of the sample. Note the proximity to a very large dust peak (logarithmic scale).

This peak has actually been avoided at sample cutting, but possibly the separation was not sharp enough so this sample could still have incorporated some fraction of the dust peak. Additionally,

## 9. Results - POC based $^{14}\text{C}$ dating of a new ice core from the high Alpine firn saddle Colle Gnifetti (Swiss Alps)

---

the temperature separation of old organic material could have not entirely worked. A hypothetical correction of this sample to the age level of the following sample at 45.12 m w.e. depth by an assumed Saharan dust bias (calculated with an average dust age of 2600 yBP, see chapter 7) would lead to a biasing dust mass of 1.6  $\mu\text{gC}$ . This is about 27 % of the total sample mass. Thus, such a bias is considered to be not unrealistic. Another possibility for the age deviation of sample KCC 75/76 will be discussed in section 9.4.3.

There is an apparently strong correlation between the completely independently developed model and the  $^{14}\text{C}$  results. The curvature and shape of the age depth relation is very similar to the course of the  $^{14}\text{C}$  data with a comparably small offset even in the basal section. At present development state, the model however uses vertical ice velocities, thus accumulation rates, which are up to four times higher than the observed values in field measurements. It is thus not yet able to represent realistic glaciological conditions and gives an additional hint to some systematical bias of the  $^{14}\text{C}$  results to younger ages than expected.

As an intermediate conclusion, from a methodological point of view there is no reason to question the retrieved  $^{14}\text{C}$  results. All results could be measured with reasonable relative errors of 1-10 % and there were no hints for measurable blank contaminations or isotope fractionation in the sample preparation system. In the following, other possible reasons for this systematical age difference of both dating methods will be discussed.

### 9.4. Discussion of potential reasons for the age difference between POC $^{14}\text{C}$ dating and annual layer counting

In this section, the possibility of artificial contaminations and natural effects causing the large systematic offset to young ages from the annual layer counting chronology will be analysed. These possible age biasing effects are:

1. Insufficient blank correction
2. Incorporation of over-modern matter
3. Incorporation of in situ  $^{14}\text{C}$  into the POC fraction

#### 9.4.1. Insufficient blank correction - artificial bias

A possible reason for the large age offset could be an insufficient blank correction of the results. No procedure blank has been observed on the 340 °C fraction so far during the processing of liquid ultrapure water, so the  $^{14}\text{C}$  results have not been blank corrected. If this assumption is not true and there is a blank contribution introduced by insufficient decontamination of the sample surface or additional input of material during ice sample handling, this would not be represented by the liquid water blank samples. Thus, hypothetical blank scenarios will be discussed to evaluate this possibility. Two hypothetical blank corrections have been performed under the following assumptions:

1. Fixed blank masses  $m_b = 1, 2$  and  $5 \mu\text{gC}$  and variable blank  $F^{14}\text{C}$
2. Fixed blank  $F^{14}\text{C}$  to modern atmospheric values and variable blank masses

## 9.4 Discussion of potential reasons for the age difference between POC $^{14}\text{C}$ dating and annual layer counting

Overall, the hypothetical blank needs to have a higher  $F^{14}\text{C}$  value than the samples to shift them to older ages during correction according to eq. 9.1. The according annual layer counting age for each sample depth was used as the expected value of the sample  $F^{14}\text{C}$ . Therefore, the two deepest  $^{14}\text{C}$  samples have not been considered, because of a missing reference value. Together with the measured sample masses  $m_m$ , the measured  $F^{14}\text{C}_m$  values and assumed blank masses  $m_b$ , the resulting hypothetical blank  $F^{14}\text{C}$  values, which are necessary to adjust the measured results to the annual layer counting chronology have been calculated. The results are shown in Fig 9.11.

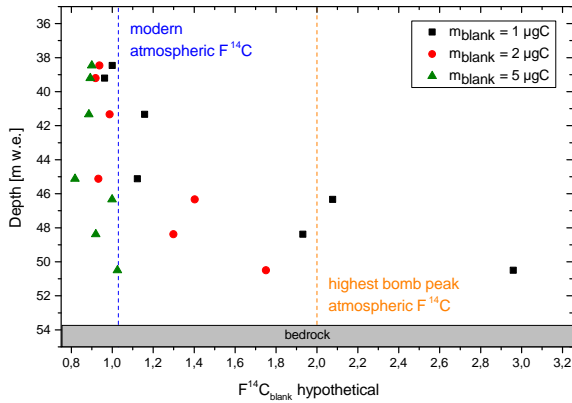


**Fig. 9.11.:** Hypothetical blank  $F^{14}\text{C}$  values based on different assumptions of blank masses for correction of the measured  $^{14}\text{C}$  results to the level of the annual layer counting chronology. Note the unrealistic high hypothetical blank  $F^{14}\text{C}$  values exceeding bomb peak levels

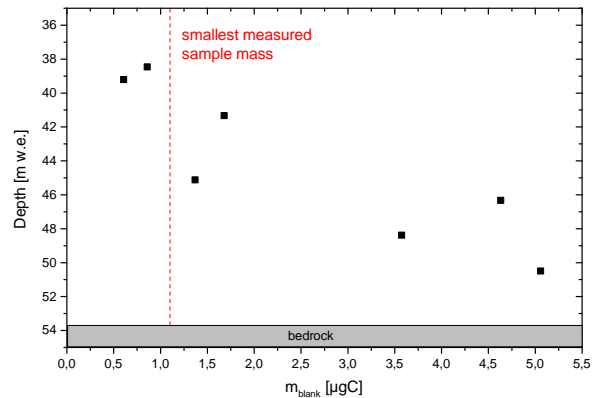


**Fig. 9.12.:** Hypothetical blank masses needed to correct the measured  $^{14}\text{C}$  results to the level of the annual layer counting chronology based on an assumed modern blank  $F^{14}\text{C}$  of 1.03 (pers. comm. Ingeborg Levin). Note the high masses above the minimal measured sample size.

The main findings of the hypothetical blank estimation with fixed blank masses are:

- For an assumed blank mass of  $2 \mu\text{gC}$ , which is in the range of the measured values for the  $800 \text{ }^\circ\text{C}$  fraction, for the samples below 45 m w.e. a highly over-modern blank  $F^{14}\text{C}$  would be needed for correction, almost reaching the highest bomb peak values.
- For a blank mass of  $1 \mu\text{gC}$ , which is in the range of the observed values for blank ice samples of the offline system, this effect is even stronger.
- Only for blank masses of  $5 \mu\text{gC}$  or more, the  $^{14}\text{C}$  values would drop below the modern atmospheric value.
- Blank masses can not exceed the smallest measured sample mass, which would be the case for  $m_b = 5 \mu\text{gC}$  for three samples out of seven.

The same effect is shown in Fig. 9.12, where the blank  $F^{14}\text{C}$  was fixed to a value of 1.03, which was the atmospheric content in the year 2013 at the time of ice core drilling. This was assumed as the highest possible value for contaminating material introduced during the drilling and handling

## 9. Results - POC based $^{14}\text{C}$ dating of a new ice core from the high Alpine firn saddle Colle Gnifetti (Swiss Alps)

---

thereafter. With such a  $F^{14}\text{C}$ , hypothetical blank masses again of up to 5  $\mu\text{gC}$  are calculated for the deepest samples. As already stated above, this is very unrealistic, because without a very high blank variability, the blank mass should on average not exceed the minimal measured sample masses of 1.1  $\mu\text{gC}$ . Such a high variability has never been observed in the course of all blank measurements.

As a result, an artificial contamination of the POC  $^{14}\text{C}$  samples, which was not considered so far could only be a realistic explanation for the top two to three POC  $^{14}\text{C}$  samples of the core. For the deeper samples, all hypothetical blank scenarios are highly unrealistic and the age offset between the counted chronology and the POC  $^{14}\text{C}$  dating can not be explained by sample contamination with organic material during processing.

### 9.4.2. Incorporation of over-modern matter

Apart from an artificial contamination with modern material after sampling, another possibility for the offset to younger ages between the  $^{14}\text{C}$  samples and the annual layer counting could be the incorporation of over-modern material, especially from the bomb peak period directly on the drilling site. Within the firn section of the glacier, volatile organic substances are able to diffuse within the open pores (see e.g. Schwander (1996)), which will lead to a smoothing of atmospheric signals (Legrand et al., 2003). This has however only been observed for gaseous substances and not for the POC fraction. In the KCC core, the bomb peak has been detected at a depth of 11 m w.e., the first POC  $^{14}\text{C}$  sample was taken at a depth of 35 m w.e., 25 m deeper, below the firn ice transition, which makes an influence of bomb  $^{14}\text{C}$  enriched material by diffusion highly unlikely.

Another phenomenon which could lead to incorporation of young material in the deep core sections is the recurringly open Bergschrund upstream of the core drilling site. This crevasse could possibly facilitate the direction of fresh, modern precipitation to basal parts of the glacier body. This hypothesis was however dismissed as unlikely by Wagenbach et al. (2012). The possibility of mechanical incorporation of (over) modern material into the ice matrix is therefore not sufficient to explain the age offset between annual layer counting and POC  $^{14}\text{C}$  results

### 9.4.3. Incorporation of in situ produced $^{14}\text{C}$ into the POC fraction - natural bias

Another possibility of a natural bias of radiocarbon ages to younger values is the in situ production of  $^{14}\text{C}$  by cosmic irradiation in the ice matrix, which has already been discussed in chapter 4. By neutron irradiation experiments it has been shown that 20-30% of the total in situ produced radiocarbon is able to enter the DOC fraction, thus excluding the possibility of ice core dating via  $^{14}\text{C}$  analyses of the DOC due to the produced age bias.

### DOC adsorption to the quartz fibre filter matrix

The in situ effect has only been shown in the DOC and not in the POC so far. A direct production of in situ in the POC fraction is regarded to be unrealistic, because of the up to ten times smaller concentration of POC compared to DOC and the very inhomogeneous and isolated distributions of particles. However, it could in principle be possible that during the melting and filtration of the ice sample a fraction of the in situ biased DOC adsorbs onto the surface of POC particles or, more probable, onto the filter matrix. This effect is widely known for POC / DOC separation in seawater samples, where the distinction between the two organic carbon fractions is usually

## 9.4 Discussion of potential reasons for the age difference between POC $^{14}\text{C}$ dating and annual layer counting

defined by particle retention on a filter with  $0.45\ \mu\text{m}$  pore size (Johnson and Wangersky, 1985; Karanfil et al., 2003). It has been observed, that for seawater samples up to 30% of the DOC is retained on glass fibre filters (Abdel-Moati, 1990; Collos et al., 2014) at variable pore sizes of  $0.4\text{--}1.2\ \mu\text{m}$ . This effect can even be enhanced for quartz fibres compared to glass fibres (Maske and Garcia-Mendoza, 1994). The effect is strongly dependent on the salinity of the water, the polarity of the DOC substances and the chain length of the organic molecules (Bates et al., 1983; Gómez-Gutiérrez et al., 2007). It was observed to increase with high salinity and lipophilic nature of the substances. However, seawater has a very different chemical composition, most notably, a very much enhanced salinity compared to high Alpine snow and is therefore not directly comparable. Also glass fibre filters can have a different surface texture and chemical properties than quartz fibre filters, which makes a direct comparison difficult.

Better comparable to the filtration of high Alpine precipitation, but still different, is the filtration of freshwater and artificial solutions, where DOC adsorption to glass fibre filters has been observed as well (Bates et al., 1983; Gómez-Gutiérrez et al., 2007). There, the effect of DOC retention of the filter is smaller. It has been measured up to 10% (Karanfil et al., 2003) in an artificial solution (1–4 mg/l) of humic and fulvic acids based on deionised water.

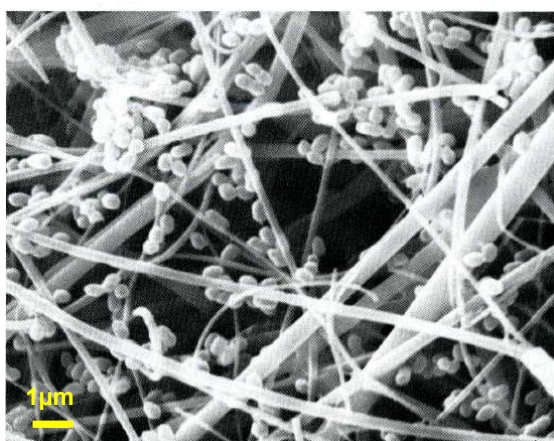


**Fig. 9.13.:** Scanning electron micrograph of bacteria adsorbed to the matrix of a fibrous filter. Note the scale. Taken from Brock (1983).

However, adsorption of particles much smaller than the nominal pore size (see Fig. 9.13 for an example of adsorbed bacteria) and even solutes to the filter matrix, especially for fibre filters, is on first order a physical process. It can also be driven by electrostatic effects (Brock, 1983) and should therefore in principle occur to a certain stage in any filtration setup using fibre filters. The adsorption processes have also been observed to be not linearly dependent on the filtered volume. This is due to a saturation of the adsorption centres on the fibre surfaces, but typically filtration of a certain amount of material a saturation is reached, strongly dependent on concentration (Brock, 1983; Abdel-Moati, 1990; Collos et al., 2014).

Based on these facts and observations, it could in principle be possible for a fraction of the in situ biased DOC to adsorb to the filter matrix, especially, because saturation of the adsorption centres will probably not be reached for the very low impurity concentrations in Alpine samples. The quantitative assessment of this fraction must however up to now remain highly speculative. In a first attempt to set up a quantitative estimation for the ice samples the 10% adsorption observed by Karanfil et al. (2003) are regarded as an upper limit. Based on the finding, that about 30% of the in situ produced  $^{14}\text{C}$  can enter the DOC fraction (see Section 4.1.3), the lower limit for calculation was in a first estimate set to 3% adsorption, which then equals a total incorporation of 1% in situ  $^{14}\text{C}$  into the POC fraction.

## 9. Results - POC based $^{14}\text{C}$ dating of a new ice core from the high Alpine firn saddle Colle Gnifetti (Swiss Alps)

---

The assumptions for in situ calculation can thus be summarised to:

- Upper limit: 30 % incorporation of in situ  $^{14}\text{C}$  to the DOC  
 $\rightarrow$  10 % adsorption of DOC to the filter  $\Rightarrow$  3 % total in situ  $^{14}\text{C}$  incorporation to the POC
- Lower limit: 30 % incorporation of in situ  $^{14}\text{C}$  to the DOC  
 $\rightarrow$  3 % adsorption of DOC to the filter  $\Rightarrow$  1 % total in situ  $^{14}\text{C}$  incorporation to the POC

Based on these assumptions a hypothetical in situ  $^{14}\text{C}$  correction of the measured POC values has been performed according to (the detailed calculation is reported in appendix A.5.4):

$$C_m = C_s + C_{insitu} \cdot m \cdot \varepsilon \quad \Leftrightarrow \quad C_s = C_m - C_{insitu} \cdot m \cdot \varepsilon \quad (9.1)$$

with  $C_m$  as the measured number of  $^{14}\text{C}$  atoms,  $C_s$  the expected number of  $^{14}\text{C}$  atoms of the samples based on the age of the annual layer counting in the according depth,  $m$  as the sample ice mass [g] and  $\varepsilon$  as the fraction of in situ  $^{14}\text{C}$  measured in the POC.  $C_{insitu}$  denotes the additional  $^{14}\text{C}$  number per gram ice due to  $^{14}\text{C}$  production and was calculated according to (see chapter 4):

$$C_{insitu}(z) = \frac{P_0}{\frac{\rho A}{\Lambda} - \lambda} \cdot \left( e^{-\frac{\lambda z}{A}} - e^{-\frac{\rho z}{\Lambda}} \right) \quad (9.2)$$

with  $P_0$  as the production rate,  $\rho$  the ice density in  $\text{g}/\text{cm}^3$ ,  $A$  the mean accumulation in cm water per year,  $z$  as the sample depth [cm w.e.],  $\lambda$  the decay constant of  $^{14}\text{C}$  and  $\Lambda$  as the mean free path length for neutrons in ice. The parameter values used in these corrections are summarised in Table 9.3.

**Tab. 9.3.:** Parameter values used for hypothetical in situ correction of the POC  $^{14}\text{C}$  ages of the KCC core.

Parameter	Value for calculation
$P_0$	380 $^{14}\text{Cg}^{-1}\text{a}^{-1}$ (Lal and Jull, 1990)
$\Lambda$	150 $\text{g} \cdot \text{cm}^{-2}$ (Lal and Jull, 1990)
$A$	22 cm w.e./year (pers comm. Pascal Bohleber)
$\rho$	0.9 $\text{g}/\text{cm}^3$
$\varepsilon$	0.01 / 0.03 / 0.1

The resulting in situ corrected calibrated POC  $^{14}\text{C}$  ages are shown in Fig. 9.14 and the main findings retrieved from this hypothetical in situ correction of the POC  $^{14}\text{C}$  can be summarised to:

- The hypothetical in situ correction has an overall rather small effect on the  $^{14}\text{C}$  ages of the samples. The calibrated ages increase about 2-30 % at 16 % average for 1 % assumed in situ incorporation. Even 3% assumed in situ incorporation is not enough to shift the samples in the bottom 10m of the core to the range of the annual layer counting.

## 9.4 Discussion of potential reasons for the age difference between POC $^{14}\text{C}$ dating and annual layer counting

- Only an assumption of 10% in situ  $^{14}\text{C}$  incorporation into the POC fraction (see Fig. 9.14) would be large enough to shift the five deepest samples to the range of the annual layer counting. This would however mean, that one third of the total DOC mass needs to be measured in the POC fraction, which is considered to be unrealistic regarding the overall low total carbon masses of the POC samples.
- The in situ correction is also dependent on sample size and has a larger influence on smaller samples (see calculations in appendix A.5.4), which causes the large deviation for the two samples at 39.21 m w.e. and 45.12 m w.e.

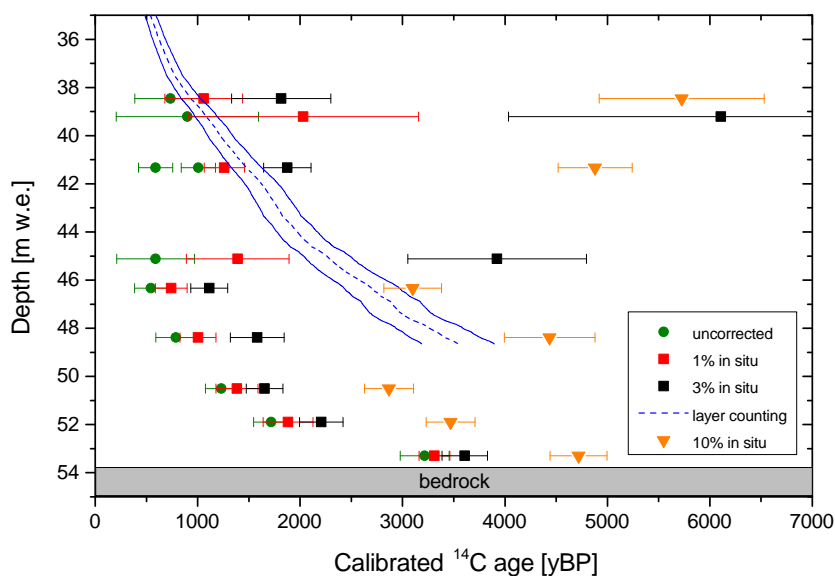


**Fig. 9.14.:** In situ production corrected POC  $^{14}\text{C}$  ages for the KCC core calculated with 1 and 3 % total in situ incorporation in the POC via 3-10 % DOC adsorption onto the quartz fibre filter. Note that only for the unrealistic assumption of 10 % in situ incorporation the basal ages are shifted to the range of the annual layer counting chronology.

A major drawback of this correction is the assumption of a constant accumulation rate over the complete core depth, which is, based on the glaciological settings stated above, not very realistic. The in situ corrections are thus regarded as a first order estimation. As a conclusion, an incorporation of in situ produced  $^{14}\text{C}$  into the POC fraction could be possible, but the effect is very likely too small to explain the large offset between the POC  $^{14}\text{C}$  dates and the annual layer counting chronology, especially in the bottom part of the core.

### Accumulation changes

Although an in situ  $^{14}\text{C}$  bias of the POC fraction is probably not able to explain the large offset between the two dating methods, it could however be a reason for the apparent shift between the top three POC samples and the bottom part, if the sample at 41.33 m w.e. depth is not regarded as an outlier biased by Saharan dust influence. Such a shift could be due to a change in accumulation regime, either temporal or spatial. Upstream of the drilling site, high on the

## 9. Results - POC based $^{14}\text{C}$ dating of a new ice core from the high Alpine firn saddle Colle Gnifetti (Swiss Alps)

slope, field measurements yielded very low accumulation rates of down to 4 cm w.e./year (Lüthi, 2000). However, reconstructions of accumulation rates based on ground penetrating radar (GPR) data, rather predict a slight increase of accumulation upstream to ca. 30 cm w.e./year (Bohleber, 2011; Konrad, 2011; Konrad et al., 2013). If, however, based on the direct field measurement, a substantial decrease in upstream accumulation is assumed, this would result in an enhanced in situ production and thus increase the bias to younger ages.

It was therefore tried to assess such an effect by application of an accumulation change below the sample at 41.33 m w.e. depth using the most probable in situ correction scenario with 1% incorporation into the POC. The results are shown in Fig. 9.15; the large deviations of the samples at 39.21 m w.e. and 45.12 m w.e. depth are due to their very small sample sizes. First, a change from 22 cm w.e./y (surface accumulation of KCC) to 14 cm w.e./y was applied (black symbols), which equals the surface accumulation of the KCI core on the same flowline as the KCC. This was however not enough to eliminate the offset between the top and bottom samples. Only for an assumed accumulation change to 5 cm w.e./y in the bottom part of the core, the top and bottom samples seem to follow the same course. This is a very large step and probably not very realistic. The apparent shift in the data is mainly caused by the deviation of the sample at 41.33 m w.e. depth, the two samples above are within error range equal to the following sample at 45.12 m w.e.

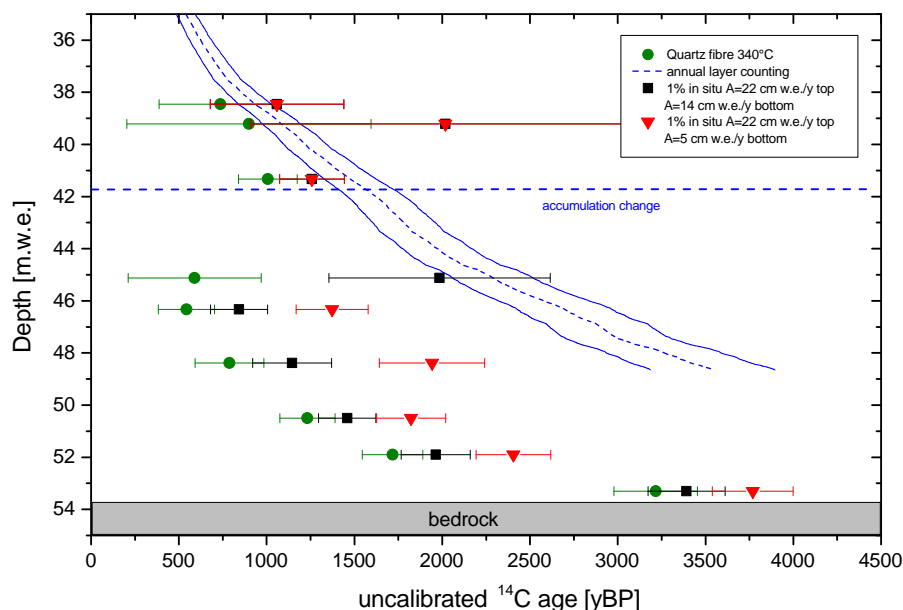


**Fig. 9.15.:** In situ corrected POC  $^{14}\text{C}$  results including an accumulation change between the top three and the bottom samples. An accumulation change from 22 cm w.e./y to 5 cm w.e./y (triangles) is needed to compensate the apparent shift between top and bottom samples.

Because the accumulation change scenarios have been found to be not very realistic, the  $^{14}\text{C}$  result at 41.33 m w.e. depth is rather considered as an outlier caused by possible influences of an adjacent dust event already discussed above.

### Bacterial activity

Another possibility to incorporate in situ produced  $^{14}\text{C}$  and its products ( $\text{CO}_2$  and DOC) directly into the POC fraction could be the fixation of  $\text{CO}_2$  and DOC by microbe and bacteria metabolism within the snow and firn section of the glacier. Bacterial activity has been found even in the cold, high Alpine regimes (Chuvochina et al., 2011). There, for example cyanobacteria have been discovered, which are able to perform photosynthesis. Also heterotrophic species have been found, that use external organic material for metabolism, (Tung et al., 2005; Anesio et al., 2009) and could be able to incorporate in situ  $^{14}\text{C}$  fixed in the DOC this way. These bacteria and microbes have typical sizes of up to a few micrometers (see e.g. Després et al. (2012)) and thus are able to contribute directly to the POC fraction. However, as already stated in Chapter 3, their total concentration and mass, which lies for high Alpine ice and snow typically in the range of 1.5 ngC/kg ice (Chuvochina et al., 2011), (pers. comm. Birgit Sattler, Innsbruck) is just too small to have a measurable contribution to the POC fraction. Thus, the fixation of in situ produced  $^{14}\text{C}$  by microbial activity and their contribution to the POC fraction is considered to be negligible and can not serve as an explanation for the age offset between the POC  $^{14}\text{C}$  results and the annual layer counting chronology.

### 9.4.4. Conclusion of potentially age biasing effects

As a conclusion of the investigations on potentially age biasing effects, no phenomenon, artificial or natural, could so far be discovered, that is large enough to completely explain the offset between the POC  $^{14}\text{C}$  dates and the annual layer working chronology. The most likely effect is the incorporation of in situ produced  $^{14}\text{C}$  into the DOC fraction. Based on the estimations for DOC adsorption this could be able to explain several hundred years of age offset, but not 2500 years for the most basal samples. However, this effect needs to be investigated further, before a final conclusion. Therefore, the POC  $^{14}\text{C}$  results should be regarded as preliminary, until further insights into the in situ effect and the nature of the internal shift in the data are gained.

## 9.5. Comparison with previous Colle Gnifetti ice core dating studies

Because the investigation of potential artificial and natural biasing effects causing younger  $^{14}\text{C}$  ages than expected in the POC fraction of the KCC core yielded no final conclusion, the results are now compared on a normalized depth scale to other  $^{14}\text{C}$  POC dating attempts at Colle Gnifetti. This is done to obtain an evaluation of the measured  $^{14}\text{C}$  data independent from the annual layer counting scenario. Such a comparison can only be performed on a qualitative base though. It can not be expected, that for a common relative core depth the total ages of two cores agree, because of a strong connection between total thickness, accumulation rate and layer thinning (Bohleber, 2008). As an example, in Fig. 9.16, the normalised age depth relationships for all IUP Colle Gnifetti ice cores are shown. The core with the lowest accumulation, KCI, yields the highest ages in already shallow depth. Note that all shown chronologies inherit an increasing uncertainty with depth, which is not shown in the picture. The aim of this data comparison is therefore in first order not to compare directly total ages, but the shape and curvature of the  $^{14}\text{C}$  datasets.

## 9. Results - POC based $^{14}\text{C}$ dating of a new ice core from the high Alpine firn saddle Colle Gnifetti (Swiss Alps)

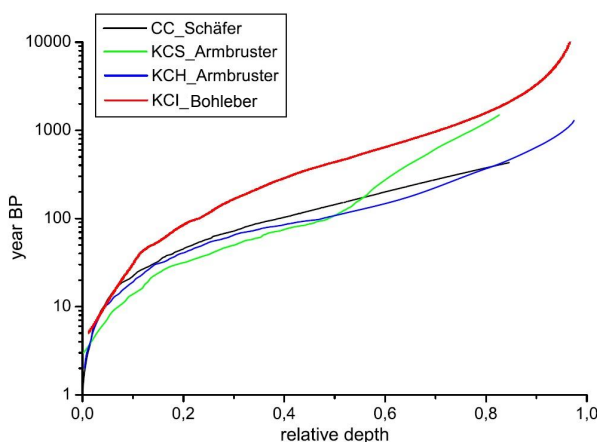


**Fig. 9.16.:** Normalised age depth relationships for all IUP Colle Gnifetti cores except KCC. Note the differences in total ages at common relative depths. Taken from Bohleber (2008)

### 9.5.1. KCC - KCI comparison

First, the results are compared to POC  $^{14}\text{C}$  ages retrieved by May (2009) from the KCI core on the same flow line as KCC (see Fig. 9.17) but with only about half the surface accumulation. The results by May (2009) for the KCI were combusted completely at  $800^\circ\text{C}$  (marked in black) and show very large errors due to a high blank correction. Based on the findings about the age differences between the different temperature fractions, they should therefore have a general tendency to older ages than the results of  $340^\circ\text{C}$  combustion only. The old KCI samples are complemented by two more samples measured within this work (blue). For the two new samples only the  $340^\circ\text{C}$  results are shown, which should be better comparable to the KCC results. The error bars of the two deepest samples are not shown completely, because this would have required a logarithmic scale, which is not very descriptive.

Overall, the curvature of both datasets is very similar. The KCI samples also show a deviation in direction to younger ages increasing with depth compared to the annual layer counting based ice slab model of the KCI. This deviation is however at a normalised core depth of 0.8-0.85 not as strong as for the KCC. The comparison of the two datasets has a very suggesting appearance regarding the one outlier of KCC. In this depiction, it seems that there is indeed a shift in the KCC data between 80 and 85 % of the core, which is not apparent in the KCI data. Nevertheless, on base of the present sparse and highly uncertain KCI data, a final decision about the shift is not possible, more data in the gap between 80 and 85 % of the KCC and KCI is needed to investigate that phenomenon. Note that since being based on a simple flow model consideration, the shape of the KCI dating is inherently analytical in contrast to the annual layer counting based dating of KCC. The KCC dating comprises frequent points of inflection, which are a realistic feature of a Colle Gnifetti age scale, due to the variable net accumulation.

## 9.5 Comparison with previous Colle Gnifetti ice core dating studies

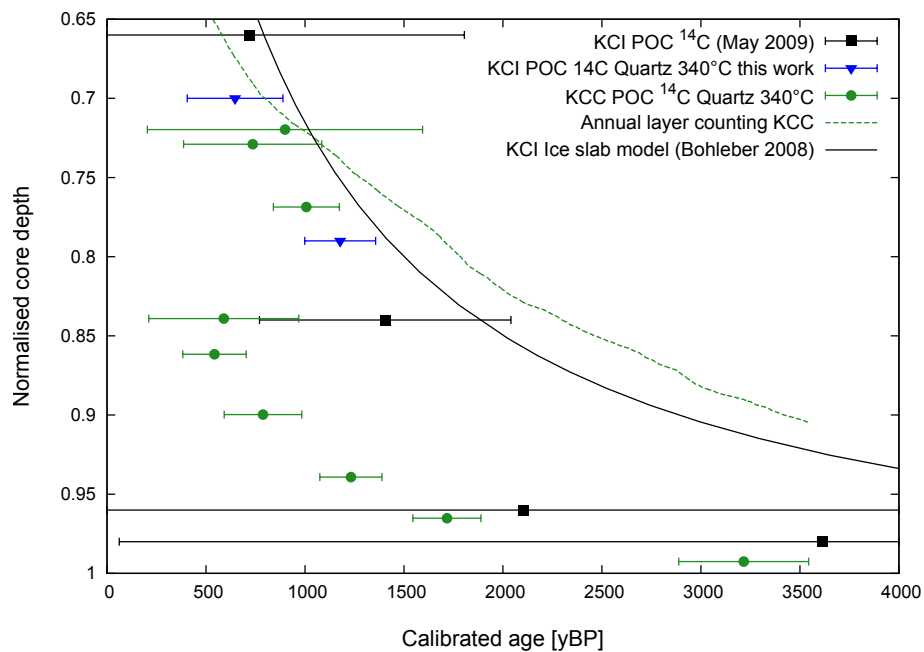


**Fig. 9.17.:** Comparison of POC  $^{14}\text{C}$  ages measured at the KCI ice core by May (2009) with  $^{14}\text{C}$  data retrieved in this study for both cores. Note the overall similarity in the curvature of age-depth relationship.

The most important finding of this comparison is the overall very similar shape and curvature in the KCI and KCC POC  $^{14}\text{C}$  data, which is contradicting to the chronologies based on annual layer counting. This finding could hint to a systematic difference in  $^{14}\text{C}$  data and annual layer counting based age data for the Colle Gnifetti.

### 9.5.2. KCC - CG 03 comparison

Apart from KCI and KCC, the only other ice core from Colle Gnifetti, which has been dated by POC  $^{14}\text{C}$  analyses so far (CG 03) has been drilled under the lead of the Paul Scherrer Institute (Switzerland) in 2003 (see Jenk et al. (2009)). The drilling position of the core near the saddle point is marked in Fig. 9.3. Nine samples from the lowest third of the core have been POC  $^{14}\text{C}$  dated, using quartz fibre filters for filtration and a two step combustion (340 °C and 650 °C). Only the 340 °C fraction has been used for dating. The radiocarbon results of this study (taken from Jenk et al. (2009)) are shown together with the KCC results in Fig. 9.18 on a normalised core depth scale.

More important is again not the absolute agreement of the data points but the very similar course and shape of the age increase with depth of both  $^{14}\text{C}$  datasets, strongly contradicting the shape of the annual layer counting chronology.

## 9. Results - POC based $^{14}\text{C}$ dating of a new ice core from the high Alpine firn saddle Colle Gnifetti (Swiss Alps)

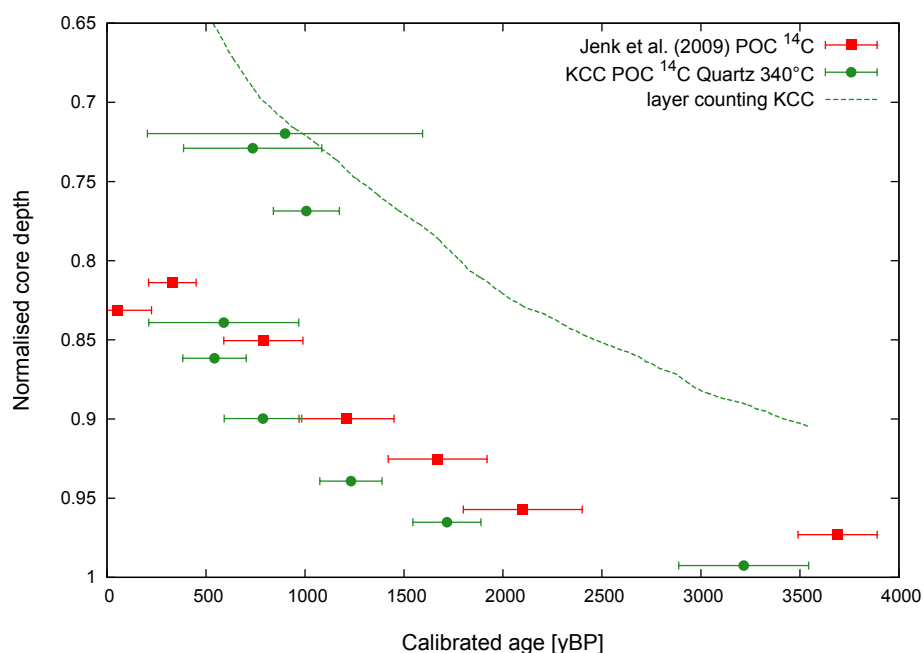


**Fig. 9.18.:** Comparison of POC  $^{14}\text{C}$  ages measured at the CG 03 ice core by Jenk et al. (2009) with  $^{14}\text{C}$  data retrieved in this study. Note the very similar curvature of both radiocarbon dating scenarios.

Both datasets show an offset of ca. 500 years, which stays almost constant in the deepest 15% of the core. At some relative depths, the results even agree within error. This is somehow surprising, because the CG 03 core is indeed located at the same flank of the saddle, but at a very different position and not the same flow line as KCI and KCC. The CG 03 core also has a surface accumulation of 46 cm w.e./year, which is almost twice as high as for the KCC. Such an age comparison on a normalised core depth scale can thus only provide a qualitative assessment. Nevertheless, combined with findings from the KCI comparison, a general trend in the POC  $^{14}\text{C}$  dates for three independent cores measured by three independent POC  $^{14}\text{C}$  methods can be deduced. In contrast to the annual layer counting based chronology, the  $^{14}\text{C}$  ages show a trend to stay younger in the deepest quarter of the core, with increasing age offset approaching bedrock.

### 9.5.3. Summary of the POC $^{14}\text{C}$ result discussion and final evaluation of the data

As a conclusion, the POC  $^{14}\text{C}$  for the KCC core retrieved within this work are not questionable from a methodological point of view. They show however a large systematical offset to the annual layer counting working chronology. The ultimate reason for this offset must remain unclear at this stage of investigation. Possibly, the in situ production of  $^{14}\text{C}$  and the incorporation into the POC has a limited influence, but this needs to be clarified in further measurements. Also the possible shift between the top three samples and the bottom part of the core needs to be investigated further by additional measurements. At the present stage, the main reason for this apparent shift is the result of the sample at 41.33 m w.e. depth, which is rather regarded to be an outlier biased by Saharan dust as long as this trend is not backed up by additional measurements.

## 9.5 Comparison with previous Colle Gnifetti ice core dating studies

---

Therefore, based on the data obtained so far it is not possible to constitute the POC  $^{14}\text{C}$  ages as a self-contained dating scenario, this can only be assessed by further  $^{14}\text{C}$  investigations which will be proposed in chapter 10.

The main findings of the POC  $^{14}\text{C}$  data evaluation of the 2013 Colle Gnifetti deep ice core KCC can thus be summarised as follows:

- The POC samples had small sample sizes ( $<10\ \mu\text{gC}$  in most cases), but could be measured to errors between 1 and 5 % on average, which is a factor of more than ten better than previous studies.
- The results show a gradual age increase with depth, as expected, but have a simultaneously increasing massive offset of up to 2500 yBP to the chronology based on annual layer counting.
- So far, a basal age of  $(3216 \pm 238)$  cal. yBP could be measured 60 cm above bedrock.
- Artificial contamination could be ruled out as reason for the offset between  $^{14}\text{C}$  and annual layer counting data.
- Incorporation of in situ produced  $^{14}\text{C}$  in the POC fraction via adsorption of DOC to the filter matrix could have an influence on the  $^{14}\text{C}$  dates, resulting in younger ages than expected, but the effect is probably not large enough to explain the complete deviation between the  $^{14}\text{C}$  and annual layer counting method.
- An apparent age shift within the upper part of the sampled core length can either be due to a bias of one sample by dust input or systematically due to accumulation rate changes. A final decision is not possible on base of the present data, but the outlier is considered to be more probable.
- Inter-core comparisons with other POC  $^{14}\text{C}$  dating studies from Colle Gnifetti yield a very good agreement of the principal shape and curvature of age increase for all  $^{14}\text{C}$  datings including a systematical shift to younger ages compared to the annual layer counting scenarios.
- The  $^{14}\text{C}$  data is not proposed as an independent dating scenario but as an alternative working hypothesis until further insights into possible in situ effects and age shifts are gained by additional measurements.



## 10. Outlook

The main goal of this work was to improve the POC  $^{14}\text{C}$  dating of high Alpine ice samples regarding the reduction of required sample ice mass, in order to make the method applicable for ice core dating, where the retrieved POC concentrations are often not exceeding  $50 \frac{\mu\text{gC}}{\text{kg}}$ . This goal has been widely achieved. The methodological key improvements were:

- The establishment of  $\text{CO}_2$  gas  $^{14}\text{C}$  measurements at the MICADAS AMS in Mannheim, which enable reproducible  $^{14}\text{C}$  dating of  $\text{CO}_2$  gas in a sample size range of 2-100  $\mu\text{gC}$  with a precision of 1-2 % for samples larger than 10  $\mu\text{gC}$  and 3-7 % for samples smaller than 10  $\mu\text{gC}$ .
- Setup of a new combined pre-cleaning, filtration and stepwise combustion system, REFILOX, by which the process blank could be reduced by a factor of four to ten compared to earlier POC extraction systems at the IUP Heidelberg. The new process blank has now a maximum value of  $(1.5 \pm 0.5) \mu\text{gC}$  for a total combustion at 800 °C and was even below detection limit for combustion at 340 °C.
- As a result, dating of samples  $> 2 \mu\text{gC}$  for the 340 °C, fraction and  $> 10 \mu\text{gC}$  for the 800 °C and total combustion is possible with a relative error introduced by the blank contribution of less than 10 % for ages up to ca. 12 000 years BP.

A systematic  $^{14}\text{C}$  age investigation of different materials (Saharan dust, cryoconite and sediment) yielded overall very high (600-22 000 years) intrinsic ages, much higher than the expected ice ages at the respective sample locations. By systematic analyses of aerosol samples of known  $^{14}\text{C}$  age, it was found that the carbon fraction best representing the real sample age already combusts at very low temperatures of only 340 °C and only this fraction should thus be used as the best representative for the ice age of a sample. In spite of this general limitation of dating accuracy, all POC  $^{14}\text{C}$  dates can serve for constraining upper ice age limits.

In a first dating application a consistent basal age, narrowed down to 4237-4784 calibrated yBP, could be measured for basal ice blocks from Titlis glacier (Switzerland), which serves like stated above as a first estimate of an upper age limit. The dating of a new ice core from Colle Gnifetti via POC  $^{14}\text{C}$  has been very successful in terms of measurement technique. Although almost all samples had a size below 10  $\mu\text{gC}$ , they could be dated to average relative errors of ca. 3% in the 340 °C fraction. A basal ice age of  $(3216 \pm 268)$  calibrated yBP, ca. 60 cm above bedrock could be found. However, the  $^{14}\text{C}$  results show a large age offset to younger ages of up to 2500 years compared to the independently established working chronology based on annual layer counting, which can not be explained by artificial contamination. A possible natural reason for this age difference could be the incorporation of in situ produced  $^{14}\text{C}$  via DOC adsorption to the POC fraction, which is however likely to be insufficient for the explanation of the whole offset. The enigma of age deviation between both dating methods must therefore at present state remain unsolved. The next steps planned in the near future for the investigation of this phenomenon are:

## 10. Outlook

---

- Filtration of synthetic solutions containing different species of DOC to quantify the adsorption effect of solutes to the filter matrix
- Comparison of normal POC filtration and DOC extraction before POC filtration for one Colle Gnifetti ice core sample to evaluate, if there is an age change in the retrieved POC  $^{14}\text{C}$  ages by removing the DOC from the sample first
- Dating of further core samples, especially in the depth range where an apparent shift in the  $^{14}\text{C}$  data is visible in the present data

Also planned for the near future are biological investigations of the POC composition of the Titlis basal ice, which will be carried out in collaboration with the University of Innsbruck. This will help to further evaluate the measured basal ice ages. In this context, also  $^{39}\text{Ar}$  dating (done by the aquatic systems group at the IUP) of the Titlis ice will help to further constrain the age. Within the next year, it is envisaged to repeat the neutron irradiation experiments, already done for in situ production in DOC as presented in this work, for the POC fraction, to evaluate the amount of in situ  $^{14}\text{C}$  possibly incorporated into the POC fraction. Also further improvements for the gas ion source can be made by optimising the mixing ratio of  $\text{CO}_2$  and Helium introduced into the ion source, to maximise the retrieved ion currents and thus minimise the statistical counting error. Also for the carbon fraction separation by combustion temperature further investigations are needed to gain deeper insights in the separation of the different organic carbon fractions. For that purpose, further analyses of aerosol samples and ice samples, where a lot of material is available for testing (e.g. block samples from Titlis glacier) are planned. These analyses will mainly focus on further tuning of separating temperatures and combustion times.

In the long run, in terms of method optimisation, speeding up the cleaning routines of the RE-FILOX system and the establishment of an online sample combustion are the next aims. By such an online combustion in a stream of oxygen instead of within a closed volume, directly supervised by a  $\text{CO}_2$  detector, the whole sample preparation process could be sped up significantly. It was already attempted to implement such a system, but this has so far been thwarted by too high process blanks of so far unknown origin, probably caused by leaks in the  $\text{CO}_2$  detector.

The method of micro POC  $^{14}\text{C}$  dating of Alpine ice samples, refined and evaluated within this work, is a valuable tool for glacier dating where stratigraphic methods fail and on this sensitivity level only complemented by one other similar system in Switzerland. It is planned to play an important role in many different projects. These include for example a project called *(C)old ice AT* (led by colleagues from Innsbruck University), in which the Titlis samples presented in this work were part of a pilote study and which aims for a better understanding of the distribution of cold, old ice bodies all over the Alps. In another Alpine context, a higher resolved dating of the ice core from Vasto ice cave (Italy) is in preparation in collaboration with colleagues from Trieste and Milano. Also a collaboration with the Climate Change Institute (CCI) at the University of Maine has been established, as part of which the POC  $^{14}\text{C}$  dating has already been applied in pilote studies for dating of selected ice samples from the Andes and South Georgia. Apart from these numerous collaborations, it is also envisaged to investigate more ice core samples from Colle Gnifetti, especially from the KCI core. This aims to complete the picture of chronologies established so far, which will be an important contribution to the interpretation of climate proxy time series retrieved from this ice core array.

# Bibliography

- [Abdel-Moati 1990] ABDEL-MOATI, A. R.: Adsorption of dissolved organic carbon (DOC) on glass fibre filters during particulate organic carbon (POC) determination. In: *Water Research* 6 (1990), Nr. 763-764
- [Anesio et al. 2009] ANESIO, A. M. ; HODSON, A. J. ; FRITZ, A. ; PSENNER, R. ; SATTLER, B.: High microbial activity on glaciers: importance to the global carbon cycle. In: *Global Change Biology* 15 (2009), pp. 955–960
- [Armbruster 2000] ARMBRUSTER, M.: *Stratigraphische Datierung hochalpiner Eisbohrkerne über die letzten 1000 Jahre*, Institut für Umweltphysik, Universität Heidelberg, Diplomarbeit, 2000
- [Arnold and Libby 1949] ARNOLD, J. R. ; LIBBY, W. F.: Age determinations by radiocarbon content: checks with samples of known age. In: *Science* 110 (1949), pp. 678–680
- [Aymoz et al. 2004] AYMOZ, G. ; JAFFREZO, J.-L. ; JACOB, V. ; COLOMB, A. ; GEORGE, Ch.: Evolution of organic and inorganic components of aerosol during a Saharan dust episode observed in the French Alps. In: *Atmospheric Chemistry and Physics Discussions* 4 (2004), pp. 3875–3909
- [Baertschi 1953] BAERTSCHI, P.: Die Fraktionierung der natürlichen Kohlenstoffisotopen im Kohlendioxidstoffwechsel grüner Pflanzen. In: *Helvetica Chimica Acta* 95 (1953), pp. 773–781
- [Bardgett et al. 2007] BARDGETT, R. D. ; RICHTER, A. ; BOL, R. ; GARNETT, M. H. ; BÄUMLER, R. ; XU, X. ; LOPEZ-CAPEL, E. ; MANNING, D. A. ; HOBBS, P. J. ; HARTLEY, I. R. ; WANEK, W.: Heterotrophic microbial communities use ancient carbon following glacial retreat. In: *Biology Letters* 3 (2007), pp. 487–490
- [Bates et al. 1983] BATES, T. S. ; HAMILTON, S. E. ; CLINE, J. D.: Collection of Suspended Particulate Matter for Hydrocarbon Analyses: Continuous Flow Centrifugation vs. Filtration. In: *Estuarine, Coastal and Shelf Science* 16 (1983), pp. 107–112
- [Bauer et al. 2002] BAUER, H. ; KASPER-GIEBL, A. ; LÖFLUND, M. ; GIEBL, H. ; HITZENBERGER, R. ; ZIBUSCHKA, F. ; PUXBAUM, H.: The contribution of bacteria and fungal spores to the organic carbon content of cloud water, precipitation and aerosols. In: *Atmospheric Research* 64 (2002), pp. 109–119
- [Becker 1993] BECKER, B.: An 11,000-year German oak and pine dendrochronology for radiocarbon calibration. In: *Radiocarbon* 35 (1993), Nr. 1, pp. 201–213
- [Benn and Evans 2010] BENN, D. I. ; EVANS, D. J. A.: *Glaciers & Glaciation*. 2. Hodder Education, 2010

## Bibliography

---

- [Biegalski et al. 1998] BIEGALSKI, S. R. ; CURRIE, L. A. ; FLETCHER, R. A. ; KLOUDA, G. A. ; WEISSENBÖK, R.: AMS and microprobe analysis of combusted particles in ice and snow. In: *Radiocarbon* 40 (1998), pp. 3–10
- [Bigler et al. 2011] BIGLER, M. ; SVENSSON, A. ; KETTNER, E. ; VALLELONGA, P. ; NIELSEN, M. E. ; STEFFENSEN, J. P.: Optimization of High-Resolution Continuous Flow Analysis for Transient Climate Signals in Ice Cores. In: *Environmental Science and Technology* 45 (2011), pp. 4483–4489
- [Bohleber 2008] BOHLEBER, P.: *Age distribution and  $\delta^{18}O$  variability in a low accumulation Alpine ice core: perspective for paleoclimate studies*, Institut für Umweltphysik, Heidelberg University, Diplomarbeit, 2008
- [Bohleber 2011] BOHLEBER, P.: *Ground-penetrating radar assisted ice core research: The challenge of Alpine glaciers and dielectric ice properties*, Institut für Umweltphysik, Heidelberg University, Dissertation, 2011
- [Bohleber et al. 2013] BOHLEBER, P. ; WAGENBACH, D. ; SCHÖNER, W. ; BÖHM, R.: To what extent do water isotope records from low accumulation Alpine ice cores reproduce instrumental temperature series? In: *Tellus B* 65 (2013)
- [Brock 1983] BROCK, T. D. ; BROCK, K. M. (Edt.) ; BROCK, T. D. (Edt.): *Membrane Filtration - A User's Guide and reference Manual*. Springer Verlag, 1983
- [Bronk Ramsey 1995] BRONK RAMSEY, C.: Radiocarbon Calibration and Analysis of Stratigraphy: The OxCal Program. In: *Radiocarbon* 37 (1995), pp. 425–430
- [Bronk Ramsey et al. 2004] BRONK RAMSEY, C. ; DITCHFIELD, P. ; HUMM, M.: Using a gas ion source for radiocarbon AMS and GC-AMS. In: *Radiocarbon* 46 (2004), Nr. 1, pp. 25–32
- [Buijsman et al. 1987] BUIJSMAN, E. ; MAAS, H. F. M. ; ASMAN, W. A. H.: Anthropogenic  $NH_3$  emissions in Europe. In: *Atmospheric Environment* 21 (1987), Nr. 5, pp. 1009–1022
- [Cachier et al. 1989] CACHIER, H. ; BREMOND, M.-P. ; BUAT-MÉNARD, P.: Determination of atmospheric soot carbon with a simple thermal method. In: *Tellus* 41B (1989), pp. 379–390
- [Cao et al. 2013] CAO, F. ; ZHANG, J.-L. ; SZIDAT, S. ; ZAPF, A. ; WACKER, L. ; SCHWIKOWSKI, M.: Microgram-level radiocarbon determination of carbonaceous particles in firn and ice samples: pretreatment and OC/EC separation. In: *Radiocarbon* 55 (2013), Nr. 2-3, pp. 383–390
- [Carcaillet 2001] CARCAILLET, C.: Are Holocene wood-charcoal fragments stratified in alpine and subalpine soils? Evidence from the Alps based on AMS  $^{14}C$  dates. In: *The Holocene* 11 (2001), Nr. 2, pp. 231–242
- [Cheminet et al. 2012] CHEMINET, A. ; LACOSTE, V. ; HUBERT, G. ; BOSCHER, D. ; BOYER, D. ; POUPENEY, J.: Experimental Measurements of the Cosmic-Ray Induced Neutron Spectra at Various Mountain Altitudes With HERMEIS. In: *IEEE Transactions on Nuclear Science* 59 (2012), Nr. 4
- [Chen et al. 1999] CHEN, C. Y. ; LI, Y. M. ; BAILEY, K. ; O'CONNOR, T. P. ; YOUNG, L. ; LU, Z.-T.: Ultrasensitive Isotope Trace Analyses with a Magneto-Optical Trap. In: *Science* 286 (1999)

- [Chuvochina et al. 2011] CHUVOCHINA, M. S. ; MARIE, D. ; CHEVALLIER, S. ; PETIT, J. R. ; NORMAND, P. ; ALEKHINA, I. A. ; BULAT, S. A.: Community Variability of Bacteria in Alpine Snow (Mont Blanc) Containing Saharan Dust Deposition and Their Snow Colonisation Potential. In: *Microbes and Environmments* 26 (2011), Nr. 3, pp. 237–247
- [Colbeck and Lazaridis 2014] COLBECK, I. (Edt.) ; LAZARIDIS, M. (Edt.): *Aerosol Science Technology and Applications*. Wiley, 2014
- [Collos et al. 2014] COLLOS, Y. ; JAUZEIN, C. ; HATEY, E.: Particulate carbon and nitrogen determinations in tracer studies: The neglected variables. In: *Applied Radiation and Isotopes* 94 (2014), pp. 14–22
- [Colucci 2013] COLUCCI, R. R.: *Some evidences of recent and holocenic evolution of the cryosphere in Friuli Venezia Giulia (Italy)*, Università degli studi di Trieste, Dissertation, April 2013
- [Colucci et al. 2014] COLUCCI, R. R. ; FONTANA, D. ; FORTE, E.: Characterization Of Two Permanent Ice Cave Deposits In The Southeastern Alps (Italy) By Means Of Ground Penetrating Radar (Gpr). In: *Ice cave processes*, 2014 (Proceeding of the International Workshop on Ice Caves VI)
- [Craig 1957] CRAIG, H.: The Natural Distribution of Radiocarbon and the Exchange Time of Carbon Dioxide Between Atmosphere and Sea. In: *Tellus* 9 (1957), pp. 1–17
- [Cuffey and Paterson 2010] CUFFEY, K. M. ; PATERSON, W. S. B.: *The Physics of Glaciers*. 4. Edition. Academic Press, 2010
- [Dansgaard 1964] DANSGAARD, W.: Stable isotopes in precipitation. In: *Tellus* 16 (1964), pp. 436–468
- [De Angelis et al. 2012] DE ANGELIS, M. ; TRAVERSI, R. ; UDISTI, R.: Long-term trends of mono-carboxylic acids in Antarctica: comparison of changes in sources and transport processes at the two EPICA deep drilling sites. In: *Tellus* 64B (2012)
- [deMenocal et al. 2000] DEMENOCAL, P. ; ORTIZ, R. A. ; GUILDERSON, T. P. ; ADKINS, J. ; SARNTHEIM, M. ; BAKER, L. ; YARUSINSKY, M.: Abrupt onset and termination of the African Humid Period: rapid climate responses to gradual insolation forcing. In: *Quaternary Science Reviews* 19 (2000), pp. 347–361
- [Després et al. 2012] DESPRÉS, V. R. ; HUFFMAN, J. A. ; BURROWS, S. M. ; HOOSE, C. ; SAFATTOY, A. S. ; BURYAK, G. ; FRÖHLICH-NOWOISKY, J. ; ELBERT, W. ; ANDREAE, M. O. ; PÖSCHL, U. ; JAENICKE, R.: Primary biological aerosol particles in the atmosphere: a review. In: *Tellus B* 64 (2012)
- [Donahue et al. 1990] DONAHUE, D. J. ; LINICK, T. W. ; JULL, A. T.: Isotope ratio and background corrections for accelerator mass spectrometry radiocarbon measurements. In: *Radiocarbon* 32 (1990), Nr. 2, pp. 135–142
- [Döscher et al. 1996] DÖSCHER, A. ; GÄGGELER, H. W. ; SCHOTTERER, U. ; SCHWIKOWSKI, M.: A historical record of ammonium concentration from a glacier in the Alps. In: *Geophysical Research Letters* 23 (1996), Nr. 20, pp. 2741–2744

## Bibliography

---

- [Dunbar and Kurbatov 2011] DUNBAR, N. W. ; KURBATOV, A. V.: Tephrochronology of the Siple Dome ice core, West Antarctica: correlations and sources. In: *Quaternary Science Reviews* 30 (2011), Nr. 13-14, pp. 1602–1614
- [Egli et al. 2001] EGLI, M. ; FITZE, P. ; MIRABELLA, A.: Weathering and evolution of soils formed on granitic, glacial deposits: results from chronosequences of Swiss alpine environments. In: *Catena* 45 (2001), pp. 19–47
- [Eglinton et al. 2002] EGLINTON, T. I. ; EGLINTON, G. ; DUPONT, L. ; SHOLKOVITZ, E. R. ; MONTLUCON, D. ; REDDY, C. M.: Composition, age, and provenance of organic matter in NW African dust over the Atlantic Ocean. In: *Geochemistry Geophysics, Geosystems* 3 (2002), Nr. 8
- [ELGA 2016] ELGA (Manual): *PURELAB Ultra Analytic*. 2016
- [EXFOR 2016] EXFOR: *Experimental Nuclear Reaction Data (EXFOR)*. 2016. – URL <https://www-nds.iaea.org/exfor/exfor.htm>. – Database version of February 02, 2016
- [Fagerli et al. 2007] FAGERLI, H. ; LEGRAND, M. ; PREUNKERT, S. ; VESTRENG, V. ; SIMPSON, D. ; CERQUEIRA, M.: Modeling historical long-term trends of sulfate, ammonium, and elemental carbon over Europe: A comparison with ice core records in the Alps. In: *Journal of Geophysical Research* 112 (2007)
- [Fahrni et al. 2013] FAHRNI, S. M. ; WACKER, L. ; SYNAL, H.-A. ; SZIDAT, S.: Improving a gas ion source for  $^{14}\text{C}$  AMS. In: *Nuclear Instruments and Methods in Physics Research B* 294 (2013), pp. 320–327
- [Feczko et al. 2007] FECZKO, T. ; PUXBAUM, H. ; KASPER-GIEBL, A. ; HANDLER, M. ; LIMBECK, A. ; GELENCSEÉR, A. ; PIO, C. ; PREUNKERT, S. ; LEGRAND, M.: Determination of water and alkaline extractable atmospheric humic-like substances with the TU Vienna HULIS analyzer in samples from six background sites in Europe. In: *Journal of Geophysical Research* 112 (2007)
- [Fischer 2013] FISCHER, A.: *Jamtalferner Massenhaushalt 2013/14 Jahresbericht des Vereines Gletscher-Klima*. 2013. – URL [www.gletscher-klima.at](http://www.gletscher-klima.at)
- [Fischer et al. 2014] FISCHER, A. ; STOCKER-WALDHUBER, M. ; SEISER, B. ; HYNEK, B. ; SLUPETZKY, H.: Glaciological monitoring in Hohe Tauern National Park. In: *eco.mont* 6 (2014), Nr. 1
- [Fischer et al. 2013] FISCHER, H. ; SEVERINGHAUS, J. P. ; BROOK, E. ; WOLFF, E. W. ; ALBERT, M. ; ALEMANY, O. ; ARTHERN, R. ; BENTLEY, C. ; BLANKENSHIP, D. ; CHAPPELLAZ, J. ; CREYTS, T. ; DAHL-JEHNSSEN, D. ; DINN, M. ; FREZZOTTI, M. ; FUJITA, S. ; GALLEE, H. ; HINDMARSH, R. ; HUDSPETH, D. ; JUGIE, G. ; KAWAMURA, K. ; LIPENKOV, V. Y. ; MILLER, H. ; MULVANEY, R. ; PARRENIN, F. ; PATTYN, F. ; RITZ, C. ; SCHWANDER, J. ; STEINHAGE, D. ; VAN OMMEN, T. ; WILHELMS, F.: Where to find 1.5 million yr old ice for the IPICS Oldest-Ice ice core. In: *Climate of the Past* 9 (2013), pp. 2489–2505
- [Forte et al. 2014] FORTE, E. ; BELLIGOI, D. ; COLUCCI, R. R. ; BONDINI, M. B. ; MAGGI, V. ; FONTANA, M. C. ; STENNI, B. ; DEL GOBBO, C. ; FILIPAZZI, M. ; FONTANA, D.: The MONICA (Monitoring of ice with cave) project: A multidisciplinary approach for the geophysical and

- paleoclimatic Characterization of Permanent ice deposits in the southeastern Alps. In: *NCKRI Symposium*, 2014 (International Workshop on Ice Caves VI)
- [Fujita et al. 2004] FUJITA, K. ; TAKEUCHI, N. ; AIZEN, S.: Glaciological Observations on the plateau of Belukha Glacier in the Altai Mountains, Russia from 2001-2003. In: *Bulletin of Glaciological Research* 21 (2004), pp. 57–64
- [Gagliardini et al. 2013] GAGLIARDINI, O. ; ZWINGER, T. ; GILLET-CHAULET, F. ; DURAND, G. ; FAVIER, L. ; FLEURIAN, B. de ; GREVE, R. ; MALINEN, M. ; MARTIN, C. ; RABACK, P. ; RUOKOLAINEN, J. ; SACCHETTINI, M. ; SCHÄFER, M. ; SEDDIK, H. ; THIES, J.: Capabilities and performance of Elmer/Ice, a new-generation ice sheet model. In: *Geoscientific Model Development* 6 (2013), pp. 1299–1318
- [Gelencsér et al. 2007] GELENCSEÉR, A. ; MAY, B. ; SIMPSON, S.-O. ; KASPER-GIEBL, A. ; PUXBAUM, H. ; CASEIRO, A. ; PIO, C. ; LEGRAND, M.: Source apportionment of PM<sub>2.5</sub> organic aerosol over Europe: Primary/secondary, natural/anthropogenic and fossil/biogenic origin. In: *Journal of Geophysical Research* 112, D23S04 (2007)
- [Gäggeler et al. 1983] GÄGgeler, H. W. ; GUNTEN, H. R. ; RÖSSLER, E. ; OESCHGER, H. ; SCHOTTERER, U.: <sup>210</sup>Pb-Dating of Cold Alpine Firn/Ice Cores From Colle Gnifetti, Switzerland. In: *Journal of Glaciology* 29 (1983), pp. 165–177
- [Gilbert et al. 2014] GILBERT, A. ; GAGLIARDINI, O. ; VINCENT, C. ; WAGNON, P.: A 3-D thermal regime model suitable for cold accumulation zones of polythermal mountain glaciers. In: *Journal of Geophysical Research: Earth Surface* 119 (2014), pp. 1876–1893
- [Gómez-Gutiérrez et al. 2007] GÓMEZ-GUTIÉRREZ, A. ; JOVER, E. ; BAYONA, J. M. ; ALBAIGÉS, J.: Influence of water filtration on the determination of a wide range of dissolved contaminants at parts-per-trillion levels. In: *Analytica Chimica Acta* 583 (2007), pp. 202–209
- [Gordon et al. 2004] GORDON, M. S. ; GOLDHAGEN, P. ; ROdBELL, K. P. ; ZABEL, T. H. ; TANG, H. H. K. ; CLEM, J. M. ; BAILEY, P.: Measurement of the Flux and Energy Spectrum of Cosmic-Ray Induced Neutrons on the Ground. In: *IEEE Transactions on Nuclear Science* 51 (2004), Nr. 6
- [Griffin 2007] GRIFFIN, D. W.: Atmospheric Movement of Microorganisms in Clouds of Desert Dust and Implications for Human Health. In: *Clinical Microbiology Reviews* 20 (2007), Nr. 3, pp. 459–477
- [Guilhermet et al. 2013] GUILHERMET, J. ; PREUNKERT, S. ; VOISIN, D. ; BADUEL, C. ; LEGRAND, M.: Major 20th century changes of water-soluble humic-like substances (HULISWS) aerosol over Europe inferred from Alpine ice cores. In: *Journal of Geophysical Research: Atmospheres* 118 (2013), pp. 3869–3878
- [Haerberli 1975] HAEBERLI, W.: Eistemperaturen in den Alpen. In: *Zeitschrift für Gletscherkunde und Glazialgeologie* 11 (1975), Nr. 2, pp. 203–220
- [Haerberli 2005] HAEBERLI, W.: Investigating glacier-permafrost relationships in high-mountain areas: historical background, selected examples and research needs. In: *The Geological Society - Special Publications* (2005)

## Bibliography

---

- [Haerberli and Alean 1985] HAEBERLI, W. ; ALEAN, J.: Temperature and Accumulation of High Altitude Firn in the Alps. In: *Annals of Glaciology* 6 (1985), pp. 161–163
- [Haerberli et al. 2004] HAEBERLI, W. ; FRAUENFELDER, R. ; KÄÄB, A. ; WAGNER, S.: Characteristics and potential climatic significance of "miniature ice caps" (crest- and cornice-type low-altitude ice archives). In: *Journal of Glaciology* 50 (2004), Nr. 168
- [Haerberli and Funk 1991] HAEBERLI, W. ; FUNK, M.: Borehole temperatures at the Colle Gnifetti core-drilling site (Monte Rosa, Swiss Alps). In: *Journal of Glaciology* 37 (1991), Nr. 125
- [Haerberli et al. 1983] HAEBERLI, W. ; SCHOTTERER, U. ; WAGENBACH, D. ; BORTENSCHLAGER, S.: Accumulation Characteristics on a Cold, High-Alpine Firn Saddle from a Snow Pit Study on Colle Gnifetti, Monte Rosa, Swiss Alps. In: *Journal of Glaciology* 29 (1983), pp. 260–271
- [Hager 2002] HAGER, P.: *Glaziologische Untersuchungen am Gipfelgrat des Vadret dal Corvatsch: Thermik und Oberflächenprozesse*, Geographisches Institut der Universität Zürich, Diplomarbeit, 2002
- [Hagler et al. 2007] HAGLER, G. S. W. ; BERGIN, M. H. ; SMITH, E. A. ; DIBB, J. E. ; ANDERSON, C. ; STEIG, E. J.: Particulate and water-soluble carbon measured in recent snow at Summit, Greenland. In: *Geophysical Research Letters* 34 (2007), Nr. 16
- [Halde 1980] HALDE, R.: Concentration of impurities by progressive freezing. In: *Water research* 14 (1980), pp. 575–580
- [Hammer 2003] HAMMER, S.: *Einsatz von Radioisotopen zur Interpretation der raum-zeitlichen Variabilität von organischem Aerosol*, Heidelberg University, Diplomarbeit, 2003
- [Heald and Spracklen 2009] HEALD, C. L. ; SPRACKLEN, D. V.: Atmospheric budget of primary biological aerosol particles from fungal spores. In: *Geophysical Research Letters* 36, L09806 (2009)
- [Herren et al. 2013] HERREN, P.-A. ; EICHLER, A. ; MACHGUTH, H. ; PAPINA, T. ; TOBLER, L. ; ZAPF, A. ; SCHWIKOWSKI, M.: The onset of Neoglaciation 6000 years ago in western Mongolia revealed by an ice core from the Tsambagarav mountain range. In: *Quaternary Science Reviews* 69 (2013), pp. 59–68
- [Higashi 1974] HIGASHI, A.: Growth and perfection of ice crystals. In: *Journal of Crystal Growth* 24 (1974), Nr. 25, pp. 102–107
- [Hoelzle et al. 2011] HOELZLE, M. ; DARMS, G. ; LÜTHI, M. P. ; SUTER, S.: Evidence of accelerated englacial warming in the Monte Rosa area, Switzerland/Italy. In: *The Cryosphere* 5 (2011), pp. 231–243
- [Hoffmann 2010] HOFFMANN, Helene: *Mikro-<sup>14</sup>C-Datierung an partikulärem organischem Kohlenstoff aus Geltschereis: Potential und Grenzen der Methode*, Institut für Umweltphysik, Heidelberg University, Diplomarbeit, 2010
- [Hoover and Pikuta 2012] HOOVER, R. B. ; PIKUTA, E. V. ; NASA MARSHALL SPACE FLIGHT CENTER; HUNTSVILLE, United S. (Ed.): *Psychrophilic and Psychrotolerant Microbial Extremophiles in Polar Environments*. CRS Press, 2012

- [Hou et al. 1980] HOU, K. ; GERBA, C. P. ; GOYAL, S. M. ; ZERDA, K. S.: Capture of Latex beads, bacteria, Endotoxin and Viruses by Charge-Modified Filters. In: *Applied and Environmental Microbiology* 40 (1980), pp. 892–896
- [Hughen et al. 2004] HUGHEN, K. ; LEHMAN, S. ; SOUTHON, J. ; OVERPECK, J. ; MARCHAL, O. ; HERRING, C. ; TURNBULL, J.:  $^{14}\text{C}$  Activity and Global Carbon Cycle Changes over the Past 50,000 Years. In: *Science* 303 (2004), pp. 202–207
- [Hughen et al. 2006] HUGHEN, K. ; SOUTHON, J. ; LEHMAN, S. ; BERTRAND, C. ; TURNBULL, J.: Marine-derived  $^{14}\text{C}$  calibration and activity record for the past 50,000 years updated from the Cariaco Basin. In: *Quaternary Science Reviews* 25 (2006), pp. 3216–3227
- [Huntzicker et al. 1982] HUNTZICKER, J. J. ; JOHNSON, R. L. ; SHAH, J. J. ; CARY, R. A.: *Particulate Carbon Atmospheric Life Cycle*. Chap. Analysis of Organic and Elemental Carbon in Ambient Aerosols by a Thermal-Optical Method, pp. 79–88, Springer US, 1982
- [IPCC 2014] IPCC ; PACHAURI, R. K. (Edt.) ; MEYER, L. A. (Edt.): *IPCC, 2014: Climate Change 2014: Synthesis Report. Contribution of Working Groups I, II and III to the Fifth Assessment Report of the Intergovernmental Panel on Climate Change*. IPCC, 2014. – IPCC, Geneva, Switzerland
- [Jaenicke 1987] JAENICKE, R. (Edt.): *Atmosphärische Spurenstoffe*. VCH Verlagsgesellschaft, 1987
- [Jaenicke and Matthias 1988] JAENICKE, R. ; MATTHIAS, S.: The primary biogenic fraction of the atmospheric aerosol. In: HOBBS, P. V. (Edt.) ; MCCORMICK, M. P. (Edt.): *Aerosols and Climate*. Deepak Publishing, Hampton, 1988, pp. 31–38
- [Jenk et al. 2009] JENK, T. M. ; SZIDAT, S. ; BOLIUS, D. ; SIGL, M. ; GÄGGELER, H. W. ; WACKER, L. ; RUFF, M. ; BRABANTE, C. ; BOUTRON, C. F. ; SCHWIKOWSKI, M.: A novel radiocarbon dating technique applied to an ice core from the Alps indicating late pleistocene ages. In: *Journal of Geophysical Research* 114, D14305 (2009)
- [Jenk et al. 2006] JENK, T. M. ; SZIDAT, S. ; GÄGGELER, H. W. ; BRÜTSCH, S. ; WACKER, L. ; SYNAL, H.-A. ; SAURER, M.: Radiocarbon analysis in an Alpine ice core: record of anthropogenic and biogenic contributions to carbonaceous aerosols in the past (1650–1940). In: *Atmospheric Chemistry and Physics* 6 (2006), pp. 5381–5390
- [Jenk et al. 2007] JENK, T. M. ; SZIDAT, S. ; SCHWIKOWSKI, M. ; GÄGGELER, H. W. ; WACKER, L. ; SYNAL, H.-A. ; SAURER, M.: Microgram level radiocarbon ( $^{14}\text{C}$ ) determination on carbonaceous particles in ice. In: *Nuclear Instruments and Methods in Physics Research B* 259 (2007), pp. 518–525
- [Joerin et al. 2006] JOERIN, U. E. ; STOCKER, T. F. ; SCHLÜCHTER, C.: Multicentury glacier fluctuations in the Swiss Alps during the Holocene. In: *The Holocene* 16 (2006), Nr. 5, pp. 697–704
- [Johnsen et al. 2001] JOHNSEN, S. J. ; DAHL-JEHNSEN, D. ; GUNDESTRUP, N. ; STEFFENSEN, J. P. ; CLAUSEN, H. B. ; MILLER, H. ; MASSON-DELMOTTE, V. ; SVEINBJÖRNSDÓTTIR, A. E. ; WHITE, J.: Oxygen isotope and paleotemperature records from six Greenland ice-core stations: Camp Century, Dye-3, GRIP, GISP2, Renland and NorthGRIP. In: *Journal of Quaternary Science* 16 (2001), pp. 299–307

## Bibliography

---

- [Johnson and Wangersky 1985] JOHNSON, B. D. ; WANGERSKY, P. J.: Seawater filtration: Particle flow and impaction considerations. In: *Limnology and Oceanography* 30 (1985), Nr. 5, pp. 966–971
- [Jouzel et al. 2007] JOUZEL, J. ; MASSON-DELMOTTE, V. ; CATTANI, O. ; DREYFUS, G. ; FALOURD, S. ; HOFFMANN, G. ; MINSTER, B. ; NOUET, J. ; BARNOLA, J.-M. ; CHAPPELLAZ, J. ; FISCHER, H. ; GALLET, J. C. ; JOHNSEN, S. J. ; LEUENBERGER, A. ; LOULERGUE, L. ; LUETHI, D. ; OERTER, H. ; PARRENIN, F. ; RAISBECK, G. ; RAYNAUD, D. ; SCHILT, A. ; SCHWANDER, J. ; SELMO, E. ; SOUCHEZ, R. ; SPAHNI, R. ; STAUFFER, B. ; STEFFENSEN, J. P. ; STENNI, B. ; STOCKER, T. F. ; TISON, J. L. ; WERNER, M. ; WOLFF, E. W.: Orbital and Millennial Antarctic Climate Variability over the Past 800,000 Years. In: *Science* 317 (2007), pp. 793–796
- [Junge 1963] JUNGE, C. E.: *Air Chemistry and Radioactivity*. Academic Press, 1963
- [Karanfil et al. 2003] KARANFIL, T. ; ERDOGAN, I. ; SCHLAUTMAN, M A.: Selecting filter membranes for measuring DOC and UV<sub>254</sub>. In: *Journal - American Water Works Association* 95 (2003), Nr. 3, pp. 86–100
- [Kaufmann et al. 2008] KAUFMANN, P. R. ; FEDERER, U. ; HUTTERLI, M. A. ; BIGLER, M. ; SCHÜPBACH, S. ; RUTH, U. ; SCHMITT, J. ; STOCKER, T. F.: An Improved Continuous Flow Analysis System for High-Resolution Field Measurements on Ice Cores. In: *Environmental Science and Technology* 42 (2008), pp. 8044–8050
- [Kawamura et al. 1996] KAWAMURA, K. ; YANASE, A. ; EGUCHI, T. ; MIKAMI, T. ; BARRIE, A.: Enhanced atmospheric transport of soil derived organic matter in spring over the high Arctic. In: *Geophysical Research Letters* 23 (1996), Nr. 25, pp. 3735–3738
- [Keck 2001] KECK, L.: *Climate significance of stable isotope records from Alpine ice cores*, Institut für Umweltphysik, Heidelberg University, Dissertation, 2001
- [Konrad 2011] KONRAD, H.: *Characterization of the age distribution and the flow field of an Alpine glacier by a combination of simple flow modeling and ground-penetrating radar*, Institut für Umweltphysik, Heidelberg University, Diplomarbeit, 2011
- [Konrad et al. 2013] KONRAD, H. ; BOHLEBER, P. ; WAGENBACH, D. ; VINCENT, C. ; EISEN, O.: Determining the age distribution of Colle Gnifetti, Monte Rosa, Swiss Alps, by combining ice cores, ground-penetrating radar and a simple flow model. In: *Journal of Glaciology* 59 (2013), Nr. 213
- [Kromer et al. 2013] KROMER, B. ; LINDAUER, S. ; SYNAL, H.-A. ; WACKER, L.: MAMS - A new AMS facility at the Curt Engelhorn Centre for Archaeometry, Mannheim, Germany. In: *Nuclear Instruments and Methods in Physics Research, Section B: Beam Interactions with Materials and Atoms* 294 (2013), pp. 11–13
- [Kuchiki et al. 2015] KUCHIKI, K. ; AOLI, T. ; NIWANO, M. ; MATOBA, S. ; KODAMA, Y. ; ADACHI, K.: Elemental carbon, organic carbon, and dust concentrations in snow measured with thermal optical and gravimetric methods: Variations during the 2007-2013 winters at Sapporo, Japan. In: *Journal of Geophysical Research: Atmospheres* 120 (2015), Nr. 2, pp. 868–882

- [Lal and Jull 1990] LAL, D. ; JULL, A.: On determining ice accumulation rates in the past 40 000 years using in situ cosmogenic  $^{14}\text{C}$ . In: *Geophysical Research Letters* 17 (1990), Nr. 9, pp. 1303–1306
- [Lal et al. 1987] LAL, D. ; JULL, A.J.T ; DONAHUE, D. J. ; BURTNER, D. ; NISHIZUMI, K.: In situ cosmogenic  $^3\text{H}$ ,  $^{14}\text{C}$  and  $^{10}\text{Be}$  for determining the net accumulation and ablation rates of ice sheets. In: *Journal of Geophysical Research, Solid earth* 92 (1987), Nr. B6, pp. 4947–4952
- [Lambert et al. 2008] LAMBERT, F. ; DELMONTE, B. ; PETIT, J. R. ; BIGLER, M. ; KAUFMANN, P. R. ; HUTTERLI, M. A. ; STOCKER, T. F. ; RUTH, U. ; STEFFENSEN, J. P. ; MAGGI, V.: Dust-climate couplings over the past 800,000 years from the EPICA Dome C ice core. In: *Nature* 452 (2008), pp. 610–619
- [Langford et al. 2010] LANGFORD, H. ; HODSON, A. ; BANWART, S. ; BOGGILD, C.: The microstructure and biogeochemistry of Arctic cryoconite granules. In: *Journal of Glaciology* 51 (2010), Nr. 56, pp. 87–94
- [Legrand and Mayewski 1997] LEGRAND, M. ; MAYEWSKI, P. A.: Glaciogeochemistry of polar ice cores: A review. In: *Reviews of Geophysics* 35 (1997), Nr. 3, pp. 219–243
- [Legrand et al. 2013a] LEGRAND, M. ; PREUNKERT, S. ; JOURDAIN, B. ; GUILHERMET, J. ; FAIN, X. ; ALEKHINA, I. A. ; PETIT, J. R.: Water-soluble organic carbon in snow and ice deposited at Alpine, Greenland, and Antarctic sites: a critical review of available data and their atmospheric relevance. In: *Climate of the Past* 9 (2013), pp. 2195–2211
- [Legrand et al. 2013b] LEGRAND, M. ; PREUNKERT, S. ; MAY, B. ; GUILHERMET, J. ; HOFFMANN, H. ; WAGENBACH, D.: Major 20th century changes of the content and chemical speciation of organic carbon archived in Alpine ice cores: Implications for the long-term change of organic aerosol over Europe. In: *Journal of Geophysical Research: Atmospheres* 118 (2013), pp. 3879–3890
- [Legrand et al. 2007] LEGRAND, M. ; PREUNKERT, S. ; SCHOCK, M. ; CERQUEIRA, M. ; KASPERGIEBL, A. ; AFONSO, J. ; PIO, C. ; GELENCSE, A. ; DOMBROWSKI-ETCHEVERS, I.: Major 20th century changes of carbonaceous aerosol components (EC, WinOC, DOC, HULIS, carboxylic acids and cellulose) derived from Alpine ice cores. In: *Journal of Geophysical Research* 112, D23S11 (2007)
- [Legrand et al. 2003] LEGRAND, M. ; PREUNKERT, S. ; WAGENBACH, D. ; CACHIER, H. ; PUXBAUM, H.: A historical record of formate and acetate from a high elevation Alpine glacier: Implications for their natural versus anthropogenic budget at the European scale. In: *Journal of Geophysical Research* 108 (2003)
- [Legrand and Puxbaum 2007] LEGRAND, M. ; PUXBAUM, H.: Summary of the CARBOSOL project: Present and retrospective state of organic versus inorganic aerosol over Europe. In: *Journal of Geophysical Research* 112 (2007)
- [Leinfelder 2012] LEINFELDER, D.: *Blankminimierung bei Radiokarbondatierung von Gletschereis anhand von partikulärem organischem Kohlenstoff*. Bachelor Thesis. 2012
- [Levin et al. 2010] LEVIN, I. ; NAEGLER, T. ; KROMER, B. ; DIEHL, M. ; FRANCEY, R. J. ; GOMEZ-PELAEZ, A. J. ; STEELE, L. P. ; WAGENBACH, D. ; WELLER, R. ; WORTHY, D. E.:

## Bibliography

---

- Observations and modelling of the global distribution and long-term trend of atmospheric  $^{14}\text{CO}_2$ . In: *Tellus B* 62 (2010), pp. 26–46
- [Libby 1946] LIBBY, W. F.: Atmospheric Helium Three and Radiocarbon from Cosmic Radiation. In: *Physical Review* 69 (1946), pp. 671–672
- [Liebl et al. 2010] LIEBL, J. ; ORTIZ, R. A. ; GOLSER, R. ; HANDLE, F. ; KUTSCHERA, W. ; STEIER, P. ; WILD, E. M.: Studies on the preparation of small  $^{14}\text{C}$  samples with an RGA and  $^{13}\text{C}$ -enriched material. In: *Radiocarbon* 52 (2010), Nr. 3, pp. 1394–1404
- [Lim et al. 2014] LIM, S. ; FAIN, X. ; ZANATTA, M. ; COZIC, J. ; JAFFREZO, J.-L. ; GINOT, P. ; LAJ, P.: Refractory black carbon mass concentrations in snow and ice: method evaluation and inter-comparison with elemental carbon measurement. In: *Atmospheric Measurement Techniques* 7 (2014), pp. 3307–3324
- [Loosli 1983] LOOSLI, H. H.: A dating method with  $^{39}\text{Ar}$ . In: *Earth and Planetary Science Letters* 63 (1983), pp. 51–62
- [Lorrain and Haerberli 1990] LORRAIN, R. ; HAEBERLI, W.: Climatic change in a high-altitude Alpine area suggested by the isotopic composition of cold basal glacier ice. In: *Annals of Glaciology* 14 (1990)
- [Lowe 1989] LOWE, D.: Problems associated with the use of coal as a source of  $^{14}\text{C}$ -free background material. In: *Radiocarbon* 31 (1989), Nr. 2, pp. 117–120
- [Lüthi 2000] LÜTHI, M. P.: Rheology of cold firn and dynamics of a polythermal ice stream. Studies on Colle Gnifetti and Jakobshavns Isbrae. In: MINOR, H.-E. (Edt.): *Mitteilungen* 165 Vol. 165. Versuchsanstalt für Wasserbau, Hydrologie und Glaziologie der Eidgenössischen Technischen Hochschule Zürich, 2000
- [Lüthi and Funk 2000] LÜTHI, M. P. ; FUNK, M.: Dating ice cores from a high Alpine glacier with a flow model for cold firn. In: *Annals of Glaciology* 31 (2000), Nr. 1, pp. 69–79
- [MacDonnel and Fitzsimons 2008] MACDONNEL, S. ; FITZSIMONS, S.: The formation and hydrological significance of cryoconite holes. In: *Progress in Physical Geography* 32 (2008), Nr. 6, pp. 595–610
- [Mann 1983] MANN, W. B.: An International reference material for radiocarbon dating. In: *Radiocarbon* 25 (1983), Nr. 2, pp. 519–527
- [Maske and Garcia-Mendoza 1994] MASKE, H. ; GARCIA-MENDOZA, E.: Adsorption of Dissolved Organic Matter to the Inorganic Filter Substrate and Its Implications for  $^{14}\text{C}$  Uptake Measurements. In: *Applied and Environmental Microbiology* 60 (1994), Nr. 10, pp. 3887–3889
- [Masson-Delmotte et al. 2013] MASSON-DELMOTTE, V. ; SCHULZ, M. ; ABE-OUCHI, A. ; BEER, J. ; GANOPOLSKI, A. ; GONZÁLEZ ROUCO, J. F. ; JANSEN, E. ; LAMBECK, K. ; LUTERBACHER, J. ; NAISH, T. ; OSBORN, T. ; OTTO-BLIESNER, B. ; QUINN, T. ; RAMESH, R. ; ROJAS, M. ; SHAO, X. ; TIMMERMANN, A.: Information from Paleoclimate Archives. In: STOCKER, T. F. (Edt.) ; QIN, D. (Edt.) ; PLATTNER, G.-K. (Edt.) ; TIGNOR, M. (Edt.) ; ALLEN, S. K. (Edt.) ; BOSCHUNG, J. (Edt.) ; NAUELS, A. (Edt.) ; XIA, Y. (Edt.) ; BEX, V. (Edt.) ; MIDGLEY, P. M. (Edt.): *Climate Change 2013: The Physical Science Basis. Contribution of Working Group I*

- to the Fifth Assessment Report of the Intergovernmental Panel on Climate Change. Cambridge University Press, Cambridge, United Kingdom and New York, NY, USA, 2013
- [Maupetit and Delmas 1994] MAUPETIT, F. ; DELMAS, R. J.: Snow chemistry of high altitude glaciers in the French Alps. In: *Tellus* 46B (1994), pp. 304–324
- [May 2005] MAY, B.: *Quantification of the fossil fraction in carbonaceous aerosol by radiocarbon analysis*, Institut für Umweltphysik, Heidelberg University, Diplomarbeit, 2005
- [May 2009] MAY, B.: *Radiocarbon microanalysis on ice impurities for dating of Alpine glaciers*, Institut für Umweltphysik, Heidelberg University, Dissertation, 2009
- [May et al. 2009] MAY, B. ; WAGENBACH, D. ; HAMMER, S. ; STEIER, P. ; PUXBAUM, H. ; PIO, C.: The anthropogenic influence on carbonaceous aerosol in the European background. In: *Tellus B* 61B (2009), pp. 464–472
- [Mazarik and Reedy 1995] MAZARIK, J. ; REEDY, R. C.: Terrestrial cosmogenic-nuclide production systematics calculated from numerical simulations. In: *Earth and Planetary Science Letters* 136 (1995), pp. 381–395
- [MODIS 2003] MODIS: *Saharan Dust over the Mediterranean Sea*. 2003. – URL <http://visibleearth.nasa.gov/view.php?id=11780>. – last access: November 2010
- [Mook 2000] MOOK, W. G. (Ed.): *Environmental Isotopes in the Hydrological Cycle - Principles and Applications*. Vol. 1. IAEA, 2000
- [Muscheler et al. 2008] MUSCHELER, R. ; KROMER, B. ; BJÖRCK, S. ; SVENSSON, A. ; FRIEDRICH, M. ; KAISER, K. F. ; SOUTHON, J.: Tree rings and ice cores reveal  $^{14}\text{C}$  calibration uncertainties during the Younger Dryas. In: *Nature Geoscience* 1 (2008), pp. 263–267
- [Narcisi et al. 2005] NARCISI, B. ; PETIT, J. R. ; DELMONTE, B. ; BASILE-DOELSCH, I. ; MAGGI, V.: Characteristics and sources of tephra layers in the EPICA-Dome C ice record (East Antarctica): Implications for past atmospheric circulation and ice core stratigraphic correlations. In: *Earth and Planetary Science Letters* 239 (2005), pp. 253–265
- [NOAA 2015] NOAA: *Warmer air and sea, declining ice continue to trigger Arctic change*. December 2015. – URL <http://www.noaanews.noaa.gov/stories2015/121515-arctic-report-card-warmer-air-and-sea-declining-ice-continue-to-trigger-arctic-change.html>
- [Nydal 1968] NYDAL, R.: Further investigation on the transfer of radiocarbon in nature. In: *Journal of Geophysical Research* 73 (1968), Nr. 12, pp. 3617–3635
- [Park et al. 2005] PARK, J. H. ; LEE, C. S. ; KWON, Y. K. ; LEE, J. H. ; KIM, J. Y. ; LEE, K. B. ; PARK, H.: Activation Cross Section Measurements of  $^{16}\text{O}(n,^3\text{He})^{14}\text{C}$  and  $^{16}\text{O}(n,t)^{14}\text{N}$  above Neutron Thresholds up to 18.1 MeV. In: *Journal of the Korean Physical Society* 47 (2005), Nr. 1, pp. 23–27
- [Parrenin et al. 2007] PARRENIN, F. ; BARNOLA, J.-M. ; BEER, J. ; BLUNIER, T. ; CASTELLANO, E. ; CHAPPELLAZ, J. ; DREYFUS, G. ; FISCHER, H. ; FUJITA, S. ; JOUZEL, J. ; KAWAMURA, K. ; LEMIEUX-DUDON, B. ; LOULERGUE, L. ; VASSON-DELMOTTE, V. ; NARCISI, B. ; PETIT, J. R. ; RAISBECK, G. ; RAYNAUD, D. ; RUTH, U. ; SCHWANDER, J. ; SEVERI, M. ; SPAHNI,

## Bibliography

---

- R. ; STEFFENSEN, J. P. ; SVENSSON, A. R. ; WAELBROECK, C. ; WOLFF, E. W.: The EDC3 chronology for the EPICA Dome C ice core. In: *Climate of the Past* 3 (2007), pp. 485–497
- [Pautler et al. 2012] PAUTLER, B. G. ; WOODS, G. C. ; DUBNICK, A. ; SIMPSON, A. J. ; SHARP, M. ; FITZSIMONS, S. J. ; SIMPSON, M. J.: Molecular Characterization of Dissolved Organic Matter in Glacial Ice: Coupling Natural Abundance  $^1\text{H}$  NMR and Fluorescence Spectroscopy. In: *Environmental Science and Technology* 46 (2012), pp. 3753–3761
- [Petit et al. 1999] PETIT, J. R. ; JOUZEL, J. ; RAYNAUD, D. ; BARKOV, N. I. ; BARNOLA, J.-M. ; BASILE, I. ; BENDER, M. ; CHAPPELLAZ, J. ; DAVIS, M. ; DELAYGUE, G. ; DELMOTTE, M. ; KOTLYAKOV, V. M. ; LEGRAND, M. ; LIPENKOV, V. Y. ; LORIUS, C. ; PÉPIN, L. ; RITZ, C. ; SALTZMAN, E. ; STIEVENARD, M.: Climate and atmospheric history of the past 420,000 years from the Vostok ice core, Antarctica. In: *Nature* 399 (1999), pp. 429–436
- [Petrenko et al. 2013] PETRENKO, V. V. ; SEVERINGHAUS, J. P. ; SMITH, A. M. ; RIEDEL, K. ; BAGGENSTOS, D. ; HARTH, C. ; ORSI, A. ; HUA, Q. ; FRANZ, P. ; TAKESHITA, Y. ; BRAILSFORD, G. ; WEISS, R. F. ; BUIZER, C. ; DICKSON, A. ; SCHAEFER, H.: High-precision  $^{14}\text{C}$  measurements demonstrate production of insitu cosmogenic  $^{14}\text{CH}_4$  and rapid loss of insitu cosmogenic  $^{14}\text{CO}$  in shallow Greenland firn. In: *Earth and Planetary Science Letters* 365 (2013), pp. 190–197
- [Petrenko et al. 2009] PETRENKO, V. V. ; SMITH, A. M. ; BROOK, E. J. ; LOWE, D. ; RIEDEL, K. ; BRAILSFORD, G. ; HUA, Q. ; SCHAEFER, H. ; REEH, N. ; WEISS, R. F. ; ETHERIDGE, D. ; SEVERINGHAUS, J. P.:  $^{14}\text{CH}_4$  Measurements in Greenland Ice: Investigating Last Glacial Termination  $\text{CH}_4$  Sources. In: *Science* 324 (2009)
- [Picciotto et al. 1967] PICCIOTTO, E. ; CROZAZ, G. ; AMBACH, W. ; EISNER, H.: Lead-210 and Strontium-90 in an Alpine Glacier. In: *Earth and Planetary Science Letters* 3 (1967), pp. 237–242
- [Pio et al. 1994] PIO, C. ; CASTRO, L. ; RAMOS, M.: Differentiated determination of organic and elemental carbon in atmospheric aerosol particles by a thermal-optical method. In: ANGELETTI, G. (Edt.) ; RESTELLI, G. (Edt.): *Proceedings of the 6th European Symposium on Physico-Chemical Behaviour of Atmospheric Pollutants, Rep. EUR 15609/2 EN*, Eur. Comm. Brussels, 1994, pp. 706–711
- [Pio et al. 2007] PIO, C. ; LEGRAND, M. ; AFONSO, J. ; SANTOS, C. ; CASEIRO, A. ; FIALHO, P. ; BARATA, F. ; PUXBAUM, H. ; SANCHEZ-OCHOA, A. ; KASPER-GIEBL, A. ; GELENCSEÉR, A. ; PREUNKERT, S. ; SCHOCK, M.: Climatology of aerosol composition (organic versus inorganic) at nonurban sites on a west-east transect across Europe. In: *Journal of Geophysical Research* 112 (2007)
- [Poeschl 2005] POESCHL, U.: Atmospheric Aerosols: Composition, Transformation, Climate and Health effects. In: *Angewandte Chemie, International Edition* 44 (2005), pp. 7520–7540
- [Preunkert and Legrand 2001] PREUNKERT, S. ; LEGRAND, M.: Sulfate trends in a Col du Dome (French Alps) ice core: A record of anthropogenic sulfate level in the European midtroposphere over the twentieth century. In: *Journal of Geophysical Research* 106 (2001), Nr. D23, pp. 31991–32004

- [Preunkert and Legrand 2013] PREUNKERT, S. ; LEGRAND, M.: Towards a quasi-complete reconstruction of past atmospheric aerosol load and composition (organic and inorganic) over Europe since 1920 inferred from Alpine ice cores. In: *Climate of the Past* 9 (2013), pp. 1403–1416
- [Preunkert et al. 2011] PREUNKERT, S. ; LEGRAND, M. ; STRICKER, P. ; BULAT, S. A. ; ALEKHINA, I. A. ; PETIT, J. R. ; HOFFMANN, H. ; MAY, B. ; JOURDAIN, B.: Quantification of Dissolved Organic Carbon at Very Low Levels in Natural Ice Samples by a UV-Induced Oxidation Method. In: *Environmental Science and Technology* 45 (2011), pp. 673–678
- [Preunkert et al. 2000] PREUNKERT, S. ; WAGENBACH, D. ; LEGRAND, M. ; VINCENT, C.: Col du Dome (Mt Blanc Massif, French Alps) suitability for ice-core studies in relation with past atmospheric chemistry over Europe. In: *Tellus* 52B (2000), pp. 993–1012
- [Pósfai et al. 2004] PÓSFAI, M. ; GELENCSEÉR, A. ; SIMONICS, R. ; ARATO, K. ; LI, J. ; HOBBS, V. ; BUSECK, P. R.: Atmospheric tar balls: Particles from biomass and biofuel burning. In: *Journal of Geophysical Research* 109, D06213 (2004)
- [Rasmussen et al. 2013] RASMUSSEN, S. O. ; ABBOTT, P. M. ; BLUNIER, T. ; BOURNE, A. J. ; BROOK, E. ; BUCHARDT, S. L. ; BUZERT, C. ; CHAPPELLAZ, J. ; CLAUSEN, H. B. ; COOK, E. ; DAHL-JEHNSEN, D. ; DAVIES, S. M. ; GUILLEVIC, M. ; KIPFSTUHL, S. ; LAEPPELE, T. ; SEIERSTAD, I. K. ; SEVERINGHAUS, J. P. ; STEFFENSEN, J. P. ; STOWASSER, C. ; SVENSSON, A. ; VALLELONGA, P. ; VINTHER, B. M. ; WILHELMS, F. ; WINSTRUP, M.: A first chronology for the North Greenland Eemian Ice Drilling (NEEM) ice core. In: *Climate of the Past* 9 (2013), pp. 2713–2730
- [Rau 2008] RAU, S.: *Stratigraphische Untersuchungen an einem tiefen Eisbohrkern der alpinen Miniatureiskappe Vadret dal Corvatsch*, Insitut für Umweltphysik, Heidelberg University, Diplomarbeit, 2008
- [Reimer et al. 2013] REIMER, P. J. ; BARD, E. ; BAYLISS, A. ; BECK, J. W. ; BLACKWELL, P. G. ; BRONK RAMSEY, C. ; BUCK, C. E. ; CHENG, H. ; EDWARDS, R. L. ; FRIEDRICH, M. ; GROOTES, P. M. ; GUILDERTSON, T. P. ; HAFLIDASON, H. ; HAJDAS, I. ; HATTE, C. ; HEATON, T. J. ; HOFFMANN, D. L. ; HOGG, A. G. ; HUGHEN, K. ; KAISER, K. F. ; KROMER, B. ; MANNING, S. W. ; NIU, M. ; REIMER, R. W. ; RICHARDS, D. A. ; SCOTT, E. M. ; SOUTHON, J. ; STAFF, R. A. ; TURNEY, C. S. M. ; VAN DER PLICHT, J.: IntCal13 and Marine13 radiocarbon age calibration curves 0-50,000 years cal BP. In: *Radiocarbon* 55 (2013), Nr. 4, pp. 1869–1887
- [Ritterbusch et al. 2014] RITTERBUSCH, S. ; WELTE, J. ; REICHEL, T. ; KERSTING, A. ; PURTSCHERT, R. ; AESCHBACH-HERTIG, W. ; OBERTHALER, M. K.: Groundwater dating with Atom Trap Trace Analysis of  $^{39}\text{Ar}$ . In: *Geophysical Research Letters* 41 (2014), pp. 6758–6764
- [Roberts and Southon 2007] ROBERTS, M. L. ; SOUTHON, J. R.: A preliminary determination of the absolute  $^{14}\text{C}/^{12}\text{C}$  ratio of Ox-I. In: *Radiocarbon* 49 (2007), Nr. 2, pp. 441–445
- [Rozanski et al. 1992] ROZANSKI, K. ; STICHLER, W. ; GONFIANTINI, R. ; SCOTT, E. M. ; BEUKENS, R. P. ; KROMER, B. ; VAN DER PLICHT, J.: The IAEA  $^{14}\text{C}$  intercomparison exercise 1990. In: *Radiocarbon* 34 (1992), Nr. 3, pp. 506–519

## Bibliography

---

- [Röthlisberger et al. 2000] RÖTHLISBERGER, R. ; BIGLER, M. ; HUTTERLI, M. A. ; SOMMER, S. ; STAUFFER, B. ; JUNGHANS, H. G. ; WAGENBACH, D.: Technique for Continuous High-Resolution Analysis of Trace Substances in Firn and Ice Cores. In: *Environmental Science and Technology* 34 (2000), pp. 338–342
- [Ruff et al. 2007] RUFF, M. ; WACKER, L. ; GÄGGELER, H. W. ; SUTER, M. ; SYNAL, H.-A. ; SZIDAT, S.: A Gas Ion Source for Radiocarbon Measurements at 200 kV. In: *Radiocarbon* 49 (2007), pp. 307–314
- [Sattler et al. 2001] SATTLER, B. ; PUXBAUM, H. ; PSENNER, R.: Bacterial growth in super-cooled cloud droplets. In: *Geophysical Research Letters* 28 (2001), Nr. 2, pp. 239–242
- [Scheffer and Schachtschabel 2010] SCHEFFER, F. ; SCHACHTSCHABEL, P. ; BLUME, H.-P. (Edt.) ; BRÜMMER, G. W. (Edt.) ; HORN, R. (Edt.) ; KANDELER, E. (Edt.) ; KÖGEL-KNABNER, I. (Edt.) ; KRETZSCHMAR, R. (Edt.) ; STAHR, K. (Edt.) ; WILKE, B.-M. (Edt.): *Lehrbuch der Bodenkunde*. Spektrum Akademischer Verlag, 2010
- [Schäfer 1995] SCHÄFER, J.: *Rekonstruktion bio-geochemischer Spurenstoffkreisläufe anhand eines alpinen Eisbohrkerns*, Institut für Umweltphysik, Heidelberg University, Diplomarbeit, 1995
- [Schotterer et al. 1998] SCHOTTERER, U. ; SCHWARZ, P. ; RAJNER, V.: From pre-bomb levels to industrial times: A complete tritium record from an alpine ice core and its relevance for environmental studies. In: VIENNA, International Atomic Energy A. (Edt.): *Isotope techniques in the study of environmental change*, 1998
- [Schwander 1996] SCHWANDER, J.: *Chemical exchange between the atmosphere and polar snow*. Chap. Gas diffusion on firn, pp. 527–540, Springer Verlag, 1996
- [Schwarz et al. 2013] SCHWARZ, J. P. ; GAO, R. S. ; PERRING, A. E. ; SPACKMAN, J. R. ; FAHEY, D. W.: Black carbon aerosol size in snow. In: *Nature Scientific reports* 3 (2013), Nr. 1356
- [Schwikowski et al. 1999] SCHWIKOWSKI, M. ; DÖSCHER, A. ; GÄGGELER, H. W. ; SCHOTTERER, U.: Anthropogenic versus natural sources of atmospheric sulphate from an Alpine ice core. In: *Tellus* 51B (1999), pp. 938–951
- [Shafique et al. 2012] SHAFIQUE, U. ; ANWAR, J. ; UZ-ZAMAN, W. ; REHMAN, R. ; SALMAN, M. ; DAR, A. ; JAMIL, N.: Forced migration of soluble and suspended materials by freezing front in aqueous systems. In: *Journal of Hydro-environment Research* 6 (2012), pp. 221–226
- [Sigl et al. 2009] SIGL, M. ; JENK, T. M. ; KELLERHALS, T. ; SZIDAT, S. ; GÄGGELER, H. W. ; WACKER, L. ; SYNAL, H.-A. ; BOUTRON, C. F. ; BARBANTE, C. ; GABRIELI, J. ; SCHWIKOWSKI, M.: Towards radiocarbon dating of ice cores. In: *Journal of Glaciology* 55 (2009), Nr. 194, pp. 985–996
- [Sigl et al. 2015] SIGL, M. ; WINSTRUP, M. ; MCCONNELL, J. R. ; WELTEN, K. C. ; PLUNKETT, G. ; LUDLOW, F. ; BÜNTGEN, U. ; CAFFEE, M. ; CHELLMAN, N. ; DAHL-JEHNSEN, D. ; FISCHER, H. ; KIPFSTUHL, S. ; KOSTICK, C. ; MASELLI, O. J. ; MEKHALDI, F. ; MULVANEY, R. ; MUSCHELER, R. ; PASTERIS, D. R. ; PILCHNER, J. R. ; SALZER, M. ; SCHÜPBACH, S. ; STEFFENSEN, J. P. ; VINTHER, B. M. ; WOODRUFF, T. E.: Timing and climate forcing of volcanic eruptions for the past 2,500 years. In: *Nature* 523 (2015), pp. 543–549

- [Singer et al. 2012] SINGER, G. A. ; FASCHING, C. ; WILHELM, L. ; NIGGEMANN, J. ; STEIER, P. ; BATTIN, T. J.: Biogeochemically diverse organic matter in Alpine glaciers and its downstream fate. In: *Nature geoscience* 5 (2012), pp. 710–714
- [Sánchez-Ochoa et al. 2007] SÁNCHEZ-OCHOA, A. ; KASPER-GIEBL, A. ; PUXBAUM, H. ; GELENCSE, A. ; LEGRAND, M. ; PIO, C.: Concentration of atmospheric cellulose: A proxy for plant debris across a west-east transect over Europe. In: *Journal of Geophysical Research* 112, D23S08 (2007)
- [Sneed et al. 2015] SNEED, S. B. ; MAYEWSKI, P. A. ; SAYRE, W. G. ; HANDLEY, M. J. ; KURBATOV, A. V. ; TAYLOR, K. C. ; BOHLEBER, P. ; WAGENBACH, D. ; ERHARDT, T. ; SPAULDING, N. E.: New LA-ICP-MS cryocell and calibration technique for sub-millimeter analysis of ice cores. In: *Journal of Glaciology* 61 (2015), Nr. 226
- [Sodemann et al. 2006] SODEMANN, H. ; PALMER, A. S. ; SCHWIERZ, C. ; SCHWIKOWSKI, M. ; WERNLI, H.: The transport history of two Saharan dust events archived in an Alpine ice core. In: *Atmospheric Chemistry and Physics* 6 (2006), pp. 667–688
- [Steier et al. 2006] STEIER, P. ; DROSG, R. ; FEDI, M. ; KUTSCHERA, W. ; SCHOCK, M. ; WAGENBACH, D.: Radiocarbon determination of particulate organic carbon in non-temperated, Alpine glacier ice. In: *Radiocarbon* 48 (2006), pp. 69–82
- [Stenström et al. 2011] STENSTRÖM, K. E. ; SKOG, G. ; GEORGIADOU, E. ; GENBERG, J. ; JOHANSSON, A.: *A guide to radiocarbon units and calculations*. Lund University, Department of Physics, Division of Nuclear Physics, Internal Report. 2011
- [Stricker 2008] STRICKER, P.: *Umbau und Charakterisierung einer Apparatur zur DOC-Analyse des organischen Kohlenstoffgehalts von Gletschereis*, Heidelberg University, Diplomarbeit, 2008
- [Stubbins et al. 2012] STUBBINS, A. ; HOOD, E. ; RAYMOND, P. A. ; AIKEN, G. R. ; SLEIGHTER, R. L. ; HERNES, P. J. ; BUTMAN, D. ; HATCHER, P. G. ; STRIEGL, R. G. ; SCHUSTER, P. ; ABDULLA, H. A. N. ; VERMILYEA, A. W. ; SCOTT, D. T. ; SPENCER, R. G. M.: Anthropogenic aerosols as a source of ancient dissolved organic matter in glaciers. In: *Nature Geoscience Letters* 5 (2012)
- [Stuiver 1983] STUIVER, M.: International agreements and the use of a new oxalic acid standard. In: *Radiocarbon* 25 (1983), Nr. 2, pp. 793–795
- [Stuiver and Polach 1977] STUIVER, M. ; POLACH, H. A.: Reporting of  $^{14}\text{C}$  Data. In: *Radiocarbon* 19 (1977), pp. 355–363
- [Stuiver and Robinson 1974] STUIVER, M. ; ROBINSON, S. W.: University of Washington Geosecs North Atlantic Carbon-14 Results. In: *Earth and Planetary Science Letters* 23 (1974), pp. 87–90
- [Suter et al. 1984] SUTER, M. ; BALZER, R. ; BONANI, G. ; WÖFLI, W.: A fast beam pulsing system for isotope ratio measurements. In: *Nuclear Instruments & Methods in Physics Research, Section B: Beam Interactions with Materials and Atoms* 5 (1984), Nr. 2, pp. 242–246
- [Svensson et al. 2008] SVENSSON, A. ; ANDERSEN, K. K. ; BIGLER, M. ; CLAUSEN, H. B. ; DAHL-JEHNSEN, D. ; DAVIES, S. M. ; JOHNSEN, S. J. ; MUSCHELER, R. ; PARRENIN, F. ;

## Bibliography

---

- RASMUSSEN, S. O. ; RÖTHLISBERGER, R. ; SEIERSTAD, I. K. ; STEFFENSEN, J. P. ; VINTHER, B. M.: A 60 000 year Greenland stratigraphic ice core chronology. In: *Climate of the Past* 4 (2008), pp. 47–57
- [Swisseduc 2004] SWISSEDOC: *Large Saharan dust deposit on the north flank of Breithorn (Monte Rosa Massif)*. 2004. – URL <http://www.swisseduc.ch/glaciers/alps/gornergletscher/gornergletscher-generell-en.html>
- [Synal et al. 2004] SYNAL, H.-A. ; DÖBELI, M. ; JACOB, S. ; STOCKER, M. ; SUTER, M.: Radiocarbon AMS towards its low-energy limits. In: *Nuclear Instruments & Methods in Physics Research, Section B: Beam Interactions with Materials and Atoms* 223-224 (2004), pp. 339–345
- [Synal et al. 2007] SYNAL, H.-A. ; STOCKER, M. ; SUTER, M.: MICADAS: A new compact radiocarbon AMS system. In: *Nuclear Instruments & Methods in Physics Research, Section B: Beam Interactions with Materials and Atoms* 259 (2007), pp. 7–13
- [Szidat et al. 2004a] SZIDAT, S. ; JENK, T. M. ; GÄGGELER, H. W. ; SYNAL, H.-A. ; FISSEHA, R. ; BALTENSPERGER, U. ; KALBERER, M. ; SAMBUROVA, V. ; WACKER, L. ; SAURER, M. ; SCHWIKOWSKI, M. ; HAJDAS, I.: Source apportionment of aerosols by  $^{14}\text{C}$  measurements in different carbonaceous particle fractions. In: *Radiocarbon* 46 (2004), pp. 475–484
- [Szidat et al. 2004b] SZIDAT, S. ; JENK, T. M. ; GÄGGELER, H. W. ; SYNAL, H.-A. ; HAJDAS, I. ; BONANI, G. ; SAURER, M.: THEODORE, a two-step heating system for the EC/OC determination of radiocarbon ( $^{14}\text{C}$ ) in the environment. In: *Nuclear Instruments & Methods in Physics Research, Section B: Beam Interactions with Materials and Atoms* 223-224 (2004), pp. 829–836
- [Takeuchi et al. 2001] TAKEUCHI, N. ; KOHSHIMA, S. ; SEKO, K.: Structure, Formation and Darkening Process of Albedo-reducing Material (Cryoconite) on a Himalayan glacier: A Granular Algal Mat Growing on the Glacier. In: *Arctic, Antarctic and Alpine Research* 33 (2001), Nr. 2, pp. 115–122
- [Thevenon et al. 2012] THEVENON, F. ; CHIARADIA, M. ; ADATTE, T. ; HUEGLIN, C. ; POTE, J.: Characterization of Modern and Fossil Mineral Dust Transported to High Altitude in the Western Alps: Saharan Sources and Transport Patterns. In: *Advances in Meteorology* 2012 (2012)
- [Thibert and Dominé 1997] THIBERT, E. ; DOMINÉ, F.: Thermodynamics and Kinetics of the Solid Solution of HCl in Ice. In: *Journal of Physical Chemistry* 101 (1997), pp. 3554–3565
- [Thompson et al. 2000] THOMPSON, L. G. ; MOSLEY-THOMPSON, E. ; HENDERSON, K. A.: Ice-core palaeoclimate records in tropical South America since the Last Glacial Maximum. In: *Journal of Quaternary Science* 15 (2000), Nr. 4, pp. 377–394
- [Tomadin et al. 1996] TOMADIN, L. ; WAGENBACH, D. ; LANDUZZI, V.: Mineral and source of high altitude glacial deposits in the western Alps: Clay mineral as Saharan dust tracers. In: GUERZONI, S. (Edt.) ; CHESTER, R. (Edt.): *The Impact of Desert Dust Across the Mediterranean* Vol. 11. Kluwer Academic Publishers, 1996

- [Trumbore 2000] TRUMBORE, S.: Age of Soil Organic matter and Spoil Respiration: Radiocarbon Constraints on Belowground C Dynamics. In: *Ecological Applications* 10 (2000), pp. 399–411
- [Tung et al. 2005] TUNG, H. C. ; BRAMALL, N. E. ; PRICE, P. B.: Microbial origin of excess methane in glacial ice and implications for life on Mars. In: *Proceedings of the National Academy of Sciences of the United States of America* 102 (2005), Nr. 21, pp. 18292–18296
- [Uhl et al. 2007] UHL, T. ; LUPPOLD, W. ; ROTTENBACH, A. ; SCHARF, A. ; KRITZLER, K. ; KRETSCHMER, W.: Development of an automatic gas handling system for microscale AMS  $^{14}\text{C}$  measurements. In: *Nuclear Instruments & Methods in Physics Research, Section B: Beam Interactions with Materials and Atoms* 259 (2007), pp. 303–307
- [Usoskin 2008] USOSKIN, I.: A History of Solar Activity over Millennia. In: *Living. Rev. Solar Phys.* 10 (2008), Nr. 1
- [Verzilov et al. 1998] VERZILOV, Y. M. ; IKEDA, Y. ; MAEKAWA, F. ; OYAMA, Y. ; SMITH, D. L.: Measurements of Tritium and  $^{14}\text{C}$  Production Cross Sections for 14.7-MeV Neutrons on  $^{17}\text{O}$  and  $^{18}\text{O}$ . In: *Nuclear Science and Engineering* 129 (1998), Nr. 1, pp. 81–87
- [Wacker et al. 2013] WACKER, L. ; FAHRNI, S. M. ; HAJDAS, I. ; MOLNAR, M. ; SYNAL, H.-A. ; SZIDAT, S. ; ZHANG, Y. L.: A versatile gas interface for routine radiocarbon analysis with a gas ion source. In: *Nuclear Instruments & Methods in Physics Research, Section B: Beam Interactions with Materials and Atoms* 294 (2013), pp. 315–319
- [Wacker et al. 2010] WACKER, L. ; NEMEC, M. ; BOURQUIN, J.: A revolutionary graphitisation system: Fully automated, compact and simple. In: *Nuclear Instruments and Methods in Physics Research B* 268 (2010), Nr. 7-8, pp. 931–934
- [Wagenbach et al. 2012] WAGENBACH, D. ; BOHLEBER, P. ; PREUNKERT, S.: Col, Alpine ice bodies revisited: What may we learn from their impurity and isotope content? In: *Geografiska Annaler: Series A, Physical Geography* (2012), pp. 245–263
- [Wagenbach and Geis 1989] WAGENBACH, D. ; GEIS, K.: The Mineral Dust Record in a High Altitude Alpine Glacier (Colle Gnifetti, Swiss Alps). In: LEINEN, M. (Edt.) ; SARNTHEIN, M. (Edt.): *Paleoclimatology and Palaeometeorology: Modern and Past Patterns of Global Atmospheric Transport*. Kluwer Academic Publishers, 1989, pp. 543–564
- [Wagenbach et al. 1996] WAGENBACH, D. ; PREUNKERT, S. ; SCHÄFER, J. ; JUNG, W. ; TOMADIN, L.: Northward Transport of Saharan Dust recorded in a deep Alpine ice core. In: GUERZONI, S. (Edt.) ; CHESTER, R. (Edt.): *The Impact of Desert Dust Across the Mediterranean* Vol. 11. Kluwer Academic Publishers, 1996, pp. 291–300
- [van de Wal et al. 1994] WAL, R. S. W. van de ; ROIJEN, J. J. van ; RAYNAUD, D. ; BORG, K. van der ; JONG, A. F. M. de ; OERLEMANS, J. ; LIPENKOV, V. Y. ; HUYBRECHTS, P.: From  $^{14}\text{C}/^{12}\text{C}$  measurements towards radiocarbon dating of ice. In: *Tellus* 46B (1994), pp. 94–102
- [Welte et al. 2010] WELTE, J. ; RITTERBUSCH, F. ; STEINKE, I. ; HENRICH, M. ; AESCHBACH-HERTIG, W. ; OBERTHALER, M. K.: Towards the realization of Atom Trap Trace Analysis for  $^{39}\text{Ar}$ . In: *New Journal of Physics* 12 (2010)

## Bibliography

---

- [Wharton et al. 1985] WHARTON, R. A. ; MCKAY, C. P. ; SIMMONS, G. M. ; PARKER, B. C.: Cryconite holes on glaciers. In: *BioScience* 35 (1985), Nr. 8
- [Whitman et al. 1998] WHITMAN, W. B. ; COLEMAN, D. C. ; WIEBE, W. J.: Prokaryotes: The unseen majority. In: *Proceedings of the National Academy of Sciences of the United States of America* 95 (1998), pp. 6578–6583
- [Woon 2002] WOON, D. E.: Modeling gas-grain chemistry with quantum chemical cluster calculations. I. heterogeneous hydrogenation of CO and H<sub>2</sub>CO on icy grain mantles. In: *The Astrophysical Journal* 569 (2002), pp. 541–548
- [Xu et al. 2010] XU, Y. ; SIMPSON, A. J. ; EYLES, N. ; SIMPSON, M. J.: Sources and molecular composition of cryoconite organic matter from the Athabasca Glacier, Canadian Rocky Mountains. In: *Organic Chemistry* 41 (2010), pp. 177–186
- [Yankwich et al. 1946] YANKWICH, P. E. ; ROLLEFSON, G. K. ; NORRIS, T. H.: Chemical Forms Assumed by <sup>14</sup>C Produced by Neutron Irradiation of Nitrogenous Substances. In: *The Journal of Chemical Physics* 14 (1946), Nr. 3
- [Zapf et al. 2013] ZAPF, A. ; NESJE, A. ; SZIDAT, S. ; WACKER, L. ; SCHWIKOWSKI, M.: <sup>14</sup>C Measurements of ice samples from the Juvfonne ice tunnel, Jotunheimen, Southern Norway - Validation of a <sup>14</sup>C dating technique for glacier ice. In: *Radiocarbon* 55 (2013), Nr. 2-3, pp. 571–578
- [Zhang et al. 2012] ZHANG, Y. L. ; PERRON, N. ; CIOBANU, V. G. ; ZOTTER, P. ; MINGUILÓN, M. C. ; WACKER, L. ; PRÉVOT, A. S. H. ; BALTENSPERGER, U. ; SZIDAT, S.: On the isolation of OC and EC and the optimal strategy of radiocarbon-based source apportionment of carbonaceous aerosols. In: *Atmospheric Chemistry and Physics* 12 (2012), pp. 10841–10856
- [Zielinski et al. 1994] ZIELINSKI, G. A. ; MAYEWSKI, P. A. ; MEEKER, L. D. ; WHITLOW, S. ; TWICKLER, M. ; MEESE, D. A. ; GOW, A. J. ; ALLEY, R. B.: Record of Volcanism Since 7000 B.C. from the GISP2 Greenland Ice Core and Implications for the Volcano-Climate System. In: *Science* 264 (1994), pp. 948–952
- [Zsolnay 2003] ZSOLNAY, A.: Dissolved organic matter: artefacts, definitions, and functions. In: *Geoderma* 113 (2003), Nr. 3-4, pp. 187–209

# List of Figures

2.1. Overview of different dating techniques for Alpine ice cores and their applicable time ranges . . . . .	8
2.2. Schematic view of the pathways for $^{14}\text{C}$ in the carbon cycle. Adapted from (Mook, 2000) . . . . .	9
2.3. The radiocarbon calibration curve IntCal13 (Reimer et al., 2013). The left panel shows the complete record up to 50 000 yBP with increasing uncertainties to the very old ages, on the right is a zoom to the last 1000 yBP. . . . .	13
2.4. Large variations in the calibration curve makes $^{14}\text{C}$ dating of samples younger than 400 years extremely difficult. . . . .	13
2.5. Example of an uncritical age calibration. No multiple age assignments are possible. The $1\sigma$ probability of the calibrated age is given. . . . .	13
2.6. Atmospheric enrichment of $\Delta^{14}\text{C}$ during the bomb peak period. Figure taken from Levin et al. (2010). . . . .	14
2.7. Schematic view of the MICADAS main components and the proposed ion pathway (red) (picture by Ionplus AG). . . . .	15
2.8. Schematic view of the MICADAS ion source with a gas target inserted. The $\text{CO}_2$ is supplied by a capillary (60 $\mu\text{m}$ diameter), which feeds the target through a hole in the holder (Fahrni et al., 2013). . . . .	17
2.9. Cross section of a target for gas measurements. The $\text{CO}_2$ -He-mixture is directed via a small slit to the front of the titan insert, where it is sputtered (modified from Ruff et al. (2007)). . . . .	17
3.1. Schematic overview of the different aerosol particle sizes and formation pathways. Figure taken from Colbeck and Lazaridis (2014). . . . .	20
3.2. <b>Left:</b> Dust transport to high Alpine glaciers. 1: long range - Saharan dust, 2: mid and short range - local sources, 3: Eolian dust input to the Mediterranean basin. Taken from Tomadin et al. (1996). <b>Right:</b> A large deposit of Saharan dust on the north flank of Breithorn in the year 2004 (Monte Rosa Massif, Switzerland); picture taken from Swissheduc (2004). . . . .	21
3.3. Temporal changes over the 20 th century of summer mass concentration of different aerosols derived from an ice core drilled at the Col du Dome site (Mont Blanc, France) WSOM: water soluble organic matter, WinOM: Water insoluble organic matter, BC: black carbon. Figure taken from Preunkert and Legrand (2013). . . . .	21
3.4. The fractions of carbonaceous compounds in glacier ice samples. . . . .	22
3.5. <b>Left panels:</b> Chemical winter and summer composition of DOC retrieved from a Col du Dome ice core (Mont Blanc) for the first half of the 20th century (adapted from Legrand et al. (2013b)). <b>Right panel:</b> Averaged POC composition of high Alpine glacier ice based on the summarised values in Table 3.1. Note the large unknown fraction. . . . .	25
3.6. A Saharan dust storm over Italy in 2003 (MODIS, 2003). . . . .	26

## List of Figures

---

3.7.	Bedrock sediment folded into the basal ice of Tunabreen glacier, Svalbard (2013), Doug Benn for scale. Picture by Helene Hoffmann. . . . .	27
3.8.	Water-filled cryoconite holes in the ablation zone of Grenzgletscher, Switzerland (2014), Pole for scale. Picture by Johanna Kerch. . . . .	27
4.1.	DOC $^{14}\text{C}$ results of samples from an ice core from the high Alpine firn saddle Colle Gnifetti. Note the $^{14}\text{C}$ values higher than modern even in large core depths and the large discrepancy to the age expectation based on a 2D-flow model (Bohleber, 2008). Figure modified from May (2009) . . . . .	29
4.2.	Neutron fluxes and energy spectra for several North American measurement sites scaled to sea level. Note the very similar shape of the energy distributions. Figure taken from Gordon et al. (2004) . . . . .	31
4.3.	Theoretically produced number of $^{14}\text{C}$ atoms per gram ice based on Eq. 4.1 depending on ice depth $z$ , for different accumulation rates $A$ . With $P_0 \approx 396 \text{ }^{14}\text{C g}^{-1} \text{ a}^{-1}$ , $\Lambda = 150 \text{ g} \cdot \text{cm}^{-2}$ and $\rho = 0.9 \text{ g/cm}^3$ . . . . .	31
4.4.	DOC- $^{14}\text{C}$ results of ice samples from an ice core from the high Alpine firn saddle Colle Gnifetti (red) together with a hypothetical correction (green) under assumption of a 20% in situ produced $^{14}\text{C}$ -contribution to the DOC fraction (modified from May (2009)) . . . . .	32
4.5.	<b>Left:</b> Schematic view of the ice sample irradiation experiment. Samples have been kept in plastic containers sealed in PE-foil and have been equipped with flux monitors to observe the actual neutron flux. The ice samples were placed inside a polystyrene container and cooled by an atmosphere of liquid nitrogen to prevent them from melting during the irradiation. <b>Right:</b> Picture of the polystyrene container from top. The sample containers can be seen to the left. Picture by Helene Hoffmann . . . . .	34
4.6.	<b>Left:</b> $^{14}\text{C}$ results of the reference samples. All results agree with the expected ranges. <b>Right:</b> $^{14}\text{C}$ results of the irradiated samples (green) together with the reference samples (red). Note the logarithmic scale and the very enriched $^{14}\text{C}$ contents of all samples. . . . .	36
4.7.	Schematic illustration of the main processing steps for POC extraction from ice samples and radiocarbon dating used at the Paul-Scherrer-Institute (Switzerland). . . . .	38
5.1.	Picture (Ionplus) and schematic view (adapted from Ruff et al. (2007)) of the Gas Inlet System (GIS) built by the Ionplus AG. The sample ampoule is cracked, $\text{CO}_2$ is released and manometrically quantified, mixed with helium to desired pressure in the syringe and pushed into the ion source via the capillary. . . . .	41
5.2.	Variation of LE $^{12}\text{C}^-$ current dependent on different syringe pressures and $\text{CO}_2$ -He-mixing ratios. The dashed lines are linear fits to the respective datasets. Note the highest current at 4,1% and ca. $10 \mu\text{A}$ . . . . .	43
5.3.	Effect of changing gas pressure on the $^{12}\text{C}$ ion current in the AMS. Note the distinct drop in current after reducing the mass flow of $\text{CO}_2$ into the source by reducing the syringe pressure . . . . .	43
5.4.	Measurements of standard material (Oxalic acid II) as $\text{CO}_2$ over the course of two years. The dashed lines mark the expected value. All results measured to ca. 0.8% counting error agree well with the expected values, the blue area marks samples with smaller measurement times and thus larger errors . . . . .	45

5.5.	<b>Left:</b> Results of small (down to ca. 3 $\mu\text{gC}$ ) oxalic acid gas samples prepared at the IUP. The $^{14}\text{C}$ results agree reasonably well with the expected value. The depletion in $\delta^{13}\text{C}$ for the very small samples is due to a fractionation in the ion source at very low ion currents. <b>Right:</b> Zoom to the section of smallest sample sizes. . . . .	46
5.6.	Measurement of blank material (fossil $\text{CO}_2$ ) over the course of two years. Results are in the range of 35 000 - 40 000 years BP (uncalibrated), which is reasonably good for all measured samples. The dashed lines mark the average values of all measurements, no trend is visible. . . . .	46
6.1.	Schematic view of the internal structure of depth filters (e.g. quartz fibre filters, left) and membrane filters (e.g. silver membranes, right). Note the very variable interstices of the fibre filter. Figures taken from Brock (1983) . . . . .	50
6.2.	Offline POC filtration system for direct filtration of meltwater and silver membrane filters still in use at the IUP. the sketch only shows the lowest part of the melting vessel (a 2l closed PFA-bottle) and the filtration unit. . . . .	51
6.3.	<b>Left:</b> MQ-water frozen in PE-foil spiked with fluorescent powder. Most of the particles accumulate in the middle, where the water freezes last, but there is also still a fraction homogeneously distributed over the complete ice block. <b>Right:</b> MQ-water frozen in PE-foil spiked with fluorescent powder and frozen on a lab shaker. By shaking, freezing is so slow that all particles have time to accumulate in the middle of the sample and can be cut out. The rest of the ice is completely particle free (pictures taken from Leinfelder (2012)) . . . . .	53
6.4.	Schematic views of the main parts of REFILOX. <b>Left:</b> Overview of the filtration combustion unit with all major components. The oven is mobile, it can be attached and removed as required. The filtration part of the system is airtight. <b>Right:</b> Detailed view of the inner part of the filtration system. The filter is placed on top of a fixed quartz frit and pressed down by the inner glass tube, which itself is fixed by the pressure of a spiral spring. Pictures of the system are shown in Fig. A.5 in Appendix A.2. . . . .	56
6.5.	Schematic view of the sample processing steps for POC extraction . . . . .	57
6.6.	Pre-heating of the quartz filter at 900 $^{\circ}\text{C}$ to remove intrinsic and by rinsing accumulated contamination. Typically two combustion peaks arise, the first starting at ca. 350 $^{\circ}\text{C}$ and the second at ca. 600 $^{\circ}\text{C}$ . . . . .	58
6.7.	Schematic overview over the complete POC extraction and cleaning system. The process starts on the right with melting and filtration of the ice sample in the REFILOX. After filtration, the sample is acidified and combusted to $\text{CO}_2$ , which is purged out with synthetic air. The $\text{CO}_2$ is then collected in the cooling traps under liquid nitrogen temperature at ca. 20 mbar total pressure to avoid condensation of $\text{O}_2$ . After cleaning of residual gases and manometric quantification, the $\text{CO}_2$ is flame sealed in a 4 mm glass ampoule and ready for AMS-measurement. The setup of the vacuum line was not part of this work, a description and characterisation can be found in Hammer (2003) and May (2005). . . . .	59
6.8.	Artificial blank ice measurements in the offline filtration system together with one natural Antarctic sample. Note the linear correlation of the blank ice samples and the low carbon mass retrieved from the Antarctic sample . . . . .	61

## List of Figures

---

6.9.	Results of the cellulose $^{14}\text{C}$ measurements processed in the offline filtration system. The error bars denote the $2\sigma$ range. Within this range, all results except one hit the expected value (red line) and so does the weighted average (black line) within error. The outlier was not considered in the average. . . . .	65
6.10.	Results of the cellulose measurements in the REFILOX filtration system. The error bars denote the $2\sigma$ range. Within this range, all results except one hit the expected value (red line) and so does the weighted average (black line) within error. . . . .	66
6.11.	Carbon extraction efficiencies for different input sample masses in both combustion systems. Note that the efficiencies for larger samples are better than for very small samples. . . . .	67
6.12.	Relative errors of the $^{14}\text{C}$ -results depending on the measured $F_m$ . . . . .	69
6.13.	Thermogram of the method for carbon fraction separation used in the CARBOSOL project. The total organic fraction is subdivided into five subfractions OC1, OC2, OC3, PC and EC by heating in an inert atmosphere before combustion with $\text{O}_2$ (Pio et al., 2007). . . . .	72
6.14.	Comparison of the retrieved carbon concentrations for the CARBOSOL system and the REFILOX for total carbon content and the $380\text{ }^\circ\text{C} + 800\text{ }^\circ\text{C}$ fraction of REFILOX. . . . .	75
6.15.	$^{14}\text{C}$ results for the different temperature carbon fractions of sample SBO-32. . . . .	78
6.16.	$^{14}\text{C}$ results for the different temperature carbon fractions of sample SIL-3/28. . . . .	78
7.1.	Map of the sampling sites for investigations of POC $^{14}\text{C}$ age biasing effects of Saharan dust, cryoconite and sediment . . . . .	79
7.2.	Aerial view of the Jamtalferner (Austria) 2013 from the south, with the sampling sites for sediment and cryoconite. Picture provided by Andrea Fischer (Innsbruck). . . . .	80
7.3.	Sampling location of Jam 2-2 sed. The greyish and sandy sediment became ice free in the year of sampling and immediately a patch of grass grew there. Picture by Andrea Fischer. . . . .	81
7.4.	Sampling site of Jam 1-1 sed. The sample was very wet, rather dark and smelly, which indicates microbial activity (Hoover and Pikuta, 2012) Picture by Andrea Fischer. . . . .	81
7.5.	Map of the Grenzgletscher sampling area downstream of the glacier in the ablation zone. The sampling sites for cryoconite are marked in blue. . . . .	82
7.6.	<b>Left:</b> Map of the cave with the sampling sites. <b>Right:</b> View inside Stubai glacier cave. Note the distinct layering visible in the walls. . . . .	83
7.7.	Microscope image of the bark particle extracted from the wall of Stubai glacier cave for $^{14}\text{C}$ dating. Note the scale. . . . .	84
7.8.	Saharan dustband in the wall of the glacier cave, which was sampled for POC $^{14}\text{C}$ dating. Picture by Andrea Fischer. . . . .	84
7.9.	Exemplary sediment band sampled for POC $^{14}\text{C}$ dating with ice screws. Picture by Andrea Fischer. . . . .	85
7.10.	<b>Left:</b> Vertical section through Vasto ice cave. The entrance is only open during summer, when the winter snow accumulated in the entrance shaft is gone (Figure taken from Colucci et al. (2014)). <b>Right:</b> The cave interior and the ice surface during core drilling. (Picture provided by Jacopo Pasotti). . . . .	85

7.11. $^{14}\text{C}$ ages of snow and ice samples clearly containing Saharan dust from sampling sites all over the European Alps. The grey symbols denote the modern dust sample results after correction of a 7% mass contribution of fossil fuel EC. Note the very narrow age range for the pre-industrial samples from Stubai glacier cave, Grenz- gletscher and Vasto ice cave. . . . .	87
7.12. POC $^{14}\text{C}$ dating results for samples from an ice core drilled in Vasto ice cave (Italy). Note the two very high ages produced by obvious Saharan dust input directly adjacent to unbiased samples. . . . .	88
7.13. POC $^{14}\text{C}$ ages of all measurable Grenz- gletscher ice blocks. The large errorbars result from the very small sample masses. Note the coincidence of the dust biased and not dust biased sample ages (shaded area). . . . .	89
7.14. Overview of all cryoconite $^{14}\text{C}$ results. Note the gradual age increase of the Gren- z- gletscher (GGT) samples. . . . .	90
7.15. Overview of all sediment $^{14}\text{C}$ results. The two samples from Jamtalferner marked in green (black material) are very young compared to all other samples. They showed clear indications of living bacterial activity, which is likely the case for the comparably young $^{14}\text{C}$ ages . . . . .	92
8.1. Schematic view of the outline of the ice tunnel at the summit of Chli Titlis. Today the cave is extended to a U-shape, roughly marked in red. Adapted from Lorrain and Haeberli (1990). . . . .	96
8.2. View into the ice tunnel at Titlis glacier (2015). A level floor has been constructed by freezing water. Note the distinct layering visible in the walls. . . . .	96
8.3. Crest of Vadret dal Corvatsch in summer 1998 (picture by Martin Hölzle), strong melting revealed the glacier ice surface . . . . .	97
8.4. Vadret dal Corvatsch in winter 2007. The VCL core drilling site is marked. Picture by Barbara May . . . . .	97
8.5. Schematic view of sampling site one (2014) and two (2015) with the calibrated $^{14}\text{C}$ ages shown in red. . . . .	98
8.6. Schematic view of sampling site 3. The calibrated age of block 3-5 in red . . . . .	99
9.1. Location of Colle Gnifetti in the European Alps. Adapted from Wagenbach et al. (2012). . . . .	101
9.2. View of the saddle of Colle Gnifetti from the top of Signalkuppe in the south east. Note the locations of the cores KCC and KCI on the same flow line. The picture was taken during the 2013 drilling campaign. . . . .	102
9.3. Schematic view of all deep ice core positions and names, where drilling was led by the IUP Heidelberg (red) and the core CG03 drilled by the Paul Scherrer Institute. . . . .	102
9.4. Cutting plan of the KCC ice core and method attribution of the aliquots. . . . .	103
9.5. POC $^{14}\text{C}$ dating attempts of the KCI core by May (2009) together with absolute time markers, annual layer counting and a simple flow model (Bohleber, 2008). Note the very large age uncertainties of the $^{14}\text{C}$ data. . . . .	105
9.6. Uncalibrated POC $^{14}\text{C}$ ages of samples processed in the offline filtration system using silver membrane filters (5 $\mu\text{m}$ poresize). No age increase with core depth is discernible. . . . .	108

## List of Figures

---

9.7. Uncalibrated $^{14}\text{C}$ ages of the 340 °C (green) and 800 °C (black) fractions. The large errorbars of the 800 °C results are caused by the blank correction. Note the large age offset between both fractions. . . . .	108
9.8. Comparison of retrieved POC concentrations for the offline filtration system and the REFILOX. The respective averages are marked by the dashed lines. Note the strong increase in the basal core section. . . . .	109
9.9. Calibrated $^{14}\text{C}$ ages of the 340°C POC fraction together with two dating scenarios based on combined CFA and laser ablation annual layer counting (blue) with a 10% error range and a preliminary age-depth model. The $^{14}\text{C}$ results seem to follow the course of the model. At present state, the model uses however glaciologically unrealistic assumptions. Note the systematical offset between the $^{14}\text{C}$ ages and the counted chronology. . . . .	110
9.10. CFA data (dust and $\text{NH}_4$ ) for sample selection (pers. comm. Tobias Erhardt, Bern). The blue box marks the depth range of the sample. Note the proximity to a very large dust peak (logarithmic scale). . . . .	111
9.11. Hypothetical blank $\text{F}^{14}\text{C}$ values based on different assumptions of blank masses for correction of the measures $^{14}\text{C}$ results to the level of the annual layer counting chronology. Note the unrealistic high hypothetical blank $\text{F}^{14}\text{C}$ values exceeding bomb peak levels . . . . .	113
9.12. Hypothetical blank masses needed to correct the measured $^{14}\text{C}$ results to the level of the annual layer counting chronology based on an assumed modern blank $\text{F}^{14}\text{C}$ of 1.03 ( pers. comm. Ingeborg Levin). Note the high masses above the minimal measured sample size. . . . .	113
9.13. Scanning electron micrograph of bacteria adsorbed to the matrix of a fibrous filter. Note the scale. Taken from Brock (1983). . . . .	115
9.14. In situ production corrected POC $^{14}\text{C}$ ages for the KCC core calculated with 1 and 3 % total in situ incorporation in the POC via 3-10 % DOC adsorption onto the quartz fibre filter. Note that only for the unrealistic assumption of 10 % in situ incorporation the basal ages are shifted to the range of the annual layer counting chronology. . . . .	117
9.15. In situ corrected POC $^{14}\text{C}$ results including an accumulation change between the top three and the bottom samples. An accumulation change from 22 cm w.e./y to 5 cm w.e./y (triangles) is needed to compensate the apparent shift between top and bottom samples. . . . .	118
9.16. Normalised age depth relationships for all IUP Colle Gnifetti cores except KCC. Note the differences in total ages at common relative depths. Taken from Bohleber (2008) . . . . .	120
9.17. Comparison of POC $^{14}\text{C}$ ages measured at the KCI ice core by May (2009) with $^{14}\text{C}$ data retrieved in this study for both cores. Note the overall similarity in the curvature of age-depth relationship. . . . .	121
9.18. Comparison of POC $^{14}\text{C}$ ages measured at the CG 03 ice core by Jenk et al. (2009) with $^{14}\text{C}$ data retrieved in this study. Note the very similar curvature of both radiocarbon dating scenarios. . . . .	122
A.1. Ice sample decontamination routine at the beginning of this work. . . . .	159
A.2. Surface of a silver membrane filter after filtration of blank ice without any further decontamination after cutting . . . . .	159

A.3.	Sawing blade of the ice band saw coated with fluorescent particles (red) (picture taken from Leinfelder (2012)) . . . . .	160
A.4.	Abrasion (red) from the blade on the surface of a freshly cut ice block (picture taken from Leinfelder (2012)) . . . . .	160
A.5.	Pictures of the main part of the REFILOX filtration-combustion system. It mainly consists of a quartz tube, with a molten in quartz frit, where the quartz fibre filter is placed on top. The zone, where the filter is located can be heated by an exactly fitting oven, which can be clipped around the tube. The oven consists of tool steel, heated by four glowplugs. . . . .	161
A.6.	<sup>14</sup> C results for the different temperature carbon fractions of sample SIL-3/24. . . .	163
A.7.	<sup>14</sup> C results for the different temperature carbon fractions of sample SIL-02/08. . . .	163
A.8.	<sup>14</sup> C results for the different temperature carbon fractions of sample AVE-31 . . . .	164
A.9.	<sup>14</sup> C results for the different temperature carbon fractions of sample AVE-03 . . . .	164
A.10.	<b>Left:</b> Map of Grenzletscher in the Monte Rosa Massif, originating in the Colle Gnifetti area. Taken from Steier et al. (2006). <b>Right:</b> Schematic view of the theoretical ice flow lines of Grenzletscher with old, cold ice resurfacing in the block sampling area . . . . .	166
A.11.	<b>Left:</b> Sampling site 1 near the cave entrance. Note the layering. <b>Middle:</b> Sampling site 2 ca. 1,2 m to the right of site 1. <b>Right:</b> Sampling site 3 deeper in the cave. Note the large stones . . . . .	168
A.12.	Linear correlation between integrated dust content of ice core samples and retrieved POC mass. Note the high Pearson correlation coefficient . . . . .	168
A.13.	Picture of KCC 76 . . . . .	170



# List of Tables

2.1.	Typical $\delta^{13}\text{C}$ values of some natural materials . . . . .	10
3.1.	Major components, sizes and sub-fractions of the POC aerosol fraction in Alpine ice and snow samples. Fractions are calculated on the base of average total POC contents for high Alpine glacier ice ( $10\text{-}60 \frac{\mu\text{gC}}{\text{kg}}$ ) . . . . .	25
4.1.	Overview of the key parameters for neutron reactions with different oxygen isotopes creating $^{14}\text{C}$ . The cross sections are given for neutron energies of 14.5 MeV. Note the large variation of measured cross section for the $^{17}\text{O}$ reaction. . . . .	33
4.2.	Extracted DOC concentrations, theoretically produced numbers of in situ $^{14}\text{C}$ atoms and $^{14}\text{C}$ contents for all irradiated and reference ice samples. Note the very enriched contents of the irradiated samples. . . . .	35
4.3.	Relative fractions of $^{14}\text{C}$ , produced by irradiation that entered the DOC fraction for all irradiated ice samples. . . . .	36
5.1.	Sequential measurements of oxalic acid and blank gas to investigate possible cross contamination within the GIS . . . . .	47
5.2.	Summary of the characteristic gas ion source system parameters . . . . .	48
6.1.	Comparison of the major elements of the old and new ice sample decontamination routine . . . . .	54
6.2.	Overview of blank ice measurements done with the REFILOX . . . . .	62
6.3.	Overview of standard material $^{14}\text{C}$ results, combusted like ice POC samples in the offline filtration system . . . . .	64
6.4.	Overview of standard material $^{14}\text{C}$ results, combusted like ice POC samples in the online filtration system REFILOX . . . . .	66
6.5.	Comparison of different technical setups, advantages and disadvantages of the offline and online POC extraction system . . . . .	70
6.6.	Summary of the main characteristic system parameters. . . . .	71
6.7.	Extracted carbon contents at different temperature steps of CARBOSOL filters processed in REFILOX referred to $\text{m}^3$ of air. The results are shown in comparison to the carbon masses extracted during the CARBOSOL project. . . . .	74
6.8.	$^{14}\text{C}$ results of all carbon fractions extracted from CARBOSOL aerosol filters processed in the REFILOX system. Additionally, as a reference the bulk TC $^{14}\text{C}$ results measured by May et al. (2009) are given. . . . .	77
7.1.	Sample parameters and $^{14}\text{C}$ results of sediment (ending: sed) and cryoconite samples (ending: cryo) and one surface Saharan dust fall collected at Jamtalferner. . . . .	81

## List of Tables

---

7.2. Sample parameters and POC $^{14}\text{C}$ results of Saharan dust, clean ice and cryoconite samples from Grenzgletscher (Swiss Alps). The samples with ending REFILOX have been processed in the REFILOX system, the ones with ending Offline in the offline filtration system. Carbon concentrations are given in $\frac{\mu\text{gC}}{\text{kg}}$ for the ice samples and mass % for the cryoconite samples . . . . .	83
7.3. Samples extracted from the walls of Stubai glacier cave, Austria, their masses and $^{14}\text{C}$ results. Stubai 1 is from a Saharan dust horizon, Stubai 3-5 are taken from sediment bands, Stubai cryo is probably old cryoconite and the last two are biological remnants (bark and a larch needle). . . . .	84
7.4. Overview of the ice samples (masses and $^{14}\text{C}$ results) prepared from an ice core from Vasto ice cave (Italy). The first two samples have been pretreated like sediment, the others were filtered in the offline system. . . . .	86
7.5. Summary of the characteristic $^{14}\text{C}$ ages of different materials in Alpine glacier ice samples . . . . .	93
8.1. POC $^{14}\text{C}$ dating results for the samples from Titlis glacier cave and the one sample from the VCL core. The Titlis samples with ending -S have been processed in the offline filtration system, the others in the REFILOX, also the VCL sample. The VCL samples are complemented by the results of May (2009) for the sample VCL 38. . . . .	97
9.1. Key parameters of all deep Colle Gnifetti ice cores drilled under the lead of the IUP Heidelberg, together with the core CG03 drilled by the Paul-Scherrer-Institute (PSI). The firn ice transition is defined by a density of $0.83 \frac{\text{g}}{\text{cm}^3}$ for all cores without KCC. Table adapted from Bohleber (2008). . . . .	103
9.2. Key sample parameters and POC $^{14}\text{C}$ results of all samples from KCC ice core. Samples with ending -S have been processed using silver membrane filters in the offline filtration system, samples with ending -R in the REFILOX. $M_{\text{ice}}$ denotes the sample ice mass and $m_{\text{corr}}$ the blank corrected carbon mass. The $^{14}\text{C}$ values measured in the $800^\circ\text{C}$ fraction of the REFILOX samples and the samples pretreated in the offline system haven been blank corrected. All $^{14}\text{C}$ results are reported as fraction modern carbon $F^{14}\text{C}$ . . . . .	106
9.3. Parameter values used for hypothetical in situ correction of the POC $^{14}\text{C}$ ages of the KCC core. . . . .	116
A.1. Parameters of the different flux monitor materials used for neutron flux calculation. . . . .	157
A.2. Ice and water sample parameters and measured neutron fluxes for calculation of in situ produced $^{14}\text{C}$ . . . . .	158
A.3. Overview of different failed attempts to produce POC free blank ice by freezing of MQ-water in different materials measured in the offline system . . . . .	159
A.4. Overview of all blank ice measurements done with the offline filtration system . . . . .	162
A.5. Overview of MQ-water blank measurements with total combustion at $800^\circ\text{C}$ in REFILOX . . . . .	162
A.6. Overview of MQ water (500 ml) blank measurements only at the second combustion temperature step $800^\circ\text{C}$ in REFILOX . . . . .	162
A.7. Comparison of the different carbon fraction masses extracted by CARBOSOL and REFILOX shown as ratios . . . . .	164
A.8. Carbon concentrations extracted for every organic carbon fraction of the CARBOSOL aerosol samples by use of the thermo-optical method. . . . .	165

A.9. Key organic and inorganic impurity contents measured on the CARBOSOL aerosol samples. . . . . 165

A.10. Saharan dust samples and POC  $^{14}\text{C}$  results from Colle Gnifetti snow (Sahara 4-6) and a Colle Gnifetti ice core (KCI 10). All samples have been pretreated in the offline filtration system at the IUP Heidelberg and were combusted completely at 800°C . . . . . 167

A.11. Selection and major results of cryoconite samples from Sulzbacherkees (title: Sulz, Austria), Venedigerkees (title: Venedig, Austria) and Karakoram (title: Kara, Central Asia) . . . . . 167

A.12. . . . . 169

A.13. Uncalibrated and calibrated  $^{14}\text{C}$  ages ( $1\sigma$ ) of the 340 °C fractions of the KCC ice core samples. . . . . 170



# A. Appendix

## A.1. Appendix to Chapter 4

### A.1.1. Neutron flux calculation and ice sample parameters

Calculation of neutron number  $n$  detected at the position of the flux monitor. The flux monitors have been measured for their  $\gamma$ -activity at VERA after the irradiation experiment.

$$n = \frac{C_{corr} \cdot M \cdot \lambda}{\sigma \cdot N_A \cdot \rho \cdot d \cdot \varepsilon \cdot I_\gamma} \quad (\text{A.1})$$

With  $C_{corr}$  as the measured  $\gamma$  count rate, corrected for the decay between time of irradiation and time of measurement,  $M$  as the molar mass of the flux monitor material,  $\lambda$  the decay constant of the respective material,  $\sigma$  the cross section for the respective neutron reactions,  $\rho$  the density of monitor material,  $d$  the thickness of the monitor foil,  $\varepsilon$  the efficiency of the detector and  $I_\gamma$  as the intensity of the  $\gamma$ -line. The values used for calculation are summarised in Table A.1.

From the number of neutrons  $n$ , the neutron density  $\rho_n$  and finally the neutron flux  $\Phi_n$  can be calculated under use of the flux monitor surface  $A_{monitor}$  and the irradiation time  $t_{irradiate}$ :

$$\rho_n = \frac{n}{A_{monitor}} \quad \Rightarrow \quad \Phi_n = \frac{\rho_n}{t_{irradiate}} \quad (\text{A.2})$$

**Tab. A.1.:** Parameters of the different flux monitor materials used for neutron flux calculation.

Half life $^{92}\text{Nb}$ :	$T_{1/2}(^{92}\text{Nb}) = 876\,960\text{ s}$
Half life $^{198}\text{Au}$ :	$T_{1/2}(^{198}\text{Au}) = 232\,848\text{ s}$
Molar mass $^{92}\text{Nb}$ :	$M_{Nb} = 92\,910\text{ mg/mol}$
Molar mass $^{198}\text{Au}$ :	$196\,970\text{ mg/mol}$
Monitor radius:	$r = 5\text{ mm}$
Monitor thickness	$d = 0.127\text{ mm}$
Density Nb:	$\rho_{Nb} = 8.57\text{ mg/mm}^3$
Density Au:	$\rho_{Au} = 19.32\text{ mg/mm}^3$
Cross section $^{93}\text{Nb}(n,2n)^{92}\text{Nb}$ :	$\sigma_{Nb} = 13.5\text{ b}$
Cross section $^{197}\text{Au}(n,\gamma)^{198}\text{Au}$ :	$\sigma_{Au} = 10.0\text{ b}$
Detector efficiency:	$\varepsilon = 0.02\%$
Intensity:	$I_\gamma = 0.97\%$

Tab. A.2.: Ice and water sample parameters and measured neutron fluxes for calculation of in situ produced  $^{14}\text{C}$

Sample type	Sample mass [g]	Density [g/cm <sup>3</sup> ]	Flux monitor	Neutron flux [n/s/cm <sup>2</sup> ]	Irradiation time [s]
MQ-water	53.5	1.0	Niobium	5.20E+08 front	3600
			Niobium	8.79E+07 back	
MQ-water ref.	54.6	1.0	Gold	4.57E+08 front	
			Gold	1.93E+08 back	
Blank ice	185.4	0.90	Niobium	3.91E+08 front	2160
			Niobium	5.34E+07 back	
			Gold	7.57E+08 front	
			Gold	3.73E+08 back	
Blank ice ref.	182.6	0.91			
Alpine snow	81.3	0.36	Niobium	2.59E+08 front	3600
			Niobium	5.30E+07 back	
			Gold	4.81E+08 front	
			Gold	1.61E+08 back	
Alpine snow ref.	80.4	0.36			
Glacier ice	86.8	0.88	Niobium	3.89E+08 front	3600
			Niobium	6.22E+07 back	
			Gold	5.53E+08 front	
			Gold	2.21E+08 back	
Glacier ice ref.	87.7	0.89			

## A.2. Appendix to Chapter 6

### A.2.1. Clean ice production

**Tab. A.3.:** Overview of different failed attempts to produce POC free blank ice by freezing of MQ-water in different materials measured in the offline system

Material	Ice mass [g]	POC mass [ $\mu\text{gC}$ ]	POC conc. [ $\frac{\mu\text{gC}}{\text{kg}}$ ]
PE-foil	337	$2.7 \pm 0.3$	8.0
PE-foil	277	$4.0 \pm 0.3$	14.4
PE-foil	270	$6.7 \pm 0.3$	24.8
PFA-pot	336	$7.1 \pm 0.3$	21.1

### A.2.2. Detailed description of the sample decontamination routine

The decontamination routine used during this work follows the scheme shown in Fig. A.1.

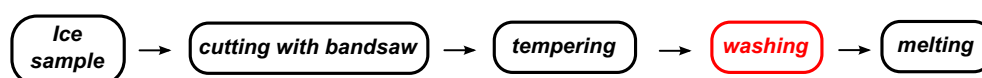


**Fig. A.1.:** Ice sample decontamination routine at the beginning of this work.

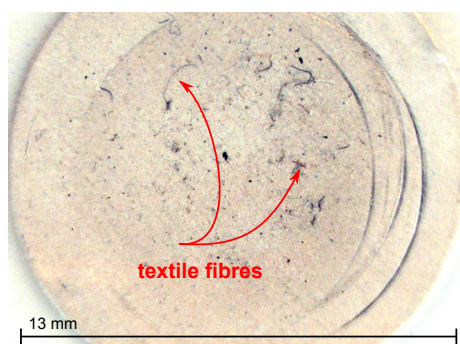


**Fig. A.2.:** Surface of a silver membrane filter after filtration of blank ice without any further decontamination after cutting

First the sample is cut by a band saw to the desired size, then it is tempered to  $0\text{ }^{\circ}\text{C}$  to avoid cracks which can lead surface contaminations to the inside, after tempering the sample is washed with ultra pure water and inserted into the melting pot. Washing of the sample proved to be the most effective cleaning step, but also the one with biggest mass loss. The initial high variability of ice blank measurements at the beginning of this work made a detailed analysis of the decontamination steps and their optimisation necessary.

Especially textile fibres (see Fig A.2) have been discovered every once in a while on the filters, although all open ice samples have been handled in a laminar flow box. As a result, it was decided to handle open ice samples only when wearing a fibre free overall and latex gloves, even in the cold room. This simple step already reduced the amount of fibres that could be found on filters significantly.

### Cutting

All ice samples have to be cut to fit into the melting vessel and to remove the outer and in terms of POC probably dirty surfaces. Sawing can not be avoided, but the abrasion from the blade, even if cleaned by sawing blank ice in advance, and the collection of cutting powder in bubbles can be a source of organic particles (e.g. lubricants). To show this, again a test with UV-fluorescent particles was performed, which made the particles smeared onto the ice surface visible in a demonstration experiment (see Fig. A.4).

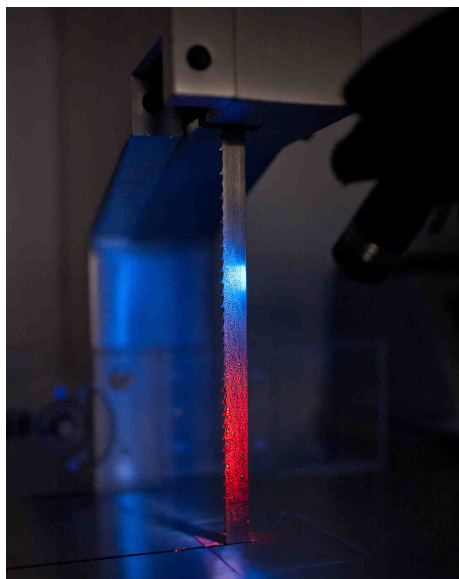


**Fig. A.3.:** Sawing blade of the ice band saw coated with fluorescent particles (red) (picture taken from Leinfelder (2012))

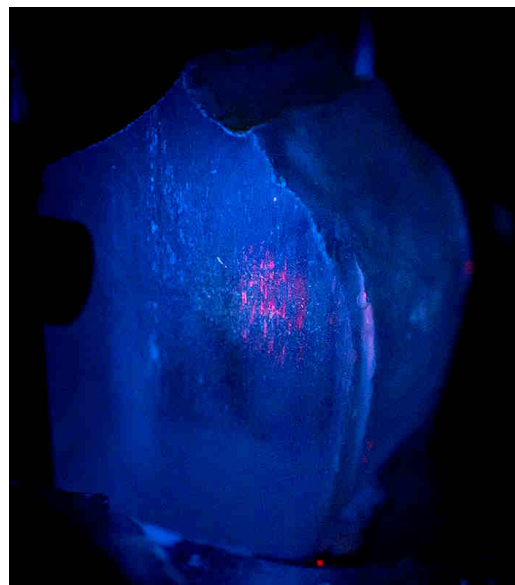


**Fig. A.4.:** Abrasion (red) from the blade on the surface of a freshly cut ice block (picture taken from Leinfelder (2012))

### Scraping

In the past, after sawing, the ice sample was directly moved to the tempering step followed by washing. Based on the insights of the fluorescent particle experiment in this work, another step was added in between sawing and tempering. This step consists of scraping of the ice surface with a ceramic knife under a laminar flow in the cold room. By scraping of the surface, all potentially contaminated cutting powder is removed mechanically, even from the surface bubbles. By this pre-cleaning step, the washing of the sample can be shortened and material is saved this way.

### Tempering

After scraping, the sample is placed inside a closed PFA container and transported out of the cold room to a laminar flow box at room temperature. The box has to remain closed during transport and until it is warmed up, to avoid condensation and transport of air dust onto the ice surface.

## Washing

When the ice reached 0°C and the first meltwater drops occur (usually after ca. 30 min), the samples are washed shortly under a jet of MQ water from each side and transferred into the melting vessel. All in a laminar flow box.

### A.2.3. Pictures of the REFILOX system

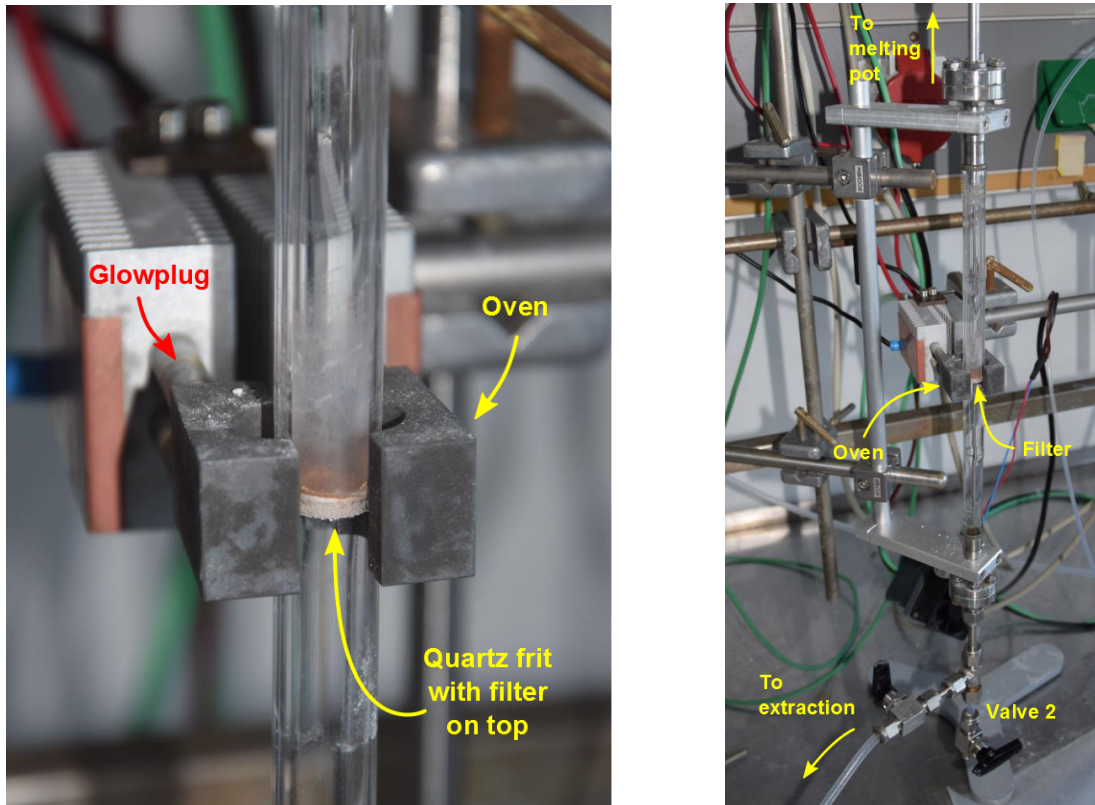


**Fig. A.5.:** Pictures of the main part of the REFILOX filtration-combustion system. It mainly consists of a quartz tube, with a molten in quartz frit, where the quartz fibre filter is placed on top. The zone, where the filter is located can be heated by an exactly fitting oven, which can be clipped around the tube. The oven consists of tool steel, heated by four glowplugs.

## A. Appendix

### A.2.4. Data for system characterisation

**Tab. A.4.:** Overview of all blank ice measurements done with the offline filtration system

Name	Type	Processing date	Ice mass [g]	POC mass [ $\mu\text{gC}$ ]	POC conc. [ $\frac{\mu\text{gC}}{\text{kg}}$ ]
POC 623	blank ice	11.4.14	210	$0.2 \pm 0.3$	0.95
POC 624	blank ice	16.4.14	218	$0.0 + 0.3$	0.0
POC 625	blank ice	25.4.14	177	$0.2 \pm 0.3$	1.12
POC 629	blank ice	22.5.15	205	$0.5 \pm 0.3$	2.4
POC 635	blank ice	20.11.14	339	$1.4 \pm 0.3$	4.1
POC 636	blank ice	26.1.15	284	$1.0 \pm 0.3$	3.5
POC 642	blank ice	6.3.15	288	$0.2 \pm 0.3$	0.69
B34-159	antarctic ice	24.4.15	326	$0.2 \pm 0.3$	0.61

**Tab. A.5.:** Overview of MQ-water blank measurements with total combustion at 800°C in REFILOX

Name	Processing date	POC mass [ $\mu\text{gC}$ ]	POC conc. [ $\frac{\mu\text{gC}}{\text{kg}}$ ]
Blank Refilox MQ 29	09.03.15	$1.4 \pm 0.3$	2.8
Blank Refilox MQ 30	20.03.15	$1.6 \pm 0.3$	3.2
Blank Refilox MQ 31	21.04.15	$1.4 \pm 0.3$	2.8
Blank Refilox MQ 32	08.05.15	$2.2 \pm 0.3$	4.4
Blank Refilox MQ 33	16.05.15	$1.6 \pm 0.3$	3.2
Blank Refilox MQ 34	16.05.15	$2.1 \pm 0.3$	4.2
Blank Refilox MQ 35	08.06.15	$0.8 \pm 0.3$	1.6
Blank Refilox MQ 36	28.07.15	$1.0 \pm 0.3$	2.0
Blank Refilox MQ 38	02.10.15	$1.9 \pm 0.3$	3.8

**Tab. A.6.:** Overview of MQ water (500 ml) blank measurements only at the second combustion temperature step 800°C in REFILOX

Name	Processing date	POC mass [ $\mu\text{gC}$ ]	POC conc. [ $\frac{\mu\text{gC}}{\text{kg}}$ ]
Blank Refilox MQ 37-2	01.10.15	$3.6 \pm 0.3$	7.2
Blank Refilox MQ 38-2	06.10.15	$0.0 + 0.3$	0.0
Blank Refilox MQ 39-2	08.10.15	$3.2 \pm 0.3$	6.4
Blank Refilox MQ 40-2	12.10.15	$1.1 \pm 0.3$	2.2
Blank Refilox MQ 41-2	27.10.15	$0.6 \pm 0.3$	1.2
Blank Refilox MQ 42-2	30.10.15	$0.5 \pm 0.3$	1.0
Blank Refilox MQ 43-2	03.11.15	$3.3 \pm 0.3$	6.6
Blank Refilox MQ 44-2	04.11.15	$1.3 \pm 0.3$	2.6
Blank Refilox MQ 45-2	09.11.15	$0.6 \pm 0.3$	1.2
Blank Refilox MQ 46-2	11.11.15	$1.3 \pm 0.3$	2.6
Blank Refilox MQ 47-2	17.11.15	$2.7 \pm 0.3$	5.4
Blank Refilox MQ 48-2	14.12.15	$2.7 \pm 0.3$	5.4

### A.2.5. Manometric quantification of carbon mass

Calculation of carbon amount  $n$  via virial expansion (see also Hammer (2003)):

$$n = V \cdot \frac{1}{2B(T)} \cdot \left[ \sqrt{1 + \frac{4B(T)p}{RT}} - 1 \right] \quad (\text{A.3})$$

With  $B(T)$  as the first virial coefficient approximated by:

$$B(T) = -149.65 + 1.2049 \cdot T - 6.87 \cdot 10^{-3} \cdot T^2 + 4.25 \cdot 10^{-5} \cdot T^3 - 1.9 \cdot 10^{-7} \cdot T^4 \left[ \frac{\text{cm}^3}{\text{mol}} \right]$$

With  $T$  as temperature,  $n$  number of moles,  $V$  measuring volume,  $p$  pressure,  $R$  gas constant for  $\text{CO}_2$ .

### A.2.6. CARBOSOL filter investigations - additional data

Results of the  $^{14}\text{C}$  measurements of different temperature fractions in REFILOX

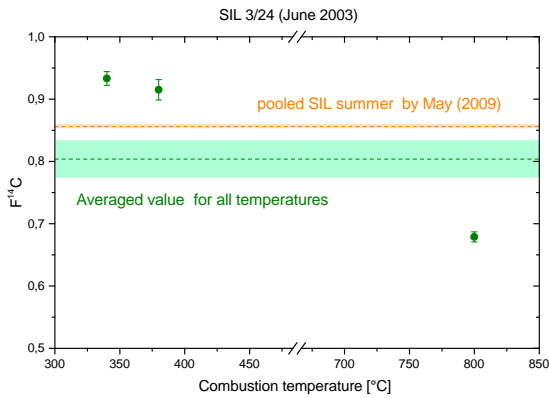


**Fig. A.6.:**  $^{14}\text{C}$  results for the different temperature carbon fractions of sample SIL-3/24.

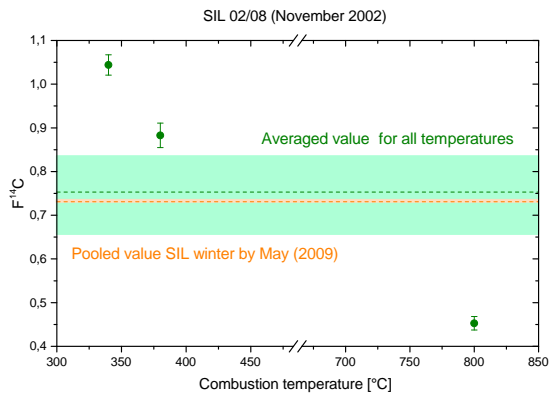


**Fig. A.7.:**  $^{14}\text{C}$  results for the different temperature carbon fractions of sample SIL-02/08.

## A. Appendix

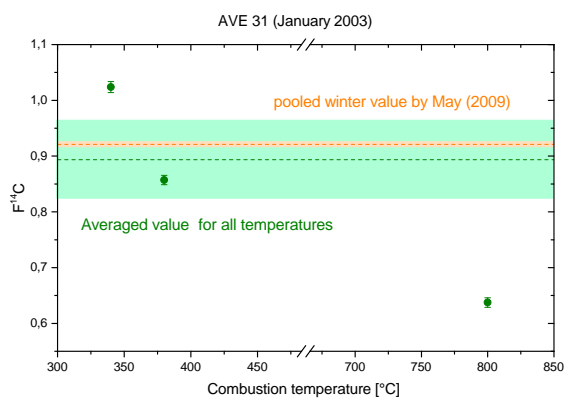


**Fig. A.8.:**  $^{14}\text{C}$  results for the different temperature carbon fractions of sample AVE-31

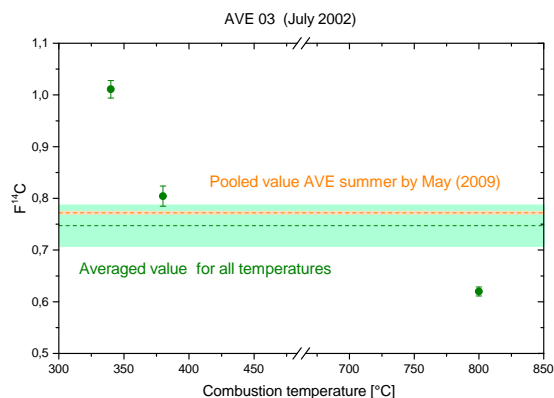


**Fig. A.9.:**  $^{14}\text{C}$  results for the different temperature carbon fractions of sample AVE-03

### Carbon fractions / ratios measured with REFILOX and CARBOSOL

**Tab. A.7.:** Comparison of the different carbon fraction masses extracted by CARBOSOL and REFILOX shown as ratios

Sample name	TC REF / TC CARB	340 °C REF / OC1+OC2 CARB	REF 380°C+ 800°C / OC3+PC+EC CARB	EC REF / EC CARB
SBO-32	0.90	0.80	0.88	6.48
SIL-02/08	0.94	1.93	0.76	1.56
SIL-3/24	1.12	1.54	0.97	6.57
SIL-3/28	1.09	1.27	0.97	7.38
AVE-31	0.87	1.61	0.64	1.42
AVE-03	1.29	1.31	1.28	6.25

**Tab. A.8.:** Carbon concentrations extracted for every organic carbon fraction of the CARBOSOL aerosol samples by use of the thermo-optical method.

Filter name	Sample volume [m <sup>3</sup> ] STP	OC1 [µgC /m <sup>3</sup> ] STP	OC2 [µgC /m <sup>3</sup> ] STP	OC3 [µgC /m <sup>3</sup> ] STP	PC [µgC /m <sup>3</sup> ] STP	EC [µgC /m <sup>3</sup> ] STP
SBO 32	3446	0.15	0.45	0.35	0.83	0.13
SIL-02/08	8429	0.02	0.12	0.19	0.31	0.23
SIL-03/24	7436	0.36	0.69	0.69	1.99	0.35
SIL-03/28	9041	0.38	0.65	0.49	2.20	0.26
AVE 31	10978	1.47	3.08	2.75	9.66	1.94
AVE 03	10661	0.40	0.61	0.64	2.21	0.52

**Tab. A.9.:** Key organic and inorganic impurity contents measured on the CARBOSOL aerosol samples.

Filter name	HULIS [µg/m <sup>3</sup> ] STP	SO <sub>4</sub> [ng/m <sup>3</sup> ] STP	NH <sub>4</sub> [ng/m <sup>3</sup> ] STP	Ca [ng/m <sup>3</sup> ] STP	Levogluconan [ng/m <sup>3</sup> ] STP	Cellulose [ng/m <sup>3</sup> ] STP
SBO 32	0.37	1628	752	87	7.1	40.6
SIL-02/08	0.44	687	241	19	19.5	6.4
SIL-03/24	1.96	3595	1179	360	19.0	316.6
SIL-03/28	1.85	5463	2020	634	23.2	95.3
AVE 31	11.75	2029	1157	165	1478.1	53.3
AVE 03	1.78	10276	3049	423	21.1	54.0

### A.3. Appendix to Chapter 7

#### A.3.1. Sample preparation routine for sediment samples used at the Klaus-Tschira-Laboratory (Mannheim)

1. washing with HCl (4 %) at 60°C for 1 hour to remove carbonates and subsequent rinsing with MQ-water
2. washing with NaOH (0.4 %) at 20°C for 1 hour to remove humic and fulvic acids, which are known to possibly bias the sample age (see section refcomp) and subsequent rinsing with MQ-water
3. washing with HCl (4 %) at 60°C for 1 hour to remove any CO<sub>2</sub> taken up from the lab air during the NaOH step and subsequent rinsing with MQ-water
4. drying of sample
5. combustion at 800°C in an Elemental Analyser and graphitisation of CO<sub>2</sub>
6. AMS-measurement

#### A.3.2. Grenzletscher sampling site additional information

In 2004, already a block sampling campaign has been carried out (Steier et al., 2006) to get large amounts of ice for testing of the Vienna POC <sup>14</sup>C dating method. The results of this study were not completely conclusive and had a large age scatter for both sites around ca. 2500 yBP <sup>14</sup>C age. Within this age range, a <sup>14</sup>C dating accuracy of higher than 1% would therefore be needed to distinguish the age difference of the two new sites.

The sampling sites chosen in 2014 (see section 7.2.2) are separated by a lateral distance of about 2 km, which results in an age difference of ca. 200 years with an assumed flow velocity of 10 m/y (Steier et al., 2006).

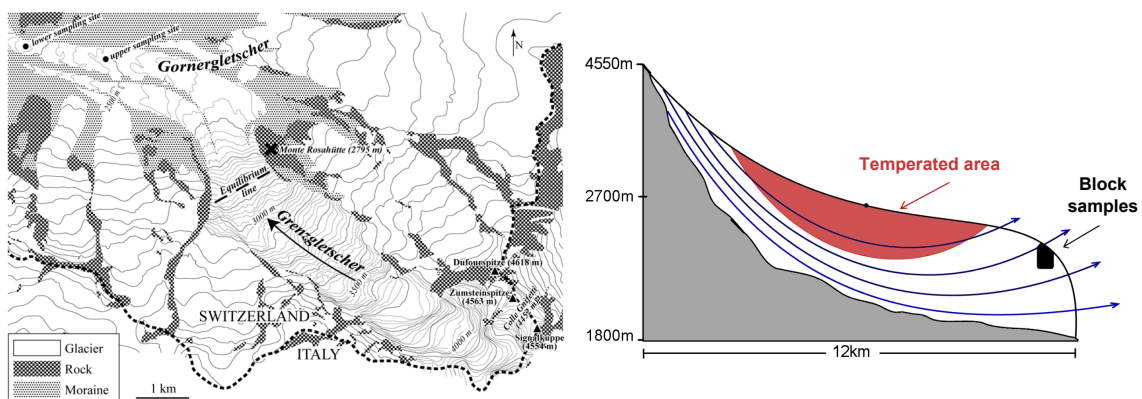


**Fig. A.10.:** **Left:** Map of Grenzletscher in the Monte Rosa Massif, originating in the Colle Gnifetti area. Taken from Steier et al. (2006). **Right:** Schematic view of the theoretical ice flow lines of Grenzletscher with old, cold ice resurfacing in the block sampling area

### A.3.3. Sample parameters of Saharan dust samples from Colle Gnifetti

All samples have been filtered and pretreated within the offline filtration system described in section 6.2 and blank corrected according to the values reported in table 6.6. Nevertheless, there is a possibility of a slightly higher blank contribution for the snow samples, because washing of the samples was difficult due to their high porosity.

**Tab. A.10.:** Saharan dust samples an POC  $^{14}\text{C}$  results from Colle Gnifetti snow (Sahara 4-6) and a Colle Gnifetti ice core (KCI 10). All samples have been pretreated in the offline filtration system at the IUP Heidelberg and were combusted completely at 800°C

Name	Mass [ $\mu\text{gC}$ ]	$F^{14}\text{C}_{corr}$	$\Delta F_{corr}$	$^{14}\text{C age}_{corr}$ [yBP]	Error [yBP]	$\delta^{13}\text{C}$ [‰]
Sahara 4-F-1	61.5	0.591	0.011	4227	152	-20.6
Sahara 4-F-2	31.4	0.635	0.02	3647	258	-22.2
Sahara 6-S-2	14.6	0.785	0.048	1943	491	-23.2
KCI 10	10.4	0.834	0.071	1460	679	-29.5

### A.3.4. Sample parameters of Cryoconite samples from Grossvenediger and Karakoram

**Tab. A.11.:** Selection and major results of cryoconite samples from Sulzbacherkees (title: Sulz, Austria), Venedigerkees (title: Venedig, Austria) and Karakoram (title: Kara, Central Asia)

Sample name	Sample mass [mgC]	$\%C_{mass}$	$F^{14}\text{C}$	$\Delta F$	$^{14}\text{C age}$ [yBP]	Error [yBP]	$\delta^{13}\text{C}$ [‰]
Sulz 1 cryo	1.196	8.0	0.820	0.002	1599	24	-20.1
Venedig 1 cryo	0.905	4.6	0.659	0.002	3353	30	-27.2
Venedig 2 cryo	1.281	6.6	0.757	0.002	2235	23	-22.5
Kara 1 cryo	3.200	2.9	0.921	0.002	661	22	-14.1
Kara 2 cryo	3.650	3.8	0.936	0.002	532	20	-14.3
Kara 3 cryo	3.620	4.6	0.961	0.003	318	22	-19.7

## A.4. Appendix to Chapter 8

Titlis glacier cave block sampling: Pictures of the extracted profiles

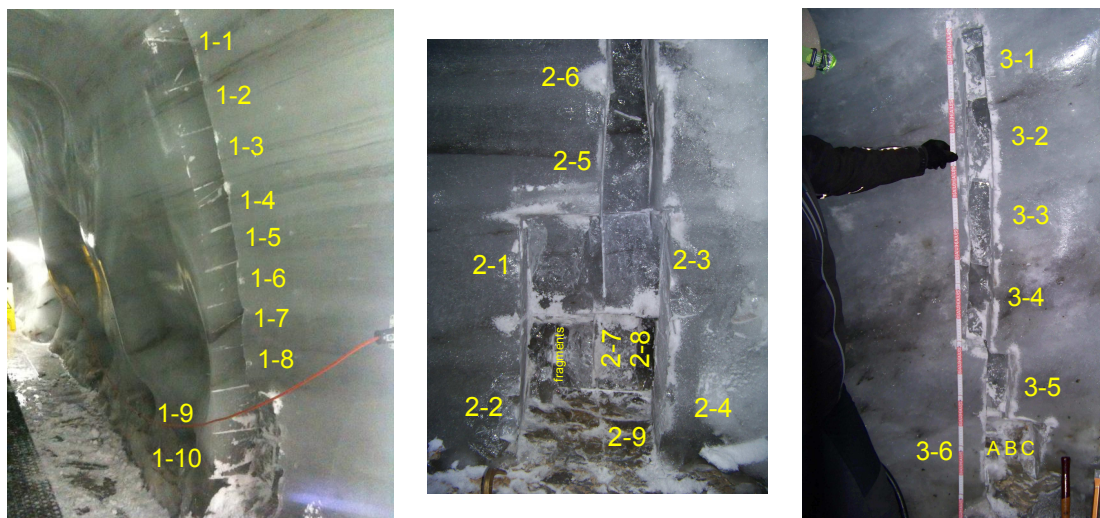


**Fig. A.11.:** **Left:** Sampling site 1 near the cave entrance. Note the layering. **Middle:** Sampling site 2 ca. 1,2 m to the right of site 1. **Right:** Sampling site 3 deeper in the cave. Note the large stones

## A.5. Appendix to Chapter 9

### A.5.1. Sample selection - additional data

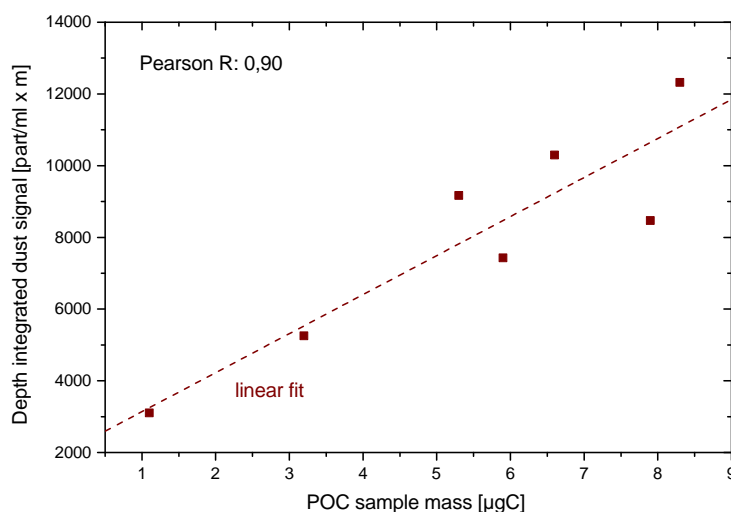


**Fig. A.12.:** Linear correlation between integrated dust content of ice core samples and retrieved POC mass. Note the high Pearson correlation coefficient

Tab. A.12.

Sample name	Dust int. [part./ml · m]	NH <sub>4</sub> int. [ng/g · m]	NO <sub>3</sub> int. [ng/g · m]	Na int. [ng/g · m]	Ca int. [ng/g · m]	δ <sup>18</sup> O average [‰]
KCC 61/62-S	15368	17	24	13	51	-14.4
KCC 68-S	1686	6	16	2	7	-16.5
KCC 69-R	5254	15	31	6	23	-13.4
KCC 70/71-R	3103	5	18	7	23	-14.5
KCC 71/72-S	8555	22	42	10	32	-12.5
KCC 75/76-R	7427	17	57	16	54	-13.3
KCC 77a/b-S	5491	4	12	8	17	-11.3
KCC 81/82a-S	11447	18	39	16	49	-12.7
KCC 83/84-R	11936	12	32	16	57	-14.5
KCC 84-S	5112	9	21	8	25	-13.2
KCC 86-R	10296	20	39	10	55	-13.7
KCC 88/89-S	12805	25	51	16	55	-13.6
KCC 90-R	9166	14	8	31	35	-15.2
KCC 94-R	8468	10	37	9	30	-15.7
KCC 97 a/b-R	12323	15	42	13	37	-17.2

A.5.2.  $^{14}\text{C}$  ages of the 340 °C fraction of the KCC samples

Tab. A.13.: Uncalibrated and calibrated  $^{14}\text{C}$  ages ( $1\sigma$ ) of the 340 °C fractions of the KCC ice core samples.

Sample name	Depth [m w.e.]	$^{14}\text{C}$ age <sub>uncal</sub> [yBP]	Error [yBP]	$^{14}\text{C}$ age <sub>cal</sub> [yBP]	Error $1\sigma$ [yBP]
KCC 69-340-R	38.46	723	375	736	349
KCC 70/71 340 R	38.7	371	824	899	695
KCC 75/76-340-R	41.33	1075	172	1007	167
KCC 83/84-340-R	45.12	478	461	590	379
KCC 86-340-R	46.33	555	172	543	160
KCC 89/90-340-R	48.38	804	218	788	196
KCC 94-340-R	50.5	1324	154	1232	157
KCC 97 a/b 340-R	51.9	1784	157	1717	172
KCC 100-340-R	53.3	3011	200	3216	238

A.5.3. Picture of KCC 76

Piece of KCC 76 directly following the sample KCC 75/76. Note the strong yellow layering caused by the fourth largest dust inclusion of the whole core.

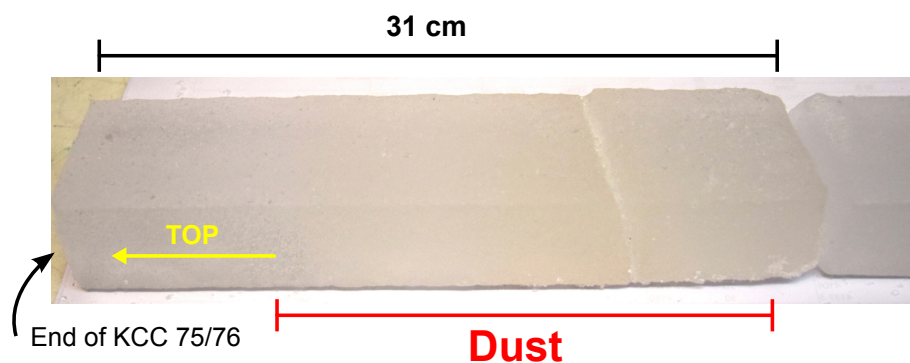


Fig. A.13.: Picture of KCC 76

### A.5.4. Hypothetical in situ correction of $^{14}\text{C}$ results - calculations

#### 1. Calculation of number of in situ produced $^{14}\text{C}$ atoms $n$ in sample depth $z$ (Eq. 4.1):

$$n_{insitu}(z) = m_{ice} \cdot \frac{P_0}{\frac{\rho A}{\Lambda} - \lambda} \cdot \left( e^{-\frac{\lambda z}{A}} - e^{-\frac{\rho z}{\Lambda}} \right)$$

With  $P_0 \approx 396 \text{ }^{14}\text{C g}^{-1} \text{ a}^{-1}$ ,  $\Lambda = 150 \text{ g} \cdot \text{cm}^{-2}$ ,  $A = 22 \text{ cm w.e./y}$ ,  $\rho = 0,9 \text{ g/cm}^3$  and  $m_{ice}$  as the ice mass of the sample in grams.

#### 2. Calculation of the number of in situ $^{14}\text{C}$ atoms incorporated into POC:

$$n_{insitu,POC}(z) = c_{insitu}(z) \cdot \varepsilon$$

With  $\varepsilon$  as the fraction of total in situ  $^{14}\text{C}$  reaching the POC via adsorption of DOC to the filter matrix.

#### 3. Calculation of the $F^{14}\text{C}_{insitu}$ of the sample

$$F^{14}\text{C}_{insitu} = \frac{n_{insitu,POC}}{n_C} \cdot \frac{1}{\left( \frac{^{14}\text{C}}{^{12}\text{C}} \right)_{OxII}}$$

With  $\left( \frac{^{14}\text{C}}{^{12}\text{C}} \right)_{OxII}$  as the measured  $^{14}\text{C}/^{12}\text{C}$  ratio of the OxII standard and  $n_C$  as the number of C-atoms in the sample, calculated via

$$n_C = N_A \cdot \frac{m_{POC}}{M_C} \cdot \frac{1}{1 - \left( \frac{^{13}\text{C}}{^{12}\text{C}} \right)_{sample}}$$

Where  $N_A$  denotes the Avogadro constant,  $m_{POC}$  the measured sample carbon mass in gram,  $M_C$  the molar mass of carbon in g/mol and  $\left( \frac{^{13}\text{C}}{^{12}\text{C}} \right)_{sample}$  the measured  $\left( \frac{^{13}\text{C}}{^{12}\text{C}} \right)$  ratio of the sample.

#### 4. Calculation of the corrected $F^{14}\text{C}$ value $F^{14}\text{C}_{corr}$ of the sample:

$$F^{14}\text{C}_{corr} = F^{14}\text{C}_{measured} - F^{14}\text{C}_{insitu}$$

#### 5. Calculation of the in situ corrected $^{14}\text{C}$ age $t_{corr}$ [yBP] of the sample:

$$t_{corr} = -8003 \cdot \ln(F^{14}\text{C}_{corr})$$



# Danksagung

Am Ende von insgesamt mehr als vier Jahren Doktorandendasein angekommen, ist es an der Zeit einigen Menschen zu danken, die mich auf diesem Weg begleitet haben.

Allen voran danke ich Dietmar Wagenbach, meinem Betreuer und Chef, der die Vollendung dieser Arbeit leider nicht mehr erleben konnte. Er hat mich in seine Eisgruppenfamilie aufgenommen und hat mir immer vertraut, auch wenn ich es selbst nicht tat. Abgesehen von dem nicht versiegenden Quell wertvoller Lebensweisheiten wie "in der Not hilft immer Schnaps" und vieler mehr, konnte ich mir immer sicher sein von ihm einen wertvollen Ratschlag zu bekommen, auch wenn ich ihn nicht immer auf Anhieb verstand und umsetzte. Die Zeit, die mir mit ihm als Betreuer vergönnt war, hat mein wissenschaftliches Arbeiten (und auch mich selbst) nachhaltig geprägt, im besten Sinne. Danke, Dietmar!

Ein großer Dank gebührt auch Ingeborg Levin, die mir im letzten Jahr eine wissenschaftliche und auch menschliche Stütze war, sich Zeit genommen hat meine Arbeit zu verstehen und schließlich sogar bereit war die offizielle Betreuung zu übernehmen, Danke.

Vielen Dank auch an Werner Aeschbach, für die Unterstützung, die Begutachtung dieser Arbeit und die immer offene und herzliche Aufnahme bei den Aquas.

Ein großes Dankeschön an Susanne Preunkert, die sich mit unermüdlichem Einsatz in meine verzwickten Daten eingefuchst hat und sich in Fragestellungen festbeißen kann wie keine Andere. Vielen lieben Dank für die unzähligen investierten Stunden des "Hirnens" und das Korrekturlesen dieses Buches. Vielen Dank auch an Michel Legrand, für die immer verfügbare fundierte Chemikermeinung.

Vielen Dank auch an Pascal Bohleber, für den wissenschaftlichen Input und die Zeit zum Korrekturlesen, das Pale Ale, aber auch das Vertrauen mich auf diverse Feldkampagnen mitzuschleppen, insbesondere den Kilimanjaro. Es waren unvergessliche Erlebnisse.

Ronny Friedrich danke ich für die vielen (kalten aber lustigen) Stunden am Beschleuniger, fürs mitleiden und mentale Händchenhalten, fürs Interesse an meinen Colle-Krampfproben und einfach allgemein für seine unkomplizierte Art.

Barbara May gebührt ein besonderer Dank, als meine Ex-Diplomarbets-Betreuerin ist sie immer noch trotz Arbeit in der echten Welt eine kompetente Diskussionspartnerin und hat mich mit wertvollem Input versorgt. Ich verspreche, es wird noch ein in situ paper geben!

Danke an Andrea Fischer, die mich nicht nur enthusiastisch mit Schlamm und Dreckproben versorgt hat, sondern mir auch ermöglichte, die Gletscher selbst anzuschauen und mich herzlich in Innsbruck aufgenommen hat.

Ich danke Bernd Kromer für die Unterstützung beim Aufbau der Gasquelle und in diesem Zusammenhang auch dem Team der Ionenstrahlphysik an der ETH Zürich, insbesondere Lukas Wacker und Simon Fahrni für die Hilfe und den Rat rund um die Gasquelle.

Danke an die vielen Kollegen, die mich mit Probenmaterial versorgt haben. An Roberto Colucci aus Triest für die Eishöhlenproben und das Vertrauen mich mit dem wertvollen Material spielen zu lassen, an Christoph Mayer aus München, der mich mit Schlamm aus dem Karakorum versorgt hat und vor allem auch an Paul Mayewski, der mich nach Maine eingeladen hat und mir ebenfalls wertvolle Proben anvertraut.

Danke auch an Peter Steier und Anton Wallner aus Wien, sowie an das Team an der Neutronenquelle im Forschungszentrum Dresden Rossendorf für ihre tatkräftige Unterstützung bei den Bestrahlungsexperimenten.

Vielen Dank an die Mitarbeiter der IUP-Werkstatt und an Herrn Stadler von der Glasbläserei, die meine Laborarbeit mehr als einmal (auch sehr spontan) gerettet haben.

Ebenso danke ich allen Mitarbeiter(innen) des Sekretariats und der Verwaltung für die Unterstützung im Bürokratiedschungel, insbesondere im letzten Jahr.

Ein besonderer Dank geht an die Eisgruppe. Speziell an Lars Zipf und Carlo Licciulli für die Beharrlichkeit bei der Aufrechterhaltung des Feierabendbieres, für die Selbstverständlichkeit sich verantwortlich zu fühlen, für den Zusammenhalt und die lustigen Gespäche abseits der Wissenschaft.

Ich danke meinen Kollegen am IUP, vergangener und aktueller Generationen, für lustige Mensabesuche und Hinterhofgrillabende und die Bereitschaft als Versuchskaninchen für schräge Stickstoffeissorten herzuhalten. Insbesondere danke ich Tilman Hüneke für den "social Monday" in der Endphase des Zusammenschreibens.

Vielen lieben Dank an meine Mädels, Jasmin, Sabrina, Esther, Miri, Steffi, Verena und Katja, die ich zum Teil jetzt schon seit fast zwanzig Jahren kenne, die mir immer Halt gegeben haben und die mich nie im Stich lassen. Danke, dass ihr euch nie ändert!

Ein besonderer Dank gilt meiner besten Freundin Johanna Kerch, ohne die ich schon lange aufgegeben hätte, die immer hinter mir steht und die Fähigkeit besitzt mit den Kopf gerade zu rücken. Danke für die vielen Jahre und die ungezwungene Albernheit und dafür, dass wir so oft dasselbe denken.

Markus danke ich, dafür, dass er es beständig mit mir aushält, auch wenn die letzte Zeit mit Sicherheit nicht immer einfach war. Danke für alles.



Zuletzt danke ich meinen Eltern. Dafür, dass sie mir in jeder Situation bedingungslosen Rückhalt geben. Danke für die Liebe und die Wärme, die Geborgenheit und den allzeit sicheren Hafen.

